Stresses in Pipe Bundles[1]

By H. PORITSKY[2] and G. HORVAY,[3] SCHENECTADY, N. Y.

For purposes of stress analysis, a closely packed bundle of very many pipes can be replaced by a homogeneous but nonisotropic solid (HNS for short). This paper deals with the derivation of the elastic constants of the HNS, the solution of its stress problem under certain conditions, and the conversion of the results into stresses and displacement of individual pipes. As an example, the thermal stresses are determined that arise in a pipe bundle due to a nonuniform axial temperature gradient.

1 Introduction

BUNDLES of thin tubes arranged in close pack hexagonal fashion, each tube or pipe being welded along six lines of contact to adjacent tubes as shown in Fig. 1, are often used in engineering structures, for instance, in heat exchangers

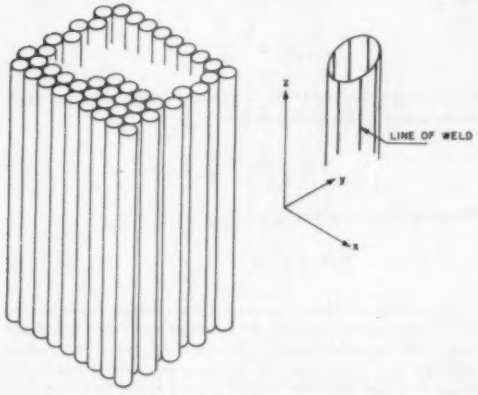

Fig. 1

and in structures where stiffness in the axial direction and flexibility in transverse directions are of interest. In the following we shall analyze the stresses and deformations which develop in the individual pipes by replacing the pipe bundle by a "homogeneous nonisotropic solid" (we shall refer to this as HNS), solve its stress problem, and then reinterpret the results for individual pipes. Evidently such an analysis is permissible only for a bundle where the number of pipes is so large that variations in stresses in the HNS over distances of 1 pipe diameter are not significant.

In Section 2 the elastic constants of the HNS are expressed in terms of the constants and dimensions of the individual pipes (Equations [2]); in the third section it is shown how the stresses and deformations of the HNS translate into stresses and deformations of individual pipes (Equations [27] to [29] and [35] to [41], also Figs. 7 to 11); in the fourth and fifth sections, the elastic equations for the HNS are derived, taking into account its nonisotropic behavior in the axial (z) and transverse (x, y, or r, θ) directions; and in the final section, as an illustration of the method, there is outlined the solution of a thermal stress problem for a cylindrical bundle, where the individual tubes are arranged in the manner of Fig. 1.

A similar method of analysis is applicable to honeycomb structures.

2 Determination of Elastic Moduli of Continuous Homogeneous Nonisotropic Solid (HNS) That is Structurally Equivalent to a Bundle of Tubes

The thermoelastic stress-strain relations of an homogeneous nonisotropic solid (HNS) which represents a bundle of tubes with axes parallel to the z-axis can be written in the form

$$\left.\begin{aligned} \epsilon_x &= \frac{\sigma_x}{E_t} - \frac{\mu_t\sigma_y}{E_t} - \frac{\mu_a\sigma_z}{E_a} + k\vartheta \\ \epsilon_y &= -\frac{\mu_t\sigma_x}{E_t} + \frac{\sigma_y}{E_t} - \frac{\mu_a\sigma_z}{E_a} + k\vartheta \\ \epsilon_z &= -\frac{\mu_a\sigma_x}{E_a} - \frac{\mu_a\sigma_y}{E_a} + \frac{\sigma_z}{E_a} + k\vartheta \end{aligned}\right\} \quad \ldots\ldots [1]$$

$$\gamma_{xy} = \tau_{xy}/G_t,\ \gamma_{xz} = \tau_{xz}/G_a,\ \gamma_{yz} = \tau_{yz}/G_a$$

where $\epsilon_x, \ldots, \gamma_{yz}$ are the strain components of the HNS, $\sigma_x, \ldots, \tau_{yz}$ the stress components; k is the coefficient of linear expansion of the material, ϑ the temperature rise. As will be noted, an axial stress σ_z produces axial elongation and transverse contractions, determined by the axial Young's modulus and Poisson's ratio, E_a, μ_a, while the transverse stresses σ_x, σ_y lead to strains determined by different, transverse, elastic constants, E_t, μ_t; similarly, the different shear moduli G_a, G_t express the shearing strains in terms of the shearing stresses τ_{xz}, τ_{yz}, and τ_{xy}, respectively.

It will be noted that the HNS, as described by Equations [1] is isotropic about the z-axis. Referring to Figs. 4, 6, it is not immediately obvious whether this is actually the case or not. However, as will be shown presently, a stress σ_y, in Fig. 1 leads to elastic constants differing by less than 1 per cent from those obtained for σ_x (see Figs. 4, 6, and Equations [21], [26]); hence the assumption of isotropy in the cross-sectional plane is an adequate approximation.

In what follows, the following values will be derived for the elastic constants of the HNS for the pipe bundle in Fig. 1

$$E_a = \frac{\pi}{\sqrt{3}}\frac{t}{\rho}E, \qquad \mu_a = \mu \quad \ldots\ldots [2a]$$

$$G_a = \frac{3\sqrt{3}}{2\pi}\frac{t}{\rho}G, \qquad G = \frac{E}{2(1+\mu)} \quad \ldots\ldots [2b]$$

[1] The writers are indebted to the Atomic Energy Commission for sponsoring this study and for permission to publish it.

[2] Engineering General Division, General Electric Company. Mem. ASME.

[3] Engineering General Division, General Electric Company.

Contributed by the Applied Mechanics Division and presented at the Annual Meeting, New York, N. Y., November 26–December 1, 1950, of The American Society of Mechanical Engineers.

Discussion of this paper should be addressed to the Secretary, ASME, 29 West 39th Street, New York, N. Y., and will be accepted until October 10, 1951, for publication at a later date. Discussion received after the closing date will be returned.

Note: Statements and opinions advanced in papers are to be understood as individual expressions of their authors and not those of the Society. Manuscript received by ASME Applied Mechanics Division, March 17, 1950. Paper No. 50—A-80.

$$E_t = \frac{8.32}{1-\mu^2}\left(\frac{t}{\rho}\right)^3 E, \quad \mu_t = 0.806 \ldots\ldots [2c]$$

$$G_t = E_t/2(1+\mu_t) \ldots\ldots [2d]$$

Here E, μ, G are the ordinary Young's modulus, Poisson ratio and shear modulus for the pipe material, ρ the tube radius, t the tube-wall thickness. We assume the pipes to be thin; $t << \rho$.

Moduli E_a, μ_a for Axial Tension σ_a.

Let the tube bundle be subject to a uniform axial tension, producing an axial strain $\epsilon_a = \epsilon$. The axial force, over a large area A, required to produce this strain is

$$F = A\sigma_a = \epsilon E f A \ldots\ldots [3]$$

where f is the ratio of the cross section of the active material over A to the area A, that is, the ratio of the tube material of the bundle to the space occupied by it. Since the space in the tube bundle can be divided equally between the tubes by allotting one circumscribed hexagon to each tube, see Fig. 2, we can write

$$f = \frac{\text{tube cross section}}{\text{hexagon area}} = \frac{\pi}{\sqrt{3}}\frac{t}{\rho} \ldots\ldots [4]$$

The equivalent Young's modulus E_a is therefore

$$E_a = \frac{F}{\epsilon A} = Ef = E\pi t/\sqrt{3}\,\rho \ldots\ldots [5]$$

It is obvious that, in spite of the reduced active area, the transverse strain under a uniform axial tension is the same fraction of the longitudinal strain as for a solid material, hence

$$\mu_a = \mu \ldots\ldots [6]$$

Axial Shear Modulus G_a.

Let the bundle of tubes be arranged relative to the axes as shown in Fig. 3(a), and let it be subject to a shear τ_{zz}. It is clear that the part of this shear carried by a particular (cross-hatched) tube can be applied to it only along the welds P_2, P_3, and will in turn be transmitted by it to the tubes to the left at P_5, P_6 only. The tubes to the right and to the left of the hatched tube are similarly loaded, and by symmetry no shear is, therefore, carried across the welds at P_1 or P_4. Thus only the tube area from P_2 to P_5 and from P_3 to P_6 is loaded in shear, while the remaining portions P_2P_3, P_5P_6 are idle.

The shear τ_{zz} leads to a shearing force $2\rho\tau_{zz}$ per tube, per unit axial length, and a shearing stress $\rho\tau_{zz}/t$ across the tube sections P_2P_5, P_3P_6. The shearing strain is, therefore

$$\rho\tau_{zz}/tG \ldots\ldots [7]$$

The total axial displacement d of P_5, P_6 relative to P_2, P_3 is obtained by multiplying this shearing strain by the arc $P_2P_5 = 2\pi\rho/3$.

$$d = \frac{2\pi\rho^2\tau_{zz}}{3tG} \ldots\ldots [8]$$

Dividing d by the chord $P_2P_5 = \rho\sqrt{3}$ leads to the shearing strain of the equivalent homogeneous solid

$$\gamma = \frac{d}{\rho\sqrt{3}} = \frac{2\pi\rho\tau_{zz}}{3\sqrt{3}tG} \ldots\ldots [9]$$

Hence the shear modulus G_a is

$$G_a = \tau_{zz}/\gamma = \frac{3\sqrt{3}\,t}{2\pi\rho}G \ldots\ldots [10]$$

A particular position of the co-ordinate axes relative to the line of centers has been used in the foregoing analysis. It is likely that a different orientation of the axes would result in a slightly different G_a. This point will be examined more closely in the analysis of the transverse moduli, where the variation turns out to be small.

Moduli E_t, μ_t for Transverse Tension.

If, in Equations [1] only σ_x, σ_y do not vanish, there results

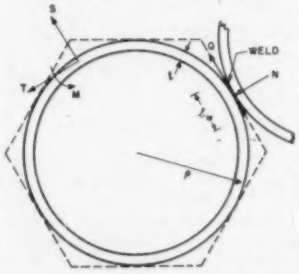

FIG. 2

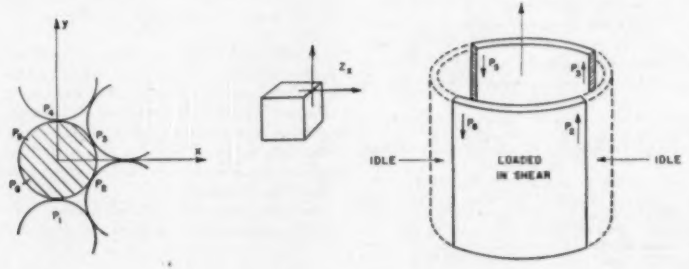

FIG. 3

$$\left.\begin{aligned} E_1\epsilon_x &= \sigma_x - \mu_1\sigma_y \\ E_1\epsilon_y &= -\mu_1\sigma_x + \sigma_y \end{aligned}\right\} \quad \ldots\ldots\ldots\ldots [11]$$

The question arises whether the tube bundle can be truly described by means of a solid which is isotropic about the z-axis, for instance, whether in Fig. 1 the elastic constants E_x, μ_x resulting from the application of a stress σ_x differ from those of a stress σ_y. This point will be examined in detail.

Turning to Fig. 4, suppose that a compression $p_y(= -\sigma_y)$ is applied to the tube bundle, while $\sigma_x = 0$. From symmetry considerations it is clear that this pressure can only be transmitted to a particular tube of the bundle, say, the hatched tube

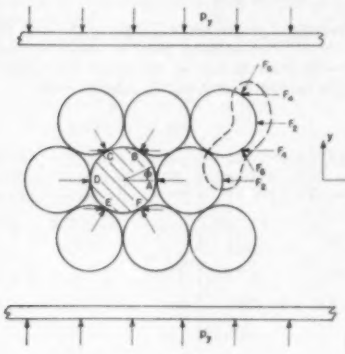

FIG. 4

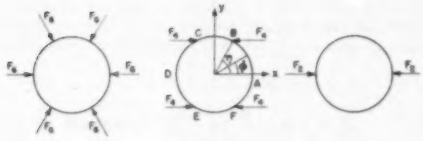

FIG. 5

in Fig. 4, in equal vertical reactions at the two points B, C and passed on in turn to other tubes at the points E, F. In addition to these, various horizontal reactions can act at A, B, C, D, E, F. The net forces (per unit height) acting at the six welds of the hatched tube will be resolved into 3 parts: first, into six equal radial components F_0 acting across each of the six points A, B, C, D, E, F; next, into four horizontal reactions F_1 across each of the four points B, C, E, F; finally, into two further horizontal reactions F_2 at the points A, D. These forces are displayed separately in Fig. 5. It will be noted that at the four points B, C, E, F, the reactions are both normal and tangential; on the other hand, at the points A, D, they are purely normal, due to symmetry. We denote by $\bar{u}$, $\bar{v}$ the radial (inward) and tangential (counterclockwise) displacements of the hatched tube in Fig. 4 (assuming its center to remain fixed) and by φ the central angle of a tube element, and obtain by superposition

$$\left.\begin{aligned} \bar{u}(\varphi) &= u_0(\varphi)\,F_0 + u_1(\varphi)F_1 + u_2(\varphi)F_2 \\ \bar{v}(\varphi) &= v_0(\varphi)F_0 + v_1(\varphi)F_1 + v_2(\varphi)F_2 \end{aligned}\right\} \quad \ldots\ldots [12]$$

where u_0, v_0, u_1, . . . , denote the displacements produced by the forces F_0, F_1, F_2, respectively, per unit F_0, F_1, F_2. An explicit form for u_0, v_0, . . . for thin-walled tubes is given by

$$u_0 = \frac{6\rho^2}{\pi D}\sum_1^\infty \frac{\cos 6n\varphi}{(36n^2-1)^2}, \qquad v_0 = \frac{6\rho^2}{\pi D}\sum_1^\infty \frac{\sin 6n\varphi}{6n(36n^2-1)^2} \quad [13a]$$

$$\left.\begin{aligned} u_1 &= \frac{4\rho^2}{\pi D}\sum_1^\infty \left(\cos\eta\cos 2n\eta + \frac{1}{2n}\sin\eta\sin 2n\eta\right)\times \frac{\cos 2n\varphi}{(4n^2-1)^2} \\ v_1 &= \frac{4\rho^2}{\pi D}\sum_1^\infty \left(\cos\eta\cos 2n\eta + \frac{1}{2n}\sin\eta\sin 2n\eta\right)\times \frac{\sin 2n\varphi}{2n(4n^2-1)^2} \end{aligned}\right\} \quad [13b]$$

$$u_2 = \frac{2\rho^2}{\pi D}\sum_1^\infty \frac{\cos 2n\varphi,}{(4n^2-1)^2}, \qquad v_2 = \frac{2\rho^2}{\pi D}\sum_1^\infty \frac{\sin 2n\varphi}{2n(4n^2-1)^2} \quad [13c]$$

Equations [13] are derived in the Appendix. The angle η defines the location of the forces F_1, Fig. 5. In our case $\eta = 60$ deg. D is the flexural rigidity of the tube wall per unit height,

$$D = E t^3/12(1-\mu^2) \quad \ldots\ldots [14]$$

The three unknowns, F_0, F_1, F_2 will now be determined from the following equilibrium and displacement conditions. First, equating the force of the pressure p_y on the tube to the vertical component of the forces F_0, F_1, F_2 in Fig. 4, there results

$$2\rho\, p_y = 2F_0\cos\frac{\pi}{6} \quad \ldots\ldots [15]$$

Since there is no lateral stress σ_x, it follows that over the right-hand edge in Fig. 4 the net horizontal resultant of the forces must be zero. These forces obviously recur for every pair of tubes. Summing the horizontal forces over the (encircled) two tubes there results

$$2\left(\sin\frac{\pi}{6}+1\right)F_0 + 2F_1 + 2F_2 = 0 \quad \ldots\ldots [16]$$

The third equation for F_0, F_1, F_2 is obtained from the condition that the strain be homogeneous; as a result of this the horizontal displacement at the point A relative to the tube center is double the horizontal displacement at the point B. In terms of $\bar{u}$ and $\bar{v}$ this condition becomes

$$\bar{u}(0) = 2\,[\bar{u}(\pi/3)\cos\pi/3 + \bar{v}\,(\pi/3)\sin\pi/3] \ldots [17]$$

where, by Equations [12], [13]

$$\left.\begin{aligned} \bar{u}(0) &= \frac{1-\mu^2}{E}\left(\frac{\rho}{t}\right)^3 [0.02017\,F_0 + 0.18781\,F_1 + 0.8927\,F_2] \\ \bar{u}(\pi/3) &= \frac{1-\mu^2}{E}\left(\frac{\rho}{t}\right)^3 [0.02017\,F_0 - 0.08388\,F_1 - 0.4363F_2] \\ \bar{v}\,(\pi/3) &= \frac{1-\mu^2}{E}\left(\frac{\rho}{t}\right)^3 [0.00830\,F_1 + 0.3603\,F_2] \end{aligned}\right\} \quad [18]$$

Solution of Equations [15], [16], [17] yields

$$F_0 = 1.1547\,\rho p_y, \quad F_1 = -2.0231\,\rho p_y, \quad F_2 = 0.2911\,\rho p_y \ldots [19]$$

The strains thus become

$$\left.\begin{aligned} \epsilon_x &= -\mathfrak{u}(0)/\rho = 0.0968\,\frac{1-\mu^2}{E}\left(\frac{\rho}{t}\right)^3 p_y \\ \epsilon_y &= \frac{\mathfrak{v}(\pi/3)\cos\pi/3 - \mathfrak{u}(\pi/3)\sin\pi/3}{\rho\sin\pi/3} \\ &= -0.1202\,\frac{1-\mu^2}{E}\left(\frac{\rho}{t}\right)^3 p_y \end{aligned}\right\} \quad [20]$$

Finally Equation [11] for $\sigma_y = -p_y$, $\sigma_x = 0$ yields

$$\left.\begin{aligned} E_t &= -p_y/\epsilon_y = 8.32\,\frac{E}{1-\mu^2}\left(\frac{t}{\rho}\right)^3 \\ \mu_t &= -\epsilon_x/\epsilon_y = 0.805 \end{aligned}\right\} \quad [21]$$

The same calculation will now be repeated for a pressure p_x applied normally to the y-axis as shown in Fig. 6. The cross-hatched tube is now subject to horizontal forces F_1 at B, C, E, F and to horizontal forces F_2 at A, D. Vertical reactions at C, B are not assumed since they would result in a pressure component p_y. Equating the pressure resultant per period of the right-hand boundary (encircled in Fig. 6) to the force resultant per period leads to

$$4\rho p_x \sin\pi/3 = 2F_1 + 2F_2 \quad [22]$$

Another equation results from the homogeneous strain condition, Equation [17].

In the present case we find for the radial and tangential displacements of point A and B the values

$$\left.\begin{aligned} \mathfrak{u}(0) &= \frac{1-\mu^2}{E}\left(\frac{\rho}{t}\right)^3 [0.18781\,F_1 + 0.8927\,F_2] \\ \mathfrak{v}(0) &= 0 \\ \mathfrak{u}(\pi/3) &= \frac{1-\mu^2}{E}\left(\frac{\rho}{t}\right)^3 [-0.08388\,F_1 - 0.4363\,F_2] \\ \mathfrak{v}(\pi/3) &= \frac{1-\mu^2}{E}\left(\frac{\rho}{t}\right)^3 [0.09830\,F_1 + 0.3603\,F_2] \end{aligned}\right\} \quad [23]$$

Noting Equations [23], solution of Equations [17], [22] gives

$$F_1 = 2.0232\,\rho p_x, \quad F_2 = -0.2911\,\rho p_x \quad [24]$$

and hence we obtain the strains

$$\left.\begin{aligned} \epsilon_x &= -0.1201\,\frac{1-\mu^2}{E}\left(\frac{\rho}{t}\right)^3 p_x \\ \epsilon_y &= 0.0970\,\frac{1-\mu^2}{E}\left(\frac{\rho}{t}\right)^3 p_x \end{aligned}\right\} \quad [25]$$

Consequently

$$E_t = -p_x/\epsilon_x = 8.33\,\frac{E}{1-\mu^2}\left(\frac{t}{\rho}\right)^3, \quad \mu_t = -\epsilon_y/\epsilon_x = 0.807 \quad [26]$$

The agreement of the values in Equations [21] and [26] indicates that in the cross-sectional plane of the tube bundle, the equivalent solid material can be considered practically as isotropic, having the elastic constants E_t, μ_t, given earlier

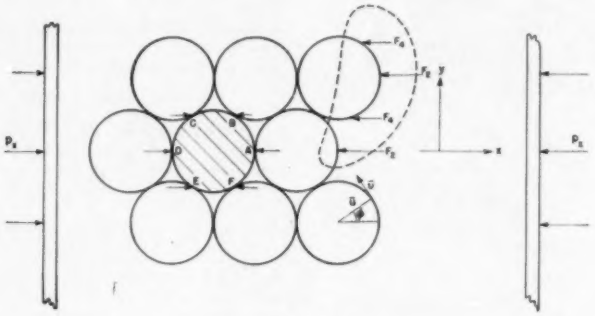

FIG. 6

$$E_t = 8.32\,\frac{E}{1-\mu^2}\left(\frac{t}{\rho}\right)^3, \quad \mu_t = 0.806 \quad [27]$$

Superpositions of equal pressures $p_x = p$, $p_y = p$ yields a uniform compression. This case can also be handled directly, since the reactions on a single tube are obviously six equal radial forces.

Transverse Shear Modulus, G_t.

The third transverse constant G_t is determined in the usual manner

$$G_t = E_t/2(1+\mu_t) \quad [28]$$

The calculations of elastic constants which have just been completed were based upon the assumption of uniform stresses (for instance, constant p_y). While these constants will be applied to cases where the stresses do vary, it is clear that they will apply only if the variation in stresses in a distance equal to one tube diameter is not significant. Otherwise a more detailed and complicated analysis of the deflections of various tubes would be required.

3 Conversion of the HNS Stresses and Displacements Into Stresses and Displacements of Individual Tubes

Continuing with the example of Section 2, it will now be shown how to convert the HNS stresses into stresses existing in the individual pipes.

From the derivation of Equation [5] it is clear that a stress σ_x gives rise to an actual axial tensile stress

$$\sigma_A = \sigma_s E/E_s \quad [29]$$

in the tube-wall material. Similarly Fig. 3 and the derivation of Equation [10] lead to

$$\tau_A = \tau_{zz}\,\rho/t \quad [30]$$

for the shearing stress in the wall material. The analysis showed that shearing reactions are transmitted across the welds, tending to slide one tube relative to the other one, of average stress magnitude

$$\tau_W = \tau_{zz}\,\rho/l_w \quad [31]$$

where l_w is the weld width (see Fig. 2).

Interpretation of the transverse tube stresses in terms of p_x, p_y is more involved.

As shown in Equations [19], [24], the pressures p_x, p_y give rise to the forces

$$\left.\begin{aligned} F_0 &= 0.577\,\rho(p_y + p_x) + 0.577\,\rho(p_y - p_x)\\ F_2 &= 2.023\,\rho(p_x - p_y)\\ F_3 &= 0.291\,\rho(p_x - p_y)\end{aligned}\right\} \quad [32]$$

at the welds, acting on the tubes, per unit length; the forces can be visualized also (see Figs. 2, 4), as normal (inward) and tangential (counterclockwise) forces

$$\left.\begin{aligned} N_A = N_D &= 0.577\,\rho(p_x + p_y) + 0.868\,\rho(p_y - p_x)\\ Q_A &= Q_D = 0\\ N_B = N_C = N_E = N_F &= 0.577\,\rho(p_y + p_x)\\ &\quad - 0.434\,\rho(p_y - p_x)\\ Q_B = Q_E = -Q_C &= -Q_F = 1.752\,\rho(p_x - p_y)\end{aligned}\right\} \quad [33]$$

acting along the welds.

The forces F_2, F_0, F_4 give rise, as seen in Fig. 2, to shear forces S, tensions T, and bending moments M, in the tube wall. They can be determined by well-known methods (see for instance, Timoshenko[4]). One finds, per unit[5] F_2, F_0, F_4, for the shears

$$\left.\begin{aligned} S_2 &= -\frac{1}{2}\cos\varphi \quad \text{for} \quad 0 < \varphi < \pi\\ S_0 &= \sin(\varphi - \pi/6) \quad \text{for} \quad 0 < \varphi < \pi/3\\ S_4 &= \begin{cases} 0 & \text{for } 0 < \varphi < \eta,\ \pi - \eta < \varphi < \pi\\ -\cos\varphi & \text{for } \eta < \varphi < \pi - \eta\end{cases}\end{aligned}\right\} \quad [34]$$

for the tensions

$$\left.\begin{aligned} T_2 &= -\frac{1}{2}\sin\varphi \quad \text{for} \quad 0 < \varphi < \pi\\ T_0 &= -\cos(\varphi - \pi/6) \text{ for } 0 < \varphi < \pi/3\\ T_4 &= \begin{cases} 0 & \text{for} \quad 0 < \varphi < \eta\\ -\sin\varphi & \text{for } \eta < \varphi < \pi - \eta\end{cases}\end{aligned}\right\} \quad [35]$$

and for the bending moments

$$\left.\begin{aligned} M_2/\rho &= \frac{1}{2}\sin\varphi - \frac{1}{\pi} \text{ for } 0 < \varphi < \pi\\ M_0/\rho &= \cos(\varphi - \pi/6) - 3/\pi \text{ for } 0 < \varphi < \pi/3\\ M_4/\rho &= \begin{cases} \frac{1}{3}\sin\eta - \frac{2}{\pi}\cos\eta \text{ for } 0 < \varphi < \eta,\\ \qquad\qquad \pi - \eta < \varphi < \pi\\ \frac{4}{3}\sin\eta - \frac{2}{\pi}\cos\eta - \sin\varphi\\ \qquad\qquad \text{for} \quad \eta < \varphi < \pi - \eta\end{cases}\end{aligned}\right\} \quad [36]$$

[4] "Strength of Materials," by S. Timoshenko, D. Van Nostrand Company, Inc., New York, N. Y., vol. 2, 1940, section 13.

[5] S_2, T_2, M_2 repeat every 60 deg; S_0, S_4, T_0, T_4, M_0, M_4 every 180 deg.

yielding for the resultant net shear, tension, and bending moment in the tube wall

$$\left.\begin{aligned} S(\varphi) &= S_s\rho(p_y + p_x) + S_d\rho(p_y - p_x)\\ T(\varphi) &= T_s\rho(p_y + p_x) + T_d\rho(p_y - p_x)\\ M(\varphi) &= M_s\rho^2(p_y + p_x) + M_d\rho^2(p_y - p_x)\end{aligned}\right\} \quad [37]$$

where the subscript s relates to the sum, d to the difference of p_y, p_x.

The tube-wall displacements (relative to the pipe axes) can be written similarly

$$\left.\begin{aligned} \bar{u}(\varphi) &= u_s\rho(p_y + p_x) + u_d\rho(p_y - p_x)\\ \bar{v}(\varphi) &= v_s\rho(p_y + p_x) + v_d\rho(p_y - p_x)\end{aligned}\right\} \quad [38]$$

In the foregoing

$$S_s = 0.577\,S_0, \quad S_d = -2.023\,S_2 + 0.577\,S_0 + 0.291\,S_4 \quad [39]$$

and $T_s, \ldots, v_d$ are obtained from Equations [39] by replacing S by $T, \ldots, v$. The coefficients S_s, S_d, T_s, T_d, M_s, M_d and $[E/(1-\mu^2)]\,(t/\rho)^3$ times u_s, u_d, v_s, v_d are plotted in Figs. 7, 8, 9, 10, 11, for the interval of $\varphi = 0$ to π. The curves repeat in the interval π to 2π.

From the curves and equations for $S(\varphi)$, $T(\varphi)$ the average stresses in the pipe wall are obtained by division by t; from $M(\varphi)$ the maximum fiber stress due to bending is obtained by multiplying by $6/t^2$; from $Q(\varphi)$, $N(\varphi)$ the average weld stresses are obtained by division by l_w.

In sections 4 to 6 the elasticity equations for the HNS will be obtained in terms of the rectangular displacement components u, v, w, and for axial symmetry in terms of cylindrical components u, w. In applying the foregoing equations for translating stresses for the HNS into pipe stresses one must first convert the transverse stresses σ_x, σ_y, τ_{xy} into principal stress components, and similarly convert τ_{xz}, τ_{yz} into a single resultant axial shear.

4 Stresses and Displacements of a Solid With Different Axial and Transverse Elastic Constants

The stress-strain relations for a solid having different axial and transverse constants were given in Equations [1]. Solving for the stresses we obtain

$$\left.\begin{aligned} \sigma_x &= A(\epsilon_x - k\vartheta) + B\epsilon_y + C\epsilon_z\\ \sigma_y &= B\epsilon_x + A(\epsilon_y - k\vartheta) + C\epsilon_z\\ \sigma_z &= C\epsilon_x + C\epsilon_y + D(\epsilon_z - k\vartheta)\\ \tau_{xy} &= G_t\gamma_{xy},\ \tau_{zx} = G_a\gamma_{zx},\ \tau_{yz} = G_a\gamma_{yz}\end{aligned}\right\} \quad [40]$$

where

$$\left.\begin{aligned} A &= (1 - E_t\mu_a^2/E_a)\,E_t/d, \quad B = (\mu_t + E_t\mu_a^2/E_a)E_t/d\\ C &= \mu_a(1 + \mu_t)\,E_t/d, \quad D = (1 - \mu_t^2)\,E_a/d\\ d &= (1 + \mu_t)\,(1 - \mu_t - 2\mu_a^2E_t/E_a)\end{aligned}\right\} \quad [41]$$

Substituting from Equations [41] into the equilibrium equations

$$\left.\begin{aligned} \frac{\partial\sigma_x}{\partial x} + \frac{\partial\tau_{xy}}{\partial y} + \frac{\partial\tau_{xz}}{\partial z} &= 0\\ \frac{\partial\tau_{xy}}{\partial x} + \frac{\partial\sigma_y}{\partial y} + \frac{\partial\tau_{yz}}{\partial z} &= 0\\ \frac{\partial\tau_{xz}}{\partial x} + \frac{\partial\tau_{yz}}{\partial y} + \frac{\partial\sigma_z}{\partial z} &= 0\end{aligned}\right\} \quad [42]$$

and expressing the strains in terms of the displacement components u, v, w

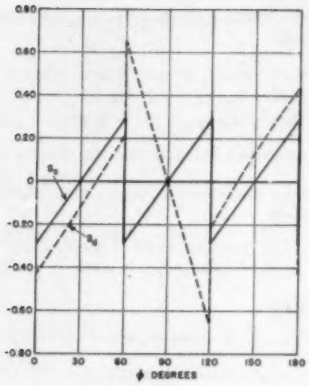

FIG. 7

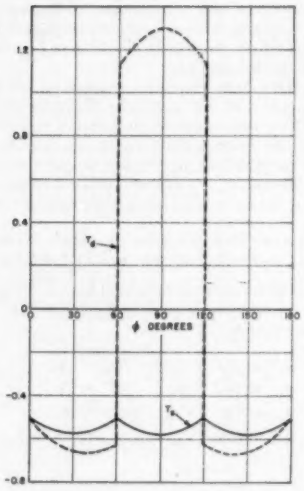

FIG. 8

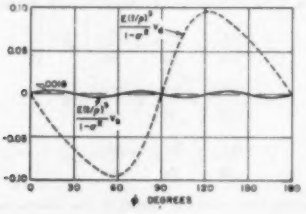

FIG. 11

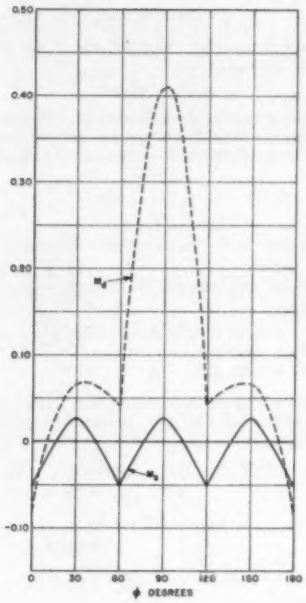

FIG. 9

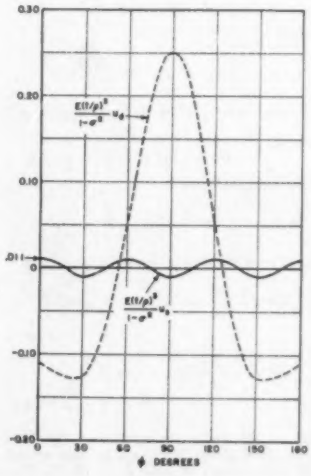

FIG. 10

$$\left.\begin{aligned} \epsilon_x &= u_{,x} \qquad \epsilon_y = v_{,y} \quad \epsilon_z = w_{,z} \\ \gamma_{xy} &= u_{,y} + v_{,x} \quad \gamma_{xz} = u_{,z} + w_{,x} \quad \gamma_{yz} = v_{,z} + w_{,y} \end{aligned}\right\} \ldots [43]$$

we arrive at the differential equations for the displacements

$$\left.\begin{aligned} Au_{,xx} + G_t u_{,yy} + G_a u_{,zz} + (B + G_t)v_{,xy} + (C + G_a)w_{,xz} &= (A + B + C)k\vartheta_{,x} \\ G_t v_{,xx} + Av_{,yy} + G_a v_{,zz} + (B + G_t)u_{,xy} + (C + G_a)w_{,yz} &= (A + B + C)k\vartheta_{,y} \\ G_a(w_{,xx} + w_{,yy}) + Dw_{,zz} + (G_a + C)(u_{,xz} + v_{,yz}) &= (2C + D)k\vartheta_{,z} \end{aligned}\right\} \ldots [44]$$

of the HNS. These equations are then to be solved for the given boundary conditions. We shall formulate the latter problem more precisely for the case of axial symmetry.

It is readily seen, by including body forces X, Y, Z in the equilibrium Equations [42], that the effect of temperature gradients is equivalent to the application of proper body forces.

5 The Case of Axial Symmetry

For axial symmetry the radial displacement $u = u(r, z)$ and the axial displacement $w = w(r, z)$ are the only nonvanishing displacement components. The strain relations, Equations 43], are replaced by

$$\left.\begin{aligned} \epsilon_r &= \partial u/\partial r, \ \epsilon_\theta = u/r \\ \epsilon_z &= \partial w/\partial z, \quad \gamma_{rz} = \frac{\partial u}{\partial z} + \frac{\partial w}{\partial r} \\ \gamma_{r\theta} &= \gamma_{z\theta} = 0 \end{aligned}\right\} \ldots\ldots [45]$$

and the stress-strain relations, Equations [40], by

$$\left.\begin{aligned} \sigma_r &= A(\epsilon_r - k\vartheta) + B\epsilon_\theta + C\epsilon_z = A(u_{,r} - k\vartheta) + B\frac{u}{r} + Cw_{,z} \\ \sigma_\theta &= B\epsilon_r + A(\epsilon_\theta - k\vartheta) + C\epsilon_z = Bu_{,r} + A\left(\frac{u}{r} - k\vartheta\right) + Cw_{,z} \\ \sigma_z &= C\epsilon_r + C\epsilon_\theta + D(\epsilon_z - k\vartheta) = Cu_{,r} + C\frac{u}{r} + D(w_{,z} - k\vartheta) \\ \tau_{r\theta} &= G_t\gamma_{r\theta} = 0, \quad \tau_{z\theta} = G_a\gamma_{z\theta} = 0 \\ \tau_{rz} &= G_a\gamma_{rz} = G_a(u_{,z} + w_{,r}) \end{aligned}\right\} \ldots [46]$$

The equations of equilibrium now take the form

$$\left.\begin{aligned} \frac{\partial\sigma_r}{\partial r} + \frac{1}{r}\frac{\partial\tau_{r\theta}}{\partial\theta} + \frac{\partial\tau_{rz}}{\partial z} + \frac{\sigma_r - \sigma_\theta}{r} &= 0 \\ \frac{\partial\tau_{r\theta}}{\partial r} + \frac{1}{r}\frac{\partial\sigma_\theta}{\partial\theta} + \frac{\partial\tau_{z\theta}}{\partial z} + \frac{2}{r}\tau_{r\theta} &= 0 \\ \frac{\partial\tau_{rz}}{\partial r} + \frac{1}{r}\frac{\partial\tau_{z\theta}}{\partial\theta} + \frac{\partial\sigma_z}{\partial z} + \frac{\tau_{rz}}{r} &= 0 \end{aligned}\right\} \ldots\ldots [47]$$

while substitution from Equations [45] into [46] yields

$$\left.\begin{aligned} A\left(u_{,rr} + \frac{u_{,r}}{r} - \frac{u}{r^2}\right) + G_a u_{,zz} + (C + G_a)w_{,rz} &= k(A + B + C)\vartheta_{,r} \\ (C + G_a)\left(u_{,rz} + \frac{u_{,z}}{r}\right) + G_a\left(w_{,rr} + \frac{w_{,r}}{r}\right) + Dw_{,zz} &= k(2c + D)\vartheta_{,z} \end{aligned}\right\} \ldots [48]$$

6 Stresses in a Pipe Bundle Produced by an Axial Temperature Gradient

As an application to the foregoing we shall consider the stresses in a bundle of pipes of lengths H forming (roughly) a cylinder of radius R, maintained at a temperature $\vartheta(z)$, which varies with the axial distance linearly over the middle third of the bundle length, from $\vartheta(H/3) = \vartheta_0$ to $\vartheta(2H/3) = \vartheta_0 + \vartheta$, in the manner shown in Fig. 12(a), and is constant over each remaining third.

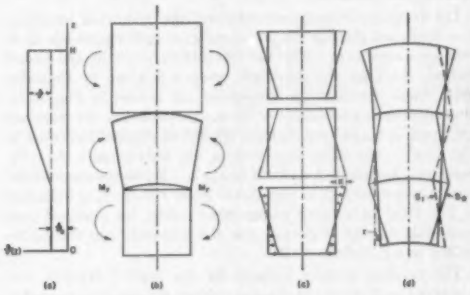

Fig. 12

Due to thermal expansion there is a tendency to produce an elongation $k\vartheta(z)$ in each direction. No stresses would result if this expansion were allowed to take place; this, however, is obviously not the case. The stresses that obtain in the present case will be analyzed as follows: Imagine the pipe bundle separated into thirds, each of axial height $H/3$, and assume that the expansions $k\vartheta(z)$ do take place over each third—this turns out to be possible without producing any stresses. It will be found then that the displacements consequent upon these expansions, produce a misfit over the common boundaries. One next tries to bring these boundaries together and join the severed thirds; the stresses introduced in the process are the thermal stresses.

Start with a uniform temperature equal to the temperature of the coolest third. Due to the thermal expansion, consequent upon the temperature distribution shown in Fig. 12(a), the first, coolest, third of the pipe bundle will not expand at all. The middle portion, if detached from the other two portions, can expand the way it should, by elongating axially an amount $k\vartheta$ per unit length, and expanding transversely a similar amount. The displacement which is obtained as a result of such expansions consists of an axial displacement, and of bending, as a result of which both of the originally plane boundaries of the middle third curve into spherical surfaces of curvature

$$c = 3k\vartheta/H \ldots\ldots [49]$$

as shown in Fig. 12(b), to a highly exaggerated extent. The remaining third of the pipe bundle, again detached from the other two thirds, will merely enlarge uniformly, corresponding to its temperature excess over the temperature of the opposite end. As a result, the distortions indicated in Fig. 12(b) would be obtained and gaps or misfits between the plane and the curved surfaces would result. We now proceed to join the severed thirds and eliminate the gaps between them. We consider the bundle as an HNS with axial and transverse elastic constants as determined by Equations [2].

One of the simplest ways of joining up the three thirds of Fig. 12(b) is by applying a proper bending moment to the cylindrical boundary of each one. The elementary bending theory of a plate, bounded by planes z = const, based as it is upon purely

transverse stresses σ_x, σ_y, will apply in the present case provided "transverse" elastic constants E_t, μ_t be used. A bending moment M_r applied as a linearly varying radial stress σ_r over the cylindrical boundary r = const of a circular plate of the thickness h will produce a curvature given by

$$c = M_r(1 - \mu_t)/E_t I_p \quad [50]$$

where $I_p = h^3/12$ is the moment of inertia of the plate side per unit length of perimeter.

Let us apply bending moments over the cylindrical boundary $r = R$ of each third of the pipe bundle, of such magnitude as to produce a curvature $c/2$ for the first section, $-c/2$ for the second section, $+c/2$ for the third one, where c is given by Equation [50]; these moments are shown by the arrows in Fig. 12(b). Since the thirds are initially of the same dimensions, the moments are equal in magnitude and are applied as stresses indicated in Fig. 12(c). The three pipe sections will then acquire the same curvature, namely, $c/2$, and will fit again. While the shape of the bundle is now conical, of semivertex angle $\tau = Rc/2$, as indicated in Fig. 12(d) to a highly exaggerated extent, for practical purposes this may be neglected, and the boundary can still be regarded as a cylinder $r = R$.

The bending stresses induced by the applied bending moments put each plane z = const in uniform tension or compression equal in magnitude to the applied σ_r stress. We call this state of stress S_0.

Over the boundary $r = R$ there are actually no stresses σ_r corresponding to those of S_0. Therefore it is necessary to counteract these stresses by applying over the boundary of the cylinder equal and opposite normal stresses, as shown in Fig. 12(d). These correcting stresses will be applied in two steps. First a "periodic" stress distribution S_1, will be applied; this is computed on the assumption that the cylinder is of infinite axial length and that a periodic zig-zag normal stress distribution acts over the cylindrical boundary. While this periodic solution S_1 will remove the applied boundary load in Fig. 12(c), it will result in a certain normal stress acting over the top and bottom ends of the cylinder. It will then be necessary to remove these stresses, too, by applying a correcting stress S_2 over these ends.

As indicated, the S_0 stresses are given by

$$\sigma_r(r, z) = \sigma_\theta(r, z) = K(z), \quad \tau_{rz}(r, z) = \sigma_z(r, z) = 0 \quad [51]$$

where $K(z)$ is the zig-zag line shown in Fig. 12(c), of maximum tension

$$K = kE_t\vartheta/2(1 - \mu_t) \quad [52]$$

at $z = H/3$, H and the same maximum compression at $z = 0$, $2H/3$.

To solve for the S_1-stresses, we shall obtain periodic solutions of the homogeneous Equations [48], subject to the boundary conditions

$$\sigma_r|_R = -K(z), \quad \tau_{rz}|_R = 0 \quad [53]$$

Expand $K(z)$ in a Fourier series

$$K(z) = -\frac{8K}{\pi^2}\sum_1^\infty \frac{1}{n^2}\cos 3n\pi z/H \quad [54]$$

Corresponding to (the negative of) each term of Equation [54], a proper solution of the Equations [48] turns out to be

$$u = aJ_1(\alpha r)\cos \gamma z, \quad w = bJ_0(\alpha r)\sin \gamma z \quad [55]$$

where $\gamma = 3\pi/H, 6\pi/H, \ldots$ and a/γ, a/b are determined from the equations

$$\left(\frac{\alpha}{\gamma}\right)^4 - \left(\frac{D}{G_a} - \frac{C^2}{AG_a} - \frac{2C}{A}\right)\left(\frac{\alpha}{\gamma}\right)^2 + \frac{D}{A} = 0 \quad [56]$$

$$-b/a = \frac{A(\alpha/\gamma)^2 - G_a}{(C + G_a)\alpha/\gamma} \quad [57]$$

which result from the substitution of the solution, Equation [55], into [48]. Adding the solutions corresponding to the two (conjugate complex) roots of Equation [56], and determining the two remaining constants so that along $r = R$ the shearing stress τ_{rz} vanishes, while the normal stress σ_r cancels the various terms in Equation [54], one arrives at the S_2 solution. This analysis has been carried out for the first term of Equation [54]. We write the resulting displacements and stresses in the form

$$\left.\begin{aligned} u &= U(r)\cos \gamma z \\ w &= W(r)\sin \gamma z \\ \sigma_r &= R(r)\cos \gamma z \\ \sigma_\theta &= \Theta(r)\cos \gamma z \\ \sigma_z &= Z(r)\cos \gamma z \\ \tau_{rz} &= X(r)\sin \gamma z \end{aligned}\right\} \quad [58]$$

The stresses R, Θ, Z, X are plotted for certain assumed tube dimensions in Fig. 13, the displacements U and W in Fig. 14.

It is of interest to note that owing to the greater transverse flexibility, there results a "skin effect," namely, a stress concentration near the boundary $r = R$.

The S_1 stress system gives rise to certain normal stresses $\sigma_z = Z_1(r)$, $-Z_1(r)$ (but to no shearing stresses τ_{rz}) over faces $z = H$, $z = 0$ of the cylinder. The S_2 stress system must now be devised so as to remove these stresses without introducing any tractions over $r = R$. The S_2 system is built up by starting with solutions of Equations [48] of the term

$$u = aJ_1(\lambda r)e^{-\beta z}, \quad w = bJ_0(\lambda r)e^{-\beta z} \quad [59]$$

(similar to Equation [55]). There results for $(\lambda/\beta)^2$ a quadratic equation similar to Equation [56], and when the solutions, Equations [59], are added for the two roots λ_a, λ_b and combined to yield zero tractions over $r = R$, one is led to a transcendental equation in Bessel functions with complex roots. Finally, the S_T-stress system is obtained as an expansion in terms of the characteristic solutions corresponding to these complex roots.

It is of interest to point out that the stress $Z(r)$, while it has a zero resultant $\int_0^R Z(r)r\,dr = 0$ over a pie-shaped portion $d\vartheta$ of the faces $z = 0$, $z = H$, does have a nonvanishing moment which is held in equilibrium only by an opposite moment over the diametrically opposite portion of the face. As a result the St. Venant principle does not apply to the S_T-stress system, and the first term of the S_T-expansion exhibits appreciable depth penetration.

Appendix

Deflections of a Ring Under Symmetrical Loading

We consider the center diagram in Fig. 5 for unit F_4 and write for the radial (inward) and tangential (counterclockwise) displacements

$$u_4 = \sum_0^\infty A_n \cos n\varphi, \quad v_4 = \sum_1^\infty B_n \sin n\varphi \quad [60]$$

Omitting the subscript 4 of u and v and recalling that the "extension" of circular ring is given by

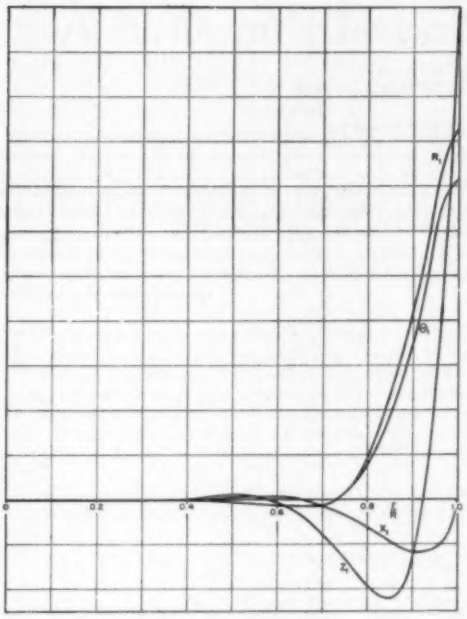

FIG. 13

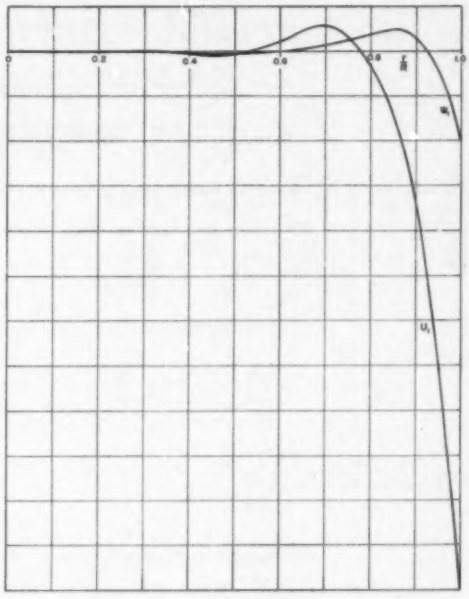

FIG. 14

$$\epsilon = \frac{1}{\rho}\left(\frac{dv}{d\varphi} - u\right) \quad \ldots\ldots [61]$$

its "curvature change" by

$$c = \frac{1}{\rho^2}\left(\frac{dv}{d\varphi} + \frac{d^2u}{d\varphi^2}\right) \quad \ldots\ldots [62]$$

we obtain for the energy of stretching and bending

$$V = \frac{1}{2} EA \int_0^{2\pi} \epsilon^2 \rho d\varphi + \frac{1}{2} EI \int_0^{2\pi} c^2 \rho d\varphi$$

$$= \frac{EA\rho\pi}{2\rho^2}\left[2A_0^2 + \Sigma\,(nB_n - A_n)^2\right] + \frac{EI\rho\pi}{2\rho^4}\,\Sigma\,(nB_n - n^2A_n)^2$$

$$\ldots\ldots [63]$$

Here I, as in Equation [14], denotes the tube-wall moment of inertia per unit height, A denotes the wall area per unit height ($A = t$). The work done by the forces F_4 during a virtual displacement δu, δv is

$$\delta W = F_\rho\,(\delta u_B + \delta u_D + \delta u_E + \delta u_F) + F_\varphi\,(\delta v_B - \delta v_D + \delta v_E - \delta v_F) = 4F_\rho\,[\delta A_0 + \delta A_2 \cos 2\eta + \delta A_4 \cos 4\eta + \ldots] + 4F_\varphi\,[\delta B_2 \sin 2\eta + \delta B_4 \sin 4\eta + \ldots] \ldots [64]$$

where

$$F_\rho = F_4 \cos\eta = \cos\eta \quad \ldots\ldots [65]$$

is the radial (u), and

$$F_\varphi = F_4 \sin\eta = \sin\eta \quad \ldots\ldots [66]$$

the tangential (v) component of the force F_4 which acts at point B. Using the abbreviation

$$q = I/\rho^2 A = (t/\rho)^2/12 \quad \ldots\ldots [67]$$

the increase in strain energy due to the displacements δu, δv is

$$\delta V = \frac{EA\pi}{\rho}\left[2A_0\delta A_0 + (1+q)\,(A_1 - B_1)\,(\delta A_1 - \delta B_1)\right] + \sum_2^\infty \delta A_n\,[A_n\,(1 + n^4q) - nB_n(1 + n^2q)] + \sum_2^\infty \delta B_n[-nA_n(1 + n^2q) + n^2B_n(1 + q)] \ldots\ldots [68]$$

Equating this to δW and comparing the δA_n, δB_n coefficients of the two expressions, we obtain

$$\left.\begin{aligned} A_0 &= \frac{4\rho}{EA\pi}\,\frac{\cos\eta}{2}\,;\quad A_n = B_n = 0 \text{ for } n \text{ odd} \\ A_n &= \frac{4\rho}{EA\pi}\,\frac{n(1+q)\cos\eta\cos n\eta + (1+qn^2)\sin\eta\sin n\eta}{qn(n^2-1)^2} \\ B_n &= \frac{4\rho^3}{EI\pi}\,\frac{(1+qn^4)\sin\eta\sin n\eta + n(1+qn^2)\cos\eta\cos n\eta}{n^2(n^2-1)^2} \end{aligned}\right\} \text{for } n \text{ even} \quad \left.\vphantom{\frac{1}{1}}\right\} \ldots [69]$$

For thin rings ($\rho >> t$) only the highest terms in ρ/t need to be kept.

Then Equations [69] reduce to Equations [13b]; making $F_4 = 1/2$, and placing $\eta = 0$ in Equations [13b] we obtain Equation [13c]; finally Equation [13a] is obtained by superposition of Equation [13c] for $\varphi = 0°$, 60°, and 120°.

A Note on Elastic Surface Deformation

By MURRAY KORNHAUSER,[1] WASHINGTON, D. C.

Surface deformation of elastic bodies having the same modulus is treated by the standard texts on elasticity, but the applicability of the solution is limited to the range of the tables of coefficients presented. This note extends the tables to cover the range that applies to bodies having one principal curvature much larger than the other. Some inaccuracy in the tables in current use also is noted. The reader is referred to any good text on elasticity for a general discussion of this problem.

THE general problem of the stresses produced by the local contact of elastic bodies was treated by Heinrich Hertz who, as long ago as 1881, developed a solution of the problem expressed in the form of a Newtonian potential function. Hertz was obliged to perform laborious computations in order to obtain the values of α and β (Table 1), constants proportional, respectively, to the major and minor axes of the ellipse of contact (1).[2]

In subsequent discussions of this problem (2, 3), Table 1 has been reproduced without extending the table of values of α and β for $\theta < 10°$. The region $0° < \theta < 10°$ is applicable to a body having one principal curvature (the principal curvatures are the maximum and the minimum curvatures, and these are in planes at right angles) much larger than the other; approaching, for example, the case of the cylinder. Table 2 was easily computed by expressing Hertz's formulas for α and β in terms of the complete elliptic integrals, K and E

$$K = \int_0^{\frac{\pi}{2}} \frac{d\psi}{\sqrt{1 - \sin^2 \alpha' \sin^2 \psi}}$$

$$E = \int_0^{\frac{\pi}{2}} d\psi \sqrt{1 - \sin^2 \alpha' \sin^2 \psi}$$

As given by Hertz

$$\alpha^3 = \frac{2}{\pi \sin^2 \frac{\theta}{2}} \int_0^{\infty} \frac{dx}{\sqrt{\left(1 + \frac{\beta^2}{\alpha^2} x^2\right)^3 (1 + x^2)}} \quad \ldots\ldots [1]$$

$$\beta^3 = \frac{2}{\pi \cos^2 \frac{\theta}{2}} \int_0^{\infty} \frac{dx}{\sqrt{\left(1 + \frac{\alpha^2}{\beta^2} x^2\right)^3 (1 + x^2)}} \quad \ldots\ldots [2]$$

Substituting $x = \tan \psi$ in Equation [1]

$$\alpha^3 = \frac{2}{\pi \sin^2 \frac{\theta}{2}} \int_0^{\frac{\pi}{2}} \frac{\sec \psi \, d\psi}{\left(1 + \frac{\beta^2}{\alpha^2} \tan^2 \psi\right)^{3/2}}$$

$$= \frac{2}{\pi \sin^2 \frac{\theta}{2}} \int_0^{\frac{\pi}{2}} \frac{\cos^3 \psi \, d\psi}{(1 - \sin^2 \alpha' \sin^2 \psi)^{3/2}}$$

TABLE 1 CONSTANTS PROPORTIONAL TO MAJOR AND MINOR AXES OF ELLIPSE OF CONTACT

θ	10°	20°	30°	40°	50°	60°	70°	80°	90°
α	6.612	3.778	2.731	2.136	1.754	1.486	1.284	1.128	1.000
β	0.319	0.408	0.493	0.567	0.641	0.717	0.802	0.893	1.000

NOTE: Auxiliary angle θ is dependent upon curvatures of bodies in contact.

TABLE 2 CONSTANTS COMPUTED BY HERTZ'S FORMULAS

θ	0	1/2°	1°	1 1/4°	2°	3°	4°	5°	8°	10°	20°
α	∞	61.40	36.89	27.48	22.26	16.50	13.31	9.790	7.860	6.604	3.813
β	0	0.1018	0.1314	0.1522	0.1691	0.1964	0.2188	0.2552	0.2850	0.3112	0.4123

where $\beta/\alpha = \cos \alpha'$

$$\alpha^3 = \frac{2}{\pi \sin^2 \frac{\theta}{2}} \frac{K - E}{1 - \beta^2/\alpha^2} \quad \ldots\ldots [3]$$

Substituting $x = (\beta/\alpha) \tan \psi$ in Equation [2]

$$\beta^3 = \frac{2}{\pi \cos^2 \frac{\theta}{2}} \int_0^{\frac{\pi}{2}} \frac{\frac{\beta}{\alpha} \cos \psi \, d\psi}{\sqrt{1 + \frac{\beta^2}{\alpha^2} \tan^2 \psi}}$$

$$= \frac{2}{\pi \cos^2 \frac{\theta}{2}} \int_0^{\frac{\pi}{2}} \frac{\frac{\beta}{\alpha} \cos^2 \psi \, d\psi}{\sqrt{1 - \sin^2 \alpha' \sin^2 \psi}}$$

$$\beta^3 = \frac{2 \frac{\beta}{\alpha}}{\pi \cos^2 \frac{\theta}{2}} \frac{E - \frac{\beta^2}{\alpha^2} K}{1 - \beta^2/\alpha^2} \quad \ldots\ldots [4]$$

Equations [3] and [4] were solved by use of tables of elliptic integrals, such as may be found in reference (5). The slight discrepancies between Tables 1 and 2 are probably due to the fact

---

[1] Navy Department, Bureau of Ships.

[2] Numbers in parentheses refer to the Bibliography at the end of the paper.

Contributed by the Applied Mechanics Division and presented at the Annual Meeting, New York, N. Y., November 26–December 1, 1950, of THE AMERICAN SOCIETY OF MECHANICAL ENGINEERS.

Discussion of this paper should be addressed to the Secretary, ASME, 29 West 39th Street, New York, N. Y., and will be accepted until October 10, 1951, for publication at a later date. Discussion received after the closing date will be returned.

NOTE: Statements and opinions advanced in papers are to be understood as individual expressions of their authors and not those of the Society. Manuscript received by ASME Applied Mechanics Division, July 10, 1950. Paper No. 50—A-30.

that Hertz did not have available the tables of elliptic integrals.

BIBLIOGRAPHY

1 "Gesammelte Werke," by H. Hertz, J. A. Barth, Leipsig, Germany, vol. 1, 1895.

2 "Theory of Elasticity," by S. Timoshenko, first edition, McGraw-Hill Book Company, Inc., New York, N. Y., 1934.

3 "A Treatise on the Mathematical Theory of Elasticity," by A. E. H. Love, fourth edition, Dover Publications, New York, N. Y., 1944.

4 "Stresses Due to the Pressure of One Elastic Solid Upon Another," by H. R. Thomas and V. A. Hoersch, Engineering Experiment Station, University of Illinois, Bulletin No. 212, 1930.

5 "Tables of Functions," by E. Jahnke and F. Emde, Dover Publications, New York, N. Y., 1943.

Velocity Distributions and Design Data for Ideal Incompressible Flow Through Cascades of Airfoils

By ROBERT RESNICK[1] AND L. J. GREEN[2]

Theoretical incompressible velocity distributions for three airfoils in various cascade arrangements and for different entering-air angles are presented. Design charts and design formulas relating cascade angle, entering-air angle, turning angle, and blade camber are presented for 10 per cent thick airfoils at solidity 1. An empirical turning-angle formula is developed and is found to be reasonably accurate and rather generally applicable.

Nomenclature

The following nomenclature is used in the paper:

β = cascade angle
λ_1 = entering-air angle
λ_2 = leaving-air angle
λ = mean air angle
α_i = angle of attack
Θ = turning angle
Θ_s = approximate turning angle derived by Constant
Θ_s' = approximate turning angle derived from Constant's
Θ_{GR} = approximate turning angle derived in present paper
γ_a = angular camber
γ_h = height camber as fraction of chord length
γ_N = camber angle at nose
γ_T = camber angle at trailing edge
t = thickness as fraction of chord length
δ = deviation of air
S = spacing between consecutive blades
C = chord length
σ = solidity of cascade = C/S
ϕ = central angle of circle used in conformal transformation
ϕ_s = value of ϕ corresponding to rear stagnation point on airfoil
K, T = constants used in conformal transformation
V_1 = magnitude of velocity of entering air
V_2 = magnitude of velocity of leaving air
V = magnitude of mean air velocity
v = magnitude of velocity of air at any point of airfoil
λ_{1D} = value of λ_1 at design operating condition
$\mu = C/2$

[1] Department of Physics, University of Pittsburgh, Pittsburgh, Pa.

[2] Department of Mathematics, Case Institute of Technology, Cleveland, Ohio.

Contributed by the Applied Mechanics Division and presented at the Annual Meeting, New York, N. Y., November 26–December 1, 1950, of THE AMERICAN SOCIETY OF MECHANICAL ENGINEERS.

Discussion of this paper should be addressed to the Secretary, ASME, 29 West 39th Street, New York, N. Y., and will be accepted until October 10, 1951, for publication at a later date. Discussion received after the closing date will be returned.

NOTE: Statements and opinions advanced in papers are to be understood as individual expressions of their authors and not those of the Society. Manuscript received by ASME Applied Mechanics Division, August 5, 1949. Paper No. 50—A-31.

Introduction

A detailed systematic analysis of the incompressible flow through a cascade of airfoils is of value in the design of compressors and turbines. There is an appreciable lack of experimental data suitable for such an analysis, although some experimental work along these lines has been published (1–4).[3] This paper is intended as a contribution to the development of such an analysis, and is based on the theory developed by Mutterperl (5).

A semiempirical turning-angle formula for typical airfoil-shaped blades of 10 per cent thickness is obtained from the cascade experiments mentioned. For any given choice of parameters, a velocity distribution over each blade of the cascade is determined from this turning-angle formula and from a suitable conformal map. If the entering-air angle is allowed to vary and the remaining parameters are kept fixed, it is possible to determine a "design range" of the cascade, that is, that range of entering-air angle which produces, for a given choice of cascade angle, solidity, and blade shape, a velocity distribution which is free from peaks near the nose. This design range has a width of at least 2 deg in all the cases tested, and its mid-point is denoted here as the design condition of the cascade. Design charts and design formulas, relating the design angle to the parameters involved, are presented here for 10 per cent thick airfoils at solidity 1.

Definitions and Notations

A lack of uniformity among authors in the definitions and nomenclature employed in airfoil cascades makes it advisable to present briefly the terminology used in this paper.

A consistent and readily applied definition of chord line for different blades is necessary, since the solidity and cascade angle depend on the choice of chord line. Here, as in references (5, 6, 7) the chord line is defined to be the "diameter" of the blade, i.e., the line joining the two points on the blade which are farthest apart. When a previously tested blade is to be considered, the given chord line is accepted, unless it departs appreciably from the blade diameter. In such a case and in the case also of an untested blade, the diameter of the blade is to be taken as the chord line.

The chord length C is defined as the projection of the airfoil on the chord line, and the solidity σ is the ratio of the chord length to the spacing between consecutive blades. This spacing is measured along a cascade line, i.e., any line connecting corresponding points of different blades of the cascade.

The geometry of the cascade is shown in Figs. 1 and 2. The cascade angle β is the angle between the cascade normal and the chord line; the entering-air angle λ_1 is the angle between the cascade normal and the air infinitely far upstream; and the leaving-air angle λ_2 is the angle between the cascade normal and the air infinitely far downstream. The signs of these angles, all lying between —90 deg and +90 deg, are determined by defining the positive direction on the cascade normal (the base line) to run

[3] Numbers in parentheses refer to the Bibliography at the end of the paper.

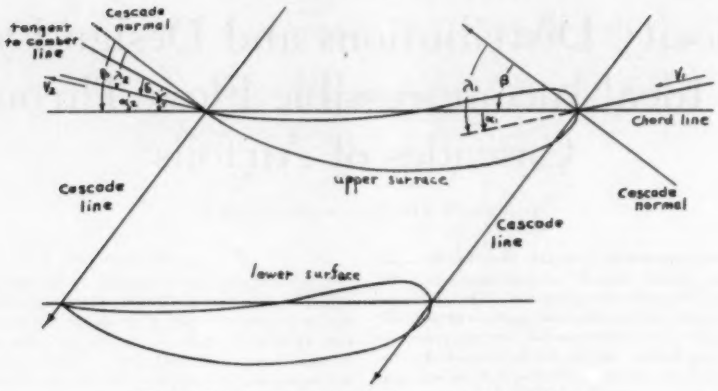

FIG. 1 GEOMETRY OF CASCADE, COMPRESSOR ARRANGEMENT

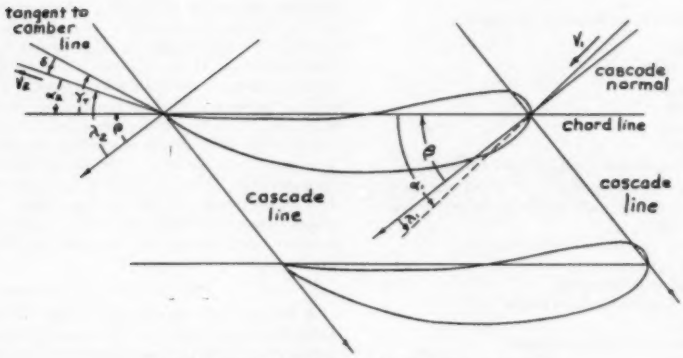

FIG. 2 GEOMETRY OF CASCADE, TURBINE ARRANGEMENT

downstream, and the positive direction on the cascade line to run from the lower (pressure) surface of any blade toward the upper (suction) surface of the same blade.

The angle of attack α is defined by

$$\alpha = \lambda_1 - \beta \quad [1]$$

the turning angle Θ has the value given by

$$\Theta = \lambda_1 - \lambda_2 \quad [2]$$

and the "angular" camber γ_a of the blade is defined by

$$\gamma_a = \gamma_N + \gamma_T \quad [3]$$

where γ_N and γ_T are the acute angles which the chord line (as defined) makes with the tangents to the mean camber line at the nose and trailing edge, respectively. A second form of camber is the "height camber," γ_h, defined as the ratio of the maximum height of the mean camber line above the chord to the chord length. Finally, the deviation, δ, defined as the angle between the leaving air infinitely far downstream and the tangent to the mean camber line at the trailing edge, has the value

$$\delta = \gamma_T + \lambda_2 - \beta \quad [4]$$

so that

$$\Theta = \lambda_1 + \gamma_T - \beta - \delta \quad [5]$$

THEORY

The basic formulas needed in the determination of the velocity distribution over the blade and the turning angle Θ are presented in this section.

The X-axis is taken as the chord line of one of the blades, the positive direction being from the trailing edge toward the nose; the origin is taken midway between the nose and the trailing edge (to conform with reference 5), the positive direction of the Y-axis running from the upper surface of a blade toward the lower surface of the same blade.

Let the Z-plane which contains the cascade of airfoils be divided into strips by lines parallel to the X-axis, the height of each strip being equal to $S \cos \beta$, with each strip containing just one airfoil of the cascade. Let the p-plane contain the unit circle. Then a conformal transformation exists which carries each strip of the Z-plane, excluding the interior of the airfoil and the point at infinity, into the p-plane, excluding the interior of the circle and two finite exterior points e^K and $-e^K$.

The boundary of each airfoil transforms into the boundary of the circle; if ϕ represents the central angle in the p-plane, the boundary transformation for the airfoil lying in the strip which contains the X-axis may be written parametrically in the form

$$X(\phi) = T + \mu \cos \beta \log_e \frac{\cosh K + \cos \phi}{\cosh K - \cos \phi} + 2\mu \sin \beta \tan^{-1} \frac{\sin \phi}{\sinh K} + \Delta X(\phi) \quad [6]$$

where

$$\left.\begin{aligned} \Delta X(\phi) &= -\frac{1}{2\pi} \int_0^{2\pi} Y(\phi') \cot \frac{\phi' - \phi}{2} \, d\phi' \\ y(\phi) &= -\Delta y(\phi) \end{aligned}\right\} \quad [7]$$

T serves as a displacement constant affecting the location of the airfoil, and $\mu = C/2\pi\sigma$. Equations [6] and [7] are derived in references (5) and (6), respectively, where C is taken equal to $2\pi\sigma$.

T and K are constants depending on β, σ, and the blade profile. The values of T and K are determined by successive approximations. If T_n, K_n, and $\Delta X_n(\phi)$ are the nth approximation values, then $X_n(\phi)$ is obtained from Equation [6] and $Y_{n+1}(\phi)$ is read from the graph of the airfoil. By numerical integration of Equations [7], as described elsewhere (8), $\Delta X_{n+1}(\phi)$ is obtained. This, together with a tentative value of K_{n+1}, is inserted into Equation [6], and the maximum and minimum values of $X_{n+1} - T_{n+1}$ are calculated. The difference between these extreme values must be equal to the chord length C, and by trial and error the proper value of K_{n+1} is found which accomplishes this. T_{n+1} is then chosen to make the extreme values of X_{n+1} equal to their known values on the graph of the airfoil. Equation [6] now gives $X_{n+1}(\phi)$ which is plotted against $Y_{n+1}(\phi)$. If the graph does not agree sufficiently well with the airfoil, then $Y_{n+2}(\phi)$ is read from the airfoil and the work is repeated.

The magnitude v of the velocity vector v at any point (X, Y) of the airfoil corresponding to the parameter ϕ is given by

$$\frac{v}{V} = \frac{2\mu(\cos^2 \lambda + \sinh^2 K)^{1/2} \left| \sin (\phi - \lambda_K) - \sin (\phi_s - \lambda_K) \right|}{(\sin^2 \phi + \sinh^2 K) \left[\left(\zeta_p - \frac{d\Delta X}{d\phi} \right)^2 + \left(\frac{dY}{d\phi} \right)^2 \right]^{1/2}} \quad [8]$$

where

$$\zeta_p = 2\mu(\cos^2 \beta + \sinh^2 K)^{1/2} \sin (\phi - \beta_K)/(\sin^2 \phi + \sinh^2 K)$$

V is the vector mean (Fig. 3) of V_1 and V_2 (the entering and leaving velocity vectors), λ is the angle between the cascade normal and V

$$\lambda_K = \tan^{-1} (\tan \lambda \tanh K)$$

$$\beta_K = \tan^{-1} (\tan \beta \tanh K)$$

and ϕ_s is the value of ϕ corresponding to the stagnation point S in the trailing-edge region of the airfoil.

The leaving-air angle is intimately related to ϕ_s. It is proved in reference (5) that

$$\Gamma/4\pi = \frac{V(\sin^2 \phi_T + \sinh^2 K)^{1/2}}{\sinh K \cosh K} \sin (\phi_{TK} - \lambda)$$

where

$$\tan \phi_{TK} = \frac{\tan \phi_T}{\tan K}$$

Transformation of form gives

$$\Gamma/4\pi = V(\cosh K \sin \phi_s \cos \lambda - \sinh K \cos \phi_s \sin \lambda)/(\sinh K \cosh K) \quad [9]$$

where Γ is the circulation about a blade. It follows from Fig. 3,

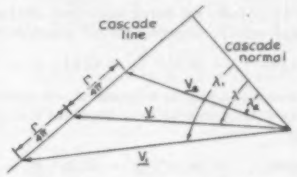

FIG. 3 RELATIONSHIP OF AIR ANGLE, AIR VELOCITY, AND CIRCULATION ABOUT BLADE IN CASCADE

also established in reference (5), that

$$\Gamma/4\pi = V \cos \lambda \tan \lambda_1 - V \sin \lambda \quad [10]$$

and

$$2 \tan \lambda = \tan \lambda_1 + \tan \lambda_2 \quad [11]$$

Elimination of Γ yields

$$\tan \lambda = (\cosh K \tan \lambda_1 - \coth K \sin \phi_s)/(\cosh K - \cos \phi_s) \quad [12]$$

which, when combined with Equation [11], gives

$$\tan \lambda_2 = A \tan \lambda_1 + B \quad [13]$$

where

$$\left.\begin{aligned} A &= \frac{\cosh K + \cos \phi_s}{\cosh K - \cos \phi_s} \\ B &= -\frac{2 \sin \phi_s \coth K}{\cosh K - \cos \phi_s} \end{aligned}\right\} \quad [14]$$

Finally, the result of solving Equation [12] for ϕ_s is

$$\sin (\phi_s - \lambda_K) = \sinh K \cosh K \cos \lambda (\tan \lambda_1 - \tan \lambda)/(\cos^2 \lambda + \sinh^2 K)^{1/2} \quad [15]$$

If β, σ, and the blade profile are considered fixed then $X(\phi)$, $Y(\phi)$, and K can be found by the method of successive approximations described previously and the following conclusions may be drawn.

For a blade with a sharp trailing edge, ϕ_s is fixed by the Kutta-Joukowski condition, so that the turning angle Θ and the velocity distribution over the blade are functions of λ_1 alone. For blades with a slightly rounded trailing edge, the turning angle Θ can be obtained in terms of λ_1 from experimental data. This will fix ϕ_s and hence determine the velocity distribution over the blade. Therefore an empirical turning-angle formula is required here, and one is developed which seems particularly accurate for the blades treated in this paper. These blades are described as follows:[4]

The 65-series blades (tested in references 1 and 2) whose members are designated 65–010, 65–110, ... satisfy the relations

[4] All angles considered are in degrees.

$$\gamma_a = 727\gamma_h, \quad \gamma_N = \gamma_T = {}^1/_2\gamma_a$$

$\gamma_h = 0$ for 65–010
$\gamma_h = 0.0055$ for 65–110
$\gamma_h = 0.0221$ for 65–410
$\gamma_h = 0.0441$ for 65–810
$\gamma_h = 0.0662$ for 65–1210

The 14.9 per cent blade, not tested experimentally but for which some theoretical velocity distributions are presented here, has

$$\gamma_h = 0.149, \ \gamma_N = 28.15°, \ \gamma_T = 42.65°, \ \gamma_a = 70.80°$$

The 8.8 per cent blade, used in reference (5) for calculating theoretical velocity distributions with the use of the Kutta-Joukowski condition, has

$$\gamma_h = 0.088, \ \gamma_N = 20.13°, \ \gamma_T = 27.35°, \ \gamma_a = 47.48°$$

Equation [13] can serve as the basis for a turning angle formula. Since the value of A given by Equation [14] is very small for all the cases for which conformal transformations were made, Equation [13] may be replaced with a high degree of accuracy by the equation

$$\lambda_2 = a \tan \lambda_1 + \beta - b \quad \ldots\ldots [16]$$

where a, b are expressible in terms of A and B. Since $\Theta = \lambda_1 - \lambda_2$, Equation [16] becomes

$$\Theta_{GR} = \lambda_1 - a \tan \lambda_1 - \beta + b \quad \ldots\ldots [17]$$

Calculations show that a and b are accurately independent of λ_1 and depend only upon β, σ, and γ_h, which characterizes the blade shape. The conformal transformations made give values of a and b for certain numerically chosen values of β, σ, and γ_h; and some of the experiments of reference (4) are used with Equation [17] to give values of $b - a \tan \lambda_1$ for numerically chosen values of β, σ, λ_1, and γ_h. On the basis of these results empirical formulas for a and b in terms of β, σ, and γ_h were obtained, namely

$$\left.\begin{aligned} a &= a_1 e^{a_2(1-\sigma)} \\ b &= 1.5\sigma^{1/4}(90\gamma_h - 1^\circ) \\ a_1 &= ({}^1/_{45})(90 - |\beta|) \\ a_2 &= 3e^{0.009|\beta|} \end{aligned}\right\} \quad \ldots\ldots [18]$$

The empirical turning-angle formula thus developed has been checked against all of the extensive data of references (1–4). A detailed comparison is available but is omitted here for the sake of brevity. Table 1 summarizes the over-all results, giving

TABLE 1 TURNING-ANGLE ERRORS

Experiment	Average of $\Theta_{GR} - \Theta_{exp}$	Average of $\Theta_C - \Theta_{exp}$
Constant (ref. 3)	1.4	1.0
Harris and Fairthorne (ref. 4)	2.1	1.9
Bogdonoff and Bogdonoff (ref. 1)	0.9	5.1
Zimney and Lappi (ref. 2)	1.3	2.1

the turning-angle errors for the blades of references (1–4); the experimental turning angles are compared with those from the empirical formula just developed, and from a formula due to Constant (3) for circular-arc cambers.
Here

$$\Theta_c = \lambda_1 + \gamma_T - \beta - 0.26\gamma_a/\sigma^{1/2} \quad \ldots\ldots [19]$$

Table 1, therefore, indicates both the degree of fit of Equations [18] and Equation [19] to experiment, and their general applicability. Θ_{GR} is seen to be quite adequate for the blades treated here and on the whole shows better agreement with experiment than Θ_c.

Velocity Distributions and Design Charts

Theoretical velocity distributions were obtained by conformal mapping and the GR turning-angle formula for the 65–810, the 65–1210, and the 14.9 per cent blades in cascade arrangements of various β, σ, and λ_1. Table 2 summarizes the cases investigated in this report.

TABLE 2 SUMMARY OF CASES INVESTIGATED

Blade	Thickness, t	Height camber, γ_h	σ	β	λ_1, deg
65–810	0.10	0.0441	2/3	35.4	36, 38, 39, 40, 42
			1	29.4	37, 39, 41, 43, 45
			1	35.4	41, 43, 45, 47, 49
			1	44.4	51, 53, 55, 57, 59
			1.5	44.4	53, 55, 57, 59, 61
65–1210	0.10	0.0662	1	35.9	47, 49, 51, 53
14.9%	0.10	0.1490	1/2	0	15, 19, 21, 23, 25, 27
			1	0	25, 27, 29, 31, 33
			1	22.5	47, 49, 51, 53, 55
			1	45	68, 70, 72, 74, 76

A set of 48 equally spaced values of ϕ was employed in the calculations of the functions $X(\phi)$, $Y(\phi)$. These functions as well as $\Delta X(\phi)$, the derivatives $[d\Delta X(\phi)]/(d\phi)$, $[dY(\phi)]/(d\phi)$ and the associated constants T and K have been obtained, but are omitted here for the sake of brevity. The derivatives were obtained by fitting a series of 6th-degree polynomials to the functions $\Delta X(\phi)$, $Y(\phi)$, as discussed, for example, in reference (9). The successive approximations were stopped when the difference between Y_a and the airfoil ordinate Y, both measured at the same abscissa, was less than 0.05 per cent of the chord throughout the leading-edge region; elsewhere along the blade this difference did not exceed 0.01 per cent of the chord.

With β, σ, and the blade shape known, each of the 48 values of ϕ thus determines a point (X, Y) on the blade. If, in addition, λ_1 and a turning-angle formula are given, then each value of ϕ determines also a velocity ratio v/V. The graph of the velocity distribution is obtained by plotting this velocity ratio against the corresponding value of X and drawing a smooth curve through the 48 points. The velocity-distribution curve is very steep in the trailing-edge region, and a 48-point method will not yield results sufficiently accurate to warrant plotting in this region.

As the velocity-distribution curves in Fig. 4 show, a velocity peak exists on the lower surface near the nose, provided the entering-air angle λ_1 is below a certain value λ_{1L}, whereas a velocity peak exists on the upper surface near the nose, provided λ_1

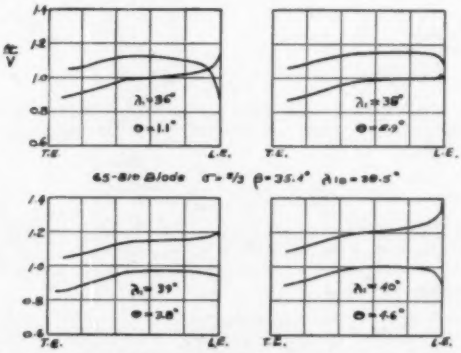

FIG. 4 VELOCITY DISTRIBUTIONS AND TURNING ANGLES FOR VARIOUS ENTERING-AIR ANGLES IN DESIGN RANGE; 65–810 BLADE; $\sigma = 2/3$ AND $\beta = 35.4$ DEG

(Abscissa gives relative distance along chord line from trailing edge to leading edge.)

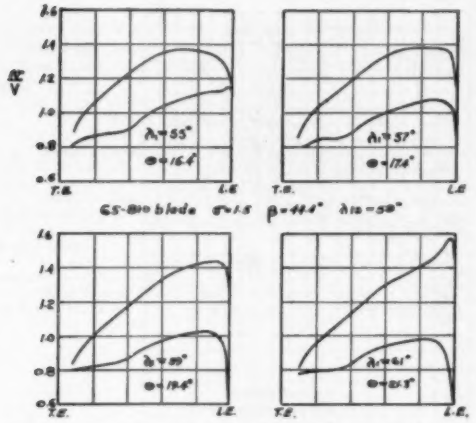

FIG. 5 VELOCITY DISTRIBUTIONS AND TURNING ANGLES FOR VARIOUS ENTERING-AIR ANGLES IN DESIGN RANGE; 65-810 BLADE; $\sigma = 1.5$ AND $\beta = 44.4$ DEG

(Abscissa gives relative distance along chord line from trailing edge to leading edge.)

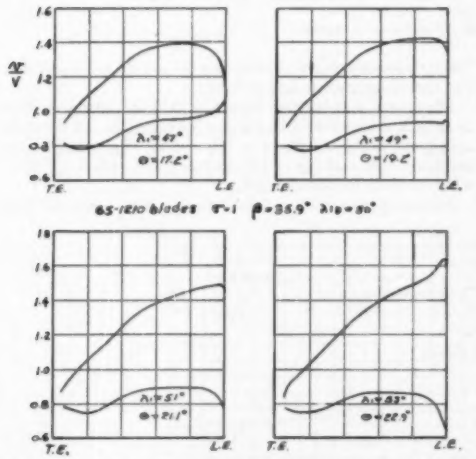

FIG. 6 VELOCITY DISTRIBUTIONS AND TURNING ANGLES FOR VARIOUS ENTERING-AIR ANGLES IN DESIGN RANGE; 65–1210 BLADE; $\sigma = 1$ AND $\beta = 35.9$ DEG

(Abscissa gives relative distance along chord line from trailing edge to leading edge.)

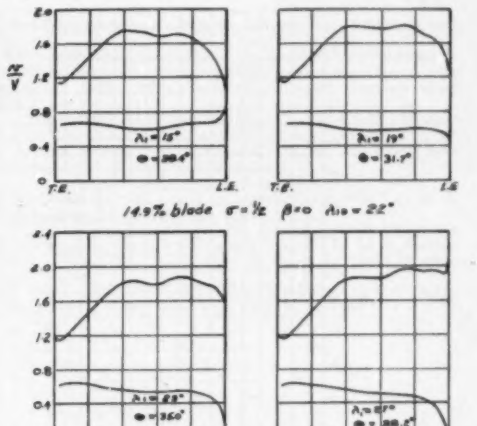

FIG. 7 VELOCITY DISTRIBUTIONS AND TURNING ANGLES FOR VARIOUS ENTERING-AIR ANGLES IN DESIGN RANGE; 14.9-PER CENT BLADE; $\sigma = 1/2$ AND $\beta = 0$

(Abscissa gives relative distance along chord line from trailing edge to leading edge.)

exceeds a certain value λ_{1u}, with $\lambda_{1u} > \lambda_{1L}$.[5] The design entering-air angle, λ_{1D}, is defined in this paper as the arithmetic mean of λ_{1L} and λ_{1u}, although it may well be chosen differently depending upon the situation at hand. Without a precise definition of the term "peak," and because the velocity ratio v/V is known only at 48 points, rather than continuously, it is impossible to determine λ_{1L} and λ_{1u} and hence λ_{1D}, with any great degree of accuracy.

Figs. 4 to 7 show some typical velocity-distribution curves for values of λ_1 in the design region along with the corresponding turning angles.[6] A peak-free region of at least 2 deg exists on each side of λ_{1D} in all the cases calculated with solidity 1.

The three solid lines in Fig. 8 represent the graphs of λ_{1D} against β at solidity 1 for the 65–810, the 65–1210, and the 14.9 per cent blades. The experimental results of references (1) and (2) are included. Furthermore, since only one conformal transformation was carried out here for the 65-1210 blade, the results of reference (7) were used to calculate values of λ_{1D} corresponding to three different values of β; these are shown also in Fig. 8.

The points plotted show the justification of a linear relation between λ_{1D} and β, and faired lines were drawn through the theoretically determined points. A single equation which fits these three lines quite well is

$$\lambda_{1D} = 0.96\beta + 164\gamma_b + 4.90 \quad (\sigma = 1, t = 0.10) \ldots [20]$$

Disagreement in Fig. 8 between the theoretical results and the experimental results of references (1) and (2) is due to (*a*) different definitions of design point, and (*b*) differences between theoretical and experimental velocity distributions. A discussion of (*b*) is given in reference (7). It should be added here that some of the experimental results of reference (1) are of questionable value (because of a disagreement in values of circulation as obtained from flow-angles measurement and integration of the experimental pressure distribution about the blades). Disagreement in the case of the 65–1210 blade between the results based upon reference (7) and the faired line drawn in Fig. 8 is due to the inaccuracy in obtaining design points by use of the 24-point method of reference (7). The 48-point method of the present paper not only yields twice as many points on the velocity-distribution curve, thereby improving the fairing; but, more im-

[5] Generally, the presence of a velocity peak indicates an undesirable operating condition. In particular, a peak on the upper surface signifies high aerodynamic loading with an increase in drag and a possibility of stalling; a peak on the lower surface, while it increases the drag somewhat, indicates inefficient operation primarily because of low aerodynamic loading.

[6] Graphs for the remaining cases listed in Table 2 are omitted for the sake of brevity, but the resulting λ_{1D} for those cases are included in the design charts.

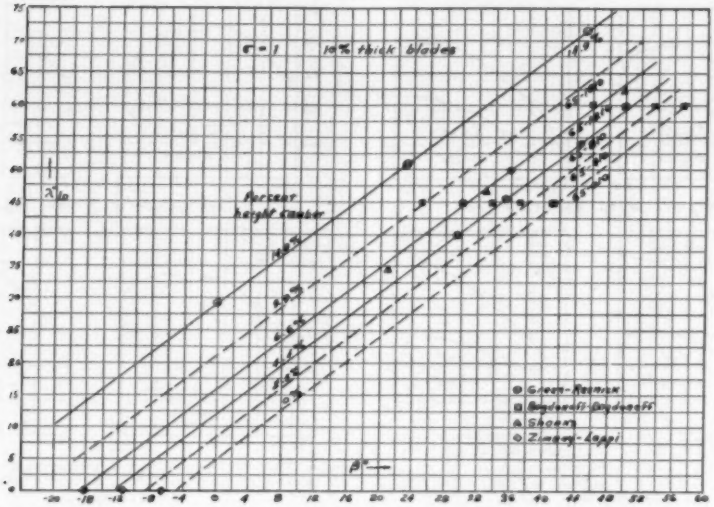

FIG. 8 ENTERING-AIR ANGLE λ_1, VERSUS CASCADE ANGLE, β, AT DESIGN CONDITION FOR VARIOUS CAMBERS
(σ = 1, 10 per cent thick blades. All angles are in degrees.)

portant, it permits greater accuracy in the determination of the derivatives of $\Delta X(\phi)$, and $Y(\phi)$ in the critical nose region, and this in turn greatly improves the velocity values themselves in this region. A 24-point method is unacceptable in determining accurately the velocity distributions, and hence the design point in the nose and trailing-edge regions.

Equation [20] when applied to the 65–010, 65–410, and 65–1810 blades yields three new lines which are shown dashed in Fig. 8. The experimental results of references (1) and (2) are shown also. The agreement is quite satisfactory.

Elimination of β between Equations [17] and [20] gives Θ in terms of λ_{1D}, with $\sigma = 1$, and with γ_A as parameter. The results are plotted in Fig. 9. For $\sigma = 1$, $t = 0.10$, Figs. 8 and 9 yield the design values of any two of the four parameters β, λ_1, Θ, γ_A when the other two are specified.

Additional theoretical velocity distributions should serve to

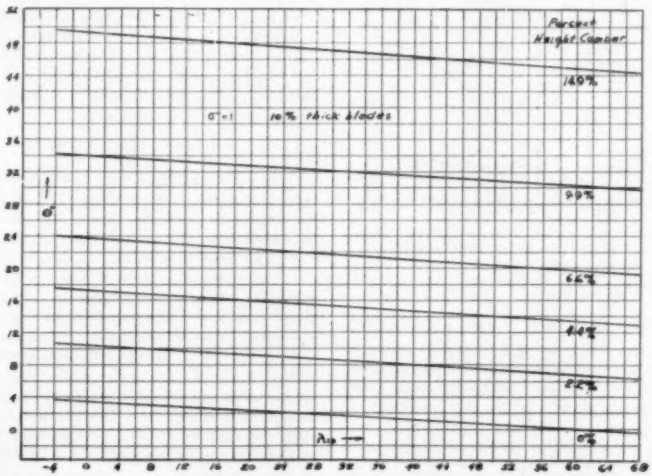

FIG. 9 TURNING ANGLE, Θ, VERSUS ENTERING-AIR ANGLE λ_1, AT DESIGN CONDITION FOR VARIOUS CAMBERS
(σ = 1, 10 per cent thick blades. All angles are in degrees.)

improve Equation [20] as well as remove the restriction $\sigma = 1$. The three cases considered for $\sigma \neq 1$ (Figs. 4 to 6), may be used to show the effects of solidity on velocity distribution and design point.

BIBLIOGRAPHY

1 "Blade Design Data for Axial-Flow Fans and Compressors," by S. M. Bogdonoff and H. E. Bogdonoff, NACA ACR L5F07a, July, 1945. Reissued as NACA Wartime Report L-635.

2 "Data for Design of Entrance Vanes From Two-Dimensional Tests of Airfoils in Cascade," by C. M. Zimney and V. M. Lappi, NACA ACR L5G18, October, 1945. Reissued as NACA Wartime Report L-188.

3 "Note on Performance of Cascades of Aerfoils," by H. Constant, Royal Aircraft Establishment, Note No. E.3696, June, 1939.

4 "Wind Tunnel Experiments With Infinite Cascades of Airfoils," by R. G. Harris and R. A. Fairthorne, Aeronautical Research Committee, Reports and Memoranda No. 1206 (Ae. 367), T.2685, September, 1928.

5 "A Solution of the Direct and Inverse Potential Problems for Arbitrary Cascades of Airfoils," by William Mutterperl, NACA ARR L4K22b, December, 1944. Reissued as NACA Wartime Report L-81.

6 "The Conformal Transformation of an Airfoil Into a Straight Line and Its Application to the Inverse Problem of Airfoil Theory," by William Mutterperl, NACA ARR L4K22a, December, 1944. Reissued as NACA Wartime Report L-113.

7 "A Comparison of Experimental and Theoretical Pressure Distributions and Turning Angles for Cascades of Airfoils," by M. E. Shanks, NACA MRE6E09, June, 1946.

8 "Numerical Evaluation of the E-integral Occurring in the Theodorsen Arbitrary Airfoil Potential Theory," by Irven Naiman, NACA ARR L4D27a, April, 1944. Reissued as NACA Wartime Report L-136.

9 "Relaxation Methods in Engineering Science," by R. V. Southwell, Oxford University Press, New York, N. Y., 1940.

Approximate Solutions of Compressible Flows Past Bodies of Revolution by Variational Method[1]

By CHI-TEH WANG[2] AND SOCRATES DE LOS SANTOS,[3] NEW YORK, N. Y.

Using the direct method of Rayleigh-Ritz in the calculus of variations, the problem of steady irrotational compressible flow past a body of revolution of arbitrary shape is formulated. In order to compare with the analytical solutions obtained by other investigators, two numerical examples have been carried out, namely, compressible flows past a sphere, and an ellipsoid of revolution. The results are found to be in excellent agreement with those computed by other approximate methods.

Introduction

In previous papers (1–6),[4] the senior author and his associates have applied variational methods to two-dimensional compressible-flow problems following Rayleigh-Ritz, Galerkin, and Biezeno-Koch procedures. For inviscid, steady, subsonic flows, the results obtained by the variational methods show excellent agreement with those obtained by other approximate methods. For viscous flows and transonic flows with shock waves, calculations (5, 7) are still being carried out and the results will be reported in subsequent papers.

In this paper, the variational method following the Rayleigh-Ritz procedure has been applied to steady irrotational compressible flows past bodies of revolution. Two numerical examples are given, namely, the flows past a sphere, and an ellipsoid of revolution of thickness ratio of 0.8. These examples are chosen because results by other approximate methods are available. In the case of flow past a sphere, Janzen (8), and Rayleigh (9) expanded the velocity potential into a power series of the Mach number and obtained explicit expression for the first approximation, i.e., terms involving only squares of the Mach number. By using Poggi's modification of the Rayleigh-Janzen method, Tamada (10) succeeded in obtaining the second approximation. Later, following the original Rayleigh-Janzen method, Kaplan (11) also arrived at the same results obtained by Tamada. The third approximation to the stream function and also to the velocity potential has been calculated by Lamla (12). In the case of the flow past ellipsoids of revolution, there is the solution obtained by Schmieden (13) who, using the Rayleigh-Janzen method, developed the Stokes stream function in powers of M^2 and calculated the flow to the first approximation. The results computed by the variational method are compared with those obtained by these investigators and the agreement appears to be excellent. The general problem of compressible flow past an arbitrary body of revolution is formulated and the method of solution is indicated.

Variational Principle

For steady, inviscid, irrotational compressible flow, the governing differential equation is

$$\left[a^2 - \left(\frac{\partial\phi}{\partial x_i}\right)^2\right]\frac{\partial^2\phi}{\partial x_i \partial x_i} - \frac{\partial\phi}{\partial x_i}\frac{\partial\phi}{\partial x_j}\frac{\partial^2\phi}{\partial x_i \partial x_j} = 0 \quad \ldots [1]$$

where

$$a^2 = \frac{\gamma - 1}{2}\left(q_m^2 - \frac{\partial\phi}{\partial x_i}\frac{\partial\phi}{\partial x_i}\right) \quad \ldots [2]$$

In Equations [1] and [2], a is the velocity of sound, ϕ is the velocity potential, x_i are the Cartesian co-ordinates, γ is the ratio of the specific heats, q_m is the maximum attainable velocity in the flow and is given by the following expression

$$q_m^2 = 2a_0^2/(\gamma - 1) + U^2 \quad \ldots [3]$$

where a_0 is the velocity of sound corresponding to the velocity of the undisturbed flow, U. A repetition of subscripts in these equations indicates summation.

It was shown by Bateman (14) that the variational integral

$$I_1 = \int_V p(\phi) dV \quad \ldots [4]$$

gives Equation [1] as its Euler's equation, where p is the pressure, dV is the elementary volume, and the integration is extended to the volume of the fluid V. The derivation of Equation [4] is also shown in detail in references (1) and (2).

To apply the variational method, following the Rayleigh-Ritz procedure, to problems where the domain is infinite, it is pointed out in references (1) and (2) that integral, Equation [4], cannot be used directly. Taking the first variation of Equation [4] in which we assume the pressure-density relationship is of the form

$$p = A + B\rho^\gamma \quad \ldots [5]$$

where ρ is the density and A, B are constants, it can be shown that

---

[1] Based partly on a thesis submitted by S. de los Santos in June, 1949, to the Graduate Division of the College of Engineering in partial fulfillment of the requirements for the degree of Doctor of Engineering Science at New York University under the direction of the senior author.

[2] Associate Professor of Aeronautical Engineering, Daniel Guggenheim School of Aeronautics, College of Engineering, New York University.

[3] Now Professor of Mathematics, Far Eastern University, Manila, Philippines.

[4] Numbers in parentheses refer to the Bibliography at the end of the paper.

Contributed by the Applied Mechanics Division and presented at the Annual Meeting, New York, N. Y., November 26–December 1, 1950, of The American Society of Mechanical Engineers.

Discussion of this paper should be addressed to the Secretary, ASME, 29 West 39th Street, New York, N. Y., and will be accepted until October 10, 1951, for publication at a later date. Discussion received after the closing date will be returned.

Note: Statements and opinions advanced in papers are to be understood as individual expressions of their authors and not those of the Society. Manuscript received by ASME Applied Mechanics Division, May 15, 1950. Paper No. 50—A-33.

$$\delta I_1 = -B^{-1/(\gamma-1)}\left(\frac{\gamma-1}{2\gamma}\right)^{1/(\gamma-1)}\left\{\int_V \delta\phi\,\frac{\partial}{\partial x_i}\left[\left(q_\infty^2-\frac{\partial\phi}{\partial x_i}\frac{\partial\phi}{\partial x_i}\right)^{1/(\gamma-1)}\frac{\partial\phi}{\partial x_i}\right]dV + \oint_S \delta\phi\left(q_\infty^2-\frac{\partial\phi}{\partial x_i}\frac{\partial\phi}{\partial x_i}\right)^{1/(\gamma-1)}\frac{\partial\phi}{\partial n}\,dS\right\} \quad [6]$$

where S is the boundary surface of the domain V, and n is the normal to the boundary surface. If the surface integral is zero, it can be shown that the condition $\delta I_1 = 0$ leads to Equation [1]. If the surface integral is not zero, a surface integral whose first variation is of the form just given must be added to I_1. If ϕ is assumed to be of the form

$$\phi = \phi_1 + \phi_2 \quad [7]$$

where ϕ_1 is the velocity potential of the corresponding incompressible flow, and ϕ_2 is the correction part due to compressibility, it is shown in reference (15) that I_1 must be replaced by I_2 as follows

$$I_2 = \int_V [p(\phi) - p(\phi_1)]dV + B^{-1/(\gamma-1)}\left(\frac{\gamma-1}{2\gamma}\right)^{1/(\gamma-1)} \times (q_\infty^2 - U^2)^{1/(\gamma-1)}\oint_S \phi_2\frac{\partial\phi_1}{\partial n}\,dS \quad [8]$$

Dropping the constant factor from Equation [8], I_2 becomes

$$I_2 = \int_V\left[\left(q_\infty^2-\frac{\partial\phi}{\partial x_i}\frac{\partial\phi}{\partial x_i}\right)^{\gamma/(\gamma-1)} - \left(q_\infty^2-\frac{\partial\phi_1}{\partial x_i}\frac{\partial\phi_1}{\partial x_i}\right)^{\gamma/(\gamma-1)}\right]dV + \frac{2\gamma}{\gamma-1}(q_\infty^2-U^2)^{1/(\gamma-1)}\oint_S \phi_2\frac{\partial\phi_1}{\partial n}\,dS \quad [8a]$$

If ϕ is not assumed as in Equation [7], then the surface integral

$$B^{-1/(\gamma-1)}\left(\frac{\gamma-1}{2\gamma}\right)^{1/(\gamma-1)}\oint_S \delta\phi\left(q_\infty^2 - \frac{\partial\phi}{\partial x_i}\frac{\partial\phi}{\partial x_i}\right)^{1/(\gamma-1)}\frac{\partial\phi}{\partial n}\,dS \quad [9]$$

must be evaluated, and a corresponding function must be taken to replace the third integral in Equation [8] or [8a]. If the factor $B^{-1/(\gamma-1)}\left(\frac{\gamma-1}{2\gamma}\right)^{\gamma/(\gamma-1)}$, which is dropped in Equation [8a], is also omitted in Equation [9], then the surface integral becomes

$$\frac{2\gamma}{\gamma-1}\oint_S \delta\phi\left(q_\infty^2-\frac{\partial\phi}{\partial x_i}\frac{\partial\phi}{\partial x_i}\right)^{1/(\gamma-1)}\frac{\partial\phi}{\partial n}\,dS \quad [9a]$$

Compressible Flow Past a Sphere

Let r, θ, and ω be the spherical co-ordinates. The boundary conditions for a compressible flow past a sphere of unit radius are

$$\left[\left(\frac{\partial\phi}{\partial r}\right)^2 + \left(\frac{1}{r}\frac{\partial\phi}{\partial\theta}\right)^2\right]^{1/2} = U \text{ at } r = \infty, \text{ and } \frac{\partial\phi}{\partial r} = 0 \text{ at } r = 1$$

To satisfy the boundary conditions, the velocity potential ϕ may be assumed to be of the following form

$$\phi = \phi_1 + \phi_2 = \left(r + \frac{1}{2r^2}\right)U\cos\theta + \sum_{m=1}^{\infty}\sum_{n=1}^{\infty} A_{mn}\left[\frac{1}{(m+1)r^{m+1}} - \frac{1}{(m+3)r^{m+3}}\right]\cos^n\theta \quad [10]$$

where, as defined before, ϕ_1 is the incompressible velocity potential, and ϕ_2 is the correction due to compressibility effect. A_{mn} are unknown parameters which can be determined by the Rayleigh-Ritz method from the condition that $\delta I_2 = 0$.

The boundary integral in Equation [8a] becomes in this case

$$\frac{2\gamma}{\gamma-1}(q_\infty^2-U^2)^{1/(\gamma-1)}\oint_S \phi_2\frac{\partial\phi_1}{\partial r}\,r^2\sin\theta\,d\theta\,d\omega \quad [11]$$

On the surface of the sphere Equation [11] is identically zero. At $r = \infty$, if Equation [11] is not to be infinite, ϕ_2 in Equation [10] must start with $m = 1$. This eliminates the $m = 0$ term from ϕ_2, although this term satisfies the boundary conditions. Taking $\gamma = 2$, Equation [11] reduces to

$$4(q_\infty^2-U^2)\int_{\theta=0}^{\theta=\pi}\int_{\omega=0}^{\omega=2\pi}\phi_2\frac{\partial\phi_1}{\partial r}\,r^2\sin\theta\,d\theta\,d\omega\Big]_{r=\infty} = 8(q_\infty^2-U^2)U[A_{11}/3 + A_{12}/5 + A_{13}/7 + \ldots + A_{1(n-1)}/(2n+1) + \ldots] \quad [12]$$

and the variational integral, Equation [8a], may be written as follows

$$I_2 = \int_{r=1}^{r=\infty}\int_{\theta=0}^{\theta=\pi}\left\{\left[q_\infty^2 - \left(\frac{\partial\phi}{\partial r}\right)^2 - \left(\frac{1}{r}\frac{\partial\phi}{\partial\theta}\right)^2\right]^2 - \left[q_\infty^2 - \left(\frac{\partial\phi_1}{\partial r}\right)^2 - \left(\frac{1}{r}\frac{\partial\phi_1}{\partial\theta}\right)^2\right]^2\right\}2\pi r^2\sin\theta\,dr\,d\theta + 8\pi(q_\infty^2-U^2)U(A_{11}/3 + A_{12}/5 + A_{13}/7 + \ldots) \quad [13]$$

The justification for using $\gamma = 2$ has been discussed in detail in references (1) and (2).

Taking six parameters, the velocity potential ϕ is as follows

$$\phi = U\left(r + \frac{1}{2r^2}\right)\cos\theta + A_{11}\left(\frac{1}{2r^2}-\frac{1}{4r^4}\right)\cos\theta + A_{21}\left(\frac{1}{3r^3}-\frac{1}{5r^5}\right)\cos\theta + A_{12}\left(\frac{1}{2r^2}-\frac{1}{4r^4}\right)\cos^2\theta + A_{22}\left(\frac{1}{3r^3}-\frac{1}{5r^5}\right)\cos^2\theta + A_{31}\left(\frac{1}{6r^6}-\frac{1}{8r^8}\right)\cos\theta + A_{13}\left(\frac{1}{2r^2}-\frac{1}{4r^4}\right)\cos^3\theta \quad [14]$$

Substituting the expression for ϕ given previously in the variational integral I_2, differentiating the resulting integral with respect to the parameters, and setting the derivatives equal to zero, which is equivalent to requiring $\delta I_2 = 0$, we obtain a set of simultaneous equations

$$\left.\begin{array}{lll}\dfrac{\partial I}{\partial A_{11}} = 0 & \dfrac{\partial I}{\partial A_{21}} = 0 & \dfrac{\partial I}{\partial A_{12}} = 0 \\ \dfrac{\partial I}{\partial A_{22}} = 0 & \dfrac{\partial I}{\partial A_{31}} = 0 & \dfrac{\partial I}{\partial A_{13}} = 0\end{array}\right\} \quad [15]$$

Integrating these equations, six nonlinear algebraic equations are obtained. These equations may be solved by a method of successive approximation. Because of the limitation of space, it was not possible to include these equations here. Examples of the equa-

tions and their solution may be found in references (1) and (2), and the detailed calculation in the present case may be found in reference (18).

To compare the results with those of other investigators, the velocity distribution q/U, which on the surface of the sphere is given by the following equations, is evaluated

$$\frac{q}{U} = \left(\frac{3}{2} + \frac{1}{4M}A'_{11} + \frac{1}{15M}A'_{21} + \frac{1}{24M}A'_{31} + \frac{3}{4M}A'_{12}\cos^2\theta + \frac{2}{5M}A'_{22}\cos^2\theta + \frac{5}{4M}A'_{13}\cos^4\theta\right)\sin\theta \quad [16]$$

where $A'_{mn} = A_{mn}/a_0$.

At $\theta = \pi/2$ the equation reduces to

$$\frac{q}{U} = \frac{3}{2} + \frac{1}{4M}A'_{11} + \frac{2}{15M}A'_{21} + \frac{1}{24M}A'_{31} \ldots . \quad [17]$$

The convergence of the function assumed for the velocity potential may be tested by evaluating the velocity q/U at any point when only one term, i.e., term containing A_{11}, or two terms, i.e., A_{11}, A_{21}, and so forth until six terms are taken. In this paper the test for convergence is evaluated on the surface of the sphere and at $\theta = \pi/2$, and the results are given in Table 1. It appears that the convergence is satisfactory.

TABLE 1 VARIATION OF $(q/U)_{max}$ WITH NUMBER OF TERMS FOR VARIOUS MACH NUMBERS

M	$(q/U)_{max}$ 1 term	2 terms	3 terms	4 terms	5 terms	6 terms
0.1	1.5018	1.5018	1.5034	1.5032	1.5032	1.5032
0.2	1.5073	1.5072	1.5140	1.5131	1.5131	1.5132
0.4	1.5315	1.5312	1.5646	1.5606	1.5597	1.5628
0.5	1.5527	1.5500	1.6131	...	...	1.6156
0.5*	1.5524	1.5516	1.6126	1.5949	1.6010	1.6117

* Linearized solution.

Once the velocity distribution is obtained, the pressure distribution for adiabatic relationship may be calculated from the following equation (11)

$$C_p = \frac{p - p_0}{\frac{1}{2}\rho_0 U^2} = \frac{1}{\frac{\gamma}{2}M^2}\left\{\left[1 + \frac{\gamma-1}{2}M^2\left(1 - \frac{q^2}{U^2}\right)\right]^{\frac{\gamma}{\gamma-1}} - 1\right\} \ldots [18]$$

For $\gamma = 2$, it can be shown (2) that

$$C_p = \frac{1}{M^2}\left\{\left[1 + \frac{1}{2}M^2\left(1 - \frac{q^2}{U^2}\right)\right]^2 - 1\right\} \ldots . [19]$$

The resulting velocity and pressure distributions at different Mach numbers are tabulated in Tables 2, 3, 4, and plotted in Figs. 1 and 2. The velocity distribution computed by the linearized solution is plotted in Fig. 3. This compares very well with those computed by the nonlinear solution. This fact has already been discussed (3). The pressure distribution at $M_0 = 0.5$ is also compared with those obtained by Lamla and Kaplan in Table 2 and Fig. 4. The maximum velocities attained on the surface of the body evaluated by various methods are listed in Table 3. The agreement between the results obtained by the present method and other methods appears to be excellent.

The so-called critical Mach number, i.e., the Mach number at which the velocity of the flow equals the local velocity of sound, may be determined as follows:

TABLE 2 PRESSURE DISTRIBUTION ON SURFACE OF A SPHERE BY VARIOUS METHODS AT M = 0.5

θ deg	Incompressible	Rayleigh-Jansen* Third approx. $\gamma = 1.408$	Rayleigh-Jansen* Second approx. $\gamma = 1.408$	Variational method $\gamma = 2$	Rayleigh-Jansen 2nd approx. $\gamma = 2$
0	1.00000	1.06405	1.06405	1.06405	1.06250
5	0.98291	1.04714	1.04712	1.04520	1.04559
10	0.93215	0.99683	0.99678	0.99395	0.99530
15	0.84928	0.91437	0.91426	0.91065	0.91293
20	0.73680	0.80179	0.80157	0.79804	0.80055
30	0.43750	0.49971	0.49693	0.49815	0.49709
40	0.07035	0.11436	0.11448	0.12183	0.11309
50	—0.32034	—0.28912	—0.31597	—0.30045	—0.31366
60	—0.68752	—0.73390	—0.73599	—0.72702	—0.73420
70	—0.98679	—1.09711	—1.11067	—1.10023	—1.09127
80	—1.18216	—1.34345	—1.33088	—1.35673	—1.33083
85	—1.23289	—1.41033	—1.39371	—1.42501	—1.39380
90	—1.25000	—1.43297	—1.41497	—1.44815	—1.41509

* Rayleigh-Jansen method; third approximation as calculated by Lamla; second approximation as calculated by Kaplan.

TABLE 3 $(q/U)_{max}$ ON SURFACE OF SPHERE AT DIFFERENT MACH NUMBERS BY VARIOUS METHODS

M	q/U_{max} $\gamma = 1.408$ Rayleigh-Jansen Second approx.	$\gamma = 1.408$ Rayleigh-Jansen Third approx.	$\gamma = 2$ Rayleigh-Jansen Second approx.	$\gamma = 2$ Variational method
0	1.5000	1.5000	1.5000	1.5000
0.1	1.5032	1.5032	1.5032	1.5032
0.2	1.5131	1.5131	1.5132	1.5132
0.3	1.5311	1.5314	1.5314	1.5317
0.4	1.5592	1.5611	1.5601	1.5628
0.5	1.6005	1.6073	1.6028	1.6156

TABLE 4 $(q/U)_{max}$ ON SURFACE OF ELLIPSOID OF REVOLUTION OF THICKNESS RATIO $t = 0.8$ AT DIFFERENT MACH NUMBERS

M	Rayleigh-Jansen, first approximation	Variational method $\phi_1 = \phi_{inc}$	Variational method $\phi_1 = \phi_{inc}$
0	1.3812	1.3812	1.3812
0.1	1.3833	1.3825	...
0.2	1.3896	1.3863	...
0.3	1.4001	1.3930	1.4039
0.4	1.4147	1.4032	1.4242
0.5	1.4336	1.4177	1.4558
0.6	1.4567	1.4382	...

The maximum velocity for a sphere occurs on the surface of the sphere at $\theta = \pi/2$. Plot (q/U) for various Mach numbers, and also plot a^*/U, where a^* is the velocity of sound at a point where the velocity of the fluid is equal to the velocity of sound, the intersection of the two curves gives the critical Mach number. The relation between a^*/U and M may be shown to be given by the equation

$$\left(\frac{a^*}{U}\right)^2 = \frac{2}{\gamma+1}\frac{1}{M^2} + \frac{\gamma-1}{\gamma+1} \ldots . [20]$$

For a sphere it was found to be (Fig. 5)

$$M_{cr} = 0.57 \ldots . [21]$$

Compressible Flow Past an Ellipsoid of Revolution

In the case of an ellipsoid of revolution, the so-called ovary semielliptic co-ordinates may be used. Let ζ, μ and ω be such co-ordinates (Fig. 6). The boundary conditions are

$$\left(\frac{\partial\phi}{\partial\zeta}\right)_{\zeta=\zeta_0} = 0$$

and

$$\left[\frac{\zeta^2-1}{\zeta^2-\mu^2}\left(\frac{\partial\phi}{\partial\zeta}\right)^2 - \frac{1-\mu^2}{\zeta^2-\mu^2}\left(\frac{\partial\phi}{\partial\mu}\right)^2\right]^{1/2} = U \text{ at } \zeta = \infty$$

where ζ_0 defines the ellipsoid of revolution. The velocity potential may again be assumed to be of the form $\phi_1 + \phi_2$, where ϕ_1 and ϕ_2 are as defined before. Thus we have

$$\phi_1 = \left(\frac{1}{2}A\zeta\log\frac{\zeta+1}{\zeta-1} - A + U\zeta\right)\mu \ldots . [22]$$

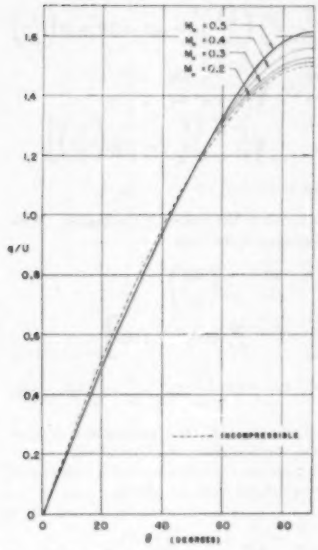

FIG. 1 VELOCITY DISTRIBUTION ON SURFACE OF SPHERE AT DIFFERENT MACH NUMBERS

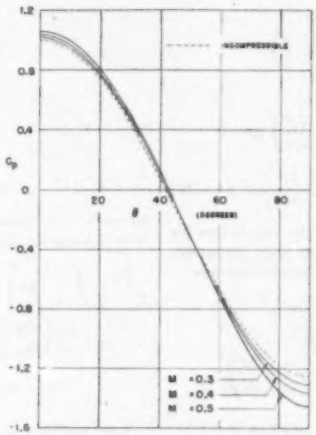

FIG. 2 PRESSURE DISTRIBUTION ON SURFACE OF SPHERE AT DIFFERENT MACH NUMBERS; $\gamma = 2$

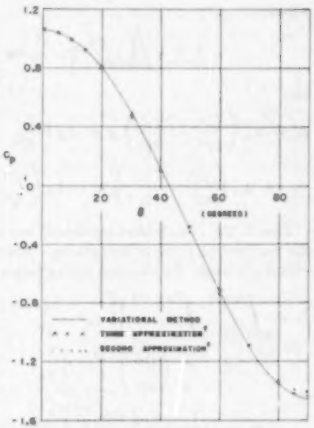

FIG. 4 PRESSURE DISTRIBUTION ON SURFACE OF SPHERE AT $M_0 = 0.5$
(Janzen-Rayleigh method.)

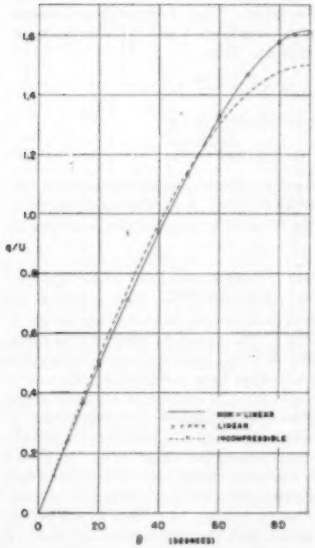

FIG. 3 VELOCITY DISTRIBUTION ON SURFACE OF SPHERE AT MACH NUMBER $M_0 = 0.5$

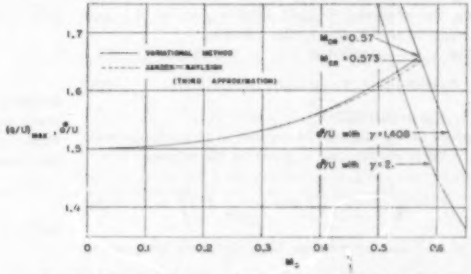

FIG. 5 CRITICAL VALUE OF MACH NUMBER FOR SPHERE

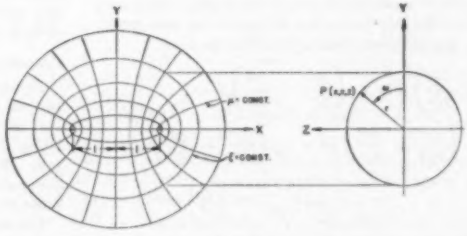

$$X = \mu\xi$$

$$Y = \sqrt{(1-\mu^2)(\xi^2-1)}\cos\omega$$

$$Z = \sqrt{(1-\mu^2)(\xi^2-1)}\sin\omega$$

FIG. 6 OVARY SEMIELLIPTIC CO-ORDINATES

where

$$A = U \Big/ \left(\frac{\zeta_0}{\zeta_0^2 - 1} - \frac{1}{2} \log \frac{\zeta_0 + 1}{\zeta_0 - 1} \right)$$

and

$$\phi_1 = A_{11} \left(\frac{\zeta_0^3}{2\zeta^2} - \frac{\zeta_0^5}{4\zeta^4} \right) \mu + A_{12} \left(\frac{\zeta_0^3}{2\zeta^2} - \frac{\zeta_0^5}{4\zeta^4} \right) \mu^3 + A_{21} \left(\frac{\zeta_0^4}{3\zeta^3} - \frac{\zeta_0^6}{5\zeta^5} \right) \mu + A_{22} \left(\frac{\zeta_0^4}{3\zeta^3} - \frac{\zeta_0^6}{5\zeta^5} \right) \mu^3 + \ldots [23]$$

Due to the complicated expression for ϕ_1, the calculations for the parameters become formidable. Therefore only one parameter A_{11} is used. In this case the variational integral becomes

$$I_1 = \int_{\zeta=\zeta_0}^{\zeta=\infty} \int_{\mu=-1}^{\mu=+1} \left\{ \left[q_\infty^2 - \frac{\zeta^2 - 1}{\zeta^2 - \mu^2} \left(\frac{\partial \phi}{\partial \zeta} \right)^2 - \frac{1 - \mu^2}{\zeta^2 - \mu^2} \left(\frac{\partial \phi}{\partial \mu} \right)^2 \right]^2 - \left[q_\infty^2 - \frac{\zeta^2 - 1}{\zeta^2 - \mu^2} \left(\frac{\partial \phi_1}{\partial \zeta} \right)^2 - \frac{1 - \mu^2}{\zeta^2 - \mu^2} \left(\frac{\partial \phi_1}{\partial \mu} \right)^2 \right]^2 \right\} 2\pi(\zeta^2 - \mu^2) d\zeta d\mu$$

$$- \frac{8}{3} \pi \zeta_0^3 (q_\infty^2 - U^2) U A_{11} \ldots . [24]$$

Substituting the expression for ϕ in the variational integral, differentiating the resulting integral with respect to A_{11}, and setting this equal to zero results in the following

$$A_{11}(0.46781436\ q_\infty^2 - 0.9999158\ U^2) - 0.08283354\ U A_{11}^2 - 0.00900455\ A_{11}^3 - 0.46677177\ U^2 = 0 \ldots\ldots [25]$$

For $M = 0.5$, $A'_{11} = 0.07297568$.

On the surface of the ellipsoid of revolution of thickness ratio $t = 0.8$, the velocity distribution is given by the relation

$$\frac{q}{U} = \sqrt{\frac{1 - \mu^2}{\zeta^2 - \mu^2}} \left(2.302 + \frac{\zeta_0}{4M} A'_{11} \right) \ldots\ldots [26]$$

The values of $(q/U)_{max}$ for various Mach numbers are given in Table 4.

The complication in the foregoing case arises because of the expression of ϕ_1. If ϕ is assumed to just satisfy the boundary conditions but not necessarily to include the incompressible velocity potential ϕ_1, the calculations can be carried out more simply. For example, ϕ may be assumed to be as follows

$$\phi = U \left(\zeta + \frac{\zeta_0^3}{2\zeta^2} \right) \mu + A_{11} \left(\frac{\zeta_0^3}{2\zeta^2} - \frac{\zeta_0^5}{4\zeta^4} \right) \mu + A_{12} \left(\frac{\zeta_0^3}{2\zeta^2} - \frac{\zeta_0^5}{4\zeta^4} \right) \mu^3 + A_{21} \left(\frac{\zeta_0^4}{3\zeta^3} - \frac{\zeta_0^6}{5\zeta^5} \right) \mu + A_{22} \left(\frac{\zeta_0^4}{3\zeta^3} - \frac{\zeta_0^6}{5\zeta^5} \right) \mu^3 \ldots\ldots [27]$$

Consider the surface integral, Equation [9a]. Since $\partial\phi/\partial\zeta = 0$ at $\zeta = \zeta_0$, the integral vanishes at the surface of the body. To compute the integral at infinity, consider first the fluid enclosed in a large ellipsoid of revolution and then let $\zeta = \infty$. There is then obtained

$$\delta\phi = \frac{\zeta_0^3}{2\zeta^2} (\mu \delta A_{11} + \mu^3 \delta A_{12}) + 0\left(\frac{1}{\zeta^2} \right)$$

$$q_\infty^2 - \frac{\partial \phi}{\partial x_i} \frac{\partial \phi}{\partial x_i} = q_\infty^2 - \frac{\zeta^2 - 1}{\zeta^2 - \mu^2} \left(\frac{\partial \phi}{\partial \zeta} \right)^2 - \frac{1 - \mu^2}{\zeta^2 - \mu^2} \left(\frac{\partial \phi}{\partial \mu} \right)^2 = q_\infty^2 - U^2 + 0\left(\frac{1}{\zeta^2} \right)$$

$$\frac{\partial \phi}{\partial n} = \sqrt{\frac{\zeta^2 - 1}{\zeta^2 - \mu^2}} \frac{\partial \phi}{\partial \zeta} = \sqrt{\frac{\zeta^2 - 1}{\zeta^2 - \mu^2}} \left[U\mu + 0\left(\frac{1}{\zeta^2} \right) \right]$$

$$dS = 2\pi \sqrt{(\zeta^2 - 1)(\zeta^2 - \mu^2)}\, d\mu$$

where $0(1/\zeta^2)$ indicates terms of the order $1/\zeta^2$ or higher. With $\gamma = 2$, Equation [9a] becomes in this case

$$\frac{2\gamma}{\gamma - 1} \int_{+1}^{-1} \delta\phi \left[q_\infty^2 - \frac{\zeta^2 - 1}{\zeta^2 - \mu^2} \left(\frac{\partial \phi}{\partial \zeta} \right)^2 - \frac{1 - \mu^2}{\zeta^2 - \mu^2} \left(\frac{\partial \phi}{\partial \mu} \right)^2 \right]^{1/(\gamma-1)} \frac{\partial \phi}{\partial \zeta} 2\pi(\zeta^2 - 1) d\mu \Big]_{\zeta=\zeta_0 \text{ and } \zeta=\infty} = -8\pi\zeta_0^2 (q_\infty^2 - U^2) U \left(\frac{1}{3} A_{11} + \frac{1}{5} A_{12} \right) \delta\phi \ldots [28]$$

Carrying out the calculation (18), the parameters A'_{mn} or A_{mn}/a_n can be determined for the given Mach numbers.

The velocity distribution on the surface of the ellipsoid of revolution may now be calculated from the relation

$$q/U = \zeta_0 \sqrt{\frac{1 - \mu^2}{\zeta_0^2 - \mu^2}} \left[\frac{3}{2} + \frac{1}{4M} A'_{11} + \frac{2}{15M} A'_{21} + \left(\frac{3}{4M} A'_{12} + \frac{2}{5M} A'_{22} \right) \mu^2 \right] \ldots\ldots [29]$$

Pressure distribution and critical Mach number follow in the same way as that of the sphere. The ratio between the semiminor axis to the semimajor axis is often referred to as the thickness ratio t, of a given ellipsoid. Thus

$$t = \sqrt{\zeta_0^2 - 1}/\zeta_0$$

and so a given t defines the ellipsoid ζ_0, i.e.

$$\zeta_0 = 1/\sqrt{1 - t^2} \ldots\ldots [30]$$

The velocity and pressure distributions on an ellipsoid of revolution with $t = 0.8$ are plotted in Figs. 7, 8, 9. The maximum velocities on the surface of the ellipsoid at various Mach numbers are given in Table 4.

Compressible Flow Past a Streamlined Body of Revolution

In the general case of compressible flow past a streamlined body of revolution, the computation can be carried out similar to that shown in reference (2). An approximate method for calculating the incompressible flow has been developed by Kaplan (16). No paper appears to have been published for the case of compressible flow past a body of revolution of arbitrary shape other than those using the Prandtl-Glauert correction factor.

Let us denote the axis of symmetry of the body by x, and the axis perpendicular to x in a meridian plane by y. It is well known that a unique conformal transformation exists which maps the region external to a given boundary of arbitrary shape in the Z-plane into the region external to a circle in the z-plane with its center at the origin, such that the regions at infinity of the two planes correspond. The function representing this conformal transformation can be developed in the region external to the circle in a convergent series of the type

$$Z = z + C_0 + \frac{C_1}{z} + \frac{C_2}{z^2} + \frac{C_3}{z^3} + \ldots\ldots\ldots [31]$$

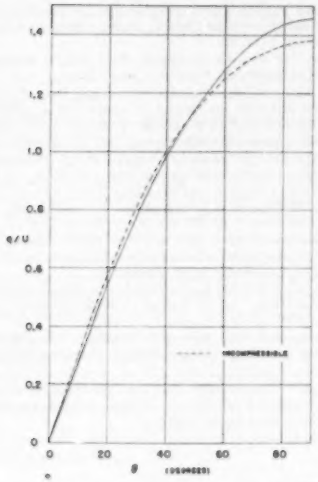

FIG. 7 VELOCITY DISTRIBUTION ON SURFACE OF ELLIPSOID OF REVOLUTION OF THICKNESS RATIO $t = 0.8$ AT $M_0 = 0.5$

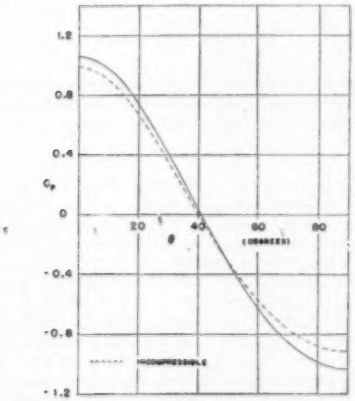

FIG. 8 PRESSURE DISTRIBUTION ON SURFACE OF ELLIPSOID OF REVOLUTION OF THICKNESS RATIO $t = 0.8$ AT $M_0 = 0.5$; $\gamma = 2$

where the coefficients C_0, C_1, C_2 are, in general, complex quantities. If, however, the meridian profile is symmetrical with respect to the axis of revolution as in our case, these coefficients are then all real. The coefficient C_n may be determined from the meridian profile in the Z-plane by such method as proposed by Theodorsen and Garrick [17].

It is shown in reference (1) that by means of a conformal mapping function, ϕ in the z-plane may be mapped into the Z-plane, while the boundary conditions are still preserved. Let $Z = X + iY$. The variational integral in the Z-plane is

$$\delta I_3 = 0 = \delta \left\{ \int_V \left[q_\infty^2 - \left(\frac{\partial \phi}{\partial X}\right)^2 - \left(\frac{\partial \phi}{\partial Y}\right)^2 \right]^{\frac{1}{\gamma}} 2\pi Y \, dX \, dY \right\}$$

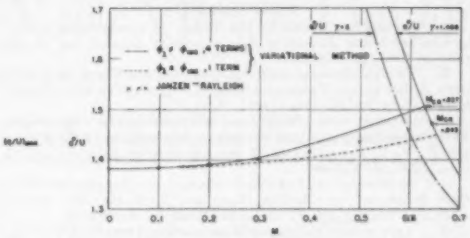

FIG. 9 CRITICAL VALUE OF MACH NUMBER FOR ELLIPSOID OF REVOLUTION OF THICKNESS RATIO $t = 0.8$

$$+ 4 \oint_S \delta\phi \left[q_\infty^2 - \left(\frac{\partial \phi}{\partial X}\right)^2 - \left(\frac{\partial \phi}{\partial Y}\right)^2 \right]^{\frac{1}{\gamma}} \frac{\partial \phi}{\partial n} \, dS$$

As is shown in reference (1), we have

$$\left(\frac{\partial \phi}{\partial X}\right)^2 + \left(\frac{\partial \phi}{\partial Y}\right)^2 = \left[\left(\frac{\partial \phi}{\partial r}\right)^2 + \left(\frac{1}{r}\frac{\partial \phi}{\partial \theta}\right)^2 \right] \Big/ \left|\frac{dZ}{dz}\right|^2$$

and

$$dX \, dY = \left|\frac{dZ}{dz}\right|^2 r \, dr \, d\theta$$

If the mapping function is in the form of Equation [31], then

$$Y = r \sin\theta + \sum_{n=1}^{N} C_n r^{-n} \sin n\theta$$

and if ϕ is in the form of Equation [10], the parameters A_{mn} may be determined from the following variational integral

$$\delta I_3 = 0 = \delta \left\{ 2\pi \int_{r=1}^{r=\infty} \int_{\theta=0}^{\theta=\pi} \left[q_\infty^2 - \frac{\left(\frac{\partial \phi}{\partial r}\right)^2 + \left(\frac{1}{r}\frac{\partial \phi}{\partial \theta}\right)^2}{\left|\frac{dZ}{dz}\right|^2} \right]^{\frac{1}{\gamma}} \left(r \sin\theta + \sum_{n=1}^{N} C_n r^{-n} \sin n\theta \right) \left|\frac{dZ}{dz}\right|^2 r \, dr \, d\theta \right.$$

$$\left. + 8\pi (q_\infty^2 - U^2) U (A_{11}/3 + A_{13}/5 + A_{15}/7 + \ldots) \right\} \quad \ldots [32]$$

The last term in Equation [32] is the same as in Equation [13] owing to the fact that the regions at infinity of the two planes correspond to each other.

If the mapping function is a complicated one, the numerical work will become formidable. In such cases, it is advisable to take more parameters and to compute only the linearized flow, i.e., neglecting the A_{mn}^2, A_{mn}^3 terms. Although ϕ_1 is no longer the incompressible velocity potential, the parameters will so adjust themselves that the discussion in reference (3) will be substantially correct.

ACKNOWLEDGMENT

The authors are indebted to Prof. F. K. Teichmann, Chairman of the Department of Aeronautical Engineering, for his kind interest and encouragement.

BIBLIOGRAPHY

1 "Variational Method in the Theory of Compressible Fluid," by Chi-Teh Wang, *Journal of the Aeronautical Sciences*, vol. 15, November, 1948, pp. 675–685.

2 "Two-Dimensional Subsonic Compressible Flows Past Arbitrary Bodies by the Variational Method," by Chi-Teh Wang, Report submitted to NACA, June, 1949.

3 "A Study of the Non-Linear Characteristic of Compressible Flow Equations by Means of Variational Method," by Chi-Teh Wang and G. V. R. Rao, *Journal of the Aeronautical Sciences*, vol. 17, June, 1950, pp. 343–348.

4 "Application of Galerkin's Method to Compressible Fluid Flow Problems," by Chi-Teh Wang and R. F. Brodsky, *Journal of Applied Physics*, vol. 20, December, 1949, pp. 1255–1256.

5 "Approximate Solution of Compressible Fluid Flow Problems by Galerkin's Method," by Chi-Teh Wang and R. F. Brodsky, to appear in the *Journal of the Aeronautical Sciences*.

6 "Application of Biezieno-Koch Method to Compressible Fluid Flow Problems," by Chi-Teh Wang and Pei-Chi Chou, *Journal of the Aeronautical Sciences*, vol. 17, no. 9, September, 1950, pp. 599–600.

7 "A Variational Method for Transonic Flows with Shock Waves," by Chi-Teh Wang, report submitted to NACA, June, 1949.

8 "Beitrag zu einer Theorie der Stationaeren Storemung Krompressibler Fluessigkeiten," by O. Janzen, *Physikalische Zeitschrift*, vol. 14, 1913, pp. 639–643.

9 "On the Flow of Compressible Fluid Past an Obstacle," by Lord Rayleigh, *Philosophical Magazine*, vol. 32, July, 1916, pp. 1–6.

10 "On the Flow of a Compressible Fluid Past a Sphere," by K. Tamada, Proceedings of the Physico Mathematical Society of Japan, vol. 21, 1939, pp. 743–752.

11 "The Flow of a Compressible Fluid Past a Sphere," by C. Kaplan, NACA Technical Note 762, May, 1940.

12 "Die Symmetrische Potentialstroemung eines Kompressiblen Gases um Kreiszylinder und Kugel im unter-Kritischen Gebiet," by E. Lamla, *Deutsche Luftfahrtforschung*, F. B. no. 1014, 1939.

13 "Die Kompressibler Stroemung um ein Rotations-Ellipsoid mach der methode von Janzen-Rayleigh," by C. Schmieden, *Jahrbuch der deutschen Luftfahrtforschung*, 1942, I 72–I 79.

14 "Notes on a Differential Equation Which Occurs in the Two-Dimensional Motion of a Compressible Fluid and the Associated Variational Problems," by H. Bateman, Proceedings of the Royal Society of London, series A, vol. 125, November, 1929, pp. 598–618.

15 "A Note on Bateman's Variational Principle for Compressible Flows," by Chi-Teh Wang, to be published.

16 "On a New Method for Calculating the Potential Flow Past a Body of Revolution," by C. Kaplan, NACA Technical Report no. 752, 1943.

17 "General Potential Theory of Arbitrary Wing Sections," by T. Theodorsen and I. E. Garrick, NACA Technical Report no. 452, 1933.

18 "Subsonic Compressible Flow Past Bodies of Revolution by the Variational Method," by S. de los Santos, Engineering ScD. thesis, New York University, April, 1949.

On the Extrusion of a Very Viscous Liquid[1]

By HERSCHEL WEIL,[2] SCHENECTADY, N. Y.

An approximation to a state of affairs occurring in the extrusion of rubber is the two-dimensional slow flow of a very viscous liquid from a half plane into a semi-infinite strip. The region surrounding the orifice or juncture of the strip and plane corresponds to the region where the extruded rubber is forced from a die box into a die. Methods are developed and carried out for numerically obtaining the stream function, the velocity components, and the pressure in this region. The general pattern of the streamlines is determined, and it is found in what way and to what extent the flow pattern in the strip near the orifice differs from plane Poiseuille flow and how far into the strip this difference is significant.

Incidental to this work, it was necessary to determine the first several complex roots of $\sin A = \pm \frac{2}{3\pi} A$. This information is useful apart from the flow problem, and the results are tabulated.

Introduction

FOR the low-Reynolds-number flows considered here it is well known that a stream function $\psi(x, y)$, defined by

$$u = \frac{\partial \psi}{\partial y} \qquad v = -\frac{\partial \psi}{\partial x} \ldots\ldots\ldots\ldots\ldots\ldots [1]$$

where u and v are, respectively, the x and y-components of velocity in a rectangular co-ordinate system (x, y), exists and, to a first-order approximation, satisfies the biharmonic equation

$$\Delta \Delta \psi = 0 \ldots\ldots\ldots\ldots\ldots\ldots [2]$$

where Δ is the Laplace operator.[3] The boundary conditions to be satisfied are that ψ be given on the boundary and that its normal derivative vanish on the boundary. In addition, ψ and all its derivatives must be finite everywhere in the region considered.

In the work which follows different representations for the solution to this problem are found for each of the three overlapping regions I, II, III, in Fig. 1. In the (x, y) co-ordinate system in Fig. 2, these regions are, respectively, the half plane $y > 0$, a narrow region enclosing the line $|x| < 1$, $y = 0$, and the semi-infinite strip $|x| < 1$, $y < 0$. In each case a method is developed for obtaining numerically approximations to these representations of the solution, and the numerical work is carried out.

The procedure is first to determine the solution ψ_{II} in region II, and in particular to determine ψ_{II} and $\partial\psi_{II}/\partial y$ along the line $\overline{RL}$. To obtain the solution ψ_I in region I, a known solution for the biharmonic equation in the half-plane $y > 0$ when $\partial\psi/\partial x$ and

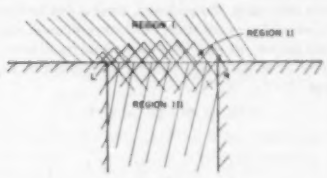

FIG. 1

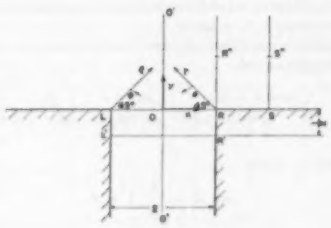

FIG. 2

$\partial\psi/\partial y$ are given on $y = 0$ may then be evaluated numerically wherever desired in $y > 0$, by using $\partial\psi_{II}/\partial x$ and $\partial\psi_{II}/\partial y$ as computed on $\overline{RL}$.

The solution ψ_{III} in region III is found by realizing that at a sufficiently large distance from the orifice, $\overline{RL}$, the flow must be a plane Poiseuille flow, that is, have a parabolic v-distribution and no u-velocity component. Accordingly, in region III near $\overline{RL}$, the flow is considered to be the Poiseuille flow plus a "correction flow" which does not alter the total flux passing through any cross section of the strip. Here ψ_{II} and $\partial\psi_{II}/\partial y$, evaluated on $\overline{RL}$, are used in the boundary conditions to determine this correction flow. Once ψ is known, the velocities may be obtained from Equation [1], and the pressures from the fact that

$$\frac{p}{\mu} + i\Delta\psi = f(z) \ldots\ldots\ldots\ldots\ldots\ldots [3]$$

is an analytic function in $z = x + iy$.

Determination of Flow in Region II

Throughout this work we shall use the polar-co-ordinate systems (r, θ), (ρ, φ), and the rectangular system (x, y) as shown in Fig. 2. The scheme in region II will be first to consider flow about the right-hand corner and to neglect the left-hand corner. When the boundary conditions along this corner only are applied, the solution will be in the form of an expansion in eigen functions in which the coefficients are undetermined. These coefficients will then be determined by bringing into account the presence of the left-hand corner.

It is known that the solution ψ in the neighborhood of R must

---

[1] This paper is based on a thesis submitted in partial fulfillment of the requirements for the degree of Doctor of Philosophy in the Graduate Division of Applied Mathematics at Brown University.

[2] General Engineering and Consulting Laboratory, General Electric Company.

[3] See for instance, "Fluid Dynamics," by von Mises and Friedrichs, Brown University, Providence, R. I., 1942, pp. 150, 151.

Contributed by the Applied Mechanics Division and presented at the Annual Meeting, New York, N. Y., November 26–December 1, 1950, of The American Society of Mechanical Engineers.

Discussion of this paper should be addressed to the Secretary, ASME, 29 West 39th Street, New York, N. Y., and will be accepted until October 10, 1951, for publication at a later date. Discussion received after the closing date will be returned.

Note: Statements and opinions advanced in papers are to be understood as individual expressions of their authors and not those of the Society. Manuscript received at ASME Headquarters, May 11, 1950. Paper No. 50—A-8.

have a branch point at R.[4] Such solutions, which at the same time do not become infinite at R, are

$$\psi = r^n [a \cos n(\theta + 2k\pi) + b \cos(n-2)(\theta + 2k\pi) + c \sin n(\theta + 2k\pi) + d \sin (n-2)(\theta + 2k\pi)] = r^n f(\theta, n) \ldots [4]$$

where k is an integer, a, b, c, d real constants, and suitable numbers n are to be determined by the boundary conditions.

When the boundary conditions are applied, all the possible eigen functions will be found by considering only the principal branch of the solution, that is, $k = 0$, so that it is sufficient to consider this case only. In addition, since ψ can be determined at most up to an additive constant, and since it must also be a constant on the corner, we can let ψ as well as its normal derivative vanish there. The boundary conditions applied to Equation [4] require that

$$\left.\begin{aligned} f(\alpha, n) = f(-\alpha, n) &= 0 \\ \text{and} \\ \left.\frac{\partial f}{\partial \theta}\right|_{\theta = \alpha} = \left.\frac{\partial f}{\partial \theta}\right|_{\theta = -\alpha} &= 0 \end{aligned}\right\} \ldots\ldots [5]$$

where $\alpha = 3\pi/4$.

Equations [5] are a set of linear homogeneous algebraic equations for the constants a, b, c, and d.

For a solution not identically zero the determinant of this set of equations must vanish

$$\begin{vmatrix} \cos n\alpha & \cos(n-2)\alpha \\ n \sin n\alpha & (n-2)\sin(n-2)\alpha \end{vmatrix} \begin{vmatrix} \sin n\alpha & \sin(n-2)\alpha \\ n \cos n\alpha & (n-2)\cos(n-2)\alpha \end{vmatrix} = 0 \ldots [6]$$

Consequently, either

$$\text{(Case I)} \qquad \sin A - \frac{2}{3\pi} A = 0 \ldots\ldots [7]$$

where

$$A = \frac{3\pi}{2}(n-1)$$

or

$$\text{(Case II)} \qquad \sin A + \frac{2}{3\pi} A = 0 \ldots\ldots [8]$$

Equations [7] and [8] are not satisfied by the same values of n, but in each case an infinite set of complex numbers n_i and their complex conjugates $\bar{n}_i$ are found to be roots of these equations. These are the eigen numbers of the problem to each of which corresponds an eigen function. For clarity we call the roots of Equation [7] α_i, and $\bar{\alpha}_i$, while we call the roots of Equation [8] β_i and $\bar{\beta}_i$.

If one solves Equation [6] for the constants, it is found that in Case I, $c = d = 0$ necessarily (even solutions), while

$$\frac{b}{a} = -\frac{\cos n\alpha}{\cos(n-2)\alpha}$$

On the other hand, in Case II, $a = b = 0$ (odd solutions), while

$$\frac{d}{c} = -\frac{\sin n\alpha}{\sin(n-2)\alpha}$$

A real solution of Equation [2] may now be written as

$$\psi_R = \sum_{i=1}^{N} [a_i Re[r^{\alpha_i} f(\theta, \alpha_i)] + a_i' Im[r^{\alpha_i} f(\theta, \alpha_i)] + b_i Re[r^{\beta_i} f(\theta, \beta_i)] + b_i' Im[r^{\beta_i} f(\theta, \beta_i)]] \ldots\ldots [9]$$

[4] For instance, see "Applications of Analytic Functions to Two-Dimensional Biharmonic Analysis," H. Poritsky, Trans. American Mathematical Society, vol. 59, 1946, pp. 248–279.

where N is any integer, Re means "real part," and Im means "imaginary part." The real constants, a_i, a_i', b_i, and b_i', which are as yet undetermined, will be used to bring into account the presence of the corner at L, Fig. 1.

To aid in determining the constants $a_i - b_i'$ of Equation [9], consider a solution ψ_L of the biharmonic equation which has a branch point at L and is expressed in terms of the left-handed co-ordinate system (ρ, φ) of Fig. 2. For the boundary conditions $\psi = -Q$, $\partial\psi/\partial\varphi = 0$ on $\varphi = \pm 3\pi/4$ the solution must, because of symmetry, be of the same form as Equation [9], except for the addition of the constant $-Q$

$$\psi_L = -\sum_{i=1}^{N} [a_i Re[\rho^{\alpha_i} f(\varphi, \alpha_i)] + a_i' Im[\rho^{\alpha_i} f(\varphi, \alpha_i)] + b_i Re[\rho^{\beta_i} f(\varphi, \beta_i)] + b_i' Im[\rho^{\beta_i} f(\varphi, \beta_i)]] - Q \ldots [10]$$

The negative sign on the sum is necessary so that $\psi_{\text{II}L}$ will be an increasing function of ρ on $\overline{RL}$ ranging from $-Q$ to zero.

By choosing the coefficients suitably, both ψ_R and ψ_L can be made to represent approximately the solution ψ_{II} of the two-corner problem in the region around 0. Note, however, that ψ_R would certainly not be a suitable solution in a region covering L, because it is necessary for a solution around L to have a branch point at L.

In a region about 0, we now assume that both solutions ψ_L and ψ_R may be expressed in a Maclaurin series in the co-ordinate system (x, y) in Fig. 2. In either case the series so obtained will be considered to represent the ψ_{II} function in the region of convergence of the Maclaurin series, and, consequently, the two series may be equated there. By comparing coefficients of like powers $x^i y^k$, one obtains a set of equations to determine the $4N$ unknown constants. By increasing N in the procedure, one would expect to obtain a more accurate solution, assuming suitable convergence properties for the infinite series which result in the limit as N becomes infinite.

To carry out the foregoing plan for obtaining the constants, note that, with the co-ordinate systems used, the following relations hold at 0

$$\left.\frac{\partial^{2k+n}\psi_L}{\partial x^{2k}\partial y^n}\right|_0 = -\left.\frac{\partial^{2k+n}\psi_R}{\partial x^{2k}\partial y^n}\right|_0 \ldots\ldots [11]$$

$$\left.\frac{\partial^{2k+n+1}\psi_L}{\partial x^{2k+1}\partial y^n}\right|_0 = \left.\frac{\partial^{2k+n+1}\psi_R}{\partial x^{2k+1}\partial y^n}\right|_0, \quad k, n \text{ integers} \ldots [12]$$

regardless of the values of the $a_i - b_i'$. Accordingly, the Relations [12] give no information about these constants, while Relations [11] furnish the desired set of algebraic equations.

The conditions, Equations [11] may all be given physical interpretations in terms of flow velocities. For instance, when $n = 0$, $k \geq 1$ they express the fact that the vertical velocity v along $\overline{RL}$ is an even function about 0.

The foregoing procedure was carried out for $N = 4$. The roots of Equations [7] and [8] were determined graphically and then improved by Newton's iteration method until values were found which made both the real and imaginary parts of these equations less in magnitude than 0.00004. The roots are given in Table 1.

TABLE 1

	Roots of $\sin A = \frac{2}{3\pi} A$		Roots of $\sin A = -\frac{2}{3\pi} A$	
i	$Re\ A_i$	$Im\ A_i$	$Re\ A_i$	$Im\ A_i$
1	2.5658	0	4.2814	0
2	7.6777	±1.0898	4.7124[a]	0
3	14.0045	±1.7622	10.84475	±1.48839
4	20.31213	±2.14648	17.15979	±1.97349
5	20.61136	±2.420770	23.46252	±2.29317
6	32.90601	±2.63473		

[a] Yields only the trivial solution, $\psi \equiv 0$.

For $N = 4$, there are 14 constants to determine after one considers that a_i' and b_i' are arbitrary and may be set equal to zero since they themselves have zero coefficients. From the physical point of view the oddness of u and the evenness of v across $\overline{RL}$ and the condition of no flow across the center line $\overline{O'O'}$ seemed the most important, so the following conditions were satisfied at 0

$$\left.\begin{aligned} &\frac{\partial^{2n} u}{\partial x^{2n}} = 0, \quad \frac{\partial^{2n+1} v}{\partial x^{2n+1}} = 0, \quad n = 0,1,2,3,4 \\ &\frac{\partial^n u}{\partial y^n} = 0, \quad n = 1,2,3; \quad \frac{\partial^2 u}{\partial y \partial x^2} = 0 \end{aligned}\right\} \quad \ldots [13]$$

and $Q = 1$ for $\overline{RL} = 2$.

The constants $a_i - b_i'$ were computed from Equations [13] by means of Crout's method.[6] The results of these computations are given in Table 2. Using these $a_i - b_i'$ the approximate u and v velocity components were computed along the three lines $\overline{RL}$, $\overline{RR''}$, and $\overline{R'L'}$. The velocities along $\overline{RR''}$ are obtainable with very little work from the computations for velocities along $\overline{RL}$, since each term in ψ_{NR} is either even or odd in θ. The resulting curves will be discussed under Numerical Results and Checks.

We should point out that with ψ_{II} given in terms of the polar co-ordinates (r, θ), as in Equation [9], the most convenient velocity components to compute are

$$q_r = \frac{1}{r}\frac{\partial \psi_{II}}{\partial \theta}, \quad q_\theta = -\frac{\partial \psi_{II}}{\partial r} \quad \ldots [14]$$

the radial and tangential components, respectively, which are linearly related to the rectangular components u_{II} and v_{II}.

Determination of Flow in Region I

The solution of the biharmonic equation for the half-plane $y > 0$, when ψ and $\partial \psi/\partial y$ are given on $y = 0$, may be arrived at by constructing the Green's function for this problem and placing this in the known integral expression for the solution of the biharmonic equation in terms of the Green's function,[6] or, alternatively, by considering the Fourier transform of the biharmonic equation. The solution is then in the form of integrals extending over $(-\infty, \infty)$ and involving as factors in the integrands ψ and $\partial\psi/\partial y$ evaluated on $y = 0$. By writing the integrands in terms of z and $\bar{z}$ and integrating once by parts, these may be reduced to integrals involving as factors the first derivatives of ψ but not ψ itself on $y = 0$. Since these derivatives vanish on $|x| > 1$, the integrals are reduced to integrals over the finite interval $(-1, 1)$. The velocities $u - iv = 2i(\partial\psi/\partial z)$ then take the form for $y > 0$.

$$u(x,y) - iv(x,y) = \frac{1}{\pi}\left[Im \int_{-1}^{1} \frac{u(s,0)}{z-s}\,ds \right.$$
$$\left. - i\, Im \int_{-1}^{1} \frac{v(s,0)}{z-s}\,ds + y\frac{\partial}{\partial x}\int_{-1}^{1} \frac{u(s,0) + iv(s,0)}{z-s}\,ds \right] \quad \ldots [15]$$

By substituting $u_{II}(s,0)$ and $v_{II}(s,0)$ for $u(s,0)$, $v(s,0)$, this problem may be reduced to evaluating integrals of the type

TABLE 2

i	a_i	a_i'	b_i	b_i'
1	−0.44578	0	0.23740	0
2	−0.69081	0.57982	1.6504	−0.68383
3	1.4880	−0.33280	−0.75054	0.064863
4	−0.24775	0.0208670	0.046362	0.011619

Note: These constants are normalised to yield a $Q = 1$. To obtain other values of Q, they must all be multiplied by Q.

$$I = \int_0^2 \frac{u^\alpha}{t+u}\,du \quad \ldots [16]$$

where α and t are complex, $I_m t > 0$ and $|t| < 2$. Although one can show

$$I = \sum_{n=0}^{\infty} \frac{(-1)^n 2^{\alpha-n}}{\alpha - n} t^n - \pi t^\alpha \csc \pi\alpha \quad \ldots [17]$$

it appeared easier in the numerical work to express the integrals in terms of $t_1 = x - 1$ and $t_2 = y$ and to evaluate them numerically by Simpson's rule.

Determination of Flow in Region III

The general idea of this section is that the flow in the strip $|x| < 1$, $y < 0$ consists of a flow possessing a parabolic v distribution $v_p = -\partial\psi_p/\partial x$ and no u velocity component, plus a correction flow which has zero net flux through any cross section of the strip, and whose effect dies out as $-y$ increases. It is assumed that the correction flow is given by a stream function ψ_c of the form $X(x)Y(y)$. Then the problem is to find the solution

$$\psi_{III} = X(x)Y(y) - \frac{3}{4}Q\left(\frac{x^3}{3} - x + \frac{2}{3}\right) = \psi_c + \psi_p \quad \ldots [18]$$

of the biharmonic equation under the conditions

$$\left.\begin{aligned} &(a)\ X(\pm 1) = X'(\pm 1) = 0 \\ &(b)\ Y(0)X(x) - \frac{3}{4}Q\left(\frac{x^3}{3} - x + \frac{2}{3}\right) \equiv f(x) \\ &(c)\ Y'(0)X(x) \equiv g(x) \\ &(d)\ \lim_{y \to -\infty} Y(y) = \lim_{y \to -\infty} Y'(y) = 0 \\ &(e)\ -X(x) = X(-x) \end{aligned}\right\} \quad \ldots [19]$$

Here $f(x)$ and $g(x)$ represent, respectively, ψ_{II} and $\partial\psi_{II}/\partial y$ expressed in terms of the (x, y) co-ordinate system. Conditions (b) and (c) express the fact that ψ_{III} and $\partial\psi_{III}/\partial y$ must be identical with ψ_{II} and $\partial\psi_{II}/\partial y$ on $\overline{RL}$.

On applying conditions (a), (d), and (e), one is led to the fact that ψ_C may be expressed as a linear combination of eigen functions similar to the solution ψ_{II}, namely

$$\psi_C = \sum_{i=1}^{M} \left[A_i\, Re\left[e^{\Lambda_i y} X(x, \Lambda_i)\right] + A_i'\, Im\left[e^{\Lambda_i y} X(x, \Lambda_i)\right]\right] \quad \ldots [20]$$

where

$$X(x, \Lambda_i) \equiv X_i = \sin \Lambda_i x - (x \cos \Lambda_i x)\tan\Lambda_i \quad \ldots [21]$$

The eigen numbers Λ_i are the roots of

$$\sin 2\Lambda = 2\Lambda \quad \ldots [22]$$

which have been computed and published.[8] The conditions (b) and (c), then yield the following identities

[6] "A Short Method for Evaluating Determinants and Solving Systems of Linear Equations With Real or Complex Coefficients," by P. D. Crout, Trans. AIEE, vol. 60, 1941, pp. 1235–1241.

[6] "Die Differential und Integralgleichungen der Mechanik und Physik," by Ph. Frank and R. von Mises, Mary Rosenberg, New York, N. Y., vol. 1, 1943, pp. 856–862.

[7] "Preliminary Conclusions Regarding the Extrusion of Viscous Liquids" by G. F. Carrier, Memo No. 3 to U. S. Rubber Company, Brown University, Providence, R. I., 1948.

[8] "Roots of Sin $z = z$," by A. P. Hillman and H. E. Salzer, *Philosophical Magazine*, seventh series, vol. 34, 1943, p. 575.

$$\sum_{i=1}^{M} (A_i \, Re \, X_i + A_i' \, Im \, X_i) \equiv f(x) + \frac{3}{4} Q \left(\frac{x^2}{3} - x + \frac{2}{3} \right) \quad \ldots\ldots [23]$$

$$\sum_{i=1}^{M} [A_i \, Re \, (\Lambda_i X_i) + A_i' \, Im \, (\Lambda_i X_i)] \equiv g(x) \ldots [24]$$

To determine the A_i and A_i' so that Equations [23] and [24] are satisfied, it is assumed that the functions involved may be expanded in MacLaurin's series which converge for $|x| < 1$. Then, differentiating each of these identities M times with respect to x and evaluating the resulting identities at 0 yields two sets of M-conditions, to be satisfied by the two sets of constants $\{A_i\}$ and $\{A_i'\}$. This procedure was carried out for $M = 3$ using Crout's method[8] to determine the constants A_i and A_i', which are tabulated in Table 3. As in Region II, one would expect the approximation to improve as the number of terms is increased.

TABLE 3

i	A_i	A_i'
1	−0.052794	−0.25748
2	0.025339	0.0061925
3	−0.0033987	0.0018875

NOTE: These constants are normalized to yield a $Q = 1$.

Numerical Results and Checks

The graphs of u_{II} and v_{II} along $\overline{RL}$ are shown in Fig. 3. It is seen that along $\overline{RL}$, at least for $|x| < 0.5$ the conditions that u be odd about 0 and that v be even are well satisfied. Beyond $r = 1.5$ the convergence is apparently slower, as would be expected, so that these conditions are not so well satisfied for $|x| > 0.5$. The solution for $r < 1.5$ is probably a good approximation to the true one.[9] The velocity curves which one would take on $\overline{RL}$ are naturally the computed ones for $r < 1$ and the curves obtained from these by symmetry for $1 < r < 2$.

For comparison purposes, in Fig. 3 the parabolic velocity distribution v_p was plotted which would give the same (unit) total flow per second through $\overline{RL}$ as would the computed v-distribution. As previously pointed out, this parabolic distribution would be expected in the strip far enough away from the orifice. It is evident that the velocity distribution across $\overline{RL}$ has a greater magnitude near the edges than the parabolic flow and correspondingly smaller magnitude at the center. In fact the "correction velocity" $v_{cII}(x, 0) = v_{II}(x, 0) - v_p(x)$ is observed to reach a maximum equal to 27 per cent of $v_{II}\,|(0, 0)|$ at $x = 0$. The horizontal velocity u_{II} may also be considered as a correction to the zero horizontal velocity to be found far down the strip.

In Figs. 4, 5, 6, and 7, v_c, u, ψ_{yy}, and ψ_{yyy} at $y = 0$ computed by the Region II (corner) method are shown. These give further information on the behavior of the solution at the orifice, but

[9] Since there is no exact solution worked out for this problem, the only criterion for judging the approximate solutions is their apparent physical reasonableness or lack of it.

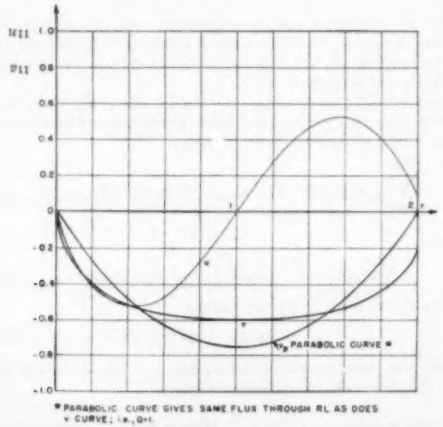

FIG. 3 VELOCITIES AT THE ORIFICE

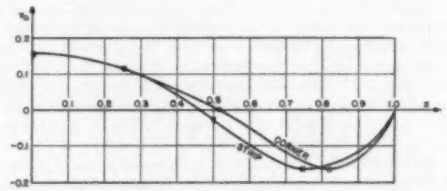

FIG. 4 CORRECTION VELOCITIES AT ORIFICE $y = 0$ COMPUTED BY CORNER EXPANSION AND STRIP EXPANSION

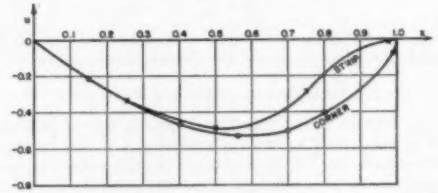

FIG. 5 CORRECTION VELOCITIES AT ORIFICE $y = 0$ COMPUTED BY CORNER EXPANSION AND STRIP EXPANSION

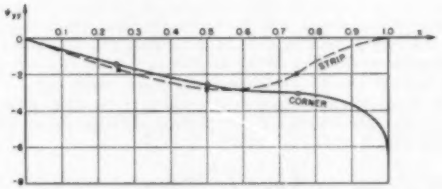

FIG. 6 ψ_{yy} COMPUTED BY CORNER EXPANSION AND BY STRIP EXPANSION

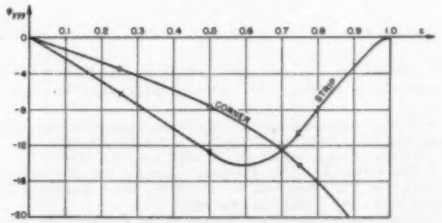

FIG. 7 ψ_{yyy} COMPUTED BY CORNER EXPANSION AND BY STRIP EXPANSION

primarily they are plotted to compare with the corresponding functions computed by the Region III (strip) method which are also plotted in these figures. They show just how smoothly the two representations of the solution join each other at $y = 0$. Toward the central part of the orifice the curves agree quite closely, although beyond $x = 0.6$ the similarity lessens considerably. This ties in with the fact that near the corner the Region III solution cannot be expected to converge to the correct solution due to its lack of a branch point. In fact, the curves computed by the partial sums of the Region II and Region III expansions can never be too similar near the corner since ψ_{yx}, ψ_{yy}, and the higher derivatives of ψ are all infinite at the corner in the Region II expansion as a result of the inequality $\alpha_1 < 2$, while each term of the Region III expansion vanishes there.

The next thing to investigate is the dependence of the correction velocities on y for $y < 0$. This is best achieved by using the solutions appropriate to Region III, the strip. Accordingly, $v_{cIII} = v_{III} - v_p$ was obtained along the y-axis as a function of y, $y < 0$. The behavior of v_{cIII} was followed on the y-axis because at the orifice $y = 0$ almost the largest correction was at $x = 0$, while at the same time the Region III solution joins the Region II solution best at $x = 0$. The results, as graphed in Fig. 8, show that $v_{cIII}(0, y)$ goes from a positive maximum at $y = 0$ to a negative minimum at $y = -1/2$ and then appears to approach zero asymptotically. This indicates that one should not consider the flow in the strip as a Poiseuille flow for, say, $-y < 1$, that is, for a distance from the orifice equal to half the width of the strip.

For the abscissa $y = -1/2$ of the minimum value of $v_{cIII}(0, y)$, it was decided to investigate the form of the correction curves $v_{cIII}(x, -1/2)$ and $u_{III}(x, -1/2)$. These curves are presented in Fig. 9. It is seen, as would be expected, that there is no flow across the center line $\overline{O'D'}$ and that, at each value of x, the magnitudes of the correction terms have decreased compared to the values at the orifice. However, the flow now had the reverse of the behavior exhibited on $\overline{RL}$. Across $\overline{R'L'}$ ($y = -1/2$) the flow is faster than the parabolic flow toward the center and slower at the edges. The streamlines must bunch toward the center line $\overline{O'O'}$ and then spread out gradually to their final configuration given by $\psi_p = \text{const.}$

From the standpoint of checking how good the Region II solution is, it is interesting to compute $v_{cII}(x, -1/2)$ and $u_{II}(x, -1/2)$. When this was done it was found that the v_{cII} curve has the same general form on $\overline{R'L'}$ as the v_{cIII} curve, although the extrema are somewhat larger in magnitude. The u_{II} velocity component on $\overline{R'L'}$, although everywhere small, indicates the existence of a slight flow across the center line which would not be the case physically. Accordingly, the Region III solutions are certainly preferable.

The velocities along $\overline{RR''}$ and $\overline{SS''}$, computed by the method outlined for Region I, are shown in Fig. 10. The results appear quite reasonable physically. For instance, on $\overline{RR''}$, $-u$, the horizontal velocity component directed toward the center line $\overline{O'O'}$ rises very quickly to a maximum near the wall, and then decreases rapidly as y increases, while the downward velocity component $-v$ continues to increase well away from the wall.

Finally, the pressure distribution on $\overline{RL}$ obtained from Equation [3] by using $\psi = \psi_{II}$ is shown in Fig. 11. This indicates the

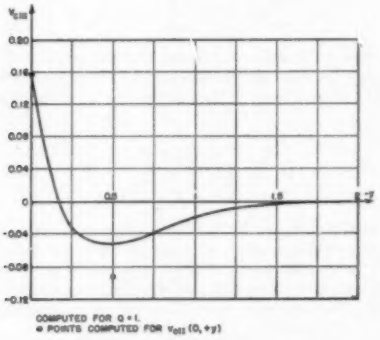

FIG. 8 CORRECTION VELOCITY, v_{cIII} (0, y)

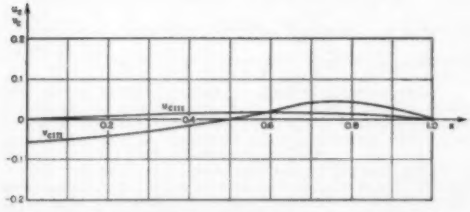

FIG. 9 CORRECTION VELOCITIES v_{cIII} AND v_{cIII} ON $R'L'$

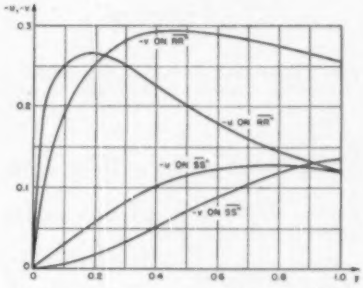

FIG. 10 $-u$ AND $-v$ ON $\overline{RR''}$ AND ON $\overline{SS''}$

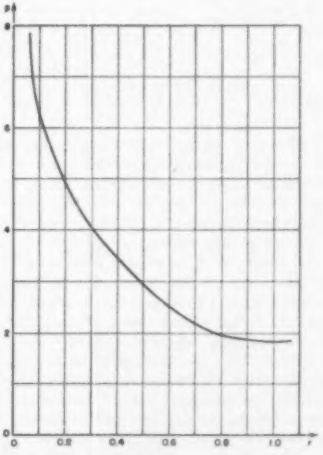

FIG. 11 PRESSURE DISTRIBUTION ON $\overline{RL}$

infinitely large pressure needed to bend the flow around the sharp corner at R.

ACKNOWLEDGMENTS

This investigation was carried out as part of a research program being conducted at Brown University for the U. S. Rubber Company. The author wishes to thank the U. S. Rubber Company for permission to publish this material and Prof. G. F. Carrier of Brown University who proposed the problem to him and whose discussions were very helpful.

On Elastic Continua With Hereditary Characteristics

By ENRICO VOLTERRA,[1] CHICAGO, ILL.

In a previous paper (1)[2] the free and forced vibrations of systems of one degree of freedom with hereditary damping characteristics were discussed. In the present paper the classical equations of motion for elastic media are extended on the basis of the general linear stress-strain law involving hereditary damping. These equations are applied to the case of free radial vibrations of a sphere. Furthermore, the free vibrations of strings, the free transverse vibrations of beams, and the free vibrations of rectangular and circular membranes are studied under the assumption of hereditary damping.

Introduction

THE equation of motion for a system of one degree of freedom with hereditary damping is given by (1)

$$M\frac{d^2q(t)}{dt^2} + a^2q(t) + \int_0^t \phi(t-\tau)\frac{dq(\tau)}{d\tau}\,d\tau = Q(t) \ldots [1]$$

when $q(t)$ is the generalized co-ordinate, M an inertia coefficient, a^2 an elastic constant, $\phi(t)$ the heredity function, and $Q(t)$ the generalized external force.

The stress-strain relationship underlying Equation [1] is of the form

$$\sigma = E\epsilon(t) + \int_0^t \phi(t-\tau)\frac{d\epsilon(\tau)}{d\tau}\,d\tau$$

In many practical cases the heredity function $\phi(t)$ is determined by experiments and is a steadily decreasing function of the time. In this instance it can be represented by a sum of exponentials

$$\phi(t) = \sum_1^n A_i e^{-\alpha_i t} \ldots\ldots\ldots\ldots [2]$$

A system whose heredity function is of this form will be said to possess heredity of degree n. The parameters A_i and α_i will be referred to as the heredity constants.

A mechanical model representing a system of one degree of freedom with heredity of the first degree is illustrated in Fig. 1(*a*).

In fact, the following relationships are verified

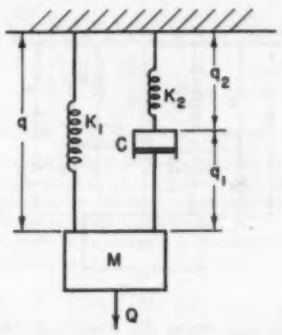

Fig. 1(*a*) Mechanical Model for Hereditary System of One Degree of Freedom With Heredity of First Degree

$$\left.\begin{aligned} Q(t) - M\frac{d^2q(t)}{dt^2} &= K_1q(t) + K_2[q(t) - q_1(t)] \\ K_2q_1(t) &= K_2[q(t) - q_1(t)] = C\frac{dq_1(t)}{dt} \end{aligned}\right\} \ldots . [3]$$

From Equation [3] we have

$$\frac{d}{dt}\left[e^{\frac{K_2}{c}t}q_1(t)\right] = e^{\frac{K_2}{c}t}\frac{K_2}{c}q(t)$$

$$q_1(t) = e^{-\frac{K_2}{c}t}\frac{K_2}{c}\int_0^t e^{\frac{K_2}{c}\tau}q(\tau)d\tau = q(t) - e^{-\frac{K_2}{c}t}\int_0^t e^{\frac{K_2}{c}\tau}\frac{dq(\tau)}{d\tau}\,d\tau$$

so that

$$M\frac{d^2q(t)}{dt^2} + K_1q(t) + K_2e^{-\frac{K_2}{c}t}\int_0^t e^{\frac{K_2}{c}\tau}\frac{dq(\tau)}{d\tau}\,d\tau = Q(t) \ldots . [4]$$

Equation [4] is identical with Equation [1] provided $K_1 = a^2$, $K_2 = A$, $K_2/c = \alpha$. Following the analogy between mechanical and electrical oscillations (2), the corresponding electrical model is shown in Fig. 1(*b*). Fig. 2 shows a mechanical model corresponding to the case of heredity of the second degree. It is readily verified that the equation of motion here again coincides with Equation [1], provided that $K_1 = a^2$, $K_2 = A_1$, $K_3 = A_2$, $K_2/c_1 = \alpha_1$, $K_3/c_2 = \alpha_2$. In the general case, corresponding to heredity of the nth degree, the model consists of a mass M together with a spring coupled in parallel with n spring dashpot elements.

In this paper vibrations of elastic continua with hereditary damping characteristics are considered. The general equations of motion for an elastic medium with hereditary damping characteristics are deduced. These equations are identical from a mathematical point of view with the corresponding equations of the classical theory of heredity (3) except for the particular physical significance of the parameters.

---

[1] Associate Professor, Illinois Institute of Technology. Mem. ASME.

[2] Numbers in parentheses refer to the Bibliography at the end of the paper.

Contributed by the Applied Mechanics Division and presented at the Annual Meeting, New York, N. Y., November 26–December 1, 1950, of The American Society of Mechanical Engineers.

Discussion of this paper should be addressed to the Secretary, ASME, 29 West 39th Street, New York, N. Y., and will be accepted until October 10, 1951, for publication at a later date. Discussion received after the closing date will be returned.

Note: Statements and opinions advanced in papers are to be understood as individual expressions of their authors and not those of the Society. Manuscript received by ASME Applied Mechanics Division, June 2, 1950. Paper No. 50—A-32.

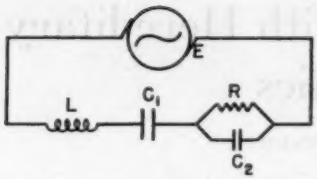

FIG. 1(b) EQUIVALENT ELECTRICAL CIRCUIT

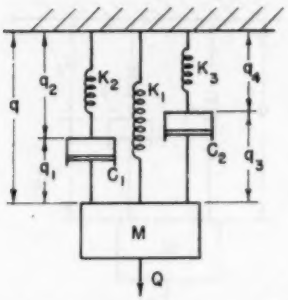

FIG. 2 MECHANICAL MODEL FOR HEREDITARY SYSTEM OF ONE DEGREE OF FREEDOM WITH HEREDITY OF SECOND DEGREE

In particular we shall study the radial vibrations of a sphere, the free vibrations of flexible strings, the lateral vibrations of bars, as well as the vibrations of rectangular and circular membranes, having hereditary damping characteristics.

All of these problems are reducible to the solution of the following integro-differer tial equation

$$\frac{d^2f(t)}{dt^2} + a^2f(t) + \int_0^t \phi(t-\tau)\frac{df(\tau)}{d\tau}d\tau = 0 \quad \ldots\ldots [5]$$

which coincides in essence with Equation [1]. The foregoing equation can be solved by elementary means in the case of heredity of degree n.

In the simplest case of heredity of the first degree, where $\phi(t) = Ae^{-\alpha t}$, and provided the coefficients of heredity α and A are small compared to the elastic constant a, the solution of Equation [5] can be given in explicit form.

SOLUTION OF GOVERNING EQUATION FOR HEREDITY OF nTH DEGREE

Equation [5] may be reduced to the classical form

$$\frac{d^2f(t)}{dt^2} + \omega^2 f(t) + \int_0^t K(t-\tau)f(\tau)d\tau = 0 \quad \ldots\ldots [6]$$

where

$$\omega^2 = a^2 + \phi(0); \; K(t-\tau) = \phi'(t-\tau)$$

by performing an integration by parts assuming, as we may, that $f(0) = 0$. Equation [6] was solved completely by Vito Volterra (3) for a wide class of functions $K(t)$.

In practical cases where the law of heredity of the nth degree given in Equation [2] is admissible, it is possible to apply an elementary method of solution. This method consists in reducing Equation [6] to an ordinary differential equation. In fact, differentiating Equation [6] n times, the integrals disappear and a linear differential equation with constant coefficients of order $n + 2$ is obtained.

Consistent with experiments (1) we may suppose the damping coefficients α_i; A_i together with ω^2 to be positive. Under the additional assumption that the α_i and A_i/ω^2 are small in the sense that their squares can be neglected compared to ω^2 and unity, respectively, all the roots of the characteristic equation belonging to the foregoing differential equation have negative real parts as was shown by D. Graffi (4).

A differentiation of Equation [6] leads to

$$\frac{d^3f(t)}{dt^3} + \alpha\frac{d^2f(t)}{dt^2} + \omega^2\frac{df(t)}{dt} + (\omega^2 - A)\alpha f(t) = 0 \ldots [7]$$

where

$$\omega^2 = a^2 + A$$

The corresponding characteristic equation there appears as

$$x^3 + \alpha x^2 + \omega^2 x + \alpha(\omega^2 - A) = 0 \ldots\ldots [8]$$

Using the foregoing linearization, the roots are

$$x_1 = -r = -\alpha\frac{(A-\omega^2)}{\omega^2}$$

$$x_2 = -p + iq = -\frac{1}{2}\frac{A\alpha}{\omega^2} + i\omega$$

$$x_3 = -p - iq = -\frac{1}{2}\frac{A\alpha}{\omega^2} - i\omega$$

The explicit solution of Equation [5] or [6] is therefore

$$\left.\begin{aligned} f(t) &= C_1e^{-rt} + C_2e^{-pt}\cos qt + C_3e^{-pt}\sin qt \\ &= C_1e^{-\alpha\frac{(A-\omega^2)}{\omega^2}t} + C_2e^{-\frac{1}{2}\frac{A\alpha}{\omega^2}t}\cos\omega t + C_3e^{-\frac{1}{2}\frac{A\alpha}{\omega^2}t}\sin\omega t \end{aligned}\right\} \ldots [9]$$

where C_1, C_2, and C_3 are arbitrary constants to be determined from the initial conditions.

It was recently show n by D. Graffi (4) that in the case of heredity of the nth degree, and under the approximate assumptions made here, the characteristic equation always has n real negative roots and a single pair of complex conjugate roots, whose real part is

$$\frac{1}{2}\sum_1^n \frac{A_i\alpha_i}{\omega^2}$$

and whose imaginary part is ω. Thus the frequency of the oscillatory term is the same as in the absence of damping, i.e., if $K(t) = 0$.

GENERAL EQUATIONS OF MOTION FOR ELASTIC MEDIUM WITH HEREDITARY CHARACTERISTICS

Consider an elastic medium having hereditary damping characteristics. Let t_{rs} be the Cartesian components of the stress, $[\rho X, \rho Y, \rho Z]$ and $[X_\sigma, Y_\sigma, Z_\sigma]$ the components of the body force and of the surface tractions, respectively, $[u, v, w]$ the components of the displacement, and n the outer normal to the boundary. The equations of motion are, as usual

$$\frac{\partial t_{11}}{\partial x} + \frac{\partial t_{12}}{\partial y} + \frac{\partial t_{13}}{\partial z} = \rho\left[X - \frac{\partial^2 u}{\partial t^2}\right]; \ldots; \ldots; \ldots [10]$$

$$t_{11}\cos nx + t_{12}\cos ny + t_{13}\cos nz = X_\sigma; \ldots; \ldots; \ldots [11]$$

The most general linear hereditary stress-strain law is of the form

$$t_{ss} = \sum_{hj} a_{ss/hj}\,\gamma_{hj} + \int_0^t \sum_{hj} \varphi_{ss/hj}\,\frac{\partial \gamma_{hj}}{\partial \tau}\,d\tau \ldots\ldots [12]$$

where γ_{hj} represent the Cartesian components of strain.

The summation appearing in Equations [12] is extended over all combinations with repetition of the letters h and j ($h, j = 1, 2, 3, \ldots\ldots 6$). The stress-strain law, Equation [12], thus involves 36 elastic coefficients $a_{ss/hj}$ and 36 heredity functions $\varphi_{ss/hj}$. In general we shall assume that the coefficients $a_{ss/hj}$ are functions of the co-ordinates x, y, z of the points of the elastic body and that the $\varphi_{ss/hj}$ are functions of x, y, z and also of the variables t and τ. Only in the case of homogeneity $a_{ss/hj}$ and $\varphi_{ss/hj}$ are independent of the co-ordinates x, y, z. The strain-displacement relations for infinitesimal deformations are

$$\gamma_{11} = \frac{\partial u}{\partial x}; \ldots; \ldots; \quad \gamma_{12} = \frac{\partial u}{\partial y} + \frac{\partial v}{\partial x}; \ldots; \ldots; \ldots [13]$$

In the case of an isotropic medium, Equations [12] must be invariant under rotation of the co-ordinate system. Therefore we obtain

$$\left.\begin{aligned} t_{rr} &= \lambda\Delta + 2G\gamma_{rr} + \int_0^t \left[\varphi(t,\tau)\,\frac{\partial \Delta}{\partial \tau} + 2\psi(t,\tau)\,\frac{\partial \gamma_{rr}}{\partial \tau}\right] d\tau \\ t_{rs} &= G\gamma_{rs} + \int_0^t \psi(t,\tau)\,\frac{\partial \gamma_{rs}}{\partial \tau}\,d\tau \end{aligned}\right\} \ldots [14]$$

where $\Delta = \gamma_{11} + \gamma_{22} + \gamma_{33}$. In the case of homogeneity λ and G are constant (Lamé's constant and shear modulus) and φ and ψ are independent of x, y, z. In the isotropic homogeneous case we are thus led to two independent elastic constants and two independent hereditary functions. We furthermore assume that

$$\varphi(t,\tau) = \varphi(t-\tau); \quad \psi(t,\tau) = \psi(t-\tau)$$

Substituting Equations [13] and [14] in Equations [10], we reach the equations of motion in terms of displacements

$$\begin{aligned} &G\nabla^2(u,v,w) + (\lambda + G)\left(\frac{\partial}{\partial x}, \frac{\partial}{\partial y}, \frac{\partial}{\partial z}\right)\Delta \\ &+ \int_0^t \left[\psi(t-\tau)\,\frac{\partial}{\partial \tau}\,\nabla^2(u,v,w) + \{\varphi(t-\tau) + \psi(t-\tau)\}\right. \\ &\left.\frac{\partial}{\partial \tau}\left(\frac{\partial}{\partial x}, \frac{\partial}{\partial y}, \frac{\partial}{\partial z}\right)\Delta\right] d\tau = \rho\{(X,Y,Z) - \frac{\partial^2}{\partial t^2}(u,v,w) \ldots [15] \end{aligned}$$

By the same method used in the classic theory of elasticity, we obtain the generalized form of the equations of motion in terms of rotation and dilatation

$$\begin{aligned} &(\lambda + 2G)\left(\frac{\partial}{\partial x}, \frac{\partial}{\partial y}, \frac{\partial}{\partial z}\right)\Delta - 2G\ \mathrm{curl}\ (\tilde{\omega}_x, \tilde{\omega}_y, \tilde{\omega}_z) \\ &+ \int_0^t \left[\{\varphi(t-\tau) + 2\psi(t-\tau)\}\left(\frac{\partial}{\partial x}, \frac{\partial}{\partial y}, \frac{\partial}{\partial z}\right)\frac{\partial \Delta}{\partial \tau}\right. \\ &\left. - 2\psi(t-\tau)\left\{2\ \mathrm{curl}\left(\frac{\partial \tilde{\omega}x}{\partial \tau}, \frac{\partial \tilde{\omega}y}{\partial \tau}, \frac{\partial \omega z}{\partial \tau}\right)\right\}\right] d\tau \\ &= \rho\left[(X,Y,Z) - \frac{\partial^2}{\partial t^2}(u,v,w)\right] \ldots\ldots [16] \end{aligned}$$

Furthermore, Equations [16] imply

$$\begin{aligned} &(\lambda + 2G)\nabla^2\Delta + \int_0^t [\varphi(t-\tau) + 2\psi(t-\tau)]\,\frac{\partial}{\partial \tau}\,\nabla^2\Delta(\tau)d\tau \\ &+ \rho\,\frac{\partial^2 \Delta(\tau)}{\partial t^2} = \frac{\partial(\rho X)}{\partial x} + \frac{\partial(\rho Y)}{\partial y} + \frac{\partial(\rho Z)}{\partial z} \ldots\ldots [17] \end{aligned}$$

$$\begin{aligned} &G\nabla^2(\tilde{\omega}x, \tilde{\omega}y, \tilde{\omega}z) + \int_0^t \psi(t-\tau)\,\frac{\partial}{\partial \tau}\,\nabla^2(\tilde{\omega}x, \tilde{\omega}y, \tilde{\omega}z)d\tau \\ &+ \rho\,\frac{\partial^2}{\partial t^2}(\tilde{\omega}x, \tilde{\omega}y, \tilde{\omega}z) = \frac{1}{2}\left[\left(\frac{\partial \rho Z}{\partial y} - \frac{\partial \rho Y}{\partial z}\right),\right. \\ &\left.\left(\frac{\partial \rho X}{\partial z} - \frac{\partial \rho Z}{\partial x}\right), \left(\frac{\partial \rho Y}{\partial x} - \frac{\partial \rho X}{\partial y}\right)\right] \ldots\ldots [18] \end{aligned}$$

Radial Free Vibrations of an Isotropic Sphere

We shall consider only those free vibrations which involve a purely radial displacement at every point, such that concentric spherical surfaces remain spherical and concentric during oscillation (5). For this mode the rotation vanishes.

Taking the origin of co-ordinates at the center of the sphere, Equations [16] become

$$\begin{aligned} &(\lambda + 2G)\left(\frac{\partial}{\partial x}, \frac{\partial}{\partial y}, \frac{\partial}{\partial z}\right)\Delta + \int^t [\varphi(t-\tau) + 2\psi(t-\tau)] \\ &\left(\frac{\partial}{\partial x}, \frac{\partial}{\partial y}, \frac{\partial}{\partial z}\right)\frac{\partial \Delta}{\partial \tau}\,d\tau = -\frac{\partial^2}{\partial t^2}\,\rho(u,v,w) \ldots\ldots [19] \end{aligned}$$

In view of the polar symmetry, and letting $r = \sqrt{x^2 + y^2 + z^2}$

$$\left.\begin{aligned} &u = \frac{x}{r}\,V(r,t),\ v = \frac{y}{r}\,V(r,t),\ w = \frac{z}{r}\,V(r,t) \\ &\text{and hence} \\ &\Delta = \frac{2}{r}\,V(r,t) + \frac{\partial V(r,t)}{\partial r} \end{aligned}\right\} \ldots [20]$$

Substituting Equations [20] into Equations [19], we are led to the following integro-differential equation which determines the unknown function $V(r,t)$

$$\begin{aligned} &(\lambda + 2G)\,\frac{\partial}{\partial r}\left[\frac{2}{r}\,V(r,t) + \frac{\partial V(r,t)}{\partial r}\right] \\ &+ \int_0^t [\varphi(t-\tau) + 2\psi(t-\tau)]\,\frac{\partial^2}{\partial r \partial \tau}\left[\frac{2}{r}\,V(r,t)\right. \\ &\left. + \frac{\partial V(r,\tau)}{\partial r}\right] d\tau = -\frac{\partial^2 V(r,t)}{\partial t^2} \ldots\ldots [21] \end{aligned}$$

Using the method of separation of variables, we put

$$V(r,t) = U(r)f(t) \ldots\ldots [22]$$

and are led to

$$\frac{d}{dr}\left[\frac{2}{r}\,U(r) + \frac{dU(r)}{dr}\right] + K^2 U(r) = 0 \ldots\ldots [23]$$

$$\begin{aligned} &\rho\,\frac{d^2 f(t)}{dt^2} + K^2\left[(\lambda + 2G)f(t) + \int_0^t [\varphi(t-\tau) + 2\psi(t-\tau)]\right. \\ &\left.\frac{df(\tau)}{d\tau}\,d\tau\right] = 0 \ldots\ldots [24] \end{aligned}$$

By integrating Equation [23], we obtain

$$U(r) = \frac{A\cos Kr - B\sin Kr}{Kr} - \frac{A\sin Kr + B\cos Kr}{K^2r^2} \quad [23a]$$

where A and B are arbitrary constants of integration. In the case of the solid sphere U must be zero when $r = 0$. It follows that $B = 0$.

If σ_r represents the radial normal stress

$$\sigma_r = (\lambda + 2G)\frac{dU}{dr} + 2G\frac{U}{r} = A\,K\left[2G\left(\frac{\cos Kr}{K^2r^2} - \frac{\sin Kr}{K^3r^3}\right)\right] - (\lambda + 2G)\left[\frac{2\cos Kr}{K^2r^2} + \sin Kr\left(\frac{1}{Kr} - \frac{2}{K^3r^3}\right)\right]$$

Applying the boundary condition $\sigma_{(r=R)} = 0$, where R is the radius of the sphere, we reach the characteristic equation

$$\frac{t_e k;\, R}{K_i\, R} = \frac{4G}{4G - (\lambda + 2G)K_i^2R^2} \quad [25]$$

Assuming heredity of the first degree, let

$$\varphi(t) = Ae^{-\alpha t};\ \psi(t) = Be^{-\beta t}$$

Equation [24] then becomes

$$\rho\frac{d^2f_i(t)}{dt^2} + K_i^2\left[(\lambda + 2G)f_i(t) + A\int_0^t e^{-\alpha(t-\tau)}\frac{df_i(\tau)}{d\tau}\,d\tau + 2B\int_0^t e^{-\beta(t-\tau)}\frac{df_i(\tau)}{d\tau}d\tau\right] = 0 \quad [26]$$

Two successive time-differentiation of Equation [26] yield

$$\frac{d^4f_i(t)}{dt^4} + (\alpha+\beta)\frac{d^3f_i(t)}{dt^3} + \left[\frac{K_i^2}{\rho}(\lambda + 2G + A + 2B) + \alpha\beta\right]\frac{d^2f_i(t)}{dt^2} + \frac{K_i^2}{\rho}[(\lambda + 2G)(\alpha+\beta) + 2\alpha B + \beta A]\frac{df_i(t)}{dt} + \alpha\beta\frac{(\lambda + 2G)K_i^2}{\rho}f_i(t) = 0 \quad [27]$$

with the characteristic equation

$$x_i^4 + (\alpha+\beta)x_i^3 + \left[\frac{K_i^2}{\rho}(\lambda + 2G + A + 2B) + \alpha\beta\right]x_i^2 + \frac{K_i^2}{\rho}[(\lambda + 2G)(\alpha+\beta) + 2\alpha B + \beta A]x_i + \alpha\beta\frac{(\lambda + 2G)K_i^2}{\rho} = 0 \quad [28]$$

The solution of Equation [22] is

$$V(r,t) = \sum_1^\infty{}_i\left(\frac{\cos K_ir}{K_ir} - \frac{\sin K_ir}{K_i^2r^2}\right)(C_{1i}e^{-m_it} + C_{2i}e^{-n_it} + C_{3i}e^{-p_it}\cos q_it + C_{4i}e^{-p_it}\sin q_it) \quad [29]$$

where $-m_i$; $-n_i$; $-p_i + iq_i$; $-p_i - iq_i$ are the roots of the algebraic Equation [28] corresponding to the characteristic values K_i of Equation [25].

The constants $C_{ri}(i = 1, 2, 3, 4)$ are found from the initial conditions

$$V(r,0) = v(r)$$

$$\frac{\partial V}{\partial t} = v'(r)$$

$$(\lambda + 2G)\frac{\partial}{\partial r}\left[\frac{2}{r}V(r,0) + \frac{\partial V(r,0)}{dr}\right] = -\frac{\partial^2 V(r,0)}{\partial t^2}$$

$$(\lambda + 2G + A + 2B)\frac{\partial^3}{\partial r\partial t}\left[\frac{2}{r}V(r,0) + \frac{\partial V(r,0)}{\partial r}\right] = -\frac{\partial^3 V(r,0)}{\partial t^3}$$

It should be noted that only the first two of these initial conditions are arbitrarily prescribed, whereas the remaining two are consequences of the equations of motion, Equation [19].

Vibrations of a Flexible String

The equation for the free vibrations of a flexible string, taking into account hereditary damping, is

$$S\frac{\partial^2 w(x,t)}{\partial x^2} + \int_0^t \phi(t-\tau)\frac{\partial^2 w(x,\tau)}{\partial x^2\partial\tau}\,d\tau = m\frac{\partial^2 w(x,t)}{\partial t^2} \quad [30]$$

where S is the tension and m the mass per unit length of the string. With

$$w(x,t) = u(x)f(t) \quad [31]$$

it follows that

$$\frac{d^2u(x)}{dx^2} - cu(x) = 0 \quad [32]$$

$$m\frac{d^2f(t)}{dt^2} - c\left[Sf(t) + \int_0^t \phi(t-\tau)\frac{df(\tau)}{d\tau}\,d\tau\right] = 0 \quad [33]$$

where c is a constant which can be shown to be negative.

Calling $c = -k^2$, where k is a real number, and integrating Equation [32] we obtain

$$u(x) = A\cos kx + B\sin kx$$

where A and B are constants.

If we suppose the string fixed at both ends, then $u(0) = u(l) = 0$ and

$$A = 0;\ k_jl = j\pi\ (j = 1, 2, 3, \ldots)$$

Equation [33] now becomes

$$m\frac{d^2f_j(t)}{dt^2} + \left(\frac{j\pi}{l}\right)^2\left[Sf_j(t) + \int_0^t \phi(t-\tau)\frac{df_j(\tau)}{d\tau}\,d\tau\right] = \quad [34]$$

Supposing heredity of the first degree

$$f_j(t) = C_{1j}e^{-r_jt} + C_{2j}e^{-p_jt}\cos q_jt + C_{3j}e^{-p_jt}\sin q_jt$$

where $-r_j$; $-p_j + iq_j$; $-p_j - iq_j$ are the roots of the cubic equation

$$x_j^3 + \alpha x_j^2 + \left(\frac{j\pi}{l}\right)^2(S + A)x_j + \left(\frac{j\pi}{l}\right)^2\alpha S = 0$$

The solution of Equation [31] is therefore

$$w(x,t) = \sum_1^\infty{}_j\psi_j(x)[C_{1j}e^{-r_jt} + C_{2j}e^{-p_jt}\cos q_jt + C_{3j}e^{-p_jt}\sin q_jt]$$

where the characteristic functions

$$\psi_j(x) = \sin\frac{j\pi x}{l}$$

satisfy the usual orthogonality conditions (6).

The constants C_i, $(i = 1, 2, 3)$ are found from the initial conditions

$$w(x,0) = v(x)$$

$$\frac{\partial w(x,0)}{\partial t} = v^1(x)$$

$$m\frac{\partial^2 w(x,0)}{\partial t^2} = S\frac{\partial^2 w(x,0)}{\partial x^2}$$

Lateral Vibrations of Bars

The equation of motion for the lateral free vibrations of a bar with hereditary damping is

$$m\frac{\partial^2 w(x,t)}{\partial t^2} + EI\frac{\partial^4 w(x,t)}{\partial x^4} + I\int_0^t \phi(t-\tau)\frac{\partial^4 w(x,\tau)}{\partial x^4 \partial \tau}d\tau = 0 \quad \ldots\ldots [35]$$

where m is the mass per unit length, and EI the flexural rigidity of the bar. Putting

$$w(x,t) = u(x)f(t) \quad \ldots\ldots [36]$$

it follows that

$$\frac{d^4u(x)}{dx^4} - k^4u(x) = 0 \quad \ldots\ldots [37]$$

$$\frac{d^2f(t)}{dt^2} + \frac{k^4I}{m}\left[Ef(t) + \int_0^t \phi(t-\tau)\frac{df(\tau)}{d\tau}d\tau\right] = 0 \quad \ldots [38]$$

where k is a constant. Integrating Equation [37] we obtain

$$u(x) = [A_1\cos kx + A_2\sin kx + A_3\cosh kx + A_4\sin hkx]$$

where $A_j (j = 1, 2, 3, 4)$ are constants.

Bar Simply Supported. Call l the length of the bar. The following end conditions hold

$$u(0) = u(l) = \frac{d^2u(0)}{dx^2} = \frac{d^2u(l)}{dx^2} = 0$$

from which $A_1 = A_3 = A_4 = 0$, $k_j = j\pi/l$; $(j = 1, 2, 3, \ldots)$. The solution of Equation [36] is thus given by

$$w(x,t) = \sum_1^\infty{}_j \psi_j(x)f_j(t)$$

where the characteristic functions

$$\psi_j = \sin\frac{j\pi x}{l}$$

Bar Clamped at One End ($x = 0$), and Free at the Other ($x = l$). The following end conditions hold

$$u(0) = \frac{du(0)}{dx} = \frac{d^2u(l)}{dx^2} = \frac{d^3u(l)}{dx^3} = 0$$

from which we obtain the characteristic equation

$$\cos k_jl\cosh k_jl = -1$$

The solution of Equation [36] is

$$w(x,t) = \sum_1^\infty{}_j \psi_j(x)f_j(t) \quad \ldots\ldots [39]$$

where the characteristic functions

$$\psi_j(x) = [\cosh k_jx - \cos k_jx] + \beta_j[\sinh k_jx - \sin k_jx] \quad \ldots [40]$$

with

$$\beta_j = -\frac{\cosh k_jl + \cos k_jl}{\sinh k_jl + \sin k_jl} = -\frac{\sinh k_jl - \sin k_jl}{\cosh k_jl + \cos k_jl}$$

Free-Free Bar. The following end conditions hold

$$\frac{d^2u(0)}{dx^2} = \frac{d^2u(0)}{dx^3} = \frac{d^2u(l)}{dx^2} = \frac{d^3u(l)}{dx^3} = 0$$

and the corresponding characteristic equation becomes

$$\cos k_jl\cosh k_jl = 1$$

The solution of Equation [36] thus is

$$w(x,t) = \sum_1^\infty{}_j \psi_j(x)f_j(t) \quad \ldots\ldots [41]$$

where the characteristic functions

$$\psi_j(x) = [\sin k_jx + \sinh k_jx] + \beta_j[\cos k_jx + \cosh k_jx]$$

with

$$\beta_j = \frac{\sin k_jl + \sinh k_jl}{\cos k_jl - \cosh k_jl} \quad \ldots\ldots [42]$$

Bar Built-In at One End ($x = 0$), and Simply Supported at the Other ($x = l$). The following end conditions hold

$$u(0) = \frac{du(0)}{dx} = u(l) = \frac{d^2u(l)}{dx^2} = 0$$

and thus

$$tghl - thkl = 0$$

The solution of Equation [36] is therefore

$$w(x,t) = \sum_1^\infty{}_j \psi_j(x)f_j(t) \quad \ldots\ldots [43]$$

where the characteristic functions

$$\psi_j(x) = [\sin k_jx - \sinh k_jx] + \beta_j[\cos k_jx - \cosh k_jx] \quad [44]$$

with

$$\beta_j = -\frac{\cos k_jl - \cosh k_jl}{\sin k_jl - \sinh k_jl}$$

The characteristic functions, Equations [38], [40], [42], [44], satisfy the usual orthogonality conditions (6). The problem of free transverse vibrations of bars is reduced to the solution of Equation [38]. Assume heredity of the first degree. Differentiating Equation [38] we obtain

$$\frac{d^2f_j(t)}{dt^2} + \alpha\frac{d^2f_j(t)}{dt^2} + \frac{k_j^4I}{m}[E + A]\frac{df_j(t)}{dt} + \alpha\frac{k_j^4I}{m}f_j(t) = 0 \quad \ldots\ldots [45]$$

The solution of Equation [45] is

$$f_j(t) = C_{1j}e^{-\sigma_jt} + C_{2j}e^{-p_jt}\cos q_jt + C_{3j}e^{-p_jt}\sin q_jt$$

where $-\sigma_j$; $-p_j + iq_j$; $-p_j - iq_j$ are the roots of the cubic equations

$$x_j^3 + \alpha x_j^2 + \frac{k_j^4I}{m}[E + A]x_j + \alpha\frac{k_j^4I}{m} = 0$$

and the constants C_{ij}; $(i = 1, 2, 3)$ are found from the initial conditions

$$w(x,0) = v(x)$$

$$\frac{\partial w(x,0)}{\partial t} = v'(x)$$

$$m\frac{\partial^2 w(x,0)}{\partial t^2} + EI\frac{\partial^4 w(x,0)}{\partial x^4} = 0$$

Vibrations of Membranes

The equation of motion for the free vibrations of a membrane taking into account hereditary damping, is

$$T\nabla^2 w(x,y;t) + \int_0^t \phi(t-\tau)\frac{\partial}{\partial \tau}\nabla^2 w(x,y;\tau)d\tau - \rho\frac{\partial^2 w(x,y;t)}{\partial t^2} = 0 \quad \ldots\ldots [46]$$

where T represents the tension per unit area, ρ the density per unit area and ∇^2 the Laplacian operator.

Rectangular Membrane. Using the method of separation of variables, we put

$$w(x,y;t) = u(x,y)f(t) \quad \ldots\ldots [47]$$

Hence

$$\frac{\partial^2 u(x,y)}{\partial x^2} + \frac{\partial^2 u(x,y)}{\partial y^2} = k^2 u(x,y) \quad \ldots\ldots [48]$$

$$\rho\frac{d^2 f(t)}{dt^2} + k^2\left[Tf(t) + \int_0^t \phi(t-\tau)\frac{df(\tau)}{d\tau}d\tau\right] = 0 \quad \ldots [49]$$

Let the boundary be defined by the equations

$$x = 0,\ x = a,\ y = 0,\ y = b$$

Substitution in Equation [48] of $u(x,y) = u_1(x)u_2(y)$ yields

$$\left.\begin{aligned}\frac{d^2 u_1(x)}{dx^2} + \omega_1^2 u_1(x) &= 0\\ \frac{d^2 u_2(y)}{dy^2} + \omega_2^2 u_2(y) &= 0\end{aligned}\right\} \quad \ldots\ldots [50]$$

where

$$\omega_1^2 + \omega_2^2 = k^2.$$

The solutions of Equations [50] are

$$u_1 = A_1\cos\omega_1 x + B_1\sin\omega_1 x$$
$$u_2 = A_2\cos\omega_2 y + B_2\sin\omega_2 y$$

where A_1, A_2, B_1, B_2 are constants.

If the membrane is fixed at the boundary, the boundary conditions are

$$u_1(0) = u_1(a) = u_2(0) = u_2(b) = 0$$

from which it follows that

$A_1 = A_2 = 0$; $a\omega_1 = m\pi$; $b\omega_2 = n\pi$ where m and n are integers. Furthermore

$$k^2 = \pi^2\left[\frac{m^2}{a^2} + \frac{n^2}{b^2}\right] \quad \begin{cases} m = 1, 2, 3\ldots \\ n = 1, 2, 3\ldots \end{cases}$$

Equation [49] now becomes

$$\rho\frac{d^2 f_{mn}(t)}{dt^2} + \pi^2\left[\frac{m^2}{a^2} + \frac{n^2}{b^2}\right]\left[Tf_{mn}(t) + \int_0^t \phi(t-\tau)\frac{df_{mn}(\tau)}{d\tau}d\tau\right] = 0 \quad \ldots\ldots [51]$$

The solution of Equation [47] is, therefore

$$w(x,y;t) = \sum_1^\infty{}_{mn}\psi_{mn}(x,y)[C_{1mn}e^{-r_{mn}t} + C_{2mn}e^{-p_{mn}t}\cos q_{mn}t + C_{3mn}e^{-p_{mn}t}\sin q_{mn}t]$$

where the characteristic functions

$$\psi_{mn}(x,y) = \sin\frac{\pi m x}{a}\sin\frac{\pi n y}{b}$$

satisfy the usual orthogonality Equations (6).

Here, $-r_{mn}$; $-p_{mn} + iq_{mn}$; $-p_{mn} - iq_{mn}$ are, in the case of heredity of the first degree, the roots of the cubic equations

$$x^3_{mn} + \alpha x^2_{mn} + \pi^2\left[\frac{m^2}{a^2} + \frac{n^2}{b^2}\right][T + A]x_{mn} + T\alpha\pi^2\left[\frac{m^2}{a^2} + \frac{n^2}{b^2}\right] = 0$$

The constants of integration C_{1mn}, C_{2mn}, C_{3mn} are found from the initial conditions

$$w(x,y;0) = v(x,y)$$

$$\frac{\partial w(x,y;0)}{\partial t} = v'(x,y)$$

$$T\nabla^2 w(x,y;0) = \rho\frac{\partial^2 w(x,y;0)}{\partial t^2}$$

Circular Membrane. Expressing the Laplacian operator in polar co-ordinates, Equations [48] and [49] assume the form

$$\frac{\partial^2 u(r,\varphi)}{\partial r^2} + \frac{1}{r}\frac{\partial u(r,\varphi)}{\partial r} + \frac{1}{r^2}\frac{\partial^2 u(r,\varphi)}{\partial \varphi^2} + k^2 u(r,\varphi) = 0 \quad \ldots [52]$$

$$\rho\frac{d^2 f(t)}{dt^2} + k^2\left[Tf(t) + \int_0^t \phi(t-\tau)\frac{df(\tau)}{d\tau}d\tau\right] = 0 \quad \ldots [53]$$

Putting

$$u(r,\varphi) = \theta(r)\psi(\varphi) \quad \ldots\ldots [54]$$

and substituting Equation [54] in Equation [52] we obtain

$$\frac{d^2\psi_n(\varphi)}{d\varphi^2} + n^2\psi_n(\varphi) = 0\ (n = 0, 1, 2, 3, \ldots) \quad \ldots [55]$$

$$\frac{r^2 d^2\theta_n(r)}{dr^2} + r\frac{d\theta_n}{dr} + (k^2r^2 - n^2)\theta_n = 0 \quad \ldots\ldots [56]$$

The solution of Equations [55] is

$$\psi_n = A_n\cos n\varphi + B_n\sin n\varphi$$

where A_n and B_n are constants of integration. Introducing in Equation [56] $\rho = rk$, we reach

$$\frac{d^2\theta_n(\rho)}{d\rho^2} + \frac{1}{\rho}\frac{d\theta_n(\rho)}{d\rho} + \left[1 - \frac{n^2}{\rho^2}\right]\theta_n(\rho) = 0 \quad \ldots\ldots [57]$$

Denoting by C_n and D_n two arbitrary constants, the general integral of Equation [57] appears as

$$\theta_n(\rho) = C_n J_n(\rho) + D_n y_n(\rho) \quad \ldots\ldots [58]$$

when J_n is the Bessel function of the first kind of order n, whereas, Y_n is the Bessel function of the second kind of order n. In the case of circular membranes, owing to the singularities of the functions Y_n for $\rho = 0$ the functions must be rejected and the integral of Equation [58] becomes

$$\theta_n(\rho) = C_n J_n(\rho)$$

If the membra ω is fastened along a boundary circle of radius R, the values of K_n are found from the characteristic equation

$$J_n(Rk_n) = 0$$

The characteristic function corresponding to the value k_{on} is

$$\psi_{on}(r,\varphi) = J_0\left(\frac{r\rho_{on}}{R}\right)$$

and the two characteristic functions corresponding to the value k_{mn}; $(m > 0)$ are

$$\psi_{emn}(r,\varphi) = \cos(m\varphi)J_m\left(\frac{r\rho_{mn}}{R}\right); \psi_{omn}(r,\varphi) = \sin(m\varphi)J_m\left(\frac{r\rho_{mn}}{R}\right)$$

These functions satisfy well-known orthogonality conditions (6).

The general solution of Equation [54] is thus given by

$$w(r,\varphi;t) = \sum_{n=1}^{\infty}\left\{\sum_{m=0}^{\infty}\psi_{emn}[C_{1emn}e^{-r_{emn}t} + C_{2emn}e^{-p_{emn}t}\cos q_{emn}t + C_{3emn}e^{-p_{emn}t}\cos q_{emn}t] + \sum_{m=1}^{\infty}\psi_{omn}[C_{1omn}e^{-r_{omn}t} + C_{2omn}e^{-p_{omn}t}\cos q_{omn}t + C_{3omn}e^{-p_{omn}t}\sin q_{omn}t\right\}$$

Here $-r_{emn}$; $-p_{emn} + iq_{emn}$; $-p_{emn} - iq_{emn}$ are the roots of the cubic equation

$$x^3_{emn} + \alpha x^2_{emn} + \frac{(T+A)}{\rho}k^2_{emn}x_{emn} + \frac{T\alpha}{\rho}k_{emn} = 0$$

and $-r_{omn}$; $-p_{omn} + iq_{omn}$; $-p_{omn} - iq_{omn}$ are the roots of the cubic equation

$$x^3_{omn} + \alpha x^2_{omn} + \frac{(T+A)}{\rho}k^2_{omn}x_{omn} + \frac{T\alpha}{\rho}k_{omn} = 0$$

The initial conditions for determining the constants of integration are

$$w(r,\varphi;0) = v(r,\varphi)$$

$$\frac{\partial w(r,\varphi;0)}{\partial t} = v'(r,\varphi)$$

$$T\Delta^2 w(r,\varphi;0) = \rho\frac{\partial^2 w(r,\varphi;0)}{\partial t^2}$$

ACKNOWLEDGMENT

The author wishes to express his appreciation to Dr. A. Nadai, Visiting Professor of Mechanics at the Illinois Institute of Technology, and to Dr. E. Sternberg, Associate Professor of Mechanics at the Illinois Institute of Technology, for most valuable suggestions and criticisms.

BIBLIOGRAPHY

1 "Vibrations of Elastic Systems Having Hereditary Characteristics," by E. Volterra, Paper No. 50—APM-8, *Journal of Applied Mechanics* (not published).

2 "Mathematical Methods in Engineering," by T. von Kármán and M. A. Biot, McGraw-Hill Book Company, Inc., New York, N. Y., and London, England, 1940.

3 "Sulle Equazioni Integro-Differenziali della Teoria dell'Elasticità," by Vito Volterra, *Rendiconti della R. Accademia dei Lincei*, vol. 18, series 5, 2nd Semestre, vol. 9, 1909, pp. 295–301.

"Lecons sur les Équations Intégrales et les Équations Intégro-Différentielles," by Vito Volterra, Gauthier-Villars, Paris, France, 1913.

"Lecons sur les Fonctions de Lignes," by Vito Volterra, Gauthier-Villars, Paris, France, 1913.

"Theory of Functionals and of Integral and Integro-Differential Equations," by Vito Volterra, Blackie and Son, London, England, 1930.

4 "Sulla Teoria delle Oscillazioni Libere in un sistema soggetto a Forze Elastiche con Ereditarieta," by Dario Graffi, *Seminario Matematico e Fisico dell'Universita di Modena*, vol. 3, 1948–1949, pp. 227–298.

5 "The Mathematical Theory of Elasticity," by A. E. H. Love, Dover Publications, New York, N. Y., 1944.

"Theory of Elasticity," by R. V. Southwell, Oxford University Press, 1949.

6 "Vibration Problems in Engineering," by S. Timoshenko, D. Van Nostrand Company, Inc., New York, N. Y., 1937.

"Mechanical Vibrations," by J. P. Den Hartog, McGraw-Hill Book Company, Inc., New York, N. Y., 1940.

"Vibration and Sound," by P. M. Morse, McGraw-Hill Book Company, Inc., New York, N. Y., 1948.

Transverse Vibrations of a Free Circular Plate Carrying Concentrated Mass

By R. E. ROBERSON,[1] WASHINGTON, D. C.

The plate under consideration carries a concentrated mass at its center, which is struck impulsively in a direction perpendicular to the undisturbed plate face. Only circularly symmetric vibrations are considered. The solution is carried out by the use of the Laplace transform method, treating the concentrated mass as a plate-density impulse. The first four natural frequencies are displayed as functions of mass ratio, and the first mode shape is displayed for three mass ratios. The natural frequencies, particularly the higher, are shown to be very sensitive to changes in mass ratio at small values of the concentrated mass.

Nomenclature

The following notation and nomenclature are used in the paper:

$A(\xi,q_n)$ = amplitude in nth normal mode
a = plate radius
$D = 2Eh^3/3(1-\nu^2)$ = flexural rigidity
E = Young's modulus
$f(r,t)$ = transverse pressure on plate face
$G(q)$, $H(\xi,q)$ = special combinations of Bessel functions defined by Equations [7] and [8]
h = half thickness of plate
I_n,J_n,K_n,Y_n = Bessel functions of order n
m = magnitude of concentrated mass
n = an integer
P = momentum transferred to plate by impulsive force loading
$q = \sqrt{is}$ = a transform variable
$q_n (n = 1, 2, \ldots)$ = real zeros of $G(q)$
r = radial co-ordinate
s = a transform variable
$s_n = -iq_n^2$ = complex frequency
t = time
$u(r,t)$ = transverse deflection of plate
$w(\xi,\tau) = \dfrac{2\pi\sqrt{2h\rho_0 D}}{P}u(r,t)$ = dimensionless deflection of plate
$W(\xi,s)$ = Laplace transform of $w(\xi,\tau)$
$\Gamma(q)$ = a combination of φ_i defined by Equation [11]
δ = "δ-function," discussed in text
$\mu = m/2\pi h\rho_0 a^2$ = mass ratio, concentrated mass/plate mass
ν = Poisson's ratio
$\xi = r/a$ = dimensionless radial co-ordinate
$\rho(r)$ = density of plate (including effect of concentrated mass)
ρ_0 = intrinsic density of plate material
$\tau = t\sqrt{D/2h\rho_0 a^4}$ = dimensionless time
$\varphi_i(q)(i = 1,2,3)$ = special combinations of Bessel functions defined by Equations [6]
$\omega_n = q_n^2$ = natural frequencies of vibration
$\nabla_\nu^2 = \dfrac{\partial^2}{\partial\nu^2} + \dfrac{1}{\nu}\dfrac{\partial}{\partial\nu}$ = Laplacian operator, ν being any variable

Subscripts r, t, ξ, τ denote partial differentiation with respect to the variable indicated, and a prime denotes differentiation with respect to argument.

Introduction

Although problems of transverse vibrations of thin plates have received considerable attention in the last century, there are relatively few exact solutions known. The general methods of solution are well developed, but there is considerable labor in carrying through the details of solution for any given problem. Among the problems amenable to solution is that of the uniform circular plate, which was treated in 1850, by Kirchhoff.[2] The case of a circular plate carrying concentrated masses may be considered the simplest generalization to nonuniform plates, and does not seem to have been discussed. This paper presents a convenient method for the treatment of such a case, based upon the use of the Laplace transform. It solves the particular problem of a circular plate with free edges, which carries a concentrated mass at its center, and is struck an impulsive blow on this mass.

While classical methods of solution or solution by the methods of the Hankel transform may be used instead of the Laplace transform, the latter seems particularly useful applied to plates carrying concentrated masses when these masses are points or flexible lines of symmetry, e.g., radial line-masses, or circular line-masses concentric with the plate edge. Such concentrated masses may be represented by suitable density "δ-functions" added to the regular plate density, the treatment of which is easily encompassed by Laplace transform methods. Although there are advantages to this (density-impulse) point of view, especially in treating line-concentrated masses, it should be emphasized that from a logical standpoint the classical methods avoiding δ-functions are perhaps still to be preferred.

The purpose of the paper, aside from illustrating the general method of solution in which concentrated masses are replaced by density impulses, is to obtain a solution for the case mentioned. In particular, the natural frequencies of vibration are exhibited as functions of the magnitude of the concentrated mass, and the first mode shape for several values of mass ratio is displayed. An important physical conclusion is that the natural frequencies are relatively sensitive to changes in the concentrated mass, becoming more so for the higher frequencies.

The System

The δ-function which is introduced in giving explicit forms for $f(r,t)$ and $\rho(r)$ is often used in formulating physical problems,

---

[1] Mechanics Division, Naval Research Laboratory. Jun. ASME.

Contributed by the Applied Mechanics Division and presented at the Annual Meeting, New York, N. Y., November 26–December 1, 1950, of The American Society of Mechanical Engineers.

Discussion of this paper should be addressed to the Secretary, ASME, 29 West 39th Street, New York, N. Y., and will be accepted until October 10, 1951, for publication at a later date. Discussion received after the closing date will be returned.

Note: Statements and opinions advanced in papers are to be understood as individual expressions of their authors and not those of the Society. Manuscript received by ASME Applied Mechanics Division, March 30, 1950. Paper No. 50—A-24.

[2] "Über das Gleichgewicht und die Bewegung einer elastischer Scheibe," by G. Kirchhoff, *Journal für Math.* (Crelle), vol. 40, 1850, p. 51.

and its properties are described by a number of authors.[3] Although δ does not represent a true function, it is useful for describing a limiting integral behavior of a sequence of functions. This integral property

$$\int_a^b \delta(x-y)f(x)dx = f(y) \quad \text{if } a \leq y \leq b$$

is the only one of which use will be made here.

The assumptions required to describe the problem at hand are that:

1 The plate is circular.
2 Circular symmetry maintains during vibration.
3 An auxiliary mass m is concentrated at the center of the plate and exerts no effect upon the flexibility of the plate.
4 The initially quiescent plate is struck impulsively in the transverse direction at its center (i.e., on the concentrated mass), a total momentum P being imparted to the plate.
5 The usual linear thin-plate theory holds.
6 The edges of the plate are free.

The choice of these conditions has been motivated by an experimental arrangement in which they are closely approximated.

Assumptions 2, 5, and 6 imply[4] that the system of equations to be solved is

$$\left.\begin{aligned} &D\nabla_r^4 u(r,t) = f(r,t) - 2h\rho u_{tt}(r,t) \\ &[u_{rr}(r,t) + r^{-1}u_r(r,t)]_{r=a} = 0 \\ &[u_{rr}(r,t) + \nu a^{-1}u_r(r,t)]_{r=a} = 0 \end{aligned}\right\} \quad \ldots\ldots [1]$$

By virtue of assumption 3, an adequate representation of the concentrated mass is

$$\rho(r) = \rho_0 + \frac{m}{4\pi h}\frac{\delta(r)}{r} \quad \ldots\ldots [2]$$

It can be seen that this density function leads to a correct expression for total mass, and that it places the concentrated mass in the correct position. Moreover, the effect of the concentrated mass is not felt in any other way, since it is presumed not to change the flexibility of the plate.[5] Finally, the pressure on the plate under assumption 4 must be given by

$$f(r,t) = \frac{P\delta(r)\delta(t)}{2\pi r} \quad \ldots\ldots [3]$$

Clearly, with this representation, the blow is effectively a point force loading at the center of the plate, and is imparted impulsively at the initial instant of time. Also, P has the desired interpretation as total added momentum.

The dimensionless variables defined at the beginning of the section may now be used in Equations [1], [2], and [3], and the results combined to give as the system to be solved the set of equations

$$\left.\begin{aligned} &\nabla_\xi^4 w(\xi,\tau) = \delta(\xi)\delta(\tau)/\xi - [1 + \delta(\xi)\mu/2\xi]w_{\tau\tau}(\xi,\tau) \\ &[w_{\xi\xi}(\xi,\tau) + \xi^{-1}w_\xi(\xi,\tau)]_{\xi=1} = 0 \\ &[w_{\xi\xi}(\xi,\tau) + \nu w_\xi(\xi,\tau)]_{\xi=1} = 0 \end{aligned}\right\} \quad \ldots [4]$$

$$w(\xi,0) = w_\tau(\xi,0) = 0 \qquad \text{(by assumption 4)}$$

From considerations of space, only the barest outline of the solution of this system is given.

The Solution

Let $W(\xi,s)$ be the Laplace transform of $w(\xi,\tau)$, and transform Equations [4] term by term. The formal manipulation proceeds straightforward provided one recognizes that[6]

$$\mathfrak{L}^{-1}\left\{\frac{\ln\left(p+\sqrt{p^2+q^2}\right)}{\sqrt{p^2+q^2}}\right\} = J_0(q\xi)\ln q - \frac{\pi}{2}Y_0(q\xi)$$

$$\mathfrak{L}^{-1}\left\{\frac{\ln\left(p+\sqrt{p^2-q^2}\right)}{\sqrt{p^2-q^2}}\right\} = I_0(q\xi)\ln q + K_0(q\xi)$$

Letting $q = \sqrt{is}$, one finds

$$W(\xi,s) = AJ_0(q\xi) + BI_0(q\xi) - (1/2q^2)\,[1 - s^2W(0,s)\mu/2]\left[\frac{\pi}{2}Y_0(q\xi) + K_0(q\xi)\right] \quad \ldots [5]$$

To this must be adjoined a consistency relation

$$\lim_{\xi\to 0} W(\xi,s) = W(0,s) \qquad \text{(which implies } W(0,s) = A + B\text{)}$$

and the two transformed boundary conditions at the free edge.

In evaluating the constants A and B of Equation [5], it is convenient to introduce the functions

$$\left.\begin{aligned} \varphi_1(q) &= \frac{\pi}{2}\left[I_0(q)Y_1(q) + I_1(q)Y_0(q) - \frac{2}{q}(1-\nu)I_1(q)Y_1(q)\right] - \frac{1}{q} \\ \varphi_2(q) &= \left[J_1(q)K_0(q) - K_1(q)J_0(q) + \frac{2}{q}(1-\nu)J_1(q)K_1(q)\right] - \frac{1}{q} \\ \varphi_3(q) &= \left[I_1(q)J_0(q) + I_0(q)J_1(q) - \frac{2}{q}(1-\nu)I_1(q)J_1(q)\right] \end{aligned}\right\} \quad \ldots [6]$$

$$G(q) = \varphi_3(q) - \frac{\mu q^2}{4}[\varphi_1(q) + \varphi_2(q)] \quad \ldots\ldots [7]$$

$$H(\xi,q) = \varphi_1(q)J_0(q\xi) + \varphi_2(q)I_0(q\xi) - \varphi_3(q)\left[\frac{\pi}{2}Y_0(q\xi) + K_0(q\xi)\right] \quad \ldots\ldots [8]$$

In these terms, $W(\xi,s)$ assumes the form

$$W(\xi,s) = H(\xi,q)/2q^2G(q) \quad \ldots\ldots [9]$$

To invert the transform of Equation [8] and obtain the actual (dimensionless) plate displacement, the singularities of $W(\xi,s)$ must be considered. Although Y_0 and K_0 separately have logarithmic singularities, the only combinations of them which enter Equation [9] do not have. Neglecting the singularity at $q = 0$ is equivalent merely to neglecting the gross motion of the plate. The only singularities which need be considered are the simple poles at the zeros of $G(q)$. If q_n are real zeros, one can show that the only other zeros are iq_n. Thus the poles of $W(\xi, s)$ may be taken as $s_n = -iq_n^2$.

From the remarks of the last paragraph, it is an exercise to invert Equation [9] to obtain

$$w(\xi,\tau) = \sum_{n=1}^{\infty} -\frac{2}{q_n}\frac{H(\xi,q_n)}{G'(q_n)}\sin q_n^2\tau \quad \ldots\ldots [10]$$

[3] For example, "Operational Methods in Applied Mathematics," by H. D. Carslaw and J. C. Jaeger, second edition, Oxford University Press, 1947, chapt. 11.

[4] "Theory of Sound," by Lord Rayleigh, first American edition, Dover Publications, New York, N. Y., 1945. (See in particular, vol. 1, chapt. 10, pp. 356 and 359.)

[5] "Dictionary of Laplace Transforms," by J. Cossar and A. Erdelyi, Admiralty Computing Service, London, England; part 1, Reference No. SRE/AC8. 53, 1944; part 3A, Reference No. SRE/AC8. 102, 1945.

This solution describes an entire class of problems, since it is in dimensionless form. It fails to be a universal solution, however, in the sense that the q_n are functions of both μ and ν. From Equation [10], by the use of the convolution integral it is possible to find the response of the plate to a force (applied to the center of the plate) having an arbitrary functional form. Also, if desired, stresses and bending moments could be calculated from this equation.

Some Numerical Results and Conclusions

The value of ν to be considered is taken as $\nu = 0.3$ at the outset. The zeros $q_n(\mu)$ can be determined graphically by representing

$$\Gamma(q) = \frac{\varphi_3(q)}{q^3[\varphi_1(q) + \varphi_2(q)]} \quad \ldots\ldots\ldots\ldots [11]$$

as a function of q, and laying off the horizontal line $\Gamma(q) = \mu/4$. The intersections of these curves are at the values q_n. Actually, it is the natural frequencies $\omega_n(\mu) = q_n^2(\mu)$ which are of interest. These are displayed graphically as functions of μ for $n = 1, 2, 3, 4$,

TABLE 1 SOME NATURAL-FREQUENCY VALUES WITH ESTIMATES FROM AN ASYMPTOTIC EXPANSION OF G

	$\omega_n(\infty)$			$\omega_n(0)$		
n	Calculated value	Estimate $[(2n-1)\pi/2]^2$	Error of estimate, per cent	Calculated value	Estimate $[n\pi]^2$	Error of estimate, per cent
1	3.73	2.47	−33.8	9.006	9.87	+9.6
2	20.9	22.20	+ 6.2	38.44	39.48	+2.7
3	60.5	61.69	+ 1.9	87.76	88.83	+1.2
4	119.7	120.91	+ 1.0	156.75	157.90	+0.7
5		199.85			246.74	
6		298.56			355.32	
7		416.98			483.60	

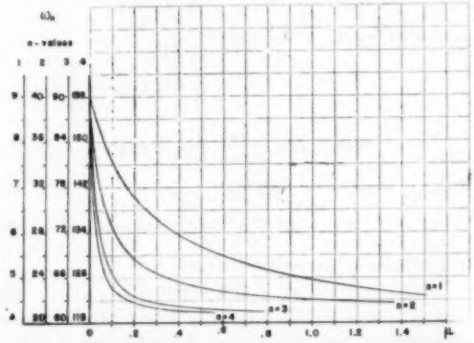

Fig. 1 Natural Frequency ω_n Versus Mass Ratio μ for Several Values of n

in Fig. 1. The first four values of $\omega_n(0)$ have been calculated more accurately by the Newton-Raphson method and their values[6] listed in Table 1, which also contains the values of $\omega_n(\infty)$, and the estimates of these values obtained by using one term of an asymptotic expansion of the Bessel functions composing $G(q)$.

Table 1 indicates that for $n > 4$, the asymptotic-expansion estimate of $\omega_n(\mu)$ may be entirely adequate for many purposes. Explicitly, this estimate may be obtained for any μ by finding the roots of the equation

$$\tan q = -\left(\frac{\pi\mu}{8}\right)q^3 \quad \ldots\ldots\ldots\ldots\ldots [12]$$

and squaring these roots to get ω_n.

An important physical conclusion from Fig. 1 is that the natural frequencies are very sensitive to changes in mass ratio, for μ near zero. This is especially true for the higher natural frequencies. It means that if masses, even small, are attached to a plate during an experimental investigation, its natural frequencies may be quite different from those of the unloaded plate. This

TABLE 2 $\left(\frac{\partial\omega_n}{\partial\mu}\right)_{\mu=0}$ AS A FUNCTION OF n

	$(\partial\omega_n/\partial\mu)_{\mu=0}$			Error in ω_n in assuming $\mu = 0$ when actually $\mu = 0.01$, per cent
n	Calculated	Asymptotic estimate	Error of asympt. estimate, per cent	
1	−18.17	−24.3	34.0	2.1
2	−190.2	−194.8	2.4	5.0
3	−647.8	−657.5	1.5	7.6
4	−1542	−1559	1.1	10.1
5		−3044		12.3
6		−5260		14.8
7		−8353		17.3

effect is shown quantitatively in Table 2, where the dependence upon n of $(\partial\omega/\partial\mu)_{\mu=0}$ is given, together with the estimates of

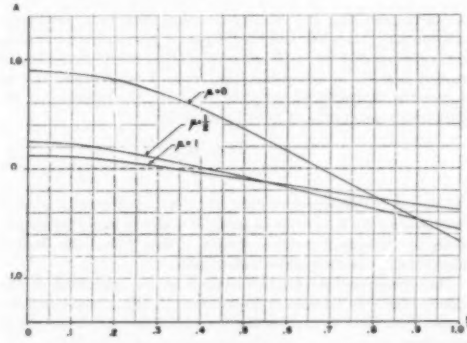

Fig. 2 First-Mode Shape for Several Values of μ

these derivatives made from Equation [12]. Also, this table records the errors in natural frequencies which would be made in assuming $\mu = 0$ when actually $\mu = 0.01$.

Finally, Fig. 2 shows the change in the first mode shape with μ. There, the amplitude function $A(\xi, q_n)$ is

$$A(\xi, q_n) = -2H(\xi, q_n)/q_n G'(q_n)$$

[6] These are not comparable to those of Poisson, since he used $\nu = 0.25$. See "Schwingungen elastischer Systeme . . .," by H. Lamb, *Encyklopadie der Math. Wiss.*, Teubner, Leipzig, Germany, IV^4 26, 1907.

Analysis of Straight and Curved Beam-Columns

By C. M. TYLER, JR.,[1] and J. G. CHRISTIANO,[2] PITTSBURGH, PA.

A method of analysis is developed for calculating the effects of deflection and axial force on the bending moments of structural members having both beam and column loadings. The member is divided into a number of segments and analyzed by a relaxation method directly in terms of the bending moments at each segment. This analysis is applicable to beam-columns of any shape and stiffness, and for any type of loading. A numerical example of an irregularly curved beam-column is included.

Nomenclature

The following nomenclature is used in the paper:

- s = length co-ordinate, measured along curve of centroidal axis
- l = length of curve of centroidal axis
- $M(s)$ = actual bending moment
- $W(s)$ = bending moment, treating member as a rigid body
- $P(s)$ = axial force acting on section normal to axis of member
- $\delta(s)$ = deflection normal to axis of member
- $E(s)$ = modulus of elasticity
- $A(s)$ = area of section normal to axis of member
- $I(s)$ = moment of inertia of section normal to axis of member
- $m(s, s')$ = bending moment at s' due to a unit dummy load applied at s at right angles to axis of member
- $p(s, s')$ = axial force due to unit dummy load

Method of Analysis

The bending moment at any point s of the axis of a beam-column may be expressed as

$$M(s) = W(s) + P(s)\delta(s) \quad \ldots\ldots\ldots\ldots\ldots [1]$$

By elastic energy theory (1)[3] the deflection is given by

$$\delta(s) = \int_0^l \frac{P(s')p(s,s')}{E(s')A(s')}\,ds' + \int_0^l \frac{M(s')m(s,s')}{E(s')I(s')}\,ds'$$

Substituting this expression in Equation [1], we obtain

$$M(s) = W(s) + P(s)\int_0^l \frac{P(s')p(s,s')}{E(s')A(s')}\,ds' + P(s)\int_0^l \frac{M(s')m(s,s')}{E(s')I(s')}\,ds' \quad \ldots\ldots [2]$$

For any specific problem $M(s)$ is the only unknown function in this equation.

Equation [2] can be solved by the relaxation method (2). With the member divided into n segments a finite-difference equivalent of Equation [2] is

$$M_j = W_j + P_j \sum_{i=1}^{n} \frac{P_i p_{ij}}{E_i A_i}\,\Delta s_i + P_j \sum_{i=1}^{n} \frac{M_i m_{ij}}{E_i I_i}\,\Delta s_i, \qquad j = 1, 2, \ldots n \quad \ldots\ldots [3]$$

These n linear algebraic equations in the unknown M_j may be solved simultaneously by any convenient means. They are particularly well adapted for solution by the relaxation process (3, 4), which briefly consists of

(*a*) Assuming any values for the unknown moments M_j.

(*b*) Calculating from these assumed moments how much each equation differs from an equality (residues).

(*c*) Reducing the value of the largest residue, say, of equation k, by altering the value of M_k (this changes all of the residues).

(*d*) Repeating (*c*) for the current value of the largest residue until all of the residues approach zero within the desired degree of accuracy.

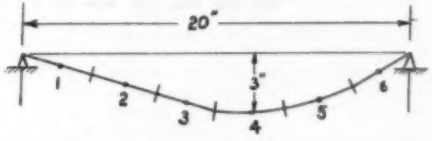

Fig. 1 Shape and Subdivisions of Example Beam-Column

As an example of the method consider a curved beam-column, Fig. 1, for which the values of Table 1 apply.

TABLE 1 PHYSICAL CONSTANTS, AXIAL FORCES, AND RIGID-BODY BENDING MOMENTS

Segment	Δs in.	I in.^{4}	A in.^{2}	E psi	P lb	W in-lb
1	3.76	0.083	1.00	10^7	8000	460
2	3.48	0.144	1.20	10^7	8000	1310
3	3.23	0.229	1.40	10^7	8500	2420
4	3.61	0.281	1.50	10^7	10500	3520
5	3.50	0.183	1.30	10^7	9900	1630
6	3.45	0.083	1.00	10^7	9500	590

In this case the second terms of Equations [3] are negligible compared with the others.

The m_{ij} coefficients due to the dummy loads (1) are tabulated in Table 2. The coefficients of the M_j with all of the terms transferred to the left side of Equations [3] are given in Table 3.

[1] Assistant Professor of Mechanical Engineering, Carnegie Institute of Technology. Jun. ASME.

[2] Assistant Professor of Mathematics, University of Pittsburgh.

[3] Numbers in parentheses refer to the Bibliography at the end of the paper.

Contributed by the Applied Mechanics Division and presented at the Annual Meeting, New York, N. Y., November 26–December 1, 1950, of The American Society of Mechanical Engineers.

Discussion of this paper should be addressed to the Secretary, ASME, 29 West 39th Street, New York, N. Y., and will be accepted until October 10, 1951, for publication at a later date. Discussion received after the closing date will be returned.

Note: Statements and opinions advanced in papers are to be understood as individual expressions of their authors and not those of the Society. Manuscript received at ASME Headquarters, May 12, 1950. Paper No. 50—A-11.

TABLE 2 m_{ij} COEFFICIENTS

Equation (j)	$i = 1$	2	3	4	5	6
1	1.696	1.341	1.013	0.672	0.376	0.107
2	1.341	3.93	2.97	1.967	1.100	0.314
3	1.013	2.97	4.78	3.17	1.772	0.506
4	0.780	1.439	3.38	4.89	2.85	0.827
5	0.442	1.232	2.02	2.89	3.81	1.170
6	0.134	0.374	0.603	0.882	1.200	1.558

As a starting point, values of M_j equal to W_j are used. An experienced computer could estimate better initial values from the coefficients of the equations. In Table 4 the residues are calculated and relaxed to zero by altering the assumed values of the M_j bending moments progressively.

Rounding off these values to agree with the initial accuracy of the data, the bending moments at the six points are 620, 1700, 2940, 4170, 2120, and 770, respectively.

BIBLIOGRAPHY

1 "Elastic Energy Theory," by J. A. Van Den Broek, second edition, John Wiley & Sons, Inc., New York, N. Y., 1942, pp. 8–10, 41–46, 64–68, 171–173.

2 "The Approximate Numerical Solution of the Non-Homogeneous Linear Fredholm Integral Equation by Relaxation Methods," by F. S. Shaw, *Quarterly of Applied Mathematics*, vol. 6, 1948, pp. 69–76.

3 "A Short Account of Relaxation Methods," by L. Fox, *The Quarterly Journal of Mechanics and Applied Mathematics*, vol. 1, 1948, pp. 253–280.

4 "Relaxation Methods in Engineering Science," by R. V. Southwell, Oxford University Press, New York, N. Y.; London, England 1940, pp. 11–16.

TABLE 3 COEFFICIENTS FOR EQUATIONS [3]

Equation (j)	$i = 1$	2	3	4	5	6	Const
1	0.9385	−0.0260	−0.0114	−0.0069	−0.0058	−0.0036	− 460
2	−0.0487	0.9239	−0.0335	−0.0203	−0.0168	−0.0104	−1310
3	−0.0396	−0.0616	0.9420	−0.0352	−0.0291	−0.0181	−2420
4	−0.0372	−0.0366	−0.0500	0.9356	−0.0572	−0.0362	−3520
5	−0.0199	−0.0295	−0.0282	−0.0369	0.9280	−0.0482	−1630
6	−0.0058	−0.0086	−0.0081	−0.0108	−0.0218	0.9384	− 590

TABLE 4 SOLUTION OF EQUATIONS [3]

Values of the M_j						Values of residues					
= 1	2	3	4	5	6	$j = 1$	2	3	4	5	6
						−460	−1310	−2420	−3520	−1630	−590
460						431.7	— 22.4	— 18.2	— 17.1	— 9.2	— 2.7
	1310					— 34.1	1210.3	— 80.7	— 47.9	— 38.7	— 11.3
		2420				— 37.6	— 81.1	2279.6	— 121.0	— 68.3	— 19.6
			3520			— 24.3	— 71.4	—123.8	3291.1	— 129.8	— 38.0
				1630		— 9.4	— 27.4	— 47.4	— 93.2	1512.6	— 35.5
					590	— 2.1	— 6.1	— 10.7	— 21.4	— 28.4	553.7
						—125.8	— 308.1	— 421.2	— 529.5	— 391.8	—142.4
			600			— 4.1	— 12.2	— 21.1	561.0	— 22.1	— 8.5
		500				— 5.7	— 16.7	471.0	— 25.6	— 14.1	— 4.0
				500		— 2.9	— 8.4	— 14.6	— 28.6	464.0	— 10.9
	400					— 10.4	389.6	— 24.6	— 14.6	— 11.8	— 3.4
					200	— 0.7	— 2.1	— 3.6	— 7.2	— 9.6	187.7
200						187.7	— 9.7	— 7.9	— 7.4	— 4.0	— 1.2
						38.1	12.4	— 22.0	— 51.9	10.6	18.3
			55			— 0.4	— 1.1	— 1.9	51.4	— 2.0	— 0.6
—40						— 37.5	1.9	1.6	1.5	0.8	0.2
		24				— 0.3	— 0.8	22.6	— 1.2	— 0.7	— 0.2
					—19	0.1	0.2	0.3	0.7	0.9	— 17.8
	—14					0.4	— 12.9	0.9	0.5	0.4	0.1
				—11		0.1	0.2	0.3	0.6	— 10.2	0.3
						0.5	— 0.1	1.8	1.6	— 0.2	0.3
		— 2				0.0	0.1	— 1.9	0.1	0.1	0.0
			—2			0.0	0.0	0.1	— 1.9	0.1	0.0
620	1698	2942	4173	2119	771	0.5	0.0	0.0	— 0.2	0.0	0.3

Sinusoidal Torsional Buckling of Bars of Angle Section Under Bending Loads, as a Problem in Plate Theory[1]

By H. J. PLASS, JR.,[2] STANFORD, CALIF.

Timoshenko has applied plate theory to each leg of an angle-section bar to determine the critical compressive load needed to cause sinusoidal torsional buckling. In this paper his idea is used to calculate the critical bending load needed to cause sinusoidal torsional buckling of an angle bar. The bending is assumed to be applied so that the extreme fibers of the angle are in compression, the vertex in tension. Approximate results are first obtained by means of the Rayleigh-Ritz method. The approximate deflection functions from which the energy terms are computed are based upon certain infinite-series solutions. After having obtained approximate results, exact values are obtained, using the approximate values as a guide to limit the amount of calculation. The results of this calculation are shown in Fig. 5, where they are compared with those predicted by bar theory. Differences between the two theories become more noticeable as the bar becomes short compared to its flange width. It is found that the critical bending load becomes larger very rapidly as the ratio of length to width of the flanges decreases. Bar theory predicts no such increase. The reason for this difference is explained.

Nomenclature

The following nomenclature is used in the paper:

a = length of plate
a_3, a_4, a_7, a_8 = const, Equation [19]
A = area of cross section of bar
$A_1, A_2, \ldots$ = series coefficients in Equations [33] and [34]
b = width of plate
$B_1, B_2, \ldots$ = series coefficients in Equations [33] and [34]
c = an adjustable parameter, Equation [18]
C = torsion constant for bar
C_1, C_2 = const, Equation [10]
D = flexural rigidity of plate = $\dfrac{Et^3}{12(1-\nu^2)}$
E = Young's modulus
$f(\eta)$ = a polynomial, Equation [19]
$F(\eta)$ = a function describing shape of cross section for buckled angle bar
$F_1(\eta), F_2(\eta)$ = two functions whose linear combination gives $F(\eta)$
G = shear modulus
$I_1, \ldots, I_5$ = integrals defined by Equations [25c]
I_x = moment of inertia of section about axis parallel to X-axis through centroid (Fig. 4)
I_y = moment of inertia of section about Y-axis (Fig. 4)
k = factor in expression for critical load; $N_o = k\dfrac{\pi^2 D}{b^2}$
k_a = approximate value of k
K = integral defined in Equation [16]
K_a = approximate value of K
M_B = critical bending moment, Equation [51]
n = an integer
N_o = maximum value of bending load per unit width of plate (Fig. 2)
N_{oa} = approximate value of N_o
$p = 2(\alpha b)^2$
$P_n = \dfrac{n^2\pi^2 EI_x}{a^2}$
$q = (\alpha b)^4 + \pi^2(\alpha b)^2$
$r = 2\pi^2 k(\alpha b)^2$
t = thickness of plate
$T_n = \left[E\Gamma\dfrac{n^2\pi^2}{a^2} + GC\right]/\rho^2$
u = deflection of angle bar in lateral direction (X-direction in Fig. 4)
U = strain energy integral, Equation [16]
U_a = approximate value of U
w = deflection of middle surface of plate
w_a = approximate value of w
x = X-co-ordinate
y = Y-co-ordinate
y_0 = Y-co-ordinate of centroid of angle section
$\alpha = \dfrac{\pi}{a}$
β = angle of rotation of section of angle bar, Equation [50]
Γ = warping constant
δ = increment notation, Equation [14]
Δ = a determinant, Equation [13]
$\eta = \dfrac{y}{b}$
$\kappa_2 = \int\int_A y(x^2 + y^2)dA - y_0 A\rho^2$
$\mu_2 = -M_B/I_x$
ν = Poisson's ratio
ρ = radius of gyration of angle section about Z-axis (Fig. 4)
$\phi(\eta)$ = a function defined by Equation [19]
$\Phi_1, \ldots, \Phi_5$ = integrals defined by Equations [25a]
$\Psi_1, \ldots, \Psi_5$ = integrals defined by Equations [25b]

---

[1] This paper presents results obtained in research carried out under contract N6-ONR-251 T.O. 12 (NR-035-241) between the Office of Naval Research and Stanford University, under the direction of J. N. Goodier.

[2] Research Assistant, Division of Engineering Mechanics, Stanford University.

Contributed by the Applied Mechanics Division and presented at the Annual Meeting, New York, N. Y., November 26–December 1, 1950, of The American Society of Mechanical Engineers.

Discussion of this paper should be addressed to the Secretary, ASME, 29 West 39th Street, New York, N. Y., and will be accepted until October 10, 1951, for publication at a later date. Discussion received after the closing date will be returned.

Note: Statements and opinions advanced in papers are to be understood as individual expressions of their authors and not those of the Society. Manuscript received by ASME Applied Mechanics Division, March 25, 1950. Paper No. 50—A-15.

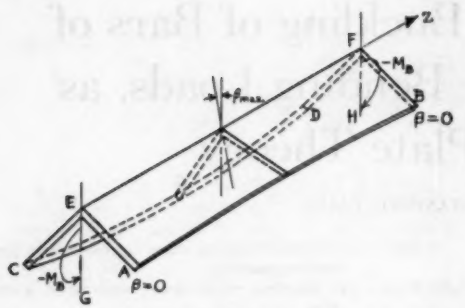

FIG. 1 SINUSOIDAL TORSIONAL BUCKLING OF ANGLE BAR UNDER BENDING LOADS

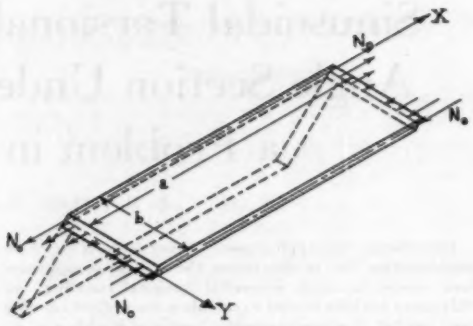

FIG. 2 DETAILS OF LOADING FOR ANGLE BAR IN BENDING

INTRODUCTION

When the walls of an angle bar are thin enough, the bar may buckle torsionally when it is subjected to bending loads such that the compressive part of the bending stress exists at the extreme fibers of the angle. Fig. 1 shows this kind of buckling. The problem of finding the critical bending moment and the buckling deformation has been solved by means of bar theory[3] for various end conditions. The deformation of the bar, if it is weaker torsionally than in bending, is expressed by means of the angle of rotation of a section, $\beta(z)$, as a function of z, the axial distance. Timoshenko[4] introduced the idea of using plate theory to solve the problem of torsional buckling of an angle bar under thrust. Each leg of the angle was treated as a plate, the vertex EF being assumed to be a simply supported edge. He also assumed that the ends AE, FB, CE, DF of the bar were simply supported, and that the extreme edges AB and CD, Fig. 1, are free.

In this paper a similar calculation is made, assuming the same boundary conditions, but a different load. A linear distribution of stress over the section is assumed such that the resultant is a pure bending moment $-M_B$, in the plane $EFGH$, Fig. 1. A more detailed idea is given in Fig. 2. In order to find the critical load and buckled form exactly, it is necessary to solve a fourth-order ordinary eigenvalue differential equation with a variable coefficient. Immediate application of this method results in the necessity for extensive tables of certain functions expressed as infinite series. The quantity of calculation can be reduced if a good approximation to the eigenvalues is known. For this reason a preliminary calculation is made using the Rayleigh-Ritz method to obtain approximate eigenvalues. The choice of approximate buckling deflection functions used in the Rayleigh-Ritz calculation is guided by the form of the infinite series solutions. Kollbrunner[5] has used other approximate functions in solving similar plate-buckling problems. However, the functions he has used do not satisfy the boundary conditions for the free edge. After the approximate eigenvalues are obtained, they are used as a guide to limit the amount of calculation needed for the exact eigenvalues found; comparison of the approximate values with these shows that there is very little error in the approximation.

[3] "Flexural-Torsional Buckling of Bars of Open Section," by J. N. Goodier, Bulletin No. 28, Cornell University Engineering Experiment Station, January, 1942.

[4] "Theory of Elastic Stability," by S. Timoshenko, "McGraw-Hill Book Company, Inc., New York, N. Y., 1936, p. 337.

[5] "Theoretische Beuluntersuchungen der T. K. V. S. B. im Jahre 1947," by C. F. Kollbrunner, *Schweizerische Bauzeitung*, vol. 66, 1948, pp. 146–149.

APPLICATION OF PLATE THEORY

We shall consider only one flange of the angle bar and choose a co-ordinate system as shown in Fig. 2.

Let b = width of plate
a = length of plate
N_o = maximum value of bending load per unit width of plate
w = deflection of middle surface of plate

The deflection w satisfies the partial differential equation

$$D\left[\frac{\partial^4 w}{\partial x^4} + 2\frac{\partial^4 w}{\partial x^2 \partial y^2} + \frac{\partial^4 w}{\partial y^4}\right] = N_o\left(1 - 2\frac{y}{b}\right)\frac{\partial^2 w}{\partial x^2} \quad \ldots [1]$$

where D = flexural rigidity of plate

$$= \frac{Et^3}{12(1-\nu^2)}$$

E = Young's modulus
ν = Poisson's ratio

Assume that the edges $x = 0$, $x = a$, $y = 0$ are simply supported, and $y = b$ is free. Then the boundary conditions which w must satisfy are as follows:

For the simply supported edges

$$\left.\begin{aligned} &w(0, y) = 0,\ w(a, y) = 0,\ w(x, 0) = 0 \\ &\frac{\partial^2 w}{\partial x^2} + \nu\frac{\partial^2 w}{\partial y^2} = 0 \quad \text{for } x = 0,\ x = a \\ &\frac{\partial^2 w}{\partial y^2} + \nu\frac{\partial^2 w}{\partial x^2} = 0 \quad \text{for } y = 0 \end{aligned}\right\} \quad \ldots\ldots [2]$$

For the free edge, $y = b$

$$\left.\begin{aligned} &\frac{\partial^2 w}{\partial y^2} + \nu\frac{\partial^2 w}{\partial x^2} = 0 \\ &\frac{\partial^3 w}{\partial y^3} + (2-\nu)\frac{\partial^3 w}{\partial x^2 \partial y} = 0 \end{aligned}\right\} \quad \ldots\ldots [3]$$

We assume a solution to Equation [1] of the form

$$w = w_0 \sin\frac{\pi x}{a} F\left(\frac{y}{b}\right) \quad \ldots\ldots [4]$$

When Equation [4] is substituted into Equation [1], we find that if Equation [4] is a solution, it is necessary that the function F satisfy the following ordinary differential equation

$$F^{IV}(\eta) - 2(\alpha b)^2 F''(\eta) + \left[(\alpha b)^4 + \frac{N_x b^2}{D}(\alpha b)^2 (1 - 2\eta)\right] F(\eta) = 0 \quad \ldots\ldots [5]$$

where

$$\eta = \frac{y}{b}, \alpha = \frac{\pi}{a}$$

and where

$$F'(\eta) = \frac{dF(\eta)}{d\eta}, F''(\eta) = \frac{d^2F(\eta)}{d\eta^2}, \text{ etc.}$$

The function, Equation [4], automatically satisfies the boundary conditions at $x = 0, x = a$. The other boundary conditions become conditions on $F(\eta)$. These are

$$\left.\begin{aligned} &F(0) = 0, F''(0) = 0 \\ &F''(1) - \nu(\alpha b)^2 F(1) = 0 \\ &F'''(1) - (2 - \nu)(\alpha b)^2 F'(1) = 0 \end{aligned}\right\} \quad \ldots\ldots [6]$$

It is possible to satisfy the differential Equation [5] and the boundary conditions, Equations [6], with a non-vanishing solution $F(\eta)$ provided that the correct value of N_x is chosen (critical value). Let $N_x = k(\pi^2 D/b^2)$. Furthermore, let

$$p = 2(\alpha b)^2$$
$$q = (\alpha b)^4 + \pi^2 k(\alpha b)^2$$
$$r = 2\pi^2 k(\alpha b)^2$$

With these abbreviations, Equation [5] becomes

$$F^{IV}(\eta) - pF''(\eta) + (q - r\eta)F(\eta) = 0 \quad \ldots\ldots [7]$$

and the boundary conditions, Equation [6], become

$$\left.\begin{aligned} &F(0) = F''(0) = 0 \\ &F''(1) - \nu\frac{p}{2}F(1) = 0 \\ &F'''(1) - (2 - \nu)\frac{p}{2}F'(1) = 0 \end{aligned}\right\} \quad \ldots\ldots [8]$$

It is possible to find solutions in the form of power series in η. Two such solutions which satisfy the conditions $F(0) = F''(0) = 0$ are

$$\left.\begin{aligned} F_1(\eta) &= \eta - \frac{q}{5!}\eta^5 + \frac{2r}{6!}\eta^6 - \frac{pq}{7!}\eta^7 + \frac{2pr}{8!}\eta^8 + \ldots \\ F_2(\eta) &= \frac{\eta^3}{3!} + \frac{p}{5!}\eta^5 + \frac{1}{7!}(p^2 - q)\eta^7 + \frac{4r}{8!}\eta^8 + \ldots \end{aligned}\right\} \quad \ldots\ldots [9]$$

Two other linearly independent solutions exist, but they do not satisfy the conditions $F(0) = F''(0) = 0$. To satisfy the other conditions (i.e., those at $\eta = 1$), it is necessary to form a linear combination of F_1 and F_2, thus

$$F(\eta) = C_1F_1(\eta) + C_2F_2(\eta) \quad \ldots\ldots [10]$$

Substitution of this combination into Equations [8] results in two linear homogeneous equations in C_1 and C_2. In order that these coefficients do not both vanish, it is necessary that their determinant be zero. This determinant depends upon the number k, which determines the critical load. Thus k can be found, and also the ratio C_1/C_2.

The details of this method will now be outlined. The last two boundary conditions of Equations [8] are

$$\left.\begin{aligned} &F''(1) - \nu\frac{p}{2}F(1) = 0 \\ &F'''(1) - (2 - \nu)\frac{p}{2}F'(1) = 0 \end{aligned}\right\} \quad \ldots\ldots [11]$$

Substitution of Equation [10] into [11] results in

$$\left.\begin{aligned} &C_1\left\{F_1''(1) - \nu\frac{p}{2}F_1(1)\right\} + C_2\left\{F_2''(1) - \nu\frac{p}{2}F_2(1)\right\} = 0 \\ &C_1\left\{F_1'''(1) - (2 - \nu)\frac{p}{2}F_1'(1)\right\} + C_2\left\{F_2'''(1) - (2 - \nu)\frac{p}{2}F_2'(1)\right\} = 0 \end{aligned}\right\} \quad [12]$$

The quantities in brackets depend on p, q, and r, hence on k and αb through the series, Equations [9]. If we are given the value of αb and wish to find k, we must find the value of k which makes the following determinant vanish:

Thus

$$\Delta = \begin{vmatrix} \left\{F_1''(1) - \nu\frac{p}{2}F_1(1)\right\} & \left\{F_2''(1) - \nu\frac{p}{2}F_2(1)\right\} \\ \left\{F_1'''(1) - (2 - \nu)\frac{p}{2}F_1'(1)\right\} & \left\{F_2'''(1) - (2 - \nu)\frac{p}{2}F_2'(1)\right\} \end{vmatrix} = 0 \quad \ldots\ldots [13]$$

The dependence of Δ on k is very complicated. In order to find the value of k which makes $\Delta = 0$, it is necessary to construct a table of functions F_1 and F_2 and their derivatives for various values of αb and k so that a table of values of Δ can be made. If we know approximately the values of k as a function of αb, then the amount of labor in the construction of this table is greatly reduced. The Rayleigh-Ritz method will be used in finding approximations for k.

Approximation Method

When buckling occurs, the work done by the end forces (the forces in this case form a bending moment) is equal to the increase in strain energy of the buckled form over that of the straight form. Expressed mathematically this is

$$N_x \int_0^b \left(1 - 2\frac{y}{b}\right)\delta u(y)\, dy = \int_0^a \int_0^b W(x, y) dy\, dx \quad \ldots [14]$$

where $\delta u(y)$ = decrease in distance between the ends due to buckling. It depends on y; $W(x, y)$ = strain energy per unit area of the plate due to buckling deformations.

Equation [14] can be expressed also as

$$N_x = \frac{U}{K} \quad \ldots\ldots [15]$$

where

$$U = \int_0^a \int_0^b W(x, y) dy\, dx = \frac{D}{2}\int_0^a \int_0^b \left\{\left(\frac{\partial^2 w}{\partial x^2} + \frac{\partial^2 w}{\partial y^2}\right)^2 - 2(1 - \nu)\left[\frac{\partial^2 w}{\partial x^2}\frac{\partial^2 w}{\partial y^2} - \left(\frac{\partial^2 w}{\partial xy\,\partial}\right)^2\right]\right\} dy dx \quad \ldots [16]$$

$$K = \frac{1}{2}\int_0^a \int_0^b \left(2\frac{y}{b} - 1\right)\left(\frac{\partial w}{\partial x}\right)^2 dy\,dx \quad \ldots\ldots [17]$$

It is assumed here that $w(x, y)$, the true deflection function, is known, so that U and K can be computed exactly. However, this is not the case.

It can be shown that if a function slightly different from $w(x, y)$, is chosen and substituted into Equations [16] and [17], and the ratio of U to K found, that the value of the ratio will always be larger than that corresponding to the true deflection function. In other words, U/K is a minimum when the deflection function is the natural one.

This idea is the basis for the Rayleigh-Ritz approximation method. Instead of considering all possible functions for the deflection, a certain class of functions characterized by a finite number of parameters is considered. It is assumed that by exercising careful judgment (based on physical intuition or experiment) in picking a class of functions, a good approximation to the true deflection can be obtained by adjusting the parameters so that U/K is a minimum for the class of functions chosen. In computing approximate values in this paper, only one adjustable parameter is used. The details of the calculation are as follows:

Let

w_a = approximate (guessed) deflection function containing one adjustable parameter c
U_a = value of U when w_a is used in Equation [16]
K_a = value of K when w_a is used in Equation [17]

$$N_{ca} = \left(\frac{U_a}{K_a}\right)_{\min} \text{ (minimum with respect to } c)$$

The form of w_a will be chosen using the series solution, Equations [9] as a guide.

Let

$$w_a(x, y) = w_0 \sin \alpha x\,[f(\eta) + c\phi(\eta)] \quad \ldots\ldots [18]$$

where

$f(\eta)$ and $\phi(\eta)$ are the polynomials

$$\left.\begin{aligned} f(\eta) &= \eta + a_3\eta^3 + a_5\eta^5 \\ \phi(\eta) &= \eta^4 + a_7\eta^7 + a_8\eta^8 \end{aligned}\right\} \quad \ldots\ldots [19]$$

and where the coefficients a_3, a_5, a_7, a_8 are chosen so that $f(\eta)$ and $\phi(\eta)$ both satisfy the conditions that the edge $y = b$, i.e., $\eta = 1$, be free. These conditions are (see Equations [8])

$$\left.\begin{aligned} f''(1) - \nu(\alpha b)^2 f(1) &= 0 \\ f'''(1) - (2-\nu)(\alpha b)^2 f'(1) &= 0 \end{aligned}\right\} \quad \ldots\ldots [20a]$$

$$\left.\begin{aligned} \phi''(1) - \nu(\alpha b)^2 \phi(1) &= 0 \\ \phi'''(1) - (2-\nu)(\alpha b)^2 \phi'(1) &= 0 \end{aligned}\right\} \quad \ldots\ldots [20b]$$

Substitution of Equations [19] into [20a] and [20b] yields the following values for a_3, a_5, a_7, a_8

$$\left.\begin{aligned} a_3 &= \frac{-(20 - 40\nu)(\alpha b)^2 - 2\nu(2-\nu)(\alpha b)^4}{120 + (50 - 42\nu)(\alpha b)^2 + \nu(2-\nu)(\alpha b)^4} \\ a_5 &= \frac{(6 - 6\nu)(\alpha b)^2 + \nu(2-\nu)(\alpha b)^4}{120 + (30 - 42\nu)(\alpha b)^2 + \nu(2-\nu)(\alpha b)^4} \end{aligned}\right\} \quad \ldots\ldots [21]$$

$$\left.\begin{aligned} a_7 &= \frac{-3360 - (192 - 312\nu)(\alpha b)^2 - 2\nu(2-\nu)(\alpha b)^4}{2352 + (112 - 182\nu)(\alpha b)^2 + \nu(2-\nu)(\alpha b)^4} \\ a_8 &= \frac{1260 + (84 - 132\nu)(\alpha b)^2 + \nu(2-\nu)(\alpha b)^4}{2352 + (112 - 182\nu)(\alpha b)^2 + \nu(2-\nu)(\alpha b)^4} \end{aligned}\right\} \quad [22]$$

Substitution of Equation [18] into [16] and [17], and making use of Equations [21] and [22], results in the following expressions for U_a and K_a

$$U_a = w_0^2\left(\frac{ab}{\pi}\right)\left(\frac{\pi^2 D}{b^2}\right)\left\{\left[\frac{1}{4(\alpha b)^2}I_1 + \frac{(\alpha b)^2}{4}I_2 - \frac{\nu}{2}I_3 + \frac{1-\nu}{2}I_4\right] + c\left[\frac{1}{2(\alpha b)^2}\Phi_1 + \frac{(\alpha b)^2}{2}\Phi_2 - \frac{\nu}{2}\Phi_3 + (1-\nu)\Phi_4\right] + c^2\left[\frac{1}{4(\alpha b)^2}\Psi_1 + \frac{(\alpha b)^2}{4}\Psi_2 - \frac{\nu}{2}\Psi_3 + \frac{1-\nu}{2}\Psi_4\right]\right\} \quad [23]$$

$$K_a = w_0^2\left(\frac{ab}{\pi}\right)\left(\frac{\pi^2}{4}\right)\{I_5 + 2c\Phi_5 + c^2\Psi_5\} \quad \ldots\ldots [24]$$

The definitions of the Φ, Ψ, and I are

$$\left.\begin{aligned} \Phi_1 &= \int_0^1 f''(\eta)\,\phi''(\eta)\,d\eta \\ \Phi_2 &= \int_0^1 f(\eta)\,\phi(\eta)\,d\eta \\ \Phi_3 &= \int_0^1 [f(\eta)\,\phi''(\eta) + f''(\eta)\,\phi(\eta)]\,d\eta \\ \Phi_4 &= \int_0^1 f'(\eta)\phi'(\eta)\,d\eta \\ \Phi_5 &= \int_0^1 (2\eta - 1)\,f(\eta)\,\phi(\eta)\,d\eta \end{aligned}\right\} \quad \ldots [25a]$$

$$\left.\begin{aligned} \Psi_1 &= \int_0^1 [\phi''(\eta)]^2\,d\eta \\ \Psi_2 &= \int_0^1 [\phi(\eta)]^2\,d\eta \\ \Psi_3 &= \int_0^1 2\,\phi(\eta)\,\phi''(\eta)\,d\eta \\ \Psi_4 &= \int_0^1 [\phi'(\eta)]^2\,d\eta \\ \Psi_5 &= \int_0^1 (2\eta - 1)\,[\phi(\eta)]^2\,d\eta \end{aligned}\right\} \quad \ldots\ldots [25b]$$

$$\left.\begin{aligned} I_1 &= \int_0^1 [f''(\eta)]^2\,d\eta \\ I_2 &= \int_0^1 [f(\eta)]^2\,d\eta \\ I_3 &= \int_0^1 f(\eta)f''(\eta)\,d\eta \\ I_4 &= \int_0^1 [f'(\eta)]^2\,d\eta \\ I_5 &= \int_0^1 (2\eta - 1)\,[f(\eta)]^2\,d\eta \end{aligned}\right\} \quad \ldots\ldots [25c]$$

In terms of the coefficients a_3, a_5, a_7, a_8, the Φ, Ψ, and I are

$$\left.\begin{aligned} \Phi_1 &= a_3[30 + 36a_7 + 42a_8] + a_5\left[75 + \frac{280}{3}a_7 + 112a_8\right] \\ \Phi_2 &= \left[\frac{1}{8} + \frac{1}{9}a_7 + \frac{1}{10}a_8\right] + a_3\left[\frac{1}{10} + \frac{1}{11}a_7 + \frac{1}{12}a_8\right] + a_5\left[\frac{1}{12} + \frac{1}{13}a_7 + \frac{1}{14}a_8\right] \\ \Phi_3 &= [5 + 6a_7 + 7a_8] + a_3\left[\frac{9}{2} + \frac{48}{9}a_7 + \frac{31}{5}a_8\right] + a_5\left[5 + \frac{62}{11}a_7 + \frac{76}{12}a_8\right] \\ \Phi_4 &= [1 + a_7 + a_8] + a_3\left[\frac{9}{4} + \frac{7}{3}a_7 + \frac{12}{5}a_8\right] + a_5\left[3 + \frac{35}{11}a_7 + \frac{10}{3}a_8\right] \\ \Phi_5 &= \left[\frac{7}{72} + \frac{4}{45}a_7 + \frac{9}{110}a_8\right] + a_3\left[\frac{9}{110} + \frac{5}{66}a_7 + \frac{11}{156}a_8\right] + a_5\left[\frac{11}{156} + \frac{6}{91}a_7 + \frac{13}{210}a_8\right] \end{aligned}\right\} \quad [26]$$

$$
\left.\begin{aligned}
\Psi_1 &= 100 + 232\,a_7 + \frac{3360}{11}\,a_8 + \frac{1764}{11}\,a_7^2 + 392\,a_7a_8 + \frac{3136}{13}\,a_8^2 \\
\Psi_2 &= \frac{1}{13} + \frac{1}{7}\,a_7 + \frac{2}{15}\,a_8 + \frac{1}{15}\,a_7^2 + \frac{1}{8}\,a_7\,a_8 + \frac{1}{17}\,a_8^2 \\
\Psi_3 &= \frac{60}{11} + 12\,a_7 + \frac{172}{13}\,a_8 + \frac{84}{13}\,a_7^2 + 14\,a_7a_8 + \frac{112}{15}\,a_8^2 \\
\Psi_4 &= \frac{36}{11} + 7\,a_7 + \frac{96}{13}\,a_8 + \frac{49}{13}\,a_7^2 + 8\,a_7a_8 + \frac{64}{15}\,a_8^2 \\
\Psi_5 &= \frac{6}{91} + \frac{13}{105}\,a_7 + \frac{7}{60}\,a_8 + \frac{7}{120}\,a_7^2 + \frac{15}{136}\,a_7a_8 + \frac{8}{153}\,a_8^2
\end{aligned}\right\} \quad \ldots [27]
$$

$$
\left.\begin{aligned}
I_1 &= 12\,a_8^2 + 48\,a_7a_8 + \frac{400}{7}\,a_8^2 \\
I_2 &= \frac{1}{3} + \frac{2}{5}\,a_8 + \frac{2}{7}\,a_8 + \frac{1}{7}\,a_8^2 + \frac{2}{9}\,a_8a_8 + \frac{1}{11}\,a_8^2 \\
I_3 &= 2\,a_8 + 4\,a_8 + \frac{6}{5}\,a_8^2 + \frac{26}{7}\,a_8a_8 + \frac{20}{9}\,a_8^2 \\
I_4 &= 1 + 2\,a_8 + 2\,a_8 + \frac{9}{5}\,a_8^2 + \frac{30}{7}\,a_8a_8 + \frac{25}{9}\,a_8^2 \\
I_5 &= \frac{1}{6} + \frac{4}{15}\,a_8 + \frac{3}{14}\,a_8 + \frac{3}{28}\,a_8^2 + \frac{8}{45}\,a_8a_8 + \frac{5}{66}\,a_8^2
\end{aligned}\right\} \quad \ldots [28]
$$

It is necessary to set

$$\frac{\partial}{\partial c}\left(\frac{U_a}{K_a}\right) = 0$$

to find the value of c which makes U_a/K_a a minimum (or maximum). This leads to a quadratic in c

$$
\begin{aligned}
c^2\,(\Psi_5 L_3 - 2\,\Psi_3 L_5) + c\,(2\Psi_5 L_1 - 2\,I_3 L_5) \\
+ (2\,\Psi_3 L_1 - I_5 L_3) = 0 \quad \ldots [29]
\end{aligned}
$$

where

$$
\left.\begin{aligned}
L_1 &= \frac{1}{4(\alpha b)^2}\,I_1 + \frac{(\alpha b)^2}{4}\,I_3 - \frac{\nu}{2}\,I_3 + \frac{1-\nu}{2}\,I_4 \\
L_2 &= \frac{1}{2(\alpha b)^2}\,\Phi_1 + \frac{(\alpha b)^2}{2}\,\Phi_2 - \frac{\nu}{2}\,\Phi_3 + (1-\nu)\Phi_4 \\
L_3 &= \frac{1}{4(\alpha b)^2}\,\Psi_1 + \frac{(\alpha b)^2}{4}\,\Psi_2 - \frac{\nu}{2}\,\Psi_3 + \frac{1-\nu}{2}\,\Psi_4
\end{aligned}\right\} \quad . [30]
$$

Two values of c result from solving Equation [29]. One of these makes U_a/K_a a minimum; the other makes it a maximum. The minimum value is the approximate critical load N_{aa}. From Equations [23] and [24] it can be seen that N_{aa} can be written

$$N_{aa} = k_a\left(\frac{\pi^2 D}{b^2}\right) \quad \ldots [31]$$

where

$$k_a = \frac{4}{\pi^2}\left[\frac{\text{bracket of [23]}}{\text{bracket of [24]}}\right]_{\min} \quad \ldots [32]$$

Computations have been made for k_a as a function of αb (i.e., $\pi b/a$) for various values of αb between 0 and 2. The value of ν was assumed to be 0.30. The results of these computations are shown on the curve labeled "k_a, approximate" in Fig. 3.

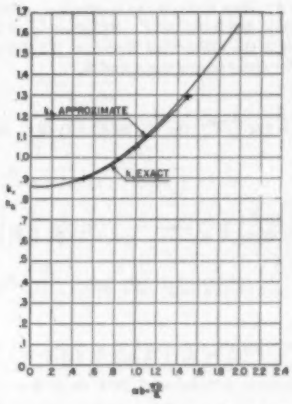

FIG. 3 CRITICAL LOAD FACTOR AS A FUNCTION OF $\frac{\pi b}{a}$, b BEING THE WIDTH, a THE LENGTH

Approximate and exact values are shown, the approximate values having been obtained by means of the Rayleigh-Ritz method.)

EXACT SOLUTION

If the approximate values just discussed are in error only by a small amount, the necessary tables of functions mentioned in the previous section can be abbreviated greatly. For a given value of αb we refer to the curve for k_a versus αb in Fig. 3, and pick several values of k above and below this value. For these values of k, we compute the values of $F_1(1)$, $F_2(1)$, $F_1'(1)$, $F_2'(1)$, $F_1''(1)$, $F_2''(1)$, $F_1'''(1)$, $F_2'''(1)$ by means of the infinite series, Equations [9]; the exact method of computation will be outlined in the next paragraph. After these are evaluated, the value of Δ is computed from Equations [13], for these values of k. By interpolation the value of k which makes $\Delta = 0$ is found.

We shall now outline the details of the computation. Note that Equations [9] can be used directly to calculate $F_1(1)$, $F_2(1)$, $F_1'(1)$, etc., provided that enough terms of the series are known to give the desired accuracy. The principal difficulty in this approach is that the coefficients in the power series for higher powers of η than those in Equations [9] are complicated algebraic expressions in p, q, and r. Since the series, especially the third-derivative series, is rather slowly convergent, it is simpler to apply certain recursion formulas numerically. Thus the arrangement of the mathematics which follows is merely a convenient one for computation, not one to aid in understanding the problem theoretically. The procedure is as follows:

Let

$$
\left.\begin{aligned}
F_1(\eta) &= \eta[A_0 + A_1\eta + A_2\eta^2 + \ldots] \\
F_1'(\eta) &= A_0' + A_1'\eta + A_2'\eta^2 + A_3'\eta^3 + \ldots \\
F_1''(\eta) &= A_0'' + A_1''\eta + A_2''\eta^2 + A_3''\eta^3 + \ldots \\
F_1'''(\eta) &= A_0''' + A_1'''\eta + A_2'''\eta^2 + A_3'''\eta^3 + \ldots
\end{aligned}\right\} \quad [33]
$$

and

$$
\left.\begin{aligned}
F_2(\eta) &= \eta^3\,[B_0 + B_1\eta + B_2\eta^2 + \ldots] \\
F_2'(\eta) &= B_0' + B_1'\eta + B_2'\eta^2 + B_3'\eta^3 + \ldots \\
F_2''(\eta) &= B_0'' + B_1''\eta + B_2''\eta^2 + B_3''\eta^3 + \ldots \\
F_2'''(\eta) &= B_0''' + B_1'''\eta + B_2'''\eta^2 + B_3'''\eta^3 + \ldots
\end{aligned}\right\} \quad [34]
$$

The primes on the A and B do not signify differentiation as they

do on the F_i they indicate the coefficients of the series for the corresponding derivative of F. Substitution of Equations [33] and [34] into the differential Equation [7] yields the following recursion formulas among the A and B

$$A_n = \frac{p}{(n+1)n} A_{n-2} - \frac{q}{(n+1)n(n-1)(n-2)} A_{n-4} + \frac{r}{(n+1)n(n-1)(n-2)} A_{n-5} \quad [35]$$

$$B_n = \frac{p}{(n+3)(n+2)} B_{n-2} - \frac{q}{(n+3)(n+2)(n+1)n} B_{n-4} + \frac{r}{(n+3)(n+2)(n+1)n} B_{n-5} \quad [36]$$

Now

$$F'(\eta) = A_0 + 2A_1\eta + 3A_2\eta^2 + \ldots = A_0' + A_1'\eta + A_2'\eta^2 + \ldots$$

Therefore we get relations between the two sets of coefficients A_n and A_n' as follows

$$A_n = \frac{A_n'}{n+1} \quad [37]$$

Similarly

$$A_n' = \frac{A_{n-1}''}{n}, n \neq 0 \quad [38]$$

$$A_n'' = \frac{A_{n-1}'''}{n}, n \neq 0 \quad [39]$$

The corresponding relations among the B_n, B_n', etc., are

$$B_n = \frac{B_{n-1}'}{n+3} \quad [40]$$

$$B_n' = \frac{B_{n-1}''}{n}, n \neq 0 \quad [41]$$

$$B_n'' = \frac{B_{n-1}'''}{n}, n \neq 0 \quad [42]$$

Substituting these relations into the recursion Equations [35] and [36] results in similar recursion formulas among the A_n''' and B_n'''. These are

$$A_n''' = \frac{p}{n(n-1)} A_{n-2}''' - \frac{q}{n(n-1)(n-2)(n-3)} A_{n-4}''' + \frac{r}{n(n-2)(n-3)(n-4)} A_{n-5}''' \quad [43]$$

$$B_n''' = \frac{p}{n(n-1)} B_{n-2}''' - \frac{q}{n(n-1)(n-2)(n-3)} B_{n-4}''' + \frac{r}{n(n-2)(n-3)(n-4)} B_{n-5}''' \quad [44]$$

When the coefficients A_0''', A_1''', A_2''', A_3''', A_4''' and B_0''' B_1''', B_2''', B_3''', B_4''' are known, all the other A_n''' and B_n''' can be found by means of Equations [43] and [44]. If we use the series expansions, Equations [9] for F_1 and F_2, we can find the needed coefficients. We have from Equations [9]

$$\left.\begin{aligned} F_1(\eta) &= \eta - \frac{q}{5!}\eta^5 + \frac{2r}{6!}\eta^6 - \frac{pq}{7!}\eta^7 + \frac{2pr}{8!}\eta^8 + \ldots \\ F_1'(\eta) &= 1 - \frac{q}{4!}\eta^4 + \frac{2r}{5!}\eta^5 - \frac{pq}{6!}\eta^6 + \frac{2pr}{7!}\eta^7 + \ldots \\ F_1''(\eta) &= -\frac{q}{3!}\eta^3 + \frac{2r}{4!}\eta^4 - \frac{pq}{5!}\eta^5 + \frac{2pr}{6!}\eta^6 + \ldots \\ F_1'''(\eta) &= -\frac{q}{2!}\eta^2 + \frac{2r}{3!}\eta^3 - \frac{pq}{4!}\eta^4 + \frac{2pr}{5!}\eta^5 + \ldots \end{aligned}\right\} \quad [45]$$

and

$$\left.\begin{aligned} F_2(\eta) &= \frac{1}{3!}\eta^3 + \frac{p}{5!}\eta^5 + \frac{1}{7!}(p^2-q)\eta^7 + \frac{4r}{8!}\eta^8 + \ldots \\ F_2'(\eta) &= \frac{1}{2!}\eta^2 + \frac{p}{4!}\eta^4 + \frac{1}{6!}(p^2-q)\eta^6 + \frac{4r}{7!}\eta^7 + \ldots \\ F_2''(\eta) &= \eta + \frac{p}{3!}\eta^3 + \frac{1}{5!}(p^2-q)\eta^5 + \frac{4r}{6!}\eta^6 + \ldots \\ F_2'''(\eta) &= 1 + \frac{p}{2!}\eta^2 + \frac{1}{4!}(p^2-q)\eta^4 + \frac{4r}{5!}\eta^5 + \ldots \end{aligned}\right\} \quad [46]$$

From Equations [45] and [46] we have

$$A_0''' = 0, A_1''' = 0, A_2''' = -\frac{q}{2}, A_3''' = \frac{r}{3}, A_4''' = -\frac{pq}{24} \quad [47]$$

$$B_0''' = 1, B_1''' = 0, B_2''' = \frac{p}{2}, B_3''' = 0, B_4''' = \frac{p^2-q}{24} \quad [48]$$

Equations [37] through [42] enable us to compute all A_n'', A_n', A_n, B_n'', B_n', B_n with the exception of A_0'', A_0', B_0'', B_0'. These are, from Equations [45] and [46]

$$A_0'' = 0, A_0' = 1, B_0'' = 0, B_0' = 0 \quad [49]$$

The reason for beginning the calculation with the A_n''' and B_n''' is that the series for the third derivatives are the most slowly convergent. When enough coefficients are known for the desired accuracy in the third derivatives, the same degree of convergence (actually better) is assured for the second and first derivatives and the functions themselves, since A_n'', A_n', A_n, $B''B_n'$, B_n are all obtained from A_n''' and B_n''' through division by integers greater than unity.

Computations were made for k as a function of αb for three values of αb, 0.5, 1.0, 1.5. The results are shown in Fig. 3 on the curve labeled "k, exact." We see that in every case the approximate value is higher than the exact value by a small amount. Table 1 shows the error in the approximation.

TABLE 1 ERROR IN APPROXIMATION OF k-VALUES

αb	k	ka	Error, per cent
0.5	0.9002	0.902	0.2
1.0	1.046	1.05	0.4
1.5	1.285	1.31	1.9

Comparison With Bar Theory

It is of interest to see whether the results just found are in agreement with those predicted by bar theory. Goodier[3] has used bar theory to find the critical bending moments for a bar having a cross section with one axis of symmetry, Fig. 4. It is

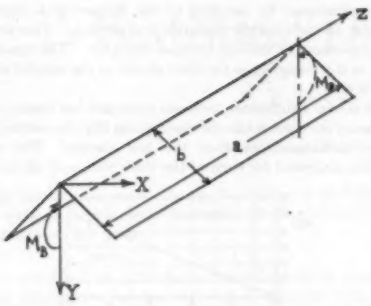

FIG. 4 ANGLE BAR, CO-ORDINATE SYSTEM AND BENDING MOMENTS REFERRED TO IN SECTION ON BAR THEORY

shown in his paper that the values of the critical bending moment M_B for buckling deflections of the type

$$\left.\begin{aligned} u &= u_0 \sin\frac{n\pi z}{a} \\ \beta &= \beta_0 \sin\frac{n\pi z}{a} \end{aligned}\right\} \quad \ldots\ldots\ldots\ldots [50]$$

where

n = an integer

are given by[4]

$$M_B = \frac{1}{2}\left\{P_n\frac{\kappa_0}{I_x} - \sqrt{P_n^2\frac{\kappa_0^2}{I_x^2} + 4\,P_n T_n \rho^2}\right\} \ldots\ldots [51]$$

where

u = deflection in X-direction
β = angle of rotation of section about Z-axis
$P_n = \dfrac{n^2\pi^2 EI_y}{a^2}$
E = Young's modulus
I_y = moment of inertia of section about Y-axis
I_x = moment of inertia of section about an axis parallel to X-axis through centroid
ρ = radius of gyration of section about Z-axis
$\rho^2 T_n = E\Gamma\dfrac{n^2\pi^2}{a^2} + GC$
$\kappa_0 = \int\int_A y(x^2 + y^2)dA - y_0 A\rho^2$
y_0 = Y-co-ordinate of centroid
A = section area
Γ = warping constant, zero for angle-section
GC = torsional rigidity,

For the angle section, when $n = 1$

$$I_y = \frac{1}{3}bt^3,\ t = \text{flange thickness}$$

$$I_x = \frac{1}{12}bt^3$$

$$y_0 = \frac{b}{2\sqrt{2}}$$

$$\rho^2 T_1 = \frac{Et^2 b}{3(1+\nu)} = 4D(1-\nu)b$$

[4] Equation [13] of reference 3.

$$\frac{\kappa_0}{I_x} = \sqrt{2}\,b$$

$$P_1 = \frac{\pi^2 Eb^3 t}{3a^2}$$

$$P_1\frac{\kappa_0}{I_x} = \frac{4\sqrt{2}\pi^2 b^4(1-\nu^2)}{a^2 t^2}D$$

Then from Equation [51]

$$M_B = \frac{1}{2}P_1\frac{\kappa_0}{I_x}\left[1 - \sqrt{1 + \frac{2}{\pi^2(1+\nu)}\left(\frac{a}{b}\right)^2\left(\frac{t}{b}\right)^2}\right]$$
$$= \frac{2\sqrt{2}\,\pi^2(1-\nu^2)b^4 D}{a^2 t^2}\left[1 - \sqrt{1 + \frac{2}{\pi^2(1+\nu)}\left(\frac{a}{b}\right)^2\left(\frac{t}{b}\right)^2}\right] \quad \ldots\ldots [52]$$

The value of M_B which is of interest is that for which the radical has the minus sign, since this corresponds to compressive stress along the free edges (M_B negative), as assumed in the problem treated by plate theory. It is

$$M_B = 2\sqrt{2}\,\pi^2(1-\nu^2)D\left(\frac{b}{a}\right)^2\left(\frac{b}{t}\right)^2$$
$$\left[1 - \sqrt{1 + \frac{2}{\pi^2(1+\nu)}\left(\frac{a}{b}\right)^2\left(\frac{t}{b}\right)^2}\right] \quad \ldots\ldots [53]$$

Or since

$$M_B = -\frac{\sqrt{2}}{6}N_c b^2$$

by definition of N_c

$$N_c = \frac{12(1-\nu^2)}{\pi^2}(ab)^2\left(\frac{b}{t}\right)^2$$
$$\left[\sqrt{1 + \frac{2}{1+\nu}\frac{1}{(ab)^2}\left(\frac{t}{b}\right)^2} - 1\right]\left(\frac{\pi^2 D}{b^2}\right) \quad \ldots\ldots [54]$$

The multiplier of $(\pi^2 D/b^2)$ in Equation [54] is plotted in Fig. 5 for $t/b = 1/50$, $\nu = 0.30$.

If the Z-axis, Fig. 4, is supported so that it remains straight,

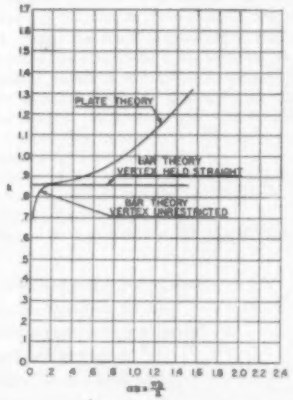

FIG. 5 COMPARISON OF CRITICAL LOAD FACTOR AS A FUNCTION OF $\frac{\pi b}{a}$ AS FOUND BY MEANS OF THREE SEPARATE THEORIES

as assumed in the plate-theory solution, the critical bending moment can be found.[4] The critical bending moment is found from the equation

$$\mu_B \kappa_z = GC \quad [55]$$

where

$$\mu_z = -\frac{M_B}{I_z}$$

for the angle section.

Therefore

$$M_B = -\frac{GC}{(\kappa_z/I_z)} = -2\sqrt{2}\,(1-\nu)D \quad [56]$$

Or, in terms of N_s

$$N_s = \frac{12\,(1-\nu)}{\pi^2}\left(\frac{\pi^2 D}{b^2}\right) \quad [57]$$

The coefficient of $(\pi^2 D/b^2)$ is independent of αb and is shown in Fig. 5 by a horizontal line.

On comparing the results of the plate-theory calculation with those of bar theory, Fig. 5, we notice differences which become larger as the bar gets shorter. The plate theory always predicts a larger value for the critical load than bar theory does. The reason for this difference is that in the bar theory the strain energy contributed by bending of the flanges in a plane perpendicular to their middle surfaces is neglected. This term becomes important as the bar becomes stubbier. The bending described in the foregoing is the kind shown in the shaded element in Fig. 6.

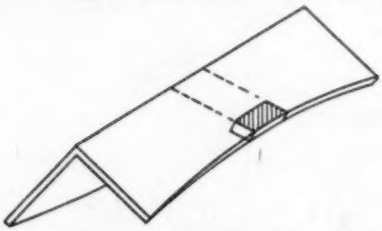

FIG. 6 SHADED ELEMENT SHOWING TYPE OF BENDING WHICH IS ACCOUNTED FOR IN PLATE THEORY BUT NOT IN BAR THEORY

There is also a difference between plate and bar theory in that plate theory does not make the assumption that the section shape remains unchanged, as does the bar theory. The section shape was computed for each of the three values of αb for which exact values of k were found. These are plotted in Fig. 7. Only for the stubbiest plate ($\alpha b = 1.5$) is the change of shape very noticeable. Near the free edge, $\eta = 1$, the section has a tendency to curl; otherwise it remains quite straight, as in pure torsional rotation. This effect, therefore, is not as much responsible as the previously discussed one for the differences between plate and bar theory.

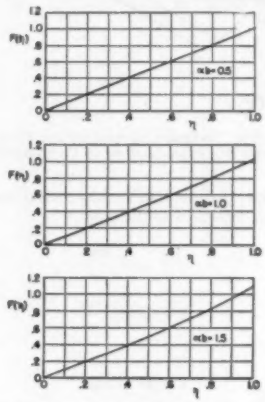

FIG. 7 CURVES SHOWING SHAPE OF CROSS SECTION (ONE LEG) FOR THREE VALUES OF αb

A Statistical Distribution Function of Wide Applicability

By WALODDI WEIBULL,[1] STOCKHOLM, SWEDEN

This paper discusses the applicability of statistics to a wide field of problems. Examples of simple and complex distributions are given.

IF a variable X is attributed to the individuals of a population, the distribution function (df) of X, denoted $F(x)$, may be defined as the number of all individuals having an $X \leq x$, divided by the total number of individuals. This function also gives the probability P of choosing at random an individual having a value of X equal to or less than x, and thus we have

$$P(X \leq x) = F(x) \quad [1]$$

Any distribution function may be written in the form

$$F(x) = 1 - e^{-\varphi(x)} \quad [2]$$

This seems to be a complication, but the advantage of this formal transformation depends on the relationship

$$(1 - P)^n = e^{-n\varphi(x)} \quad [3]$$

The merits of this formula will be demonstrated on a simple problem.

Assume that we have a chain consisting of several links. If we have found, by testing, the probability of failure P at any load x applied to a "single" link, and if we want to find the probability of failure P_n of a chain consisting of n links, we have to base our deductions upon the proposition that the chain as a whole has failed, if any one of its parts has failed. Accordingly, the probability of nonfailure of the chain, $(1 - P_n)$, is equal to the probability of the simultaneous nonfailure of all the links. Thus we have $(1 - P_n) = (1 - P)^n$. If then the df of a single link taker the form Equation [2], we obtain

$$P_n = 1 - e^{-n\varphi(x)} \quad [4]$$

Equation [4] gives the appropriate mathematical expression for the principle of the weakest link in the chain, or, more generally, for the size effect on failures in solids.

The same method of reasoning may be applied to the large group of problems, where the occurrence of an event in any part of an object may be said to have occurred in the object as a whole, e.g., the phenomena of yield limits, statical or dynamical strengths, electrical insulation breakdowns, life of electric bulbs, or even death of man, as the probability of surviving depends on the probability of not having died from many different causes.

Now we have to specify the function $\varphi(x)$. The only necessary general condition this function has to satisfy is to be a positive, nondecreasing function, vanishing at a value x_u, which is not of necessity equal to zero.

The most simple function satisfying this condition is

$$\frac{(x - x_u)^m}{x_0}$$

and thus we put

$$F(x) = 1 - e^{-\frac{(x - x_u)^m}{x_0}} \quad [5]$$

The only merit of this df is to be found in the fact that it is the simplest mathematical expression of the appropriate form, Equation [2], which satisfies the necessary general conditions. Experience has shown that, in many cases, it fits the observations better than other known distribution functions.

The objection has been stated that this distribution function has no theoretical basis. But in so far as the author understands, there are—with very few exceptions—the same objections against all other df, applied to real populations from natural or biological fields, at least in so far as the theoretical basis has anything to do with the population in question. Furthermore, it is utterly hopeless to expect a theoretical basis for distribution functions of random variables such as strength properties of materials or of machine parts or particle sizes, the "particles" being fly ash, Cyrtoideae, or even adult males, born in the British Isles.

It is believed that in such cases the only practicable way of progressing is to choose a simple function, test it empirically, and stick to it as long as none better has been found. In accordance with this program the df Equation [5], has been applied not only to populations, for which it was originally intended, but also to populations from widely different fields, and, in many cases, with quite satisfactory results. The author has never been of the opinion that this function is always valid. On the contrary, he very much doubts the sense of speaking of the "correct" distribution function, just as there is no meaning in asking for the correct strength values of an SAE steel, depending as it does, not only on the material itself, but also upon the manufacturer and many other factors. In most cases, it is hoped that these factors will influence only the parameters. However, accidentally they may even affect the function itself.

The purpose of this paper has been to illustrate with a few examples the experience that the df, Equation [5], may sometimes render good service.

The number of examples has, by space, been limited to the following:

1 Yield strength of a Bofors steel
2 Size distribution of fly ash
3 Fiber strength of Indian cotton
4 Length of Cyrtoideae
5 Fatigue life of a St-37 steel

In the Appendix:

6 Statures for adult males, born in the British Isles
7 Breadth of beans of Phaseolus Vulgaris

---

[1] Professor at the Royal Institute of Technology; Scientific Adviser to AB Bofors; mailing address Bofors, Sweden.

Contributed by the Applied Mechanics Division for presentation, by title, at the Annual Meeting, Atlantic City, N. J., November 25–30, 1951, of The American Society of Mechanical Engineers.

Discussion of this paper should be addressed to the Secretary, ASME, 29 West 39th Street, New York, N. Y., and will be accepted until October 10, 1951, for publication at a later date. Discussion received after the closing date will be returned.

Note: Statements and opinions advanced in papers are to be understood as individual expressions of their authors, and not those of the Society. Manuscript received by ASME Applied Mechanics Division on January 15, 1951. Paper No. 51—A-6.

The correctness of fit has been checked by applying the chi-square method

Of those populations, Nos. 1–3 are distributed in good agreement with the df Equation [5], whereas the four remaining populations have to be split up into two components, before such an agreement is obtained. The first type will be called a "simple" and the second type a "complex" distribution.

The fundamental question now arises, whether this splitting-up is a purely formal operation, or whether it might unveil some hidden real causes. It may be said that any distribution may be represented by a sum of a sufficiently great number of simple distributions, just as any periodical function may be developed in a Fourier series. However, if the number of the components be small and the number of observations sufficiently large, the likelihood of real causes seems to increase. In any case, it is very easy to produce real complex distributions by syntheses.

It seems obvious that the components of examples 4 and 5 are due to real causes. In examples 6 and 7 it is impossible to decide whether the division is a formal one or a real one, but the fact itself may be a valuable stimulus to a closer examination of the observed material.

The specific data for the examples follow.

Yield Strength of a Bofors Steel

The observed values are obtained as routine tests of a Bofors steel, the quality of which was chosen at random for purposes of demonstration only. Fig. 1 gives the curve and Table 1 the values, observed and calculated. The parameters are $x_u = 38.57$ kg/mm², $x_0 = 7.74$ kg/mm², $m = 2.934$. Without pooling, the degrees of freedom (d of f) are $9 - 3 = 6$. Then $\chi^2 = 5.40$ gives $P = 0.49$. The agreement is thus very satisfactory.

As a comparison, the values expected on the hypothesis of a normal distribution have been computed and are given in the last column of Table 1. If the classes 9–10 are pooled, the d of f are $8 - 2 = 6$. Then a $\chi^2 = 18.17$ gives a $P = 0.008$, which is not satisfactory at all.

TABLE 1 YIELD STRENGTH OF A BOFORS STEEL

(x = yield strength in 1.275 kg/mm²)

	x	Expected values n	Observed values n	Normal distribution n
1	32	10	10	8
2	33	36	33	28
3	34	84	81	71
4	35	150	161	141
5	36	224	224	225
6	37	291	289	301
7	38	340	336	351
8	39	369	369	376
9	40	383	383	386
10	42	389	389	388

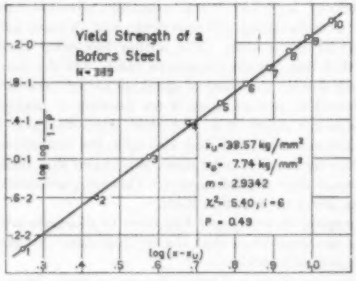

FIG. 1 YIELD STRENGTH OF A BOFORS STEEL

Size Distribution of Fly Ash

The observed values are taken from J. M. Dalla Valle's work.[2] Fig. 2 gives the curve and Table 2 the values. The parameters are $x_u = 30\mu$, $x_0 = 128\ \mu$, $m = 2.288$. Without pooling, the d of f are $12 - 3 = 9$. Then $\chi^2 = 8.44$ gives a $P = 0.49$. If the classes 2–3 and 13–14 are pooled, the d of f are 7 and $\chi^2 = 8.44$ gives a $P = 0.29$.

TABLE 2 SIZE DISTRIBUTION OF FLY ASH

(x = particle diameter in 20 microns)

x	Expected values n	Observed values n
2	3	3
3	14	11
4	34	34
5	62	58
6	92	85
7	122	126
8	150	138
9	172	175
10	188	188
11	199	197
12	205	202
13	209	208
14	211	211

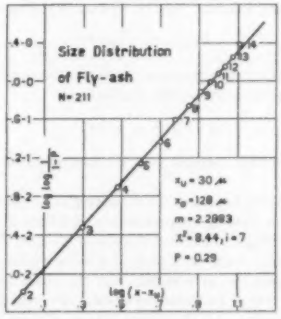

FIG. 2 SIZE DISTRIBUTION OF FLY ASH

Fiber Strength of Indian Cotton

The observed values are taken from R. S. Koshal and A. J. Turner.[3] Fig. 3 gives the curve, and Table 3 the values. The parameters are $x_u = 0.59$ gram, $x_0 = 3.73$ grams, $m = 1.456$. If the classes 14 to 16 are pooled, the d of f are $13 - 3 = 10$. Then $\chi^2 = 11.45$ gives a $P = 0.35$.

The authors[3] have pointed out that the most striking feature about the frequency curve is its asymmetry, showing a well-marked predominance of weak fibers. It was found—they say—that the observation curve would be well fitted by a theoretical curve of Pearson's Type 1, having the following equation

$$y = 599.3\left(1 + \frac{x}{18.777}\right)^{6.878718}\left(1 - \frac{x}{29.1947}\right)^{13.631394}$$

In this equation y represents the frequency of any strength x, expressed in grams.

The values computed from this not very handy equation are shown in the last column of Table 3. The d of f are $13 - 5 = 8$ (as there are 5 parameters). Then $\chi^2 = 14.43$ gives a $P = 0.07$.

---

[2] "Micromeritics," by J. M. Dalla Valle, Pitman Publishing Corporation, New York, N. Y., 1948, p. 57, Fig. 2.

[3] "Studies in the Sampling of Cotton for the Determination of Fiber Properties," by R. S. Koshal and A. J. Turner, Journal of the Textile Institute Transactions, vol. 21, 1930, pp. 325–370.

TABLE 3 FIBER STRENGTH OF INDIAN COTTON

(x = tensile strength in grams)

x	Expected values n	Observed values n	Pearson Type 1 n
1	118	177	127
2	646	667	659
3	1232	1219	1255
4	1751	1729	1777
5	2161	2153	2184
6	2461	2465	2480
7	2667	2664	2683
8	2802	2813	2816
9	2886	2887	2899
10	2937	2933	2949
11	2966	2962	2978
12	2982	2985	2994
13	2991	2991	3003
14	2996	2995	3007
15	2999	2999	3009
16	3000	3000	3010

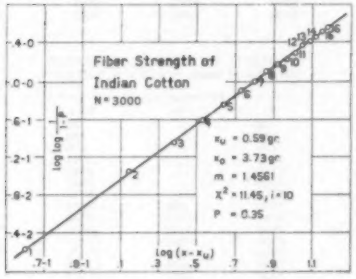

FIG. 3 FIBER STRENGTH OF INDIAN COTTON

TABLE 4 LENGTH OF CYRTOIDEAE

(x = length in microns)

	x	Expected values n_1	n_2	n_{1+2}	Observed values n_{1+2}
1	10	1	..	1	0
2	20	5	..	5	5
3	30	13	..	13	12
4	40	23	..	23	24
5	50	35	..	35	38
6	60	47	..	47	45
7	70	58	..	58	58
8	80	67	..	67	69
9	90	74	..	74	70
10	100	79	..	79	80
11	110	82	..	82	82
12	120	85	..	85	84
13	130	86	..	86	86
14	140	86	4	90	90
15	150	86	7	93	93
16	160	86	9	95	95
17	170	86	11	97	97
18	180	86	12	98	98
19	190	86	13	99	99
20	200	86	14	100	100

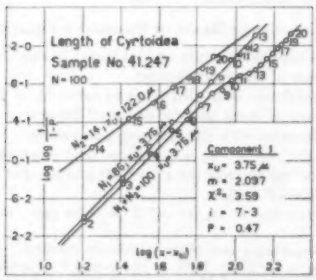

FIG. 4 LENGTH OF CYRTOIDEAE

In spite of the greater number of parameters, the fit of this distribution function is not as close as that of the first one.

LENGTH OF CYRTOIDEAE

This is the first example of a complex distribution. The observed values have been obtained from investigations by Dr. Gustaf Arrhenius, on submarine cores from the Swedish Deep-Sea Expedition With *Albatross*. The measurements were made by Dr. C. Jungk, taking samples from each 10 cm of the core, corresponding to an age interval of about 100,000 years. Some fifty populations have been analyzed statistically. About 20 per cent of the populations showed a simple distribution, as exemplified in a previous paper.[4] The remaining samples showed a two-component distribution.

Fig. 4 gives the curves and Table 4 the values of one of the complex populations. The undivided sample gives the curve marked $N_1 + N_2$. It is easy to see that the distribution is a complex one, and that it is necessary to split up the population in two parts. By trial it was found that 86 of the individuals belonged to component No. 1, and 14 to component No. 2.

The parameters are: Component No. 1: $x_u = 3.75\ \mu$, $x_0 = 63.2\ \mu$, $m = 2.097$. Pooling the classes 2–3, 9–10, and 11–13 gives $\chi^2 = 3.59$. The d of f are $7 - 3 = 4$, and $P = 0.47$.

Component No. 2: $x_u = 122.0\ \mu$, $x_0 = 124.1\ \mu$, $m = 1.479$. The number of individuals is too small for the χ^2-test.

FATIGUE LIFE OF AN ST-37 STEEL

The observed values are taken from Müller-Stock.[5] The frequency curve in Fig. 5[5] gives no impression of a complex distribution, which, on the other hand, may easily be seen when

[4] "A Statistical Analysis of the Size of Cyrtoideae in Albatross Cores From the East Pacific Ocean," by W. Weibull, *Nature*, vol. 164, 1949, p. 1047.

[5] "Der Einfluss dauernd und unterbrochen wirkender, schwingender Überbeanspruchung auf die Entwicklung des Dauerbruchs," by H. Müller-Stock, *Mitteilungen Kohle- und Eisenforschung*, (March, 1938), by measurements from his Fig. 13; reproduced in Fig. 5 of this paper.

TABLE 5 FATIGUE LIFE OF ST-37
(Rotating-beam test at ±32 kg/mm²)

	N 10^3	Expected values n_1	n_2	n_{1+2}	Observed values n_{1+2}
1	17.5	4.6	...	4.6	4.6
2	22.5	47.4	...	47.4	47.4
3	27.5	125.1	...	125.1	125.1
4	32.5	161.2	8.1	169.3	169.2
5	37.5	164.9	28.0	192.9	192.7
6	42.5	165.0	41.9	206.9	207.3
7	47.5	165.0	51.0	216.0	215.9
8	52.5	165.0	57.0	222.2	222.2
9	57.5	165.0	61.0	226.0	225.9
10	62.5	165.0	63.7	228.7	228.7
11	67.5	165.0	65.6	230.6	230.5
12	72.5	165.0	66.9	231.9	231.9
13	77.5	165.0	67.9	232.9	232.9
14	82.5	165.0	68.6	233.6	233.5
15	87.5	165.0	69.1	234.1	233.9
16	92.5	165.0	70.0	235.0	235.0

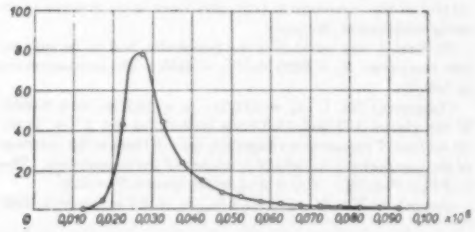

FIG. 5 FREQUENCY CURVE OF FATIGUE LIFE OF ST-37 STEEL
(Number of specimens versus number of stress cycles.)

using the plottings in Fig. 6. The parameters are: Component No. 1: $x_u = 4.032$, $m = 5.956$; Component No. 2: $x_u = 4.484$, $m = 1.215$. Table 5 shows the close agreement between the observed and the calculated values.

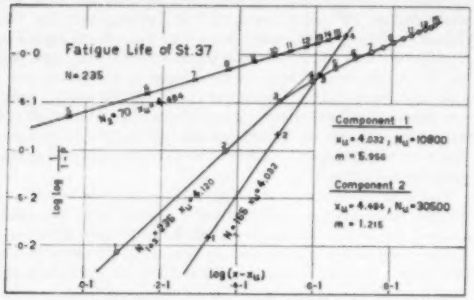

FIG. 6 FATIGUE LIFE OF ST-37 STEEL

It may be pointed out that the frequency curve in Fig. 5 seems to be the result of a smoothing operation on the cumulative frequency curve. Accordingly, the sampling errors of the observed values in Table 5 have been eliminated almost entirely (without affecting the function), which explains the really too good representation of the observed values.

The real causes of this splitting up in two components may be found by examining the frequency curve of the yield strength of the same material, Fig. 7. It is easy to see that the material, probably not being killed, is composed of two different kinds. If we suppose that all the specimens with a yield strength of less than 25 kg/mm² belong to Component No. 1, we obtain 14 specimens out of 20, making 70 per cent. Exactly the same proportion has been found by the statistical analysis, as 165/235 = 70 per cent.

The reason why this partition is so easily seen in Fig. 7 and not at all in Fig. 5, depends, of course, upon the much larger scatter in fatigue life than in yield strength.

Appendix

The foregoing statistical methods have been applied to many problems outside the field of applied mechanics. It may perhaps be of interest to have examples of this kind, and for this reason, the following two are given with the tables only:

STATURES FOR ADULT MALES BORN IN THE BRITISH ISLES

The observed values are taken from Yule and Kendall.[6] This distribution is classified by the authors as being approximately of the symmetrical type, and there is no mention of its being composed of two parts.

By trial it was found that the population had to be split up into two parts: $N_1 = 6200$ and $N_2 = 2385$. The parameters are as follows:

Component No. 1: $x_u = 50.0$ in., $x_0 = 16.2$ in., $m = 9.6865$. If the classes 1–2 and 14–15 are pooled, we get $\chi^2 = 11.80$. As we have 7 parameters altogether, (one of them is the partition of the population), we take $3^1/_2$ to each of the components. The d of f are then $12 - 3^1/_2 = 8^1/_2$, which gives a $P = 0.20$.

Component No. 2: $x_u = 67.4$ in., $x_0 = 2.3$ in., $m = 1.4662$.

[6] "An Introduction to the Theory of Statistics," by G. U. Yule and M. G. Kendall, eleventh edition, J. B. Lippincott Company, Philadelphia, Pa., 1937, pp. 94 and 111.

TABLE 6 STATURES FOR ADULT MALES BORN IN THE BRITISH ISLES
(x = height in inches)

	Expected values			Observed values
x	n_1	n_2	n_{1+2}	n_{1+2}
57	2	...	2	2
58	6	...	6	6
59	20	...	20	20
60	56	...	56	61
61	143	...	143	144
62	333	...	333	313
63	702	...	702	707
64	1350	...	1350	1376
65	2351	...	2351	2366
66	3641	...	3641	3589
67	4917	...	4917	4918
68	5787	339	6126	6148
69	6134	1079	7213	7211
70	6197	1671	7868	7857
71	6200	2039	8239	8249
72	6200	2233	8433	8451
73	6200	2324	8524	8530
74	6200	2363	8563	8562
75	6200	2378	8578	8578
76	6200	2383	8583	8583
77	6200	2385	8585	8585

TABLE 7 PHASEOLUS VULGARIS
(Breadth of beans = 0.25 x + 6.70 mm)

	Expected values			Observed values
x	n_1	n_2	n_{1+2}	n_{1+2}
1	32	...	32	32
2	130	...	130	135
3	400	...	400	374
4	1011	...	1011	998
5	2145	...	2145	2185
6	3832	...	3832	3835
7	5718	...	5718	5718
8	7140	486	7626	7648
9	7761	1525	9286	9286
10	7890	2510	10400	10416
11	7900	3229	11129	11153
12	7900	3671	11571	11580
13	7900	3908	11808	11801
14	7900	4022	11922	11911
15	7900	4071	11971	11968
16	7900	4091	11991	11992
17	7900	4098	11998	11998
18	7900	4100	12000	12000

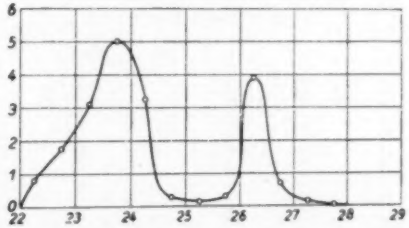

FIG. 7 FREQUENCY CURVE OF YIELD STRENGTH OF ST-37 STEEL
(Number of specimens versus yield strength in kg/mm².)

If the classes 20–21 are pooled, $\chi^2 = 5.11$. The d of f are $8 - 3^1/_2 = 4^1/_2$, which gives a $P = 0.35$.

BREADTH OF BEANS OF PHASEOLUS VULGARIS

This is a classical example, quoted from Charlier[7] to exemplify the expansion in Edgeworth's series.

If the population is divided into two parts, $N_1 = 7900$ and $N_2 = 4100$, each of them may be very well fitted to a simple distribution function with the following parameters:

Component No. 1: $x_u = -3.0$ (= 5.95 mm), $m = 6.2805$. Without pooling we have the $\chi^2 = 7.70$, and the d of f $10 - 3^1/_2 = 6^1/_2$ giving a $P = 0.29$.

Component No. 2: $x_u = +7.2$ (= 8.50 mm), $m = 1.6098$.

[7] "Die Grundlagen der Mathematischen Statistik," by C. V. L. Charlier, second edition, 1920, p. 73, quoted by Harald Cramér in his book: "Mathematical Methods of Statistics," Princeton University Press, Princeton, N. J., 1945, p. 440.

If the classes 17–18 are pooled, the value of $\chi^2 = 4.50$, and the d of f $9 - 3^1/_2 = 5^1/_2$ give a $P = 0.56$.

It may be of interest to compare this result with those of Charlier and Cramér.

Charlier says that, at the first look, the agreement with the normal distribution seems very satisfactory, but that a closer examination shows a small negative skewness and a small positive kurtosis.

Cramér has calculated the values of χ^2 on the hypotheses of normal distribution and asymptotic expansions from it. The result was as follows:

Normal distribution	$\chi^2 = 196.5$	d of f 13 $P < 0.001$
First approximation	$\chi^2 = 34.3$	d of f 12 $P < 0.001$
Second approximation	$\chi^2 = 14.9$	d of f 11 $P = 0.19$

The agreement is satisfactory in the third case only, requiring four terms of the series. This operation is certainly of a purely formal character.

Design Data and Methods

It is important that the data contained in technical papers be made readily available to designing engineers. In order to satisfy these needs of industry, this section of the Journal includes a concise presentation of data and information drawn chiefly from papers previously published by the Applied Mechanics Division of The American Society of Mechanical Engineers.

Applying Bearing Theory to the Analysis and Design of Journal Bearings—I

By JOHN BOYD[1] AND ALBERT A. RAIMONDI,[2] EAST PITTSBURGH, PA.

Nomenclature

The following nomenclature is used in the paper. Some of the terms are shown diagrammatically in Fig. 1.

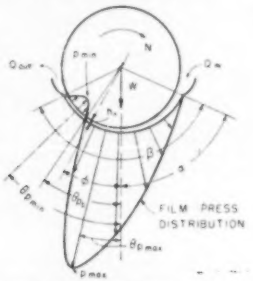

Fig. 1 Bearing Nomenclature

W = load, lb
N = speed, rpm
R = journal radius, in.
C = radial clearance, in.
L = axial length of bearing, in.
B = length of bearing arc in direction of motion, in.
P = load per unit projected bearing area = $W/2RL$, psi
μ = viscosity of lubricant in reyns, lb sec/in.^{2}
h_o = minimum film thickness, in.
f = coefficient of friction, dimensionless
H = power consumed in friction, hp
Q = flow of lubricant drawn into clearance space by journal, cu in. per min
Q_s = flow of lubricant out both sides of bearing, cu in. per min
β = angular length of bearing arc, deg
α = leading angle of bearing arc, extending from beginning of arc to line of action of load, deg
ϕ = position minimum film thickness, deg
$\theta_{p(max)}$ = position maximum film pressure, deg
$\theta_{p(min)}$ = position minimum film pressure, deg
$\theta_{p(s)}$ = position at which film pressure becomes less than supply pressure, deg
p_{max} = maximum pressure developed in lubricant film, psi
S = bearing characteristic number, or Sommerfeld number, sec/min
S_o = provisional value of S used in problems in which side flow is considered, sec/min
Δt = temperature rise of lubricant as it travels across bearing arc, deg F
c = specific heat of lubricant, Btu/lb deg F
γ = weight per unit volume of lubricant, lb per cu in.
J = mechanical equivalent of heat = 9336 in-lb/Btu
K_F, K_W, K_Q, K_T = correction factors used when accounting for effects of side flow, dimensionless

Introduction

Although much has been written on the subject of bearings, the average person wishing to analyze or design a journal bearing usually finds the available data inadequate in several respects.

Some of the difficulties he encounters are that most treatments are unnecessarily complicated, involve inconvenient conversions from one set of units to another, and do not include systematic methods for solving problems involving various known conditions. The purpose of this paper is to eliminate as many of these objections as possible and thus to simplify the problem of making accurate bearing calculations.

As an aid to this end, standard methods for the solution of problems have been set up, and viscosity data on several representative oils have been given in a form which requires no conversion.

The charts and tables contained herein yield the results to be expected on the basis of what is generally regarded to be the

[1] Manager, Lubrication Section, Research Laboratories, Westinghouse Electric Corporation. Mem. ASME.
[2] Research Engineer, Research Laboratories, Westinghouse Electric Corporation. Jun. ASME.

Discussion of this paper should be addressed to the Secretary, ASME, 29 West 39th Street, New York, N. Y., and will be accepted until October 10, 1951, for publication at a later date. Discussion received after the closing date will be returned.

Note: Statements and opinions advanced in papers are to be understood as individual expressions of their authors and not those of the Society. Manuscript received by ASME Applied Mechanics Division, February 2, 1951.

most usable theory and are applicable to a large number of problems.

It is not within the scope of this paper to recommend proper bearing proportions, allowable temperature rises, etc. These must be left to the judgment of the designer to be decided upon the basis of experience and test.

General Types of Journal Bearings

Journal bearings may be grouped broadly into two main classes—full bearings and partial bearings, as illustrated in Fig. 2.

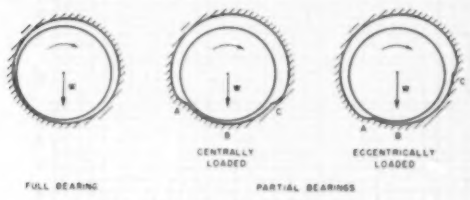

Fig. 2 Types of Journal Bearings

In the full bearing, the active bearing area extends completely around the journal for the full 360 deg, while in the partial bearing the active bearing area, or arc *ABC*, extends only partly around the journal. If the direction of the load in a partial bearing bisects the arc *ABC*, the bearing is said to be centrally loaded, but if the direction of the load does not bisect the arc, *ABC*, the bearing is then said to be eccentrically loaded. Partial bearings of less than 180 deg arc can be classified further into clearance bearings and fitted bearings. In the former, the radius of the bearing is slightly greater than the radius of the journal while, in the latter, both radii are the same.

The full journal bearing and the centrally loaded partial bearing of the clearance type are the more common, and it is to these bearings that the following analysis applies.

Assumptions Involved

Before proceeding with methods for solving problems, it is necessary to state the assumptions upon[1] which the resulting solutions are based. A detailed description of the many premises involved is out of place for present purposes but may be found in textbooks on the subject. Only the more important assumptions will be mentioned here.

Of these, the one most apt to have an important effect is whether or not side flow has been taken into account, Fig. 3(*a* and *b*).

Mathematically, it is much easier to calculate bearing characteristics on the assumption that the lubricant flows only in the circumferential direction, as shown in Fig. 3(*a*). However, the

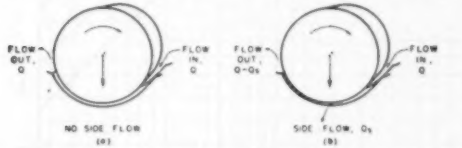

Fig. 3 Illustrating Assumption of Side Flow and No Side Flow

more accurate representation of actual conditions results from taking the side flow (sometimes called side leakage) into consideration. Although the assumption of no side flow obviously does not duplicate actual conditions, particularly if a bearing is short in the axial direction, the simpler analysis which results from this premise makes it easier to visualize how the various variables influence bearing performance. For this reason, methods for solving problems based on the assumption of no side flow will be treated first. Following this, methods which take side flow into account will be described.

Another assumption on which the analysis is based is that the viscosity of the lubricant remains constant as it passes through the film area. Although it is known that the viscosity varies with both temperature and pressure, the error made by assuming that it remains constant is usually relatively small.

In the majority of bearing problems, the pressure at all points in the film is either equal to or greater than the lubricant-supply pressure. Under certain conditions, however, the calculated pressure in some parts of the film may be negative, i.e., less than zero psi absolute. Since liquids, ordinarily, will not withstand "negative pressures," the present analysis which does not exclude such pressures will be somewhat in error. Such error is usually restricted to high loads, low speed, and low viscosities. More will be said on this matter later.

Viscosity of Lubricant

As all of the other quantities involved are given in English units, it is highly desirable to have the viscosity of the lubricant similarly expressed. The standard unit of viscosity (or absolute viscosity as it is often called), in the English system is the reyn which has the units of lb-sec/in.^{2}. Since the reyn is relatively large, the microreyn (or 10^{-6} reyn) is often more convenient for use in charts and tables. In terms of the better known centipoise unit, one microreyn = 6.9 centipoise. For calculating bearing performance according to the methods of the present treatment, the viscosity should be expressed in reyns. V-T* Chart 1 shows the viscosity in reyns of a series of typical SAE numbered motor oils.

Since lubricants other than oils are also on occasion used in bearings, the viscosities of a number of other fluids are given in V-T Chart 2, for reference and comparison.[2]

Bearing-Characteristic Number

Since the equations involved in solving bearing problems are tedious to work with, calculations are most easily made by the use of bearing-performance charts. Such charts can, of course, be plotted in many ways. In the authors' opinion, the best method of presentation is to plot the various performance factors as functions of the bearing-characteristic number, or Sommerfeld number, as it is frequently called. The characteristic number S is given by the following relation

$$S = \left(\frac{R}{C}\right)^2 \frac{\mu N}{P}$$

The advantage of this number as a parameter is that it unites in one dimensionless variable most of the factors (only the bearing arc is omitted) over which one has direct control and, when once this number has been established for a given condition of operation, all of the operating characteristics become fixed.

As used in this treatment, the characteristic number is not strictly dimensionless but is in units of sec/min. This has been done so that the speed can be expressed in revolutions per

* V-T = Viscosity Temperature.

[2] If one wishes to add curves for other lubricants to these charts when the viscosities are given in centipoises, centistokes, or Saybolt seconds, the following conversion factors may be used:
Viscosity in microreyns = $1.45 \times 10^{-1} \times$ viscosity in centipoises
Viscosity in microreyns = specific gravity $\times 1.45 \times 10^{-1} \times$ viscosity in centistokes
Viscosity in microreyns = specific gravity $\times$ 1.45×10^{-4} (0.219 SUV—149.7/SUV) where SUV is the viscosity in Saybolt seconds.

VISCOSITY-TEMPERATURE CHART 1 FOR DETERMINING VISCOSITY OF TYPICAL SAE NUMBERED OILS AT VARIOUS TEMPERATURES

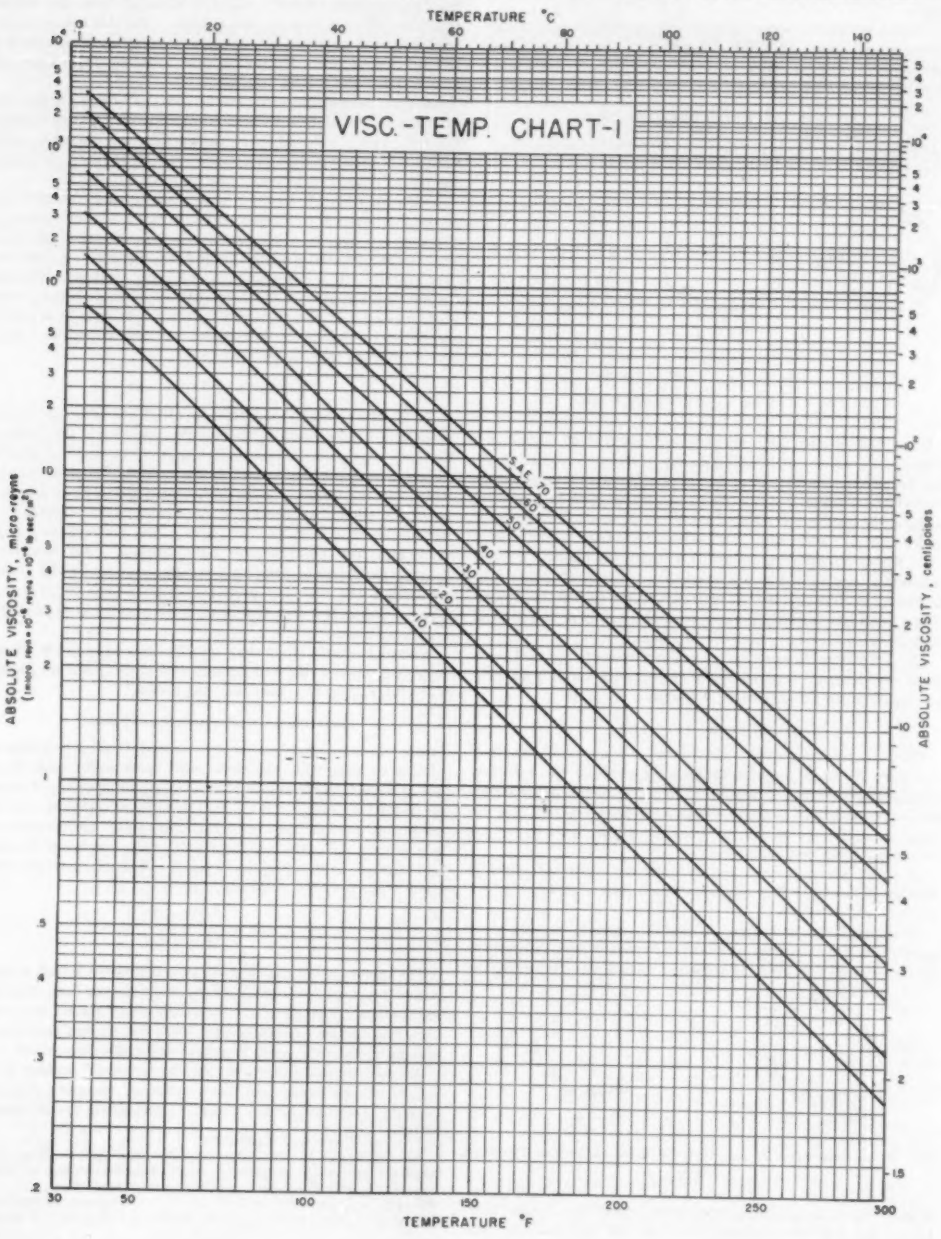

VISCOSITY-TEMPERATURE CHART 2 SHOWING RELATIVE VISCOSITIES OF A NUMBER OF FLUIDS AT VARIOUS TEMPERATURES

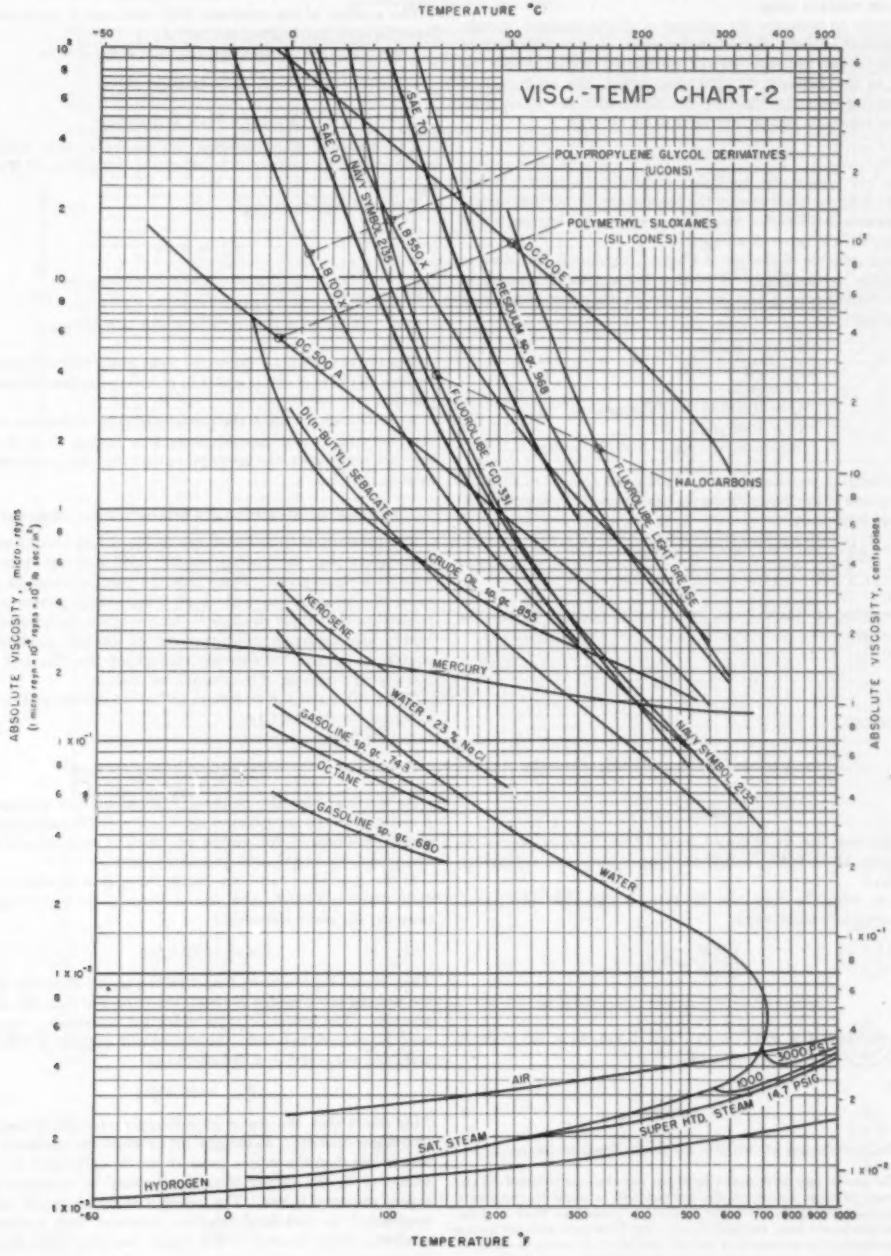

minute rather than in revolutions per second, the former being the more common usage.

In order to minimize the number of charts required, certain bearing-performance characteristics such as the coefficient of friction, power loss, etc., cannot be plotted explicitly with respect to the number, S. For this reason, the coefficient of friction, for example, has been combined with the ratio, R/C, to form the coefficient-of-friction variable $(R/C)f$.

Coefficient of Friction

Chart 1 shows the coefficient-of-friction variable plotted[4] against S for various values of the bearing arc, β. Also shown are the running positions of the journal within the bearing which correspond to the given S-numbers.

As an example of the use of Chart 1, suppose it is desired to determine the coefficient of friction for a 180-deg bearing in which the following quantities are known, the effect of side flow being neglected

$W = 12{,}500$ lb
$D = 2R = 10$ in.
$L = 10$ in.
$C = 0.010$ in. (radial clearance)
$N = 1000$ rpm
$\mu = 5$ microreyns $= 5 \times 10^{-6}$ reyns

The bearing pressure per unit of projected area, $P = W/2RL$, on the basis of the foregoing data is found to be 125 psi, and the S-number is given by

$$S = \left(\frac{R}{C}\right)^2 \frac{\mu N}{P} = \left(\frac{5}{1 \times 10^{-3}}\right)^2 \frac{5 \times 10^{-6} \times 10^3}{125} = 10 \text{ sec/min}$$

According to Chart 1, the coefficient-of-friction variable for this bearing is

$$\frac{R}{C} f = 1.92$$

from which

$$f = \frac{C}{R} \times 1.92 = \frac{1 \times 10^{-3} \times 1.92}{5} = 0.0038$$

Power Loss[5]

Power loss can be obtained from Chart 2, which shows the quantity, $10^6 H/WNC$, called the power-loss variable, plotted against S.

Thus, using the data from the foregoing example, the power-loss variable is found to be

$$\frac{10^6 H}{WNC} = 3.1$$

or

$$H = 10^{-6} \times 3.1 \times WNC = \frac{10^{-6} \times 3.1 \times 1.25 \times 10^4 \times 10^3 \times}{10^{-2}}$$

giving

$$H = 3.80 \text{ hp}$$

[4] The co-ordinates of this plot are proportional to the arc hyperbolic sine.

[5] The power loss determined by these calculations is based on the frictional moment acting on the journal and is equal to the power which must be applied to the journal to overcome fluid friction. Unless the power loss, calculated from the frictional moment acting on the bearing is corrected to include the effect of journale ecentricity, considerable error in the power requirements may result.

Position of Minimum Film Thickness

The position of the minimum film thickness ϕ, as measured from the load line, is given in Chart 3.

The angle ϕ, for the foregoing example, is found to be

$$\phi = 60 \text{ deg}$$

Minimum Film Thickness

The minimum film thickness can be found from Chart 4, which shows the minimum film-thickness variable, h_n/C, plotted against S.

For the foregoing example

$$\frac{h_n}{C} = 0.78$$

from which

$$h_n = 0.78\, C = 0.78 \times 0.010 = 0.0078 \text{ in.}$$

The insert in Chart 4 shows the locus of the journal center for various values of S and is useful in picturing the journal running position.

As will be shown later, the portions of these curves for values of S between O and approximately 2 is subject to error since they are based upon the assumption that negative pressures can exist in the film.

Position of Maximum and Minimum Film Pressure

The pressure distribution shown in Fig. 1 was plotted on the assumption that the bearing supply and discharge pressures were both atmospheric. Since both the maximum and the minimum film pressure (as well as all intermediate pressures) are referred to the supply pressure as datum, raising or lowering the supply and discharge pressures a given amount produces an equivalent increase or decrease throughout the film, but does not alter the position of the maxima or minima.

The positions of the maximum and of the minimum film pressures are shown in Chart 5.

For the foregoing example

$$\theta_{p(\max)} = 4 \text{ deg}$$

As the curve for the position of minimum film pressure for $\beta = 180$ deg does not intersect the line $S = 10$, it indicates that, within the limits of the bearing arc, there is no point where the film pressure is less than the supply pressure.

If the S-number had been smaller, say, $S = 2$, which would correspond to lower speed, lower viscosity or higher bearing pressure, the curve shows that

$$\theta_{p(\min)} = 69.5 \text{ deg}$$

There would thus be more than 20.5 deg on the discharge side of the bearing in which the pressure would be less than the supply pressure. The actual point at which the transition takes place may be determined from the right-hand portion of Chart 5, and, for a value of $S = 2$, is found to be

$$\theta_{p(z)} = 54.5 \text{ deg}$$

This shows that the region of subsupply pressure extends 90–54.5 deg or 35.5 deg. As the amount by which the minimum pressure is less than the supply pressure can be quite large for small values of S, the former theoretically may be negative if the supply pressure is low. The inability of liquids (under normal conditions) to withstand negative pressures thus renders the analysis subject to error in this region, the error increasing as S decreases.

CHART 1 FOR DETERMINING COEFFICIENT OF FRICTION
(Curves based upon no side flow.)

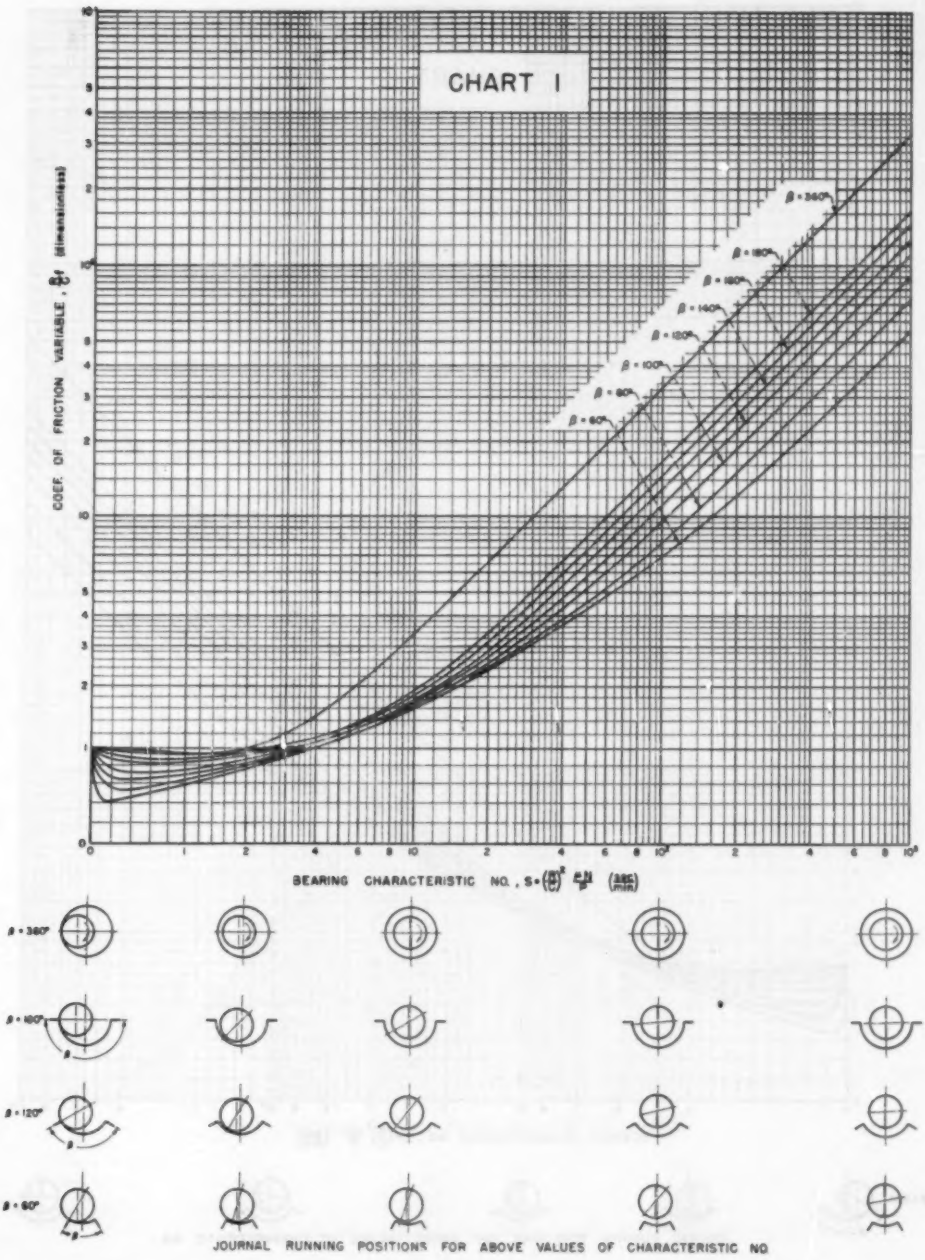

CHART 2 FOR DETERMINING POWER LOSS
(Curves based upon no side flow.)

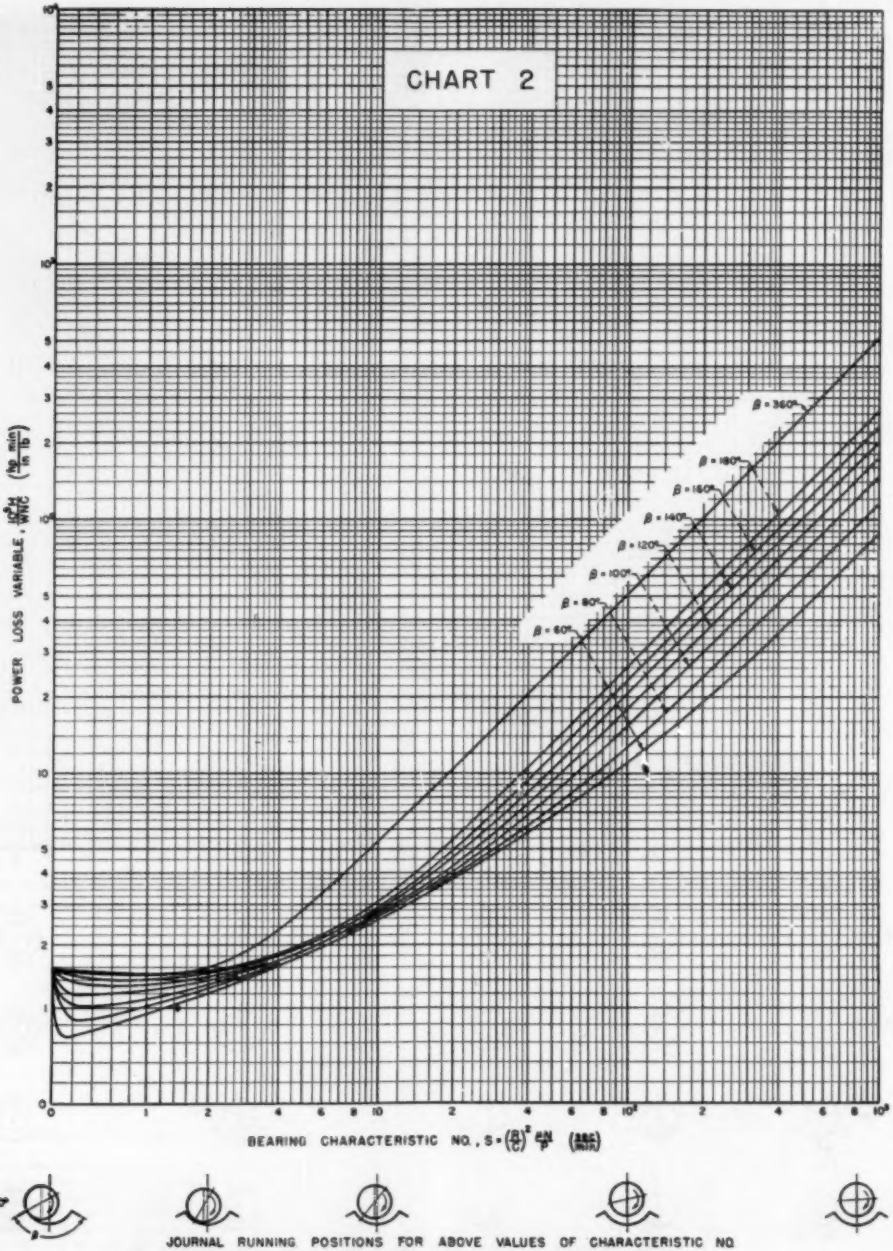
CHART 2
POWER LOSS VARIABLE, $\frac{10^6 H}{WNC}$ $\left(\frac{\text{hp. min}}{\text{in lb}}\right)$
BEARING CHARACTERISTIC NO., $S=\left(\frac{R}{C}\right)^2 \frac{\mu N}{P}$ $\left(\frac{\text{sec}}{\text{min}}\right)$
β = 360°
β = 180°
β = 160°
β = 140°
β = 120°
β = 100°
β = 80°
β = 60°
β = 120°
JOURNAL RUNNING POSITIONS FOR ABOVE VALUES OF CHARACTERISTIC NO.

CHARTS 3 AND 4 FOR DETERMINING MAGNITUDE AND POSITION OF MINIMUM FILM THICKNESS
(Curves based upon no side flow.)

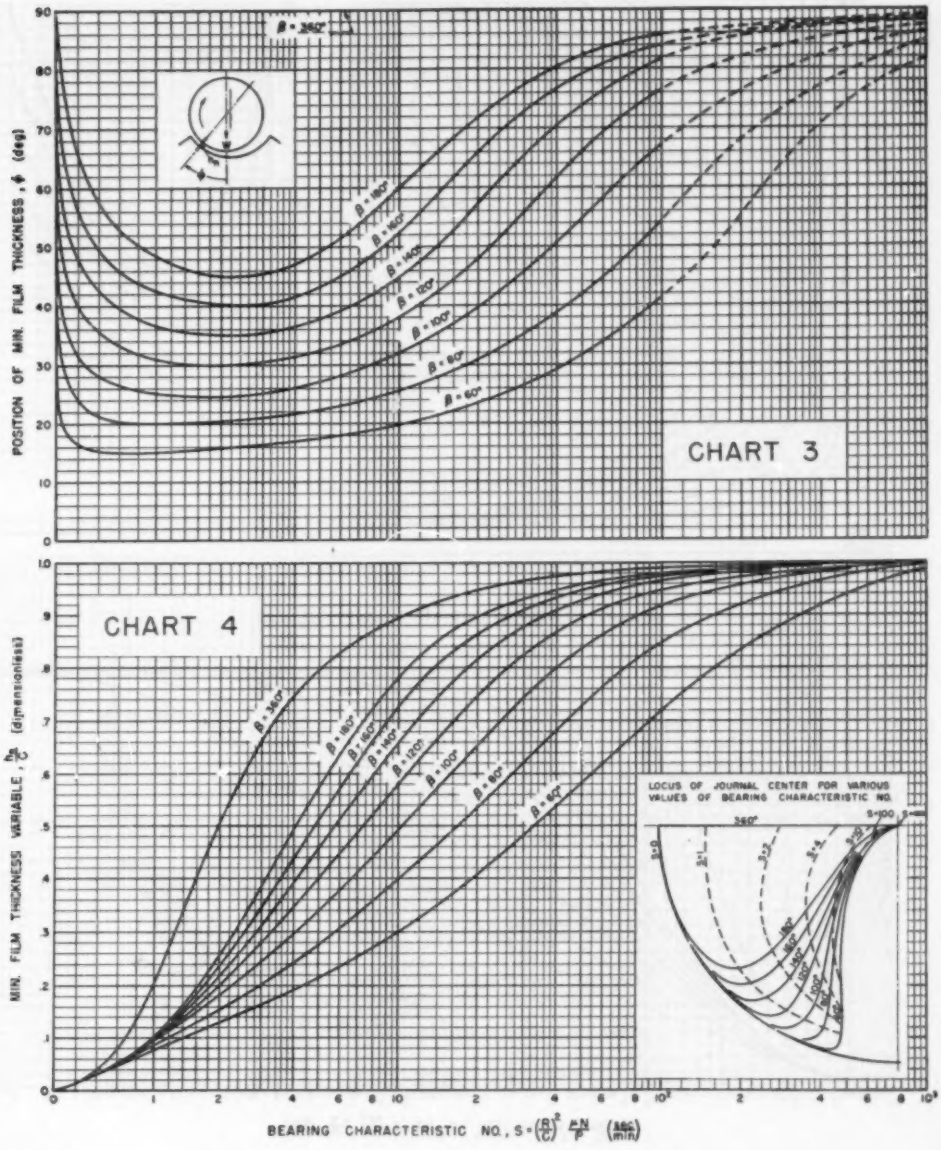
CHART 3
POSITION OF MIN. FILM THICKNESS, φ (deg)
β = 360°
β = 180°
β = 160°
β = 140°
β = 120°
β = 100°
β = 80°
β = 60°
CHART 4
MIN. FILM THICKNESS VARIABLE, h/c (dimensionless)
LOCUS OF JOURNAL CENTER FOR VARIOUS VALUES OF BEARING CHARACTERISTIC NO.
BEARING CHARACTERISTIC NO., S = (R/c)² μN/P (sec/min)

JOURNAL RUNNING POSITIONS FOR ABOVE VALUES OF CHARACTERISTIC NO.

CHARTS 5 AND 6 FOR DETERMINING LUBRICANT FLOW AND POSITION OF MAXIMUM AND MINIMUM FILM PRESSURES
(Curves based upon no side flow.)

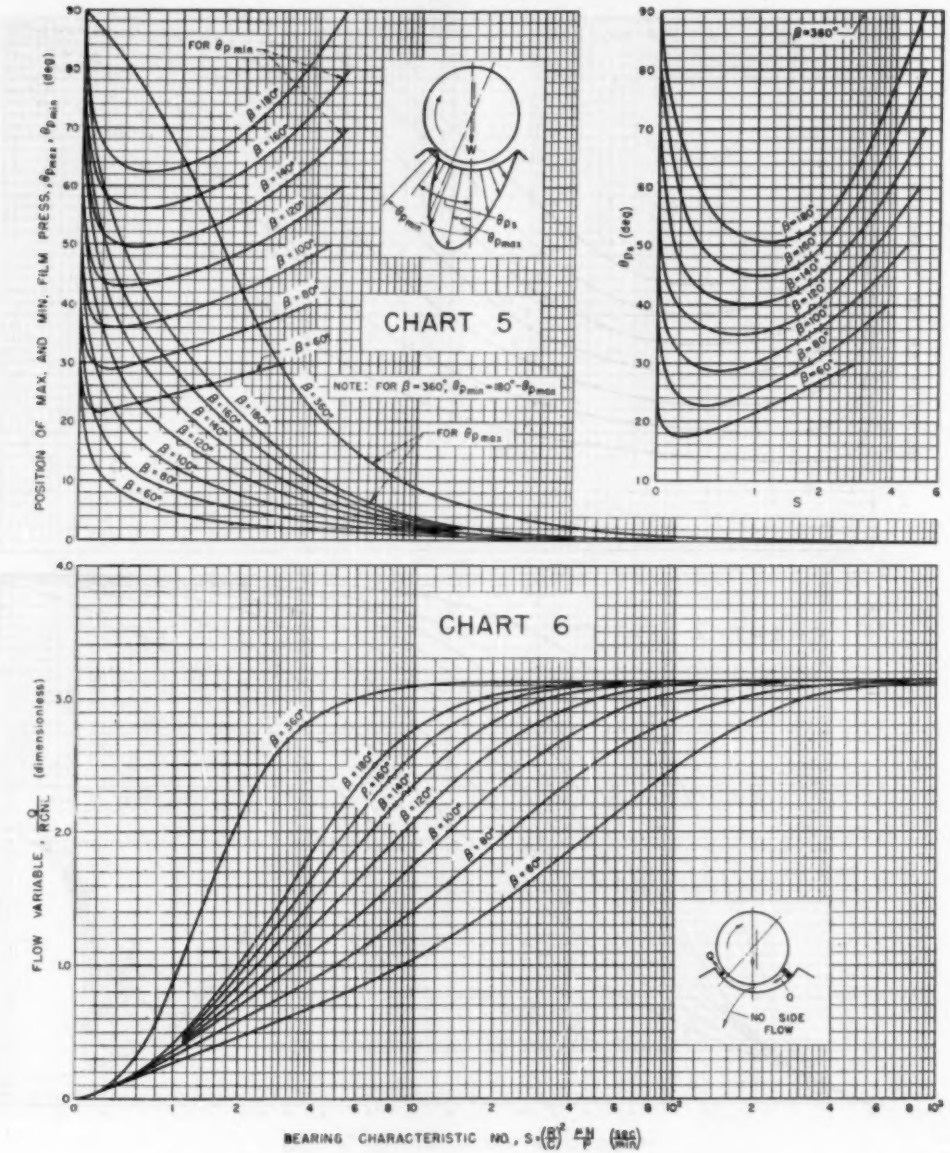
CHART 5
POSITION OF MAX. AND MIN. FILM PRESS., $\theta_{p_{max}}$, $\theta_{p_{min}}$ (deg)
FOR $\theta_{p\,min}$
FOR $\theta_{p\,max}$
NOTE: FOR $\beta = 360°$, $\theta_{p_{min}} = 180° - \theta_{p_{max}}$
β = 180°, 160°, 140°, 120°, 100°, 80°, 60°
θ_{p_s} (deg)
S
CHART 6
FLOW VARIABLE, $\frac{Q}{RCNL}$ (dimensionless)
NO SIDE FLOW
BEARING CHARACTERISTIC NO., $S = \left(\frac{R}{C}\right)^2 \frac{\mu N}{p}$ $\left(\frac{sec}{min}\right)$
β = 120°
JOURNAL RUNNING POSITIONS FOR ABOVE VALUES OF CHARACTERISTIC NO.

CHART 7 FOR DETERMINING FILM TEMPERATURE RISE
(Curves based upon no side flow.)

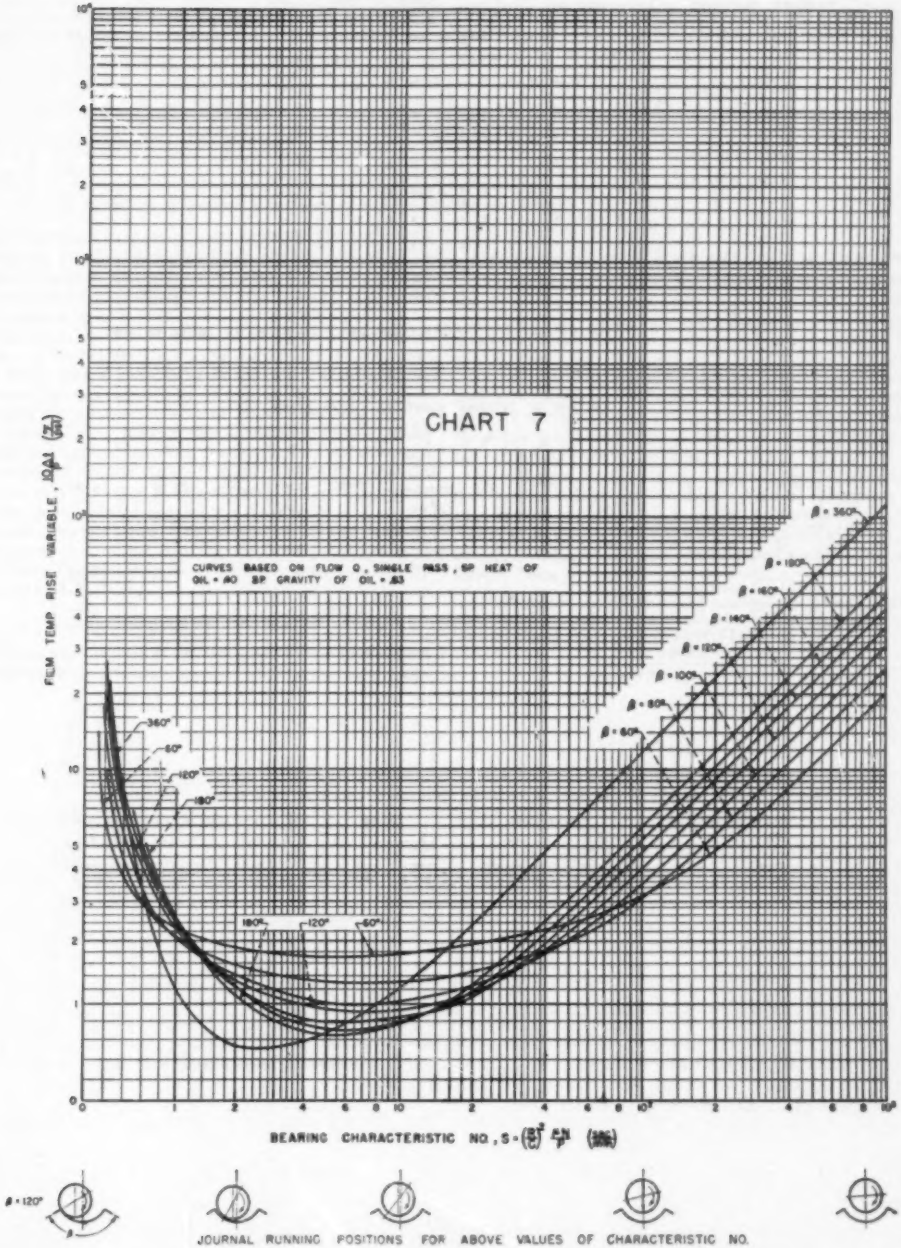
CHART 7
CURVES BASED ON FLOW Q, SINGLE PASS, SP HEAT OF OIL = .40 SP GRAVITY OF OIL = .83
FILM TEMP RISE VARIABLE, $10^6 J \left(\frac{T_2}{W}\right)$
BEARING CHARACTERISTIC NO., $S = \left(\frac{R}{C}\right)^2 \frac{\mu N}{P}$ $\left(\frac{lb\text{-}sec}{in^2}\right)$
β = 360°
β = 180°
β = 160°
β = 140°
β = 120°
β = 100°
β = 80°
β = 60°
360°
180°
120°
60°
β = 120°
JOURNAL RUNNING POSITIONS FOR ABOVE VALUES OF CHARACTERISTIC NO.

TABLE 1 METHOD OF SOLUTION FOR PROBLEMS WHERE EFFECT OF SIDE FLOW IS NEGLECTED

CASE NO.	GIVEN VARIABLES AND CONDITIONS											
	VARIABLES									CONDITIONS		
	θ/β	β	W	N	R	L	C	h_n	μ	MAX. W	MIN. f	MIN. H
1	50	X	X	X	X	X	X	X		–	–	–
2	50	X	X	X	X	X	X		X	–	–	–
3	50	X		X	X	X	X	X	X	–	–	–
4	50	X	X		X	X	X	X	X	–	–	–
5	50	X		X	X	X		X	X	X	–	–
6	50	X	X	X	X	X		X		–	X	X

DETERMINE CASE NO. FROM ABOVE. THEN WORK FROM LEFT TO RIGHT IN TABLE BELOW

CASE NO.	METHOD OF OBTAINING QUANTITIES LISTED BELOW											
	β	R	L	$\frac{h_n}{C}$	W	P	S	C	h_n	ϕ	μ	N
1	given	given	given	given	given	$\frac{W}{2RL}$	from chart 4	given	given	from chart 3	$\left(\frac{C}{R}\right)^2 \frac{PS}{N}$	given
2	"	"	"	from † chart 4	"	"	$\left(\frac{R}{C}\right)^3 \frac{\mu N}{P}$	"	$C\left(\frac{h_n}{C}\right)$	"	given	"
3	"	"	"	given	$\frac{2\mu R^3 LN}{SC^2}$ ■	"	from chart 4	"	given	"	"	"
4	"	"	"	"	given	"	"	"	"	"	"	$\left(\frac{C}{R}\right)^2 \frac{PS}{\mu}$
5	"	"	"	† from chart 14	$\frac{2\mu R^3 LN}{SC^2}$ ▲	"	"	$h_n - \left(\frac{h_n}{C}\right)$	"	"	"	given
6	"	"	"	"	given	"	"	"	"	"	$\left(\frac{C}{R}\right)^2 \frac{PS}{N}$	"

CASE NO	METHOD OF OBTAINING QUANTITIES LISTED BELOW (CONT'D)								
	COEF OF FRICTION		POWER LOSS		FLOW		FILM TEMP. RISE		PRESSURE
	$\frac{R_f}{C}$	f	$\frac{10^3 H}{WNC}$	H	$\frac{Q}{RCNL}$	Q	$\frac{10\Delta t}{P}$	Δt	$\theta p_{max.}$ $\theta p_{min.}$
1	from chart 1	$\left(\frac{R_f}{C}\right)\frac{C}{R}$	from chart 2	$\left(\frac{10^3 H}{WNC}\right)\frac{WNC}{10^3}$	from chart 6	$\left(\frac{Q}{RCNL}\right)RCNL$	from chart 7	$\left(\frac{10\Delta t}{P}\right)\frac{P}{10}$	from chart 5
2	"	"	"	"	"	"	"	"	"
3	"	"	"	"	"	"	"	"	"
4	"	"	"	"	"	"	"	"	"
5	"	"	"	"	"	"	"	"	"
6	"	"	"	"	"	"	"	"	"

■ S from appropriate column at right

▲ S and C from appropriate columns at right

† Calculate S before entering chart 4

Lubricant Flow

The lubricant-flow requirements of a bearing may be found from the flow variable, $Q/RCNL$, shown plotted against S in Chart 6. For the foregoing example

$$\frac{Q}{RCNL} = 2.77$$

or

$$Q = 2.77\,RCNL = 2.77 \times 5 \times 10^{-3} \times 10^{3} \times 10$$

giving

$$Q = 1385 \text{ cu in. per min} = 6.0 \text{ gpm}$$

This is the amount of lubricant which enters the film at the leading edge of the active bearing arc at atmospheric pressure and is pumped through to the trailing edge by the action of the journal. For the assumption of no side flow, the quantity leaving the trailing edge is equal to that entering the leading edge.

If the rate at which lubricant is supplied to the leading edge is less than Q, the bearing is said to be starved. It will not necessarily fail to operate under these conditions but its performance characteristics obviously will be altered—the degree of alteration increasing the smaller the amount of lubricant supplied.

If a bearing is so arranged that lubricant is supplied under pressure, it is again obvious that the performance characteristics will be altered. Under these conditions, part of the lubricant may flow over the top of the journal, appreciably changing the total amount of lubricant chargeable to the bearing.

It is also clear that certain types of grooving will alter radically the flow and performance characteristics of a bearing as computed in the foregoing manner. Such cases must be solved by special methods.

Temperature Rise of Lubricant

If it is assumed that all of the heat generated by friction goes into increasing the temperature of the lubricant flowing through the bearing, the resulting increase can be determined through the use of the temperature-rise variable, $10\,\Delta t/P$. Chart 7 shows $10\Delta t/P$ plotted against S for a typical petroleum oil having a specific gravity of 0.83 and a specific heat of 0.40.[6] For the foregoing example

$$\frac{10\Delta t}{P} = 0.79$$

from which

$$\Delta t = \frac{12{,}500 \times 0.79}{10 \times 10 \times 10}$$

or

$$\Delta t = 9.9 \text{ deg F}$$

Method of Solution Table and Optimum Conditions

The steps taken to obtain the various operating characteristics of the bearing in the above example are outlined in their proper sequence in Table 1, case 2. With other combinations of given variables, different methods of solution are required. The procedure for a few of the more useful cases is given in the table.

To use this table, one should list the known quantities and determine the proper case number by comparing them with those given for the various cases shown in the upper portion of Table 1. He should then proceed to the same case number in the main table and work from left to right.

When designing a bearing for a given application, it is clear that an infinite number of solutions is possible. This being the case, one may wish to select the solution which gives, say, the maximum load capacity, or the minimum power loss. This is termed designing for optimum conditions and is covered by cases 5 and 6.

[6] The temperature rise for a lubricant having a different specific gravity and a different specific heat may be found by multiplying the temperature rise as computed from Chart 7, by

$$\frac{0.332}{\text{specific gravity} \times \text{specific heat}}$$

Applying Bearing Theory to the Analysis and Design of Journal Bearings—II

By JOHN BOYD[1] and ALBERT A. RAIMONDI,[2] EAST PITTSBURGH, PA.

Solution of Problems When Side Flow is Considered

As previously mentioned, taking account of side flow generally has an important influence on the accuracy of bearing calculations. It can be done rather simply, however, by employing a provisional value of S, here referred to as S_o, which is used with the charts for no side flow in a manner similar to that described in Part 1, and modifying the results thus obtained by the introduction of correction factors which take side flow into consideration. The correction factors K_W, K_F, K_Q, and K_T for load, friction, flow, and temperature rise, respectively, are shown plotted against the B/L ratio (length of bearing arc/axial length) in Charts 8, 9, 12, and 13.

It is usually assumed that the angular positions of the minimum film thickness, the maximum and minimum pressure, etc., are not greatly affected when side flow is considered. Consequently, no correction factors are used for these quantities.

Problems in which side flow is taken into account may be solved with the aid of Table 2, which is employed in the same way as Table 1. An example will illustrate this use.

Suppose, in a bearing already built, one wishes to determine the load which can be carried at a specified minimum film thickness with an oil of a given viscosity. The given information is as follows

$R = 2$ in. $\quad C = 0.005$ in. (radial clearance)
$L = 4$ in. $\quad h_o = 0.002$ in.
$\beta = 120$ deg $\quad \mu = 5 \times 10^{-6}$ reyns
$N = 3600$ rpm

Referring to the uppermost portion of Table 2, it is seen that the given variables correspond to case 3. Following the main part of the table from left to right gives

$$\frac{B}{L} = \frac{2\pi R}{L}\frac{\beta}{360} = \frac{2 \times \pi \times 2 \times 120}{4 \times 360} = 1.05$$

$$\frac{h_o}{C} = \frac{0.002}{0.005} = 0.4$$

$K_W = 0.495$ (from Chart 9)
$S_o = 5.0$ (from Chart 4)

$$W = \frac{2\mu R^3 LNK_w}{S_o C^2} = \frac{2 \times 5 \times 10^{-6} \times 2^3 \times 4 \times 3.6 \times 10^3 \times 0.495}{5 \times (5 \times 10^{-3})^2}$$

$W = 4560$ lb

This is the load that can be carried under the foregoing conditions and is all that was asked for in the problem. If the remaining operating characteristics are also desired they may be found as follows

$$P = \frac{W}{2RL} = \frac{4560}{2 \times 2 \times 4} = 275 \text{ psi}$$

$\phi = 32.5$ deg (from Chart 3)
$K_F = 0.945$ (from Chart 8)

$$\left(\frac{R}{C}f\right)_o = 1.2 \text{ (from Chart 1)}$$

$$f = \left(\frac{R}{C}f\right)_o \frac{C}{R}\frac{K_F}{K_W} = \frac{1.2 \times 5 \times 10^{-3} \times 0.945}{2 \times 0.495}$$

$f = 5.72 \times 10^{-3} = 0.00572$

$$\left(\frac{10^5 H}{WNC}\right)_o = 1.9 \text{ (from Chart 2)}$$

$$H = \left(\frac{10^5 H}{WNC}\right)_o \frac{WNC}{10^5}\frac{K_F}{K_W} = \frac{1.9 \times 4.56 \times 10^3 \times 3.6 \times 10^3 \times 5 \times 10^{-3} \times 0.945}{10^5 \times 0.495}$$

$H = 2.98$ hp

$K_Q = 1.6$ (from Chart 12)

$$\left(\frac{Q}{RCNL}\right)_o = 1.46 \text{ (from Chart 6)}$$

$$Q = \left(\frac{Q}{RCNL}\right)_o RCNLK_Q = 1.46 \times 2 \times 5 \times 10^{-3} \times 3.6 \times 10^3 \times 4 \times 1.6$$

$Q = 336$ cu in. per min $= 1.46$ gpm

$$\frac{Q_s}{Q} = 0.40 \text{ (from Chart 10)}$$

$Q_s = 0.40 \times Q = 0.4 \times 1.46 = 0.582$ gpm (both sides)
$K_T = 0.60$ (from Chart 13)

$$\left(\frac{10\Delta t}{P}\right)_o = 0.93 \text{ (from Chart 7)}$$

$$\Delta t = \left(\frac{10\Delta t}{P}\right)_o \frac{P}{10}\frac{K_T}{K_W} = \frac{0.95 \times 275 \times 0.60}{10 \times 0.495}$$

$\Delta t = 31.0$ deg F

$$\frac{p_{max}}{P} = 2.90 \text{ (from Chart 11)}$$

$p_{max} = 2.90 \times 275 = 798$ psi
$\theta_{p(max)} = 5$ deg (from Chart 5)
$\theta_{p(min)} = 60$ deg (from Chart 5)

---

[1] Manager, Lubrication Section, Research Laboratories, Westinghouse Electric Corporation. Mem. ASME.

[2] Research Engineer, Research Laboratories, Westinghouse Electric Corporation. Jun. ASME.

Discussion of this paper should be addressed to the Secretary, ASME, 29 West 39th Street, New York, N. Y., and will be accepted until October 10, 1951, for publication at a later date. Discussion received after the closing date will be returned.

Note: Statements and opinions advanced in papers are to be understood as individual expressions of their authors and not those of the Society. Manuscript received by ASME Applied Mechanics Division, February 2, 1951.

The given viscosity of 5×10^{-6} reyns is the mean value for the film. Viscosity-Temperature Chart 1 shows that an oil such as SAE 20 would have a viscosity of 5×10^{-6} reyns, or 5 microreyns, at 121 F. Thus, assuming 121 F to be the average of the inlet and outlet temperatures for the calculated temperature rise of 31 F, the inlet temperature would have to be 121–31/2 or 105.5 F to fulfill the given conditions. The corresponding outlet temperature would be 136.5 F.

If one wished to supply the lubricant at a temperature of, say, 90 F rather than 105.5 F, it is clear that this could not be done with an SAE 20 oil and still keep the viscosity at the given value of 5×10^{-6} reyns. It would thus be necessary to select another oil which, upon calculation, would give the required inlet temperature.

Usually, one does not know the mean viscosity or the mean temperature of the film when starting a problem, but he does know what inlet temperature he can maintain. Under these conditions he should select an oil temporarily and make two or more temperature calculations with assumed values of the mean viscosity. By comparing the given value of the inlet temperature with those found by calculation, the proper mean film viscosity may be found by interpolation. If the oil chosen does not yield a reasonable solution, a different oil should be tried.

It should be noted that the temperatures calculated in the foregoing are based on all the friction heat being taken away by the lubricant. If appreciable amounts of heat enter or leave the bearing by conduction, etc., this analysis cannot be expected to give accurate results.

Problems Having Other Given Conditions

The application of Table 2 to problems based on cases 1 to 6 is similar to that for Table 1. Two comments, however, should be made in connection with case 7.

In case 7 the bearing arc, in addition to the clearance and viscosity, is unknown. The proper bearing arc for a given L/D ratio is taken from Chart 15 as directed in the table.

If, in case 7, the bearing arc had been given instead of the L/D ratio, the problem would have been quite different for with the load, speed, and minimum film thickness given, the power loss decreases as the L/D becomes infinite. Under these conditions, the choice of the proper L/D must be left to the judgment of the designer.

Agreement Between Theory and Test

To determine how well the theoretical predictions just outlined agree with actual bearing performance, accurate and extensive tests are required. Unfortunately, many of the published test results are either inapplicable or are too inaccurate or too incomplete to permit a satisfactory comparison. The best data for this purpose that has come to the authors' attention is contained in the tests by Boswall (1)[8] on a $2^1/_2$-in-diam × 4-in-long, 105 deg centrally loaded journal bearing. Figs. 4 and 5 show how Boswall's results compare with calculations based upon methods discussed in this paper.

Fig. 4 shows Boswall's coefficient-of-friction data corrected for no side-flow conditions and plotted against the curve for a bearing of 105 deg arc as interpolated from Chart 1. Also shown is a curve based on the work of Swift (2), indicating how the theoretical friction curve is altered if the inability of the film to withstand negative pressures is taken into account.

It will be seen that the effect of such pressures, for a bearing of 105 deg arc, is confined to S-numbers below approximately 10. Above 10, both curves blend together. Below a value of S of about 2 the corrected curve turns downward and approaches zero. This probably would be the case in practice if it were possible to construct a perfect bearing, operate it in exact alignment, and lubricate it with an ideal fluid. Since this cannot be done, however, the coefficient-of-friction variable always turns upward as the S-number approaches zero, in the manner shown by the dotted extension of the test data.

From Fig. 4 it can be concluded that in so far as frictional considerations are concerned the foregoing methods give results that agree quite well with experiment, at least for the particular bearing chosen. A somewhat closer agreement could be obtained if corrections are made for negative pressure, but the additional work thus involved does not appear to be warranted.

Fig. 5 shows Boswall's results for the value and position of the minimum film thickness plotted against the curves for a 105-deg bearing, as interpolated from Chart 4.

Here it will be seen that the agreement between theory and experiment is not as satisfactory as in the case of friction. While the correction for negative pressures does not have much effect on the h_m/C curve, it will be seen from the journal-position diagram that it completely alters the locus of the journal center in the region of small S-numbers.

BIBLIOGRAPHY

Charts 1 to 7 were obtained by direct calculation from the formulas given by Kingsbury (3), using the substitutions suggested by Duffing (4) in the discussion of Kingsbury's paper and are in agreement with the work of Sommerfeld (5) and Harrison (6). The form of presentation is similar to that of Norton (7), and the data are more extensive than those given by Howarth (8) for centrally loaded bearings.

Charts 8 to 13, which are used when side flow is taken into account, are based upon Needs' (9) results for a 120-deg bearing and are assumed to be applicable to bearings of other arcs.

Charts 14 to 15 were drawn from Kingsbury's data dealing with optimum conditions.

1 "The Film Lubrication of the Journal Bearing," by R. O. Boswall and J. C. Brierley, Proceedings of The Institution of Mechanical Engineers, vol. 122, 1932, pp. 423–509.

2 "The Stability of Lubricating Films in Journal Bearings," by H. W. Swift, Proceedings of the Institution of Civil Engineers, vol. 233, 1932, pp. 267–323.

3 "Optimum Conditions in Journal Bearings," by A. Kingsbury, Trans. ASME, vol. 54, 1932, pp. 123–148.

4 Discussion of Kingsbury's paper, reference (3), by G. Duffing, p. 146.

5 "Zur Hydrodynamischen Theorie die Schmiermittelreibung," ("On the Hydrodynamic Theory of Lubrication"), by A. Sommerfeld, *Zeitschrift für Mathematik und Physik*, vol. 50, 1904, pp. 97–155.

6 "The Hydrodynamical Theory of Lubrication With Special Reference to Air as a Lubricant," by W. J. Harrison, Trans. Cambridge Philosophical Society, vol. 22, 1913, pp. 39–54.

7 "Lubrication," by A. E. Norton, McGraw-Hill Book Company, Inc., New York, N. Y., 1942, p. 119.

8 "A Graphical Study of Journal Lubrication, Part II," by H. A. S. Howarth, Trans. ASME, vol. 46, 1924, pp. 809–832.

9 "Effect of Side Leakage in 120° Centrally Supported Journal Bearings," by S. J. Needs, Trans. ASME, vol. 56, 1934, pp. 721–732; vol. 57, 1935, pp. 135–138.

[8] Numbers in parentheses refer to the Bibliography at the end of the paper.

TABLE 2 METHOD OF SOLUTION FOR PROBLEMS WHERE ALLOWANCE IS MADE FOR EFFECT OF SIDE FLOW BY USE OF CORRECTION FACTORS

CASE NO.	GIVEN VARIABLES AND CONDITIONS											
	VARIABLES									CONDITIONS		
	S_0/β	β	W	N	R	L	C	h_n	μ	MAX. W	MIN. f	MIN. H
1	.50	X	X	X	X	X	X	X		–	–	–
2	.50	X	X	X	X	X	X		X	–	–	–
3	.50	X		X	X	X	X	X	X	–	–	–
4	.50	X	X		X	X	X	X	X	–	–	–
5	.50	X		X	X	X		X	X	X	–	–
6	.50	X	X	X	X	X		X		–	X	X
7	.50		X	X	X	X		X		–	X	X

DETERMINE CASE NO. FROM ABOVE. THEN WORK FROM LEFT TO RIGHT IN TABLE BELOW.

CASE NO.	METHOD OF OBTAINING QUANTITIES LISTED BELOW													
	β	R	L	β/L	$\frac{h_n}{C}$	K_w	W	P	S_0	C	h_n	ϕ	μ	N
1	given	given	given	$\frac{2\pi R}{L}\left(\frac{\beta^\circ}{360}\right)$	given	from chart 9	given	$\frac{W}{2RL}$	from †† chart 4	given	given	from † chart 3	$\left(\frac{C}{R}\right)^2\frac{PS_0}{N}\frac{1}{K_w}$	given
2	"	"	"	"	assume **	"	"	"	$\left(\frac{R}{C}\right)^2\frac{\mu N}{P}K_w$	"	$C\left(\frac{h_n}{C}\right)$	"	given	"
3	"	"	"	"	given	"	$\frac{2\pi R^3 LN}{S_0C^2}K_w$ ■	"	from †† chart 4	"	given	"	"	"
4	"	"	"	"	"	"	given	"	"	"	"	"	"	$\left(\frac{C}{R}\right)^2\frac{PS_0}{\mu}\frac{1}{K_w}$
5	"	"	"	"	from chart 14	"	$\frac{2\pi R^3 LN}{S_0C^2}K_w$ ▲	"	"	$h_n-\left(\frac{h_n}{C}\right)$	"	"	"	given
6	"	"	"	"	"	"	given	"	"	"	"	"	$\left(\frac{C}{R}\right)^2\frac{PS_0}{N}\frac{1}{K_w}$	"
7	from chart 15	"	given	"	"	"	"	"	"	"	"	"	"	"

CASE NO.	METHOD OF OBTAINING QUANTITIES LISTED BELOW (CONT'D)													
		COEF. OF FRICTION		POWER LOSS		FLOW				FILM TEMP. RISE			PRESSURE	
	K_T	$\left(\frac{\beta}{C}\right)_0$ *	f	$\left(\frac{10^6 H}{WNC}\right)_0$ *	H	K_Q	$\left(\frac{Q}{RCNL}\right)_0$ *	Q	Q_S	K_T	$\left(\frac{10\Delta t}{P}\right)_0$ *	Δt	P_{max}	$\frac{P_0}{P_{max}}\frac{P_0}{P_{min}}$
1	from chart 8	from chart 1	$\left(\frac{\beta}{C}\right)_0\frac{C}{R}\frac{K_T}{K_w}$	from chart 2	$\left(\frac{10^6 H}{WNC}\right)_0\frac{WNC}{10^6}\frac{K_T}{K_w}$	from chart 12	from chart 6	$\left(\frac{Q}{RCNL}\right)_0 RCNL\cdot K_Q$	from chart 10	from chart 13	from chart 7	$\left(\frac{10\Delta t}{P}\right)_0\frac{P}{10}\frac{K_T}{K_w}$	from chart 11	from † chart 5
2	"	"	"	"	"	"	"	"	"	"	"	"	"	"
3	"	"	"	"	"	"	"	"	"	"	"	"	"	"
4	"	"	"	"	"	"	"	"	"	"	"	"	"	"
5	"	"	"	"	"	"	"	"	"	"	"	"	"	"
6	"	"	"	"	"	"	"	"	"	"	"	"	"	"
7	"	"	"	"	"	"	"	"	"	"	"	"	"	"

** Assume h_n/C, get K_w, calculate S_0; then using $S=S_0$ find actual h_n/C from chart 4. Repeat until assumed h_n/C = actual h_n/C. Then continue solution of problem. Note: h_n/C may vary between 0 and 1.0. A good value to assume at start is $h_n/C = .4$.

■ S_0 from appropriate column at right

* Quantities marked thus ( )$_0$ are values which correspond to $S=S_0$.

† Obtained by entering chart using $S=S_0$.

†† In this case $S_0=S$.

▲ S_0 and C from appropriate columns at right

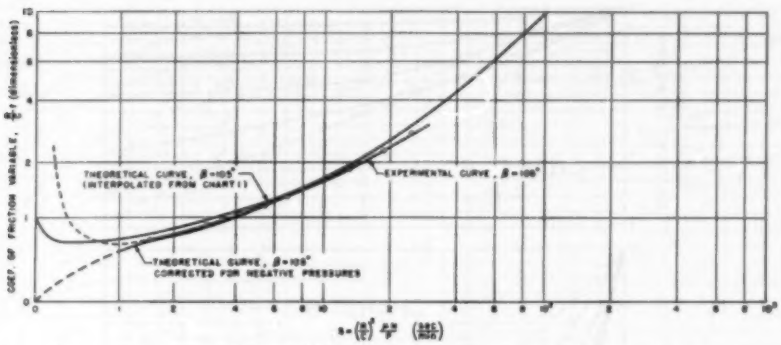
COEF. OF FRICTION VARIABLE, $\frac{R}{P}f$ (dimensionless)
THEORETICAL CURVE, $\beta=105°$ (INTERPOLATED FROM CHART I)
EXPERIMENTAL CURVE, $\beta=105°$
THEORETICAL CURVE, $\beta=105°$ CORRECTED FOR NEGATIVE PRESSURES
$S=\left(\frac{R}{C}\right)^2\frac{\mu N}{P}$ $\left(\frac{\text{sec}}{\text{min}}\right)$

FIG. 4 COMPARISON OF THEORY WITH EXPERIMENT FOR COEFFICIENT-OF-FRICTION VARIABLE

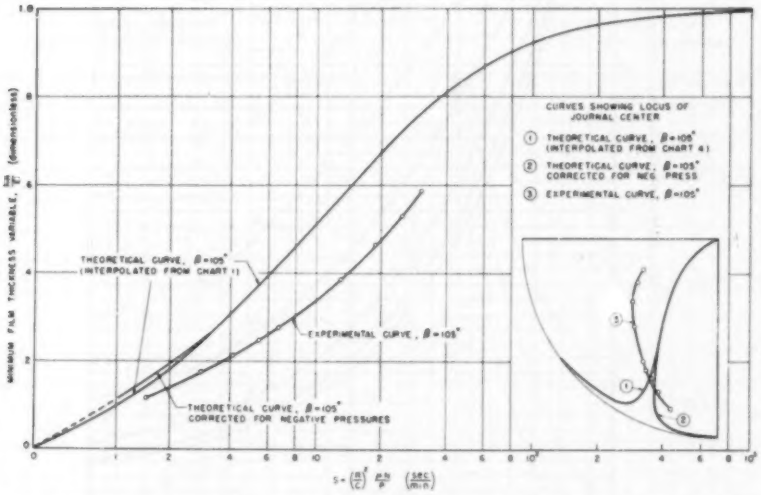
MINIMUM FILM THICKNESS VARIABLE, $\frac{h_0}{C}$ (dimensionless)
CURVES SHOWING LOCUS OF JOURNAL CENTER
① THEORETICAL CURVE, $\beta=105°$ (INTERPOLATED FROM CHART 4)
② THEORETICAL CURVE, $\beta=105°$ CORRECTED FOR NEG. PRESS
③ EXPERIMENTAL CURVE, $\beta=105°$
THEORETICAL CURVE, $\beta=105°$ (INTERPOLATED FROM CHART I)
EXPERIMENTAL CURVE, $\beta=105°$
THEORETICAL CURVE, $\beta=105°$ CORRECTED FOR NEGATIVE PRESSURES
$S=\left(\frac{R}{C}\right)^2\frac{\mu N}{P}$ $\left(\frac{\text{sec}}{\text{min}}\right)$

FIG. 5 COMPARISON OF THEORY WITH EXPERIMENT FOR MINIMUM FILM THICKNESS AND JOURNAL POSITION

CHARTS 8 AND 9 LOAD AND FRICTION CORRECTION FACTORS FOR VARIOUS VALUES OF B/L
(Used when allowing for side flow.)

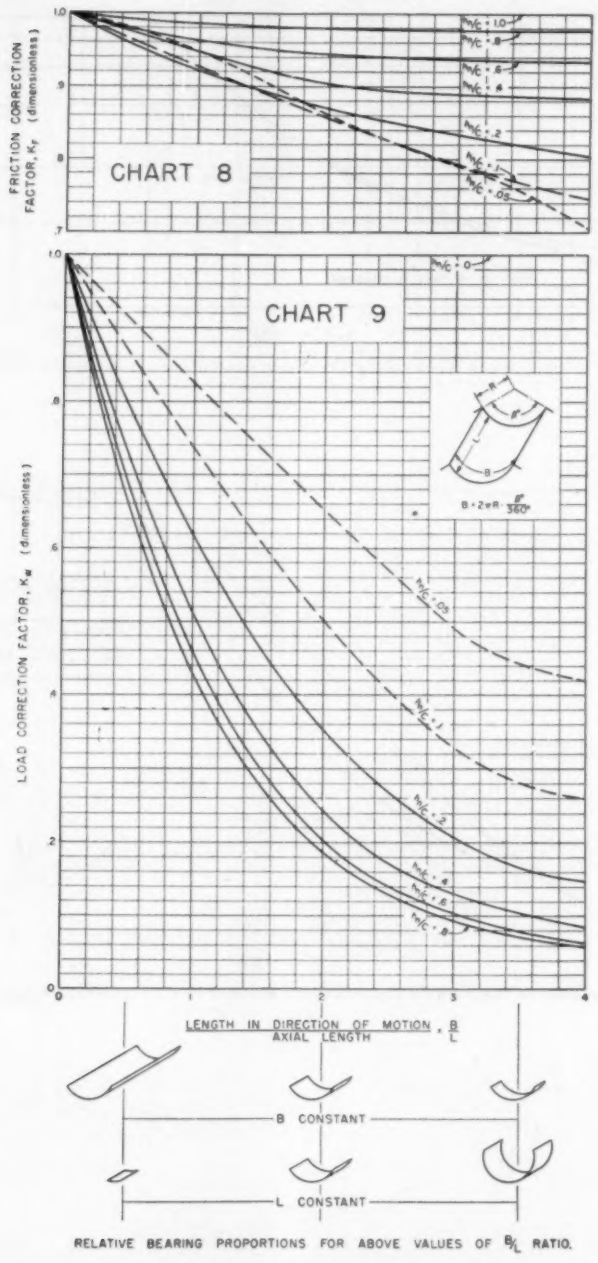

CHART 10 RATIO OF SIDE FLOW TO TOTAL FLOW FOR VARIOUS VALUES OF B/L

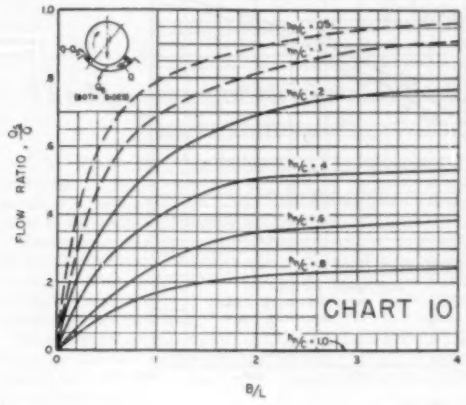

CHART 11 RATIO OF MAXIMUM FILM PRESSURE TO UNIT BEARING LOAD FOR VARIOUS VALUES OF B/L

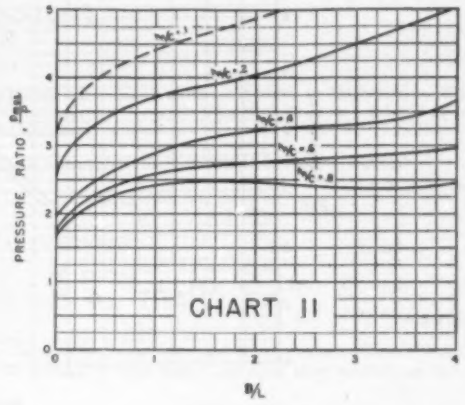

CHART 12 LUBRICANT FLOW CORRECTION FACTORS FOR VARIOUS VALUES OF B/L
(Used when allowing for side flow.)

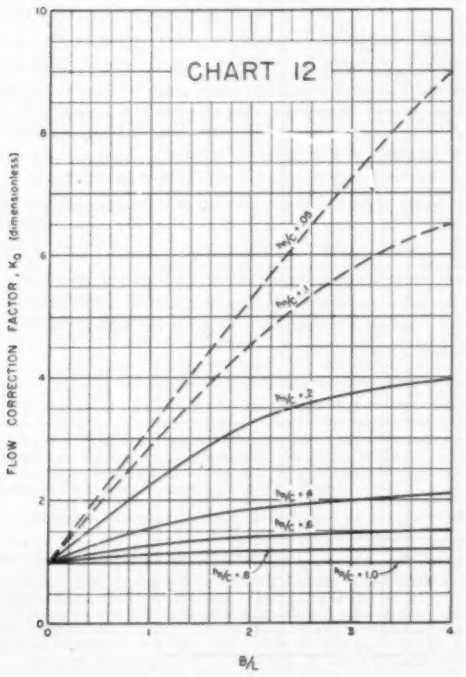

CHART 13 FILM TEMPERATURE RISE CORRECTION FACTORS FOR VARIOUS VALUES OF B/L
(Used when allowing for side flow.)

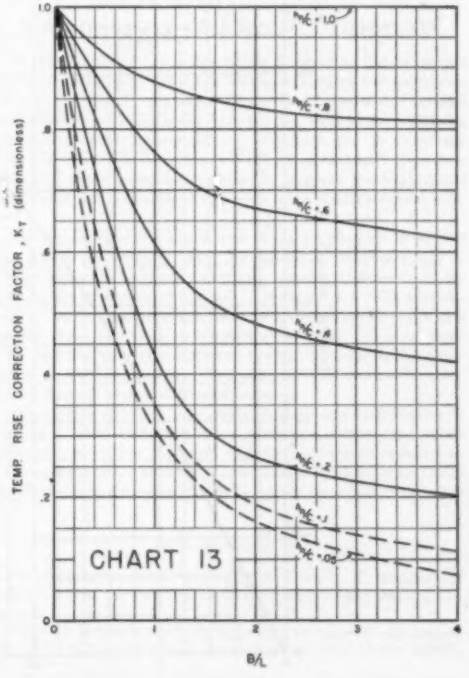

CHART 14 FOR DETERMINING VALUES OF h_o/c CORRESPONDING TO MAXIMUM LOAD OR MINIMUM POWER LOSS FOR VARIOUS BEARING ARCS

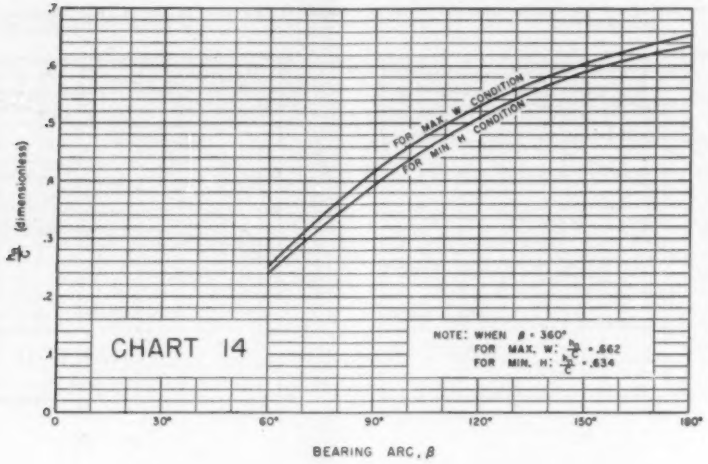

CHART 15 FOR DETERMINING OPTIMUM VALUE OF BEARING ARC β WHEN DESIGNING FOR LEAST POWER LOSS

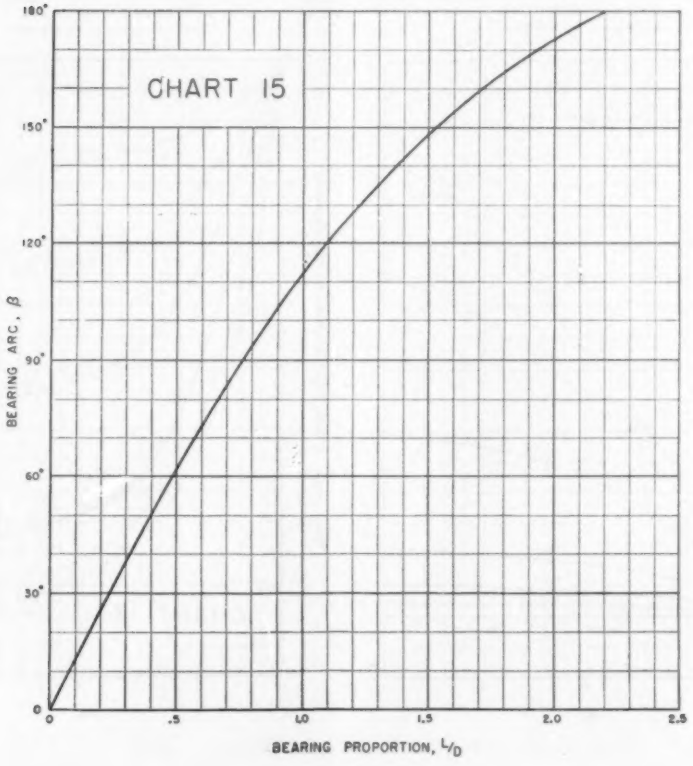

Discussion

The Dynamics of the Buckling of Elastic Columns[1]

C. M. Tyler, Jr.[2] The author should be commended for providing a rather complete treatment of dynamic-column action in a testing machine. This work should prove a useful guide to the solution of other dynamic-column problems.

Readers may be interested in an alternate solution, applicable at least to the small deflections case, in terms of Airy integral functions. This has become numerically practical with the tabulation of a function[3] which appeared after the author's manuscript was submitted.

With the transformation $Z_1 = -\Omega^{1/3}z$, Equation [15] of the paper and the initial conditions become $f'' - Z_1 f = \Omega^{1/3}e$; when $Z_1 = -\Omega^{1/3}$, $f = e$ and $f' = 0$. The solution of this equation is known to be[4]

$$f = \alpha Ai(Z_1) + \beta Bi(Z_1) - \Omega^{1/3}e\pi Gi(Z_1)$$

where $Ai(Z_1)$, $Bi(Z_1)$, and $Gi(Z_1)$ are Airy integral function and α and β are arbitrary constants.

For any particular value of Ω, the constants α and β can be evaluated using the initial conditions. For the author's value of $\Omega = 2.25$, the initial value of $Z_1 = -2.25^{1/3} = -1.3084$. Then applying the initial conditions

$$e = \alpha Ai(-1.3084) + \beta Bi(-1.3084) - 1.3084e\pi Gi(-1.3084)$$
$$0 = \alpha Ai'(-1.3084) + \beta Bi'(-1.3084) - 1.3084e\pi Gi'(-1.3084)$$

Numerical values of the functions and their derivatives are taken from published tables[5,6] with the exception of the Gi' value which is obtained by numerical differentiation

$$e = 0.51080\alpha - 0.08077\beta + 1.3084 \times \pi \times 0.03503e$$
$$0 = 0.17760\alpha + 0.59513\beta - 1.3084 \times \pi \times 0.66089e$$

Solving these equations simultaneously, $\alpha = 0.3211e$, and $\beta = 3.3929e$. Then

$$f = 0.3211eAi(Z_1) + 3.3929eBi(Z_1) - 1.3084e\pi Gi(Z_1)$$

The numerical value for f for $z = 0$ as given by the author can be recalculated. When $z = 0$, $Z_1 = 0$ and then

$$f = 0.3211 \times 0.35503e + 3.3929 \times 0.61493e - 1.3084 \times \pi \times 0.20498e$$

$$f = 1.358e$$

The foregoing solution is also valid when the author's time parameter $\xi > 1$ and is thus applicable to his Equation [33]. Numerically for $\Omega = 2.25$, when $\zeta = 0.1$, $z = -0.1$ and $Z_1 = 0.13084$ then

$$f = 0.3211 \times 0.32129e + 3.3929 \times 0.67382e - 1.3084 \times \pi \times 0.22189e$$

$$f = 1.477e$$

In a similar manner

$$\frac{df}{d\zeta} = \frac{df}{dZ_1}\frac{dZ_1}{dz}\frac{dz}{d\zeta} = 1.0061e \times (-1.3084) \times (-1.0) = 1.316e$$

These three values correspond to the author's values of $1.36e$, $1.5e$, and $1.326e$, respectively, and check them within 2 per cent.

Author's Closure

The author appreciates the comments made by the discusser and agrees with him fully when he says that the new tables of Airy integrals allow a convenient evaluation by means of the discusser's solution.

Pressure Distribution in the Calendering of Plastic Materials[6]

R. E. Gaskell.[7] It is interesting to observe that in certain experiments listed in Table 1 of the paper, notably in experiments Nos. 27, 51, 204, 71, the point of maximum pressure and the exit are definitely not equidistant from the nip, while in the remaining experiments they are equidistant, or nearly so. Is there any cause to which this discrepancy could be attributed? Is it possible that these particular experiments involved materials under conditions that caused them to possess some elastic recovery ability?

On examination of Table 1, one might be tempted to believe that here is a method by which the rheological diagram might be constructed—the viscosity found as a function of shear rate—by running the rolls at varying speeds. However, the "effective viscosity," as its name implies, is not a measurement of viscosity at a specific shear rate, but an average of viscosity taken at shear rates varying from zero midway between the rolls to the value $3\mu U/(t_0 - t_1)/t_0^2$ at the rolls. It is impossible to deduce the rheological diagram from this information alone.

The authors certainly have made an important contribution to rheology. With such ingenious applications of the latest scientific tools, the writer can agree with their optimistic conclusion: "An approach to the problem of establishing the flow properties of non-Newtonian materials should lie within the realm of possibility."

Authors' Closure

The occurrence, noted by Professor Gaskell, of instances in Table 1 where the point of maximum pressure and the exit are

---

[1] By N. J. Hoff, published in the March, 1951, issue of the Journal of Applied Mechanics, Trans. ASME, vol. 73, pp. 68–74.

[2] Assistant Professor of Mechanical Engineering, Carnegie Institute of Technology, Pittsburgh, Pa. Jun. ASME.

[3] "Numerical Evaluation of Integrals of Form $I = \int_{X_1}^{X_2} f(x)e^{i\phi(x)}dx$ and the Tabulation of the Function $Gi(Z) = \frac{1}{\pi}\int_0^\infty \sin(uZ + 1/3u^3)du$," by R. S. Scorer, *The Quarterly Journal of Mechanics and Applied Mathematics*, vol. III, part I, March, 1950, pp. 107–112.

[4] "Notes on the Solution of the Equation $y'' - xy = f(x)$," by J. C. P. Miller and Z. Mursi, *The Quarterly Journal of Mechanics and Applied Mathematics*, vol. III, part I, March, 1950, pp. 113–118.

[5] "The Airy Integral," by J. C. P. Miller, British Association for the Advancement of Science, Mathematical Tables Part-Volume B, Cambridge University Press, London, England, 1946.

[6] By J. T. Bergen and G. W. Scott, Jr., published in the March, 1951, issue of the Journal of Applied Mechanics, Trans. ASME, vol. 73, pp. 101–106.

[7] Associate Professor of Mathematics, Iowa State College, Ames, Iowa.

equidistant for certain non-Newtonian materials, we consider to be fortuitous. In most cases the point of maximum pressure is less than or equal to the exit though it may be greater, as in Experiment 204. The results of many experiments, not included in this paper, confirm this point.

In addition, a graphical comparison of such experimental data with a plot of Equation [1] indicated a marked discrepancy between the shape of the curves which was independent of the constant parameters of Equation [1]. In the absence of a more rigorous analysis of this situation it seems best to conclude that the non-Newtonian materials did not behave the same as a simple viscous liquid.

Book Reviews

Fluid Mechanics

FLUID MECHANICS. By Victor L. Streeter. McGraw-Hill Book Company, New York, N. Y., 1951. Cloth, 6 × 9 in., 315 illus., bibliography, appendixes, index viii and 366 pp., $5.

REVIEWED BY H. L. LANGHAAR[1]

THIS is an introductory text on fluid mechanics for undergraduate engineering students. The principal emphasis is on incompressible flow. The material that is covered includes statics of fluids, Bernoulli's equation, the steady-flow momentum equation, jets, vanes, principles of turbomachines, simple problems of laminar flow, elements of lubrication theory, Venturi meters, Pitot tubes, orifices, weirs, the modern theory of steady flow in closed conduits, elementary open-channel theory, boundary-layer theory, and a discussion of separation and drag coefficients.

Some topics are treated in considerable detail; notably, statics of fluids, turbomachines, pipe networks, and oil hydraulic systems. The chapter dealing with forces on immersed bodies includes an introduction to potential flow theory. There are many excellent problems in the book, including a large number of multiple-choice questions that are useful for classroom discussion.

The book contains no formal presentation of dimensional analysis, and very little reasoning based on the hypothesis of dimensional homogeneity. Newton's equations of particle dynamics are employed as the basis for nearly all the theory. In general, the material is well organized.

There has been a widely felt need for new texts on fluid mechanics. Undoubtedly, Streeter's work will help to alleviate this need. However, the book may lack the simplicity and the generality that are requisites for popular texts. The analytical level of the presentation is somewhat advanced for the average engineering undergraduate. The nature of the presentation has been influenced, perhaps too strongly, by classical hydrodynamics. For example, the energy principle of flow theory has been derived from Newton's laws of dynamics, rather than from the first law of thermodynamics. This example may illustrate two irreconcilable points of view; a circumstance that precludes any text on fluid mechanics that will receive the approbation of a large majority of engineering teachers.

[1] Professor, Theoretical and Applied Mechanics Department, University of Illinois, Urbana, Ill. Mem. ASME.

Creep of Metals

CREEP OF METALS. By L. A. Rotherham. (Physics in Industry.) The Institute of Physics, 47 Belgrave Square, London S.W.1., England, 1951. Cloth, 6 × 9½ in., 80 pp., 24 figs., 3 tables, references, index, 15/—.

REVIEWED BY JOHN M. LESSELLS[2]

THIS is a short monograph of the series Physics in Industry on creep of metals, bringing together into one volume the various papers recently published. While the subject matter deals more with the viewpoints of the physicist and metallurgist rather than those of the engineer, the treatment given will be of extreme interest to all those working in this field of high temperature. There is, however, a need for bringing together the new data on design interpretations.

The first three chapters cover such aspects as characteristics of the creep curve, crystalline flow, and metallographic feature. The next four chapters deal with grain-boundary creep, transient creep, steady-state and tertiary creep. The last chapter covers the recent developments in creep-resistant alloys.

As stated above, the book will be of more use to the physicist although some useful discussion is made of the engineering interpretations of McVetty and of Tapsell. A useful bibliography which refers to each particular chapter is given at the end.

[2] Associate Professor of Mechanical Engineering, Massachusetts Institute of Technology, Cambridge, Mass. Mem. ASME.

Abstracts of Papers

presented at the

First U. S. National Congress of Applied Mechanics

Appearing below are authors' abstracts of all the papers which have been presented at the First U. S. National Congress of Applied Mechanics, held at Illinois Institute of Technology, Chicago, Illinois, from June 11 to June 16, 1951. All papers submitted prior to June 11, 1951, and accepted by the Editorial Committee of the Congress with the advice of referees, will be printed in full in Proceedings of the Congress. These Proceedings, which will be published by The American Society of Mechanical Engineers, are to appear within the year following the Congress.

The abstracts given here are grouped according to subject matter and session schedule. In view of the current space limitations of the JOURNAL OF APPLIED MECHANICS, it has been necessary to omit at this place the titles of the authors as well as any references to sponsorship of the investigations concerned; complete information of this nature will be contained in the Proceedings. If necessary, authors may be reached through the Chairman of the Editorial Committee, Professor Eli Sternberg, Illinois Institute of Technology, Chicago 16, Illinois.

The Editorial Committee wishes to express its sincere appreciation to the staff of the JOURNAL OF APPLIED MECHANICS, in particular to the editor, Professor John M. Lessells, for their efforts in connection with the present publication of these abstracts.

Session 1: Friction; Failure of Material

Further developments in the measurement of the coefficient of static friction. H. Dean Baker, W. Claypoole, D. D. Fuller, Columbia University.

A sensitive friction tester, described in an earlier paper, has been rearranged to provide for automatic photographic recording of results, and mounted on a specially designed Julius suspension. Automatic photographically recorded data are given for controlled variation in disturbance down to very low levels. It is shown that the low values of the coefficient of static friction reported in the earlier work are attributable to the effects of mechanical disturbances. The coefficient of static friction measured at the low disturbance level attained in the present work has essentially the same value as was found by previous investigators.

Fatigue tests of single crystals of ingot iron. F. A. McClintock, Massachusetts Institute of Technology.

Single crystals of ingot iron were tested in a rotary bending-fatigue machine and examined microscopically. As had been reported by others, slip was found to take place on surfaces of high shear stress parallel to a body-diagonal direction in the crystal lattice. In contrast to some recent work, the slip appeared to occur on wavy surfaces rather than pairs of crystallographic planes. Fatigue cracks started from inclusions and spread on surfaces of high shear stress containing a body diagonal of the crystal lattice. The life under a reversed bending stress of 20,000 psi was of the order of 300,000 cycles. Cleavage fractures on the cube face were observed in two exceptional instances.

Use of a recrystallization method to study the nature of damage in fatigue of metals. G. M. Sinclair, T. J. Dolan, University of Illinois.

Based on the assumption that the initiation of a fatigue crack is preceded by a period of work-hardening, a study was made to determine the relative extent to which permanent fatigue damage occurs during the early stages of a fatigue test. Periodical reheating to the recrystallization temperature was employed as a means of removing the effects of work-hardening developed by the repeated stressing. Since this processing did not affect the finite fatigue life significantly, it was concluded that permanent damage (probably in the form of submicroscopic cracks) is initiated in local regions during a relatively early stage of cyclic stressing. Statistical methods were employed to evaluate the data.

The formation of a necked region and fracture along an oblique line in flat tensile bars. J. S. Aronofsky, Magnolia Petroleum Company.

A study is made of the necked region which forms along an oblique line in flat tensile bars. Several series of tension tests were run in order to investigate the transition from the symmetrical-type neck to the oblique neck and oblique fracture. In one series of tests the b/h ratio of width to thickness was varied, and in another series the strain-hardening due to cold-rolling was varied in order to observe the mode of necking. The method of characteristics of the hyperbolic partial differential equation is used to predict slip lines for the state of plane stress—either uniaxial or biaxial.

On the inelastic behavior of concrete. A. M. Freudenthal, Columbia University.

Concrete may be considered a two-phase material consisting of an essentially viscous cement paste in which the essentially elastic stone aggregate is suspended. Therefore, the volume concentration of the aggregate will affect both the deformational response and the fracture of various concrete mixes. The results of compression tests of cylinders with hyperbolic circumferential notches of different root radii, for which the elastic solution is known, made of three types of concrete representing, respectively,

a (not necessarily linear) viscoelastic material, a high-density elastic aggregate with filled voids, and an intermediate type, indicate the influence of the internal structure of the concrete on the character of its failure under nonuniform stress distribution. The results also show that the more nearly viscoelastic the material, the better does the elastic stress distribution account for the observed behavior. It is attempted to evaluate the test results in terms of a general theory of fracture of heterogeneous materials.

Session 2: Plates

Surface stress singularities resulting from various boundary conditions in angular corners of plates under bending. M. L. Williams, Jr., California Institute of Technology.

By considering product solutions to the plate equation in polar co-ordinates, six combinations of (homogeneous) boundary conditions—clamped, free, and simply supported edges—are investigated along the radial boundaries of a sector plate. Inasmuch as the deflection function is of the form $w(r,\theta) = Ar^{\lambda+1}F(\theta;\lambda)$, the determinant of the four linear homogeneous equations given by the two boundary conditions on each of the radial edges determines the parameter λ. It is found that of the cases investigated, only the free-free and clamped-clamped combinations have minimum values of λ greater than unity for all values of the opening angle less than 180 deg. The other four cases give values less than unity for angles greater than 90 deg, which means the stresses, being essentially two derivatives of the deflection function, become (mathematically) unbounded at the origin.

Circular and rectangular plates under lateral load and supported by an elastic solid foundation. Gerald Pickett, F. J. McCormick, Kansas State College.

Both circular and rectangular plates with free edges and under a general distribution of loading are considered. The supporting foundation is assumed to be a homogeneous elastic solid of uniform thickness and to extend a great distance beyond the plate boundaries. The elastic solid foundation is in turn assumed to be supported by a rigid base. The pressure and deflection of the circular plate, expressed as double Fourier series, are equated, respectively, to the pressure and deflection of the surface of the elastic solid, expressed as Fourier integral-series, by the use of Fourier-Bessel transforms. The method of finite differences is used to obtain an approximate solution for the rectangular plate. Numerical examples are given.

Large deflections of rectangular plates. M. Stippes, University of Illinois.

The method of Ritz is used to obtain approximate solutions of von Kármán's equations for large deflections of plates. Solutions are made available for a class of boundary conditions. This group of boundary conditions is characterized by the fact that two opposite edges are simply supported and the remaining two parallel edges may be either simply supported, free, or elastically supported. Under these assumptions, it is possible to write the potential energy of the plate and applied loads in a particularly simple fashion. A numerical example is computed for a square plate simply supported on all four sides under a uniform load. The maximum deflection obtained is compared with the linear theory, an approximate expression due to Föppl, and the results of an experiment. As a by-product, one can also obtain the influence surfaces for a plate undergoing small deflections but still satisfying the foregoing boundary conditions.

Determination of the effective width of plates with small deviations from flatness by the method of split rigidities. P. P. Bijlaard, Cornell University.

The approach is analogous to the derivation of the deflection of an initially bent column as given in the *Journal of the Aeronautical Sciences*, May, 1951, as an introduction to the author's analysis of the stability of sandwich plates. For a given initial deflection, the average edge compressive stress required for further deflection is expressed in the postbuckling stress of initially flat plates as derived by S. Levy. This is done by comparing the average deflecting and resisting forces that act on an element of the plate. Subsequently, the relation between average edge compressive stress and unit shortening is derived, which gives the variation of effective width with average edge compressive stress. Results are in excellent agreement with those obtained previously in another way by Hu, Lundquist and Batdorf (NACA TN 1124, 1946).

On the optimum distribution of material in sandwich plates. P. P. Bijlaard, Cornell University.

For a sandwich plate with given thickness and given weight per unit surface, the ratio of elastic moduli of core and faces, that leads to a maximum buckling load, is computed. Various cases of loading and boundary conditions are considered. A direct method is given for calculating for a given load the dimension of a sandwich plate with optimum properties. Assuming a material of which the elastic modulus varies proportionally to its density, the optimum continuous distribution of material in a plate, subjected to compression or shear in its own plane or a combination of that, is computed by the calculus of variations. Also a plate with five different layers is considered.

Session 3: Creep

Derivation of stress-strain equation from creep or relaxation data for plastics. W. N. Findley, University of Illinois.

The development of an equation is described which represents the creep behavior of a canvas laminate as a function of time, temperature, and stress, and which is in agreement with pertinent theory. From the equation of creep versus time, temperature, and stress was derived an expression for stress versus strain in a tension test at known strain rates. Similarly, expressions for relaxation, for recovery, and for stress versus strain at known stress rates are described. The significance of the various terms in the equations are discussed and some of the equations are compared with test data on plastics.

A theory for combined creep strain-stress relations for materials with different tension and compression properties. Joseph Marin, Yoh-Han Pao, The Pennsylvania State College.

This paper presents a new theory for creep strain-stress relations for materials with directional properties and subjected to combined stresses. The theory is applied to determine theoretical creep deformation-time relations for materials subjected to

torsion where the simple tension and simple compression creep constants are different. Torsion creep-test results on a plastic material are reported in confirmation of the proposed new theory.

Deflection of members subjected to bending accompanied by creep. Joseph Marin, L. W. Hu, The Pennsylvania State College.

The determination of creep deflection in beams and other members subjected to bending becomes mathematically complicated when even theories based upon the simplest tension or compression creep-stress-time relations are used. A semigraphical method is described in this paper for determining creep deflections in members subjected to bending. Actual creep deflection-time relations for pure bending were determined for four laminated plastics. These experimental results are compared with the theoretical results using the graphical method developed. The theoretical values are based on simple tension and compression creep constants obtained from 1000-hr creep-time relations and for various stress values. For the four laminated plastics tested, good agreement was found between the theoretical and experimental values of the creep deflections.

Theory of linear creep in pin-jointed structures. R. C. Meacham, Carnegie Institute of Technology.

A solution is obtained for the stress and total strain (elastic plus anelastic) in a pin-jointed truss, each bar of which exhibits a creep rate proportional to the stress. Two cases are studied: (1) The stress in each bar is below the elastic limit; (2) some of the redundant members are perfectly plastic. The geometry of stress space is employed to present the results (Prager and Symonds, Third Annual Symposium of Applied Mathematics, 1949). For case (1) there are h equilibrium equations, r compatibility equations, and n creep-rate equations ($h + r = n$). The r compatibility equations are obtained by employing a minimum principle enunciated by Colonnetti (*Journal de mathematiques pures et appliquees*, **17**, 233–255, 1938). The stresses and the anelastic strains are obtained as unique functions of time if the anelastic strains are known initially. The results of case 1 are extended in case 2 to describe the behavior of the structure during any one "phase" when certain known bars are perfectly plastic.

An elementary theory of creep buckling of columns. D. Rosenthal, H. W. Baer, University of California.

A simplified theory of creep buckling of columns with small initial eccentricity has been developed. The actual creep behavior was approximated by elementary models which distinguished the transient from the steady-state creep in tension. It was assumed that under a constant tensile stress the transient deformation tended to a finite value and the steady-state deformation progressed at a constant rate. With this assumption, a criterion of creep buckling for an indefinite time of service was predicted if the creep in tension was transient. This criterion was equivalent to the Euler buckling criterion. However, if the creep in tension contained a steady-state component, the theory showed that the column would become unstable under any stress. Since the change of dimensions was not considered this prediction was likely to be a conservative one. The existence of a critical stress in creep buckling has been demonstrated in a series of preliminary tests of short duration (48 hr) on 99.5 per cent aluminum at 95 F. Further tests appear necessary before practical conclusions can be drawn.

Session 4: Theoretical and Experimental Methods

A study in photoplasticity. M. Hetényi, Northwestern University.

Certain nylon copolymers were found to have a practically linear stress-strain relationship with a sharply defined yield point, accompanied by considerable birefringence in polarized light. This paper describes tests made with such nylon specimens beyond the elastic range. The stress patterns observed around the edges of yielded regions indicate conditions which facilitate the propagation of the plastic front and afford an explanation of the known instability of the yielding process. The appearance of the slip lines and the formation of plastic enclaves are compared with observations made on steel specimens and with the results of analytical studies.

Studies in three-dimensional photoelasticity; the application of the shear difference method to the general space problem. M. M. Frocht, Roscoe Guernsey, Jr., Illinois Institute of Technology.

It is known that purely optical procedures cannot solve the general three-dimensional stress problem. Photoelasticity furnishes five independent equations whereas the state of stress at a point is given by six independent components. This paper deals with methods which, when combined with photoelastic data, will yield the complete state of stress. The methods now in existence are reviewed and shown to be either limited in nature or impractical. A new, general, and practical method is described. It consists of supplementing the photoelastic data with a numerical integration of one of the differential equations of equilibrium in Cartesian co-ordinates. This permits the determination of all stress components at each point of an arbitrary straight line traversing the body. Preliminary work with this procedure shows possibilities of high accuracy.

Determination of stress-strain curve in shear by twisting square plate. Walter Ramberg, J. A. Miller, National Bureau of Standards.

A method is presented for determining the stress-strain curve in shear for an isotropic flat sheet from measurements of deflection or of extreme fiber bending strain in the center portion of a twisted square plate. The octahedral stress derived from the stress-strain curve in shear for a twisted plate of aluminum alloy agreed within about 5 per cent with the octahedral stress derived from tensile and compressive tests of the same material. The difference was much greater for specimens of mild steel with a definite yield point. Unfortunately, the method is difficult to perform on thin sheet because of the small size of the specimen. An examination of alternate methods indicates particular promise for the use of an annulus of constant thickness.

Extrapolation formulas in finite difference processes. M. G. Salvadori, Columbia University.

Problems involving differential or integral processes are often solved by means of successive approximations based upon use of finite differences. When the successive approximations are obtained by decreasing the mesh size h as $1/n$ (n = an increasing integer), extrapolated values corresponding to $n = \infty$ may be computed easily by means of formulas, whose coefficients are

presented in the paper, with considerable saving in numerical labor. The formulas are applied to typical problems in differentiation, integration, solution of ordinary and partial differential equations, and the evaluation of characteristic values.

Bounds and convergence of relaxation and iteration procedures. N. M. Newmark, University of Illinois.

This paper discusses a number of general concepts relating to relaxation procedures, methods of "steepest descent," and iteration procedures. The relationship between these is indicated for certain systematic ways in which relaxation patterns may be developed. An extrapolation procedure is developed for problems in which the successive approximations technique, in its usual form, diverges. The procedure is a generalization of an observation by Hartree and others that in many cases such divergent problems can be treated by considering the divergence to be a geometric one. The study of upper and lower bounds to the errors in relaxation procedures is a second major part of the paper. General procedures are developed for determining the maximum and minimum errors in any of the quantities for which bounds to an influence function can be determined. Use of the theorems derived makes it possible, for example, to estimate the error due to all sources including "round off" at any stage in the numerical solution of Laplace's or Poisson's equation.

Session 5: Plasticity (general theory)

The principle of minimum work applied to states of finite, homogeneous, plane, plastic strain. A. Nadai, Pittsburgh, Pa.

Sequences of finite, homogeneous, plane strain for an ideally plastic substance are defined by plotting in a plane figure the conventional finite shear as a function of the quadratic finite elongation (the square of one plus the unit strain) for two straight lines which in the unstrained condition of the body were perpendicular. The plastic work of deformation is evaluated for different sequences originating in the unstrained and ending in the same strained condition of the body. There is one and only one particular pathway for which the axes of the incremental tensor of strain continuously coincide with the axes of the tensor of finite strain. For this sequence of finite strains the work of permanent deformation is a minimum. It is shown that the curves corresponding to these minimum work sequences are the extremal curves of the Euler differential equation of the problem of variational calculus for the minimum of plastic work done.

On the general plane problem of mathematical plasticity. Hilda Geiringer, Wheaton College.

Taking as starting point the three-dimensional problem of an isotropic perfectly plastic body it is shown that both, "general plane strain," and "general plane stress" lead to the following set of five equations: Two equilibrium conditions, one general yield condition, and the "strain-stress" relations

$$(\epsilon_x - \epsilon_y)/\gamma = \cot 2\theta, \quad (\epsilon_x + \epsilon_y)/\gamma = -\cos 2\varphi / \sin 2\theta$$

Here, $\epsilon_x = \partial v_x/\partial x$, ϵ_y, γ denote components of strain-rate tensor, θ angle between x and first principal stress direction, φ angle between that direction and each of the symmetric, double counting, characteristics, C^+, C^-. Relations between these characteristics and their mappings onto "stress graph" and onto "velocity plane" are studied and used. Also, in this general case, "characteristic" velocity equations are established, stating that the strain rate in a characteristic direction vanishes. The theory is applied to "simple waves"; stress distribution and velocity distribution corresponding to given initial conditions are completely and explicitly determined.

A review of the definitions of finite strain. A. V. Hershey, U. S. Naval Proving Ground.

An elementary sphere in a deforming medium is transformed into an elementary ellipsoid. The principal components of the strain tensor may be defined as the increase in length per unit length along the principal radii of the ellipsoid, and the principal axes of the strain tensor may be defined as the principal axes of the ellipsoid. This conventional definition of strain has long been recognized in connection with homogeneous strain, but apparently has only recently been extended to the general case of strains of any type. Various published representations of strain are compared in the present paper with the conventional strain. The analysis is illustrated by an application to the practical case of a surface grid which is simultaneously stretched and sheared at variable rates.

On the coincidence of plasticity solutions obtained with incremental and deformation theories. F. Edelman, Radio Corporation of America.

A theorem due to Ilyushin is generalized in two directions. Ilyushin postulated a body composed of a work-hardening material for which strain equals a constant times stress to some power in simple tension, and for which, in general, the octahedral shear stress is the criterion of loading. The theorem states that if all boundary loads applied to such a body increase in proportion, all components of stress at each point increase in the same proportion. It is shown that the theorem is valid for a large class of loading criteria which depend on plastic strain, as well as on stress so that the material work-hardens anisotropically. Ilyushin's requirement on the simple tension stress-strain relation is proved necessary, not merely sufficient. Consideration is also given to states of stress for which the stress components at each point increase in proportion, but the constant of proportionality is a function of position.

The general theory of a continuous medium. P. F. Chenea, University of Michigan.

The continuous medium model is the basis for most of the classical theory of deformable bodies. The wide use of this model is a consequence of its simplicity, its adaptability to real substances, and the large amount of mathematical apparatus available for its analysis. It is the purpose of this paper to establish the general properties and limitations of this model. The basic states of a continuous medium are the initial, deformed, and relaxed states. The most convenient description of the relaxed state may involve the introduction of a nonphysical, curved space. All three states may be defined by nine kinematical variables. In addition to these nine quantities, the complete theory introduces sixteen other quantities. These quantities are matched by twenty-five fundamental equations which, together with the initial and boundary conditions, complete the statement of the general theory. The thermal and mechanical behavior of the medium is interrelated. Suitable approximations may be introduced to obtain special theories, such as the theory of elasticity.

Session 6: Thermal Stresses; Heat Transfer

On the temperature developed at the shear plane in the metal-cutting process. R. S. Hahn, The Heald Machine Company.

By the use of the theory of heat conduction from sources and sinks, an analysis is made of the temperature distribution on the shear plane. The analytical results are presented in graphical form in terms of dimensionless factors. Experimental determinations of chip temperatures from actual cutting tests are presented, and it is shown that the calculated shear-plane temperature is in accord with the experimental data.

Thermal stresses in perforated plates. G. Horvay, General Electric Company.

A method is developed for the analysis of perforated plates of triangular layout when the loading is applied in the plane of the plate. The method consists in replacing the perforated plate by a homogeneous plate of suitably determined effective constants E^*, G^*,* so that the homogeneous plate deforms in the same manner as the original plate. The stresses developed in the ligaments between the perforations are evaluated readily in terms of the stresses calculated for the homogeneous plate. As an example, the method is applied to the determination of the stresses and distortions that result in a tube sheet, supported by six radial spokes from an outer shell, when the temperature of the sheet is lowered below the temperature of the shell.

Thermal stresses in media exhibiting temperature-dependent viscoelastic properties. H. H. Hilton, University of Illinois.

This paper presents an analysis of the problem of thermal stresses at elevated temperatures. A linear Maxwell viscoelastic model is assumed to represent the actual anelastic behavior of metals. Hence the obtained solutions take into account the time dependent response of the material, as well as the variations of the material properties with temperature. It is found that for the incompressible Maxwell body, under conditions of plane strain and plane stress, unidirectional steady-state temperature gradients give rise to thermal stresses which relax from their initial elastic values at zero time to zero at an infinite time, and to time-independent thermal strains equal to their elastic counterparts. The analysis indicates that under the conditions mentioned, the elastic thermal stresses and strains (based on temperature-dependent elastic properties) represent the maximum values of the anelastic problem.

Mean temperature difference in multipass crossflow heat exchangers. H. H. Korst, University of Illinois.

An analytical method is presented for determining mean temperature differences for heat exchangers utilizing multipass cross flow with both fluids unmixed in the passes which are arranged in the general form of counterflow, and with the fluids between the passes mixed or unmixed in both inverted and identical order. The mathematical configuration appears as a characteristic initial value problem of a partial differential equation of second order, hyperbolic type, where the domains of dependence upon given initial values overlap. An iteration of initially arbitrarily chosen distributions along "inner" boundaries of the overlapping domains by a cyclic process of computation is proved to converge toward the solution. The integration can be done numerically by replacing the differential equations along the characteristics by difference equations. A numerical example illustrates the procedure of computation to establish dimensionless charts for practical use. The method applies for any number of crossflow passes.

Free convection due to a point source of heat. Chia-Shun Yih, Colorado Agricultural and Mechanical College.

A point source of heat is considered to be situated in an infinite plane above which the atmosphere was originally isothermal and at rest, and the resulting steady temperature and velocity distribution are sought. As can be observed from the behavior of smoke from a burning cigarette, the flow caused by the heat source is laminar at first, then at some height above it becomes unstable, and the subsequent flow is turbulent. The interdependent distributions of temperature and velocity are obtained in the laminar zone by solving a pair of simultaneous differential equations, and in the turbulent zone by systematic experimentation guided by a dimensional analysis. The transition from laminar to turbulent flow is also investigated. The results are applicable to similar problems of diffusion.

Session 7: Plasticity (stress-strain relations, plasticity solutions)

A more fundamental approach to plastic stress-strain relations. D. C. Drucker, Brown University.

Essentially thermodynamic definitions of work-hardening and of ideally plastic materials are re-employed to remove an unnecessary assumption in the derivation of the general Mises-Prager plastic potential stress-strain relations. Additional insight is thus obtained into the significance of yield or loading functions. In particular it is shown that the loading surface or any of the customary yield curves for work-hardening or ideally plastic materials must be convex. The meaning of corners in such curves or vertices in the loading surfaces is discussed with especial reference to problems of uniqueness.

Experimental studies of polyaxial stress-strain laws of plasticity. Bernard Budiansky, N. F. Dow, R. W. Peters, R. P. Shepherd, National Advisory Committee for Aeronautics.

Thin-walled cylinders of 14S-T4 aluminum alloy were stressed into the plastic range in axial compression and then twisted. As the twist was applied, the compressive load was varied in such a manner that the ratio of increments of shear stress and compressive stress were approximately constant for a given cylinder, but the magnitude of this ratio varied substantially from cylinder to cylinder. Discussion is made of the significance of the results with respect to stress-strain laws of plasticity.

Influence of the Bauschinger effect on inelastic bending of beams. O. M. Sidebottom, University of Illinois; Che-Tyan Chang, The Johns Hopkins University.

This investigation was undertaken to determine the influence of the Bauschinger effect on reducing the magnitude of the residual stresses in an inelastically deformed beam as well as on lowering the load-carrying capacity of such a beam when the sense of the loads is reversed. Two rectangular beams were tested; one made of a SAE 1020 steel which did not exhibit strain-

hardening for small inelastic strains and one made of railroad rail steel which did exhibit strain-hardening. Both the residual stresses and the load-carrying capacity of the beams were appreciably lower than the theoretical values which were derived on the assumption of no Bauschinger effect. However, the experimentally determined moment-strain diagram for each beam was found to check the moment-strain relation which was calculated from stress-strain diagrams obtained from specimens tested to follow the same strain history as the different fibers of the beams.

Plastic flow in a closed-end tube with internal pressure. R. Hill, University of Bristol; E. H. Lee, Brown University; S. J. Tupper, Ministry of Supply, England.

In a previous paper a geometrical method of representing stress and strain in a plane diagram was discussed, and used to determine the stress and strain distributions in a thick tube subjected to internal pressure for the case when longitudinal strain was prevented. The treatment differed from the usual one in that elastic strains were taken into account in the plastic region. In the present paper, using the same methods, the problem is considered for a closed-end tube with internal pressure. It is shown that as the flow develops, the longitudinal strain increases toward a limit, and the longitudinal stress approaches the mean of the other principal stresses. The error in the longitudinal stress, according to the conventional treatment, which assumes incompressible material and neglects elastic strains, has a maximum value of 18 per cent in the present case, compared with over 60 per cent for the plane-strain problem. Use of a deformation-type approximate elastic-plastic law gives an error of only 5 per cent in stresses, but predicts an incorrect longitudinal strain variation.

Unsymmetrical bending of rectangular beams beyond the elastic limit. M. S. Aghbabian, E. P. Popov, University of California.

The behavior of rectangular beams subjected to unsymmetrical bending and stressed beyond the elastic limit is analyzed in this paper. The analysis is based upon the assumption of idealized plasticity of the material above the yield point. General equations are derived for the elastoplastic bending capacity of a rectangular beam in pure unsymmetrical bending, and the rotation of the neutral axis of such beams is discussed. Experimental results obtained with steel specimens are given which verify the analytical work. It is also shown analytically that the shape factor, i.e., the ratio of the ultimate moment of the member to the moment when the extreme fibers reach the yield stress, always exceeds 1.5. The latter ratio is known to apply to rectangular beams bent about either principal axis.

Session 8: Shells; Structures

Membrane theory of shells of general shape. Luigi Broglio, Purdue University.

A membrane theory for shells of general shape has been developed. With the use of the Cartesian co-ordinates, the theory results in a differential equation of the second order in which a stress function ϕ is introduced as the unknown quantity. The theory can be applied to shells that are nonsymmetrical and nonsymmetrically loaded. The solution of the differential equation is carried out for certain specific shells.

Stress distribution and effective width adjacent to stiffeners in cylindrical shells. B. Thurlimann, R. Bereuter, Lehigh University; B. G. Johnston, University of Michigan.

This paper presents an analytical and experimental study of thin cylindrical shells reinforced with ribs in the circumferential direction, simulating on a $^1/_{20}$ scale the cross-sectional proportions of thin shell hangar-roof construction. The circumferential length is sufficient to remove the center section from local end effects and at the same time permit the line of thrust during test to be near the shell, or on either side of it. Strains and deflections were measured and analytical expressions derived. The results are applicable when the loads are small in proportion to the buckling loads of the combination of rib and shell. The results confirm the concept of an "effective width" (participation of the shell in helping the ribs). The effective width is a function of $K\sqrt{ah}$ when a is the radius of the shell, h = thickness of the shell, and K is a constant depending upon the restraint of the shell by the rib and upon the loading. Therefore it is allowable to assume an effective width and to calculate the ribs as arches independent of the shell.

A means for obtaining rapidly convergent series in the solution of shear-lag problems. M. B. Tate, University of Missouri.

The present paper has a dual purpose: (*a*) It illustrates a means for obtaining rapidly convergent series in solving shear-lag problems by inclusion of the procedure in steps of the derivation of equations for stresses in a symmetrical tension panel; and (*b*) it makes available a new solution of this particular problem, which is of general interest. The analysis is developed as a boundary-value problem in the theory of elasticity for stressed isotropic media. Functional expressions are presented for the spanwise flange stresses and for spanwise and chordwise normal and shearing stresses in the web sheet. It is found that finite values of these stresses can be computed at all points in the tension panel and along its boundaries. In closing, the author gives a formula for the maximum spanwise normal stress in the web sheet.

Shortening of column with initial curvature and eccentricity and its influence on the stress distribution in indeterminate structures. T. H. Lin, University of Detroit.

A method of calculating the shortening of a pin-ended compressive member with initial curvature and eccentricities at different loads is shown. This extra shortening of the column, due to lateral deflection, changes the rigidity of the member at different loads. The change of rigidity of this member as one in an indeterminate structure affects the stresses in other members. The discrepancy between the stresses with and without considering the initial curvature and eccentricities is shown in an illustrative example. It is suggested that initial curvature and eccentricities of compressive members used in indeterminate structures should be controlled with the maximum values specified and considered in design.

The effect of prestressing on the buckling loads of statically redundant, rigid-jointed trusses. E. F. Masur, Illinois Institute of Technology.

It is shown in this paper that, for a rigid-jointed truss which is statically indeterminate with respect to its axial force distribution, the critical loads corresponding to neutral equilibrium generally can be increased through the introduction of initial stresses. The equations governing the extremum values of the

buckling loads are derived and applied to the case of a simply redundant truss. Elastic behavior is assumed throughout.

Session 9: Limit Design; Plastic Failure

Limit design of plates. W. H. Pell, W. Prager, Brown University.

The paper is concerned with the limit design of thin plates made of a perfectly plastic material which obeys the stress-strain law of Prandtl and Reuss. A method is given which furnishes bounds for the flow limit (limiting load) of such plates. As an example, the flow limit of a simply supported circular plate under uniform load is determined to within 5.3 per cent.

Approximate methods in the limit design of structures. Jacques Heyman, William Nachbar, Brown University.

Plane frames of an elastic-plastic material are considered loaded in their plane by concentrated or distributed loads; the loading is increased proportionally until collapse. Starting from the principles of the statically admissible and kinematically sufficient multipliers of Greenberg and Prager, practical methods are given for the calculation of upper and lower bounds on the collapse factor. A quick procedure for rough computation of this factor, and a refined technique for narrowing the bounds to close limits are both offered with an illustrative example.

On plastic-rigid solutions and limit design theorems for elastic-plastic bodies. D. C. Drucker, Brown University; H. J. Greenberg, Carnegie Institute of Technology; E. H. Lee, W. Prager, Brown University.

The theorems recently developed by Drucker, Greenberg, and Prager determine upper and lower bounds for the collapse or limit load of a supported elastic-plastic body subjected to external loads. Recent work on complete solutions of plane-strain boundary-value problems for plastic-rigid bodies has determined some stress and velocity fields which satisfy the laws of plasticity and equilibrium. If the limit-load theorems are applied to such complete solutions the upper and lower bounds coincide, and so the exact limit load for the elastic-plastic problem is obtained. Examples of such solutions are given, including problems for which, because of the general form of the boundaries, it would be virtually impossible to attempt the elastic-plastic problem. Incorrect solutions which satisfy all conditions in the plastic regions only are also discussed.

New techniques for computing plastic failure loads on continuous frame structures. P. S. Symonds, Brown University; B. G. Neal, Cambridge University.

The paper shows how plastic failure loads can be readily calculated even for complex frames. Two types of failure are considered. In the simplest and usual type, plastic hinges form under a single load application at sufficient sections to transform the frame into a mechanism, which then deforms indefinitely under constant loads. In the new technique for computing this failure load the true collapse mechanism is regarded as a combination of certain elementary mechanisms, which are easily recognized and enumerated. The correct mechanism and load is determined by a series of trials of combinations of elementary mechanisms, making use of the principle of virtual work. The process is especially rapid for rectangular frames. A different type of plastic failure may occur if individual loads are applied repeatedly in random or cyclic order. Different physical concepts but similar analytical techniques determine the appropriate failure load limits. The paper illustrates methods by solutions for several frames, and shows typical differences between magnitudes of failure loads of the two types.

Analysis of rotating disks of arbitrary contour and radial temperature distribution in the region of plastic deformation. S. S. Manson, National Advisory Committee for Aeronautics.

Using finite-difference methods and deformation theory of plasticity, a method has been developed for determining displacements, stress and strain distributions in rotating disks of arbitrary profile, and radial temperature distribution subjected to either partial or total plasticity. Calculations using this method make possible the determination of such quantities as wheel stretch at a given speed, burst speed, significance of ductility on burst speed, and significance of temperature gradient on wheel stretch and burst speed. While radial temperature gradient may introduce residual stresses of importance in cycling, it does not affect the burst speed unless the temperatures involved significantly reduce material properties. For sound materials increasing ductility up to approximately 3 per cent elongation in a tensile test is useful in increasing burst speed; above this value no increases in burst speed are obtained with increase in ductility for a given tensile strength. The possibility of instability occurring in rotating disks as a result of stretch and reduction in thickness is also discussed. The validity of the method is established by favorable comparison of theoretical results with experimental data.

Session 10: Fluid Flow (optical methods; porous media)

A new quantitative optical method applied to fluid-flow problems. E. E. Weibel, University of Colorado.

In attempting to adapt the "Schlieren" method to electron optics, workers at the National Bureau of Standards developed a related "mesh-shadow" method which has yielded quantitative values of magnetic fields. Distortions of the shadow of a suitably placed square mesh superposed on the image of the object are used to compute field strengths. The present paper examines the feasibility of applying this method to problems involving light optics in which the distortions of the mesh shadow give quantitative information about the variation of refractive index of a medium such as air. Relative advantages of the method in convective heat flow and compressible flow problems over presently available methods are considered. The sensitivity and accuracy of the method as applied to light optics are discussed.

Unsteady flow of gas through porous media; one-dimensional case. J. S. Aronofsky, R. Jenkins, Magnolia Petroleum Company.

The basic differential equation which describes unsteady flow of gases through porous media is nonlinear, and no explicit solutions for specified boundary and initial conditions have been derived. This paper presents a nonanalytic method for describing one-dimensional transient flow of gases through a porous medium

in which the initial and terminal pressures and/or rates are specified. The computations were carried out by means of punch-card machines. Dimensionless pressure distributions in infinite tubes of porous media for various ratios of terminal to initial pressures have been computed, and compared with the case of flow of elastic liquids (diffusion equation) to characterise the degree of nonlinearity. The dimensionless rate of gas flow into or out of an infinite tube for these same pressure ratios is determined by integrating graphically the pressure-distribution curves. The pressure distribution in finite tubes of porous media has been calculated similarly for various boundary conditions. These results compare favorably with previous electric analog calculations reported by L. Green.

Unsteady flow of a gas through a porous medium. R. C. Roberts, University of Maryland.

A general method is developed for finding the approximate solution of unsteady flow problems in one dimension, subject to the conditions that the gas behaves isothermally and the flow obeys Darcy's law. The permeability, porosity, and viscosity are assumed to be constant. The present paper is concerned with finding the flow in a sand-filled tube of finite length closed at one end, and at whose other end the gas is drawn off with either constant velocity or constant flux. The approximate method of solution may be described as follows: The entire time interval that has elapsed since the flow started is subdivided into a sequence of suitably small time intervals. In each of these latter intervals the equation of flow is linearized and the solution found using the pressure at the end of the previous interval as the initial condition. The method is carried out numerically for the two cases previously cited and an extension to radial flow is proposed.

Nonsteady flow of gas through a porous wall. Leon Green, Jr., North American Aviation, Inc.; C. H. Wilts, California Institute of Technology.

A method of solution to a typical boundary-value problem arising from the nonsteady, isothermal flow of gas through a porous medium is presented. The nonlinear differential equation governing the pressure distribution in the medium is approximated by a finite-difference equation, which is satisfied by means of an electrical analogy.

Exact solutions of the laminar boundary-layer equations for a porous plate with variable fluid properties and a pressure gradient in the main stream. W. B. Brown, National Advisory Committee for Aeronautics.

Calculations of velocity and temperature distribution have been made for air with low Mach number by equations which include the simultaneous effects of pressure gradients in the main stream, flow through porous walls, and changes in fluid properties due to temperature variation through the boundary layer. The largest effects were due to flow through the porous wall, which reduced the heat-transfer rate to one eleventh of its value on the impermeable flat plate. A favorable pressure gradient nearly doubled the heat transfer and almost quadrupled the wall friction, while a small adverse pressure gradient reduced the wall friction to zero and the heat transfer to two thirds of the flat-plate value. When the wall was impermeable, the temperature effect was slight, less than 8 per cent for Euler number 1 and ratio of stream to wall temperature of 4. A high flow rate through the wall changed this effect to about 50 per cent.

Session 11: Elasticity

A method for the solution of the restrained cylinder under compression. E. D'Appolonia, Carnegie Institute of Technology; N. M. Newmark, University of Illinois.

In a lattice analogy method for the solution of stress problems the deformation of a solid body is approximated by a framework of pin-connected bars. An arrangement of bars suitable for the solution of radially symmetric problems is determined. Bar areas are obtained from the equivalence of deformation of solid and framework for similar load systems. The component displacements required for a solution of a problem are found by solving numerically two sets of displacement equations. Bar forces are obtained from the solution of the component displacements. From a consideration of the resultant forces on axial and radial planes, component stress distributions are determined. Two solutions of a short cylinder compressed between rigid end blocks are given.

On the axisymmetric problem of elasticity theory for a region bounded by two concentric spheres. E. Sternberg, R. A. Eubanks, M. A. Sadowsky, Illinois Institute of Technology.

The available treatments of the boundary-value problems of elasticity theory for a spherical shell are somewhat limited in their usefulness as far as actual numerical evaluations are concerned. This paper contains an exact series solution in explicit form for the stresses and displacements in a spherical shell under arbitrary axisymmetric surface tractions. The solution is based upon the Boussinesq stress-function approach referred to spherical co-ordinates and covers also the limiting case of the solid sphere as well as that of a spherical cavity in a medium of infinite extent. In particular, the known closed solution corresponding to a traction-free cavity is re-established systematically.

Estimation of torsional rigidity and other physical quantities. J. B. Diaz, University of Maryland.

The numerical determination of many physical quantities requires the estimation of a quadratic integral of an unknown function, the solution of a linear boundary-value problem. A systematic procedure for obtaining monotone sequences of upper and lower bounds for these quadratic integrals has been given earlier (Diaz, Symposium on Differential and Eigenvalue Problems, Oklahoma A. and M., 1950). Monotone sequences of upper and lower bounds follow immediately from Bessel's inequality, while maximum and minimum principles for solutions of the boundary-value problems follow from Schwarz' inequality. The present paper considers the special case of estimating the torsional rigidity, or stiffness. The desired upper and lower bounds for the torsional rigidity are derived directly, without appealing to the general formulas obtained earlier. The starting point is the formula for the torsional rigidity given by J. B. Diaz and A. Weinstein (*American Journal of Mathematics*, vol. 50, 1948, 107–116).

Solution for the exterior of a general ovaloid under arbitrary loading and its application to square rigid core problems. Yi-Yuan Yu, Northwestern University.

The two fundamental boundary-value problems in two-dimensional elasticity have been solved by the author for the exterior of a general ovaloid (Greenspan) under arbitrary loading and subject to constant or zero stresses at infinity. Their solu-

tion was obtained by Muschelisvili's complex variable method, and its general form is given in this paper. By means of the general solution, a number of particular problems were worked out. Solutions are presented for problems concerning a rigid core of the shape of a square with rounded corners. The problems include that of the core in a uniaxial tension field of arbitrary inclination, that of the core subjected to a concentrated force, and that of the core subjected to a couple. Finally, the solution of the problem of the core in a beam subjected to pure bending is given, which illustrates a case in which the stress at infinity is not constant but varies with the co-ordinates. Numerical examples are included.

The stresses around a small opening in a beam subjected to bending with shear. S. R. Heller, Jr.

This paper contains an exact closed solution for the stress distribution around a small opening in the web of a beam subjected to bending with shear. The complex variable method of solution for plane-stress problems (Muschelisvili) is used. It is applied to the case of a general ovaloid opening (Greenspan). Curves showing the tangential stresses around the boundary are given for several common openings found in engineering structures (Joseph and Brock). Maximum stress-concentration factors obtained are compared with those for similar openings subjected to tension, shear, and pure bending, as well as for similar cases of simpler geometry. The effect of small eccentricities in location is included.

Session 12: Fluid Flow Around Obstacles and Drag

Direct measurements of local skin friction in low-speed and high-speed flow. H. W. Liepmann and S. Dhawan, California Institute of Technology.

A device has been developed to measure local skin friction on a flat plate by measuring the force exerted upon a very small movable part of the surface of a flat plate. These forces, which range from about 1 mg to about 100 mg, are measured by means of a reluctance measuring device. The apparatus was first applied to measurements in the low-speed range, both for laminar and turbulent boundary layers. The measured skin-friction coefficients show excellent agreement with Blasius' and Kármán's results, respectively. The device was then applied to high-speed subsonic flow, and the turbulent skin-friction coefficients were determined up to a Mach number of about 0.8. A few measurements in supersonic flow were also made. The paper describes the design and construction of the device and the results of the measurements within the general frame of the present state of knowledge of high-speed skin friction. Extensions of the method are also stressed.

Cylindrical boundaries and the drag of spheres. J. S. McNown, State University of Iowa; J. T. Newlin, Rose Polytechnic Institute.

For the flow of air past a smooth sphere mounted centrally in a cylindrical conduit, the distribution of pressure around the sphere and the coefficient of drag have been determined for a variety of ratios of sphere diameter to cylinder diameter and for Reynolds numbers between 10,000 and 100,000. An approximate theory for large values of the diameter ratio and the results of earlier experiments at smaller Reynolds numbers have made possible the preparation of a graph indicating the variation of the drag coefficient for all values of the diameter ratio between 0 and 1 and for all Reynolds numbers from 0 to 100,000. Marked fluctuations in pressure for Reynolds numbers of about 100,000 result in temporal fluctuations of the drag coefficient and in the likelihood of transient lateral forces.

The extension to a two-dimensional subsonic flow of the Joukowski force of ideal fluid theory. G. S. S. Ludford, Harvard University.

We consider the disturbance caused by the introduction of a profile into a uniform subsonic flow of a compressible inviscid fluid. The object is to show that the drag force on the profile is zero and the lift force is of exactly the same form as the Joukowski force of ideal fluid theory with the density now that at infinity. In order to show this rigorously, it is necessary to investigate the form of the expansion of the potential function at infinity. This is done by approximating successively to the solution of the potential equation of compressible flow starting with the known form of the expansion at infinity for an incompressible flow, and insuring that at each stage the approximation is periodic. Finally a large circle is used as a control contour to evaluate the force on the profile.

Blade profiles. E. J. McBride, American Machine and Foundry Company.

This paper presents a method of developing blade profiles associated with known velocity distribution under potential flow. A criterion is offered whereby self-intersection of the profile may be avoided. A plotting function is introduced for the velocity distribution, permitting it to be obtained as a combination of velocity components whose individual physical effects are interpreted readily. This in turn permits a complete study, by analysis or experiment, of controlled variations in these components.

Methods for the determination of subsonic flows around profiles. Stefan Bergman, Harvard University.

Using the kernel function, it is possible to replace the classical methods in the theory of functions by new ones which have two important advantages: (1) They give simple formulas for the computation of Green's and Neumann's functions, and mapping functions into canonical domains; (2) they permit immediate generalization to the theory of linear partial differential equations, in particular, to equations of compressible fluids considered in the hodograph plane (see Bergman, *Mathematical Surveys*, vol. 5; Bergman and Schiffer, *Duke Mathematical Journal*, vol. 14, 1947, pp. 609–638). A flow of a compressible fluid around a given hodograph can be expressed in terms of the kernel function. (It is noted that to a given hodograph there does not always exist a flow of compressible fluid.) In the case where the domain is bounded by straight lines and segments of free boundaries, we obtain a formula for the stream function (in the physical plane) for the incompressible case (of different form from that of Cisotti) which can be generalized to subsonic flows.

Session 13: Kinematics; Dynamics

Some formulas for bar linkages. A. W. Wundheller, Illinois Institute of Technology.

The paper attempts a partial linearization of precision design of all-pivot linkages. The bar angles are replaced by certain master functions, determined by the linkage structure, in which the bar lengths and the angular design corrections are linear. The angular velocities are quotients of quantities linear in the master functions; thus differential equations are obtained for all the functions generated by bar angles, for a given linkage structure. The formulas are designed with large bar numbers in mind. To express conditions of higher contact, an algorithm is developed for the computation of the higher derivatives by recurrence, the formulas being linear in certain differential forms, standard for a given linkage structure.

Transient analysis of nonlinearized single-lag servomechanisms. I. S. Blumenthal, F. J. Beck, Yale University.

Suggestions have been made that the over-all performance of feedback control systems might be improved by introducing nonlinear elements into otherwise linear systems. One such nonlinear element is a nonlinear voltage divider or an error-sensitive relay which would cause the loop gain of the control system to increase when the dynamic error became large. This paper presents a semigraphical method for calculating the exact step-function response of a nonlinearized control system comprised of a subtractor, an amplifier, a time lag, and an integrator. The nonlinearities considered are those which cause the amplifier gain to increase by any finite amount when the system error exceeds a predetermined value. Generalized curves are presented for systems which are critically damped for small errors. It is shown that these solutions are applicable to the exactly analogous problems of the spring-mass oscillator with nonlinear springs and the parallel resonant circuit with an iron-cored coil.

Transient analysis of servomechanisms. Andrew Vazsonyi, U. S. Naval Ordnance Test Station.

The transient analysis of servomechanism is usually quite laborious because the roots of high-order algebraic equations must be computed. The purpose of this paper is to show that often the optimum performance can be determined without much numerical work. The essence of the method is to derive relationships defining the optimum performance and then devising charts for the solution of the set of characteristic equations associated with the optimum performance. The paper begins by presenting certain special mathematical relationships in connection with the third and fourth-order equations. Then follows the analysis of certain steam-turbine governors, angular positioning mechanisms, variable-voltage angular positioning mechanisms, and electric turret-traversing mechanisms.

Errors introduced by finite space and time increments in dynamic-response computations. Samuel Levy, Wilhelmina D. Kroll, National Bureau of Standards.

An investigation is made of the accuracy and convergence of numerical integration methods when applied to the computation of the dynamic response of structures to impact loads. The effect of finite time increments is studied both by obtaining analytical solutions for a single-degree-of-freedom system and by carrying out numerical integrations for many-degree-of-freedom systems; the effect of finite space increments is studied by replacing a continuous beam by a discrete number of elastically connected point masses. It is found that, of the methods investigated, only Houbolt's gives convergent results for time increments large compared to the natural periods of the system. Errors are introduced by Houbolt's method, in this case, which result in the damping out of the responses in the higher modes of vibration. The results indicate that a time increment of about 1/30 the fundamental period and a space increment of about 1/5 of the length will give good results in many cases.

A method for the graphical determination of the motion of a structure with one degree of freedom under blast loading. F. P. Beer, Lehigh University.

The structure is assumed equivalent to a mass M attached to a "plastic spring" with nonlinear restoring force $R(x)$. A force $P(t)$ is applied. The differential equation of motion is

$$M\ddot{x} = P(t) - R(x)$$

The equation is solved by graphical construction after the curves representing $P(t)$ and $R(x)$ have been approximated by means of oblique straight-line segments. By drawing arcs of circle corresponding to time intervals, the values of $M\dot{x}$ and $M\ddot{x}$ are obtained for any value of t, respectively, as abscissa and ordinate on a "velocity-acceleration" diagram. Subtracting $M\dot{x}$ from $P(t)$ yields the value of the restoring force for any t, and the curve representing $R(t)$ may be plotted. The displacement x is determined for any t by matching points of the $R(x)$ and $R(t)$ curves with equal ordinates. It may also be obtained from the moment of the area between the $P(t)$ and $R(t)$ curves.

Session 14: Experimental Stress Analysis; Buckling of Columns

Stress distribution in plates under uniaxial state of stress with multiple semicircular and flat-bottom notches. A. J. Durelli, R. L. Lake, E. A. Phillips, Armour Research Foundation.

The paper presents a photoelastic investigation of the distribution of stresses in plates under uniaxial stress parallel to the plate edge for the following cases: (1) one to five semicircular notches along the edge with center to center spacings between the notches ranging from zero to six notch diameters, and (2) a series of flat-bottom notches with distances between the centers of the two circular end fillets ranging from zero to eighteen fillet radii. It is shown that the maximum stress in the plate is lowered as the number of notches is increased while maintaining the same spacings between adjacent notches, and is lowered as the number of notches in a given space is increased to the limiting case of a flat-bottom notch. A study is made of the stress values at the bottom of all notches and of the angles of inclination of the maximum stresses. The effect of varying the ratio of plate width to notch diameter is investigated and comparison made with some theoretical results obtained for semi-infinite plates.

Photoelastic determination of stresses on the surface of poppet valves. M. M. Leven, Westinghouse Electric Corporation; M. M. Frocht, Illinois Institute of Technology.

Using relatively large Fosterite models and the method of "stress-freezing and slicing," the stresses on the surface of poppet

valves were investigated for three basic types of head designs, namely, flat, dished, and umbrella heads. The results obtained from Fosterite models are then compared with results obtained from previous tests which were made using small bakelite models, approximately one third the size of the Fosterite ones. The results are compared further with the findings from two-dimensional tests using flat models of celluloid and bakelite.

Elastic instability of cantilever struts under combined axial and shear loads at the free end. H. C. Martin, University of Washington.

The problem investigated here is that of a deep cantilever beam subjected to both axial and shear loads applied at the free end. Failure by elastic instability, due to the combined action of the applied loads, forms the subject of this paper. The governing differential equations are derived and the critical load combinations determined. The problem is solved in detail for both a uniform beam and one tapering linearly to a point. Solutions for the special cases, which occur when either load component vanishes, are shown to agree with previous results obtained, respectively, by Euler, Prandtl, Dinnik, and Federhofer. Experimental determinations of various critical-load combinations for the uniform strut are also presented. These agree well with calculated values.

Residual stresses in columns. W. R. Osgood, Illinois Institute of Technology.

A general expression is obtained for the buckling load of a column containing residual stresses assumed to be the same at every cross section and so distributed over the cross section that the Engesser-Shanley theory may be applied.

Experimental study of inelastic buckling of columns of varying section. R. E. Newton, Washington University.

Experiments were made to determine the buckling loads of centrally loaded straight columns of continuously varying compact section. Three materials—hot-rolled mild steel, magnesium alloy, and aluminum alloy—were used. For each material two series of columns of varying section, a series of columns of constant section, and several compression stress-strain specimens were tested. It is concluded that the differential equation initially derived by Euler satisfactorily predicts the load at which bending will begin if the tangent modulus of elasticity is substituted for the initial modulus in this equation; that for all except the very short columns, the ultimate load does not exceed appreciably the load at which bending begins; and that the ultimate load of short columns made from a material with a pronounced yield stress may exceed appreciably the tangent modulus load because of the phenomenon of work-hardening.

Session 15: Aeroelasticity

A problem of the theory of oscillating airfoils. Eric Reissner, Massachusetts Institute of Technology.

This note deals with the oscillations of an infinite airfoil in incompressible flow under the assumption that the deformations of the airfoil vary periodically in the direction of the span. This problem has previously been considered by W. R. Sears (Proceedings of the Fifth International Congress of Applied Mechanics, 1938). It is shown that the integral equation of the problem which was obtained in the author's earlier work (NACA Technical Note 946 and NACA Technical Note 1194) can be solved explicitly in terms of elementary functions for the case under consideration. Use is made of this result for a discussion of the behavior of the solution as a function of aspect ratio and of reduced frequency.

Some contributions to the study of vibrating beams and wings. R. H. Scanlan, Rensselaer Polytechnic Institute.

The investigations described in this paper are concerned with the following: (*a*) The determination of structural influence coefficients and vibration characteristics of beams. (*b*) The gyroscopic effect on wing vibration and flutter of elastically attached propulsive units (*c*) The theory of flight flutter testing. Under (*a*) influence coefficients are determined for swept box beam. Experimental check is made on a theory accounting for rotational inertias in beam-bending vibration. Theoretical and experimental check is made on range of validity of typical matrix beam vibration-mode calculation. Under (*b*) classical gyroscopic patterns are studied. Results of gyroscopic coupling of an aircraft propeller to its elastic wing are examined in several ways. Theory for predicting gyroscopic effect of propellers on wing flutter is developed. Under (*c*) approximate theory of subcritical flutter response is examined experimentally. Theory of wing-flutter response is developed which is intended for all incompressible air speeds.

Aeroelastic studies on a high-performance swept-wing airplane. David Benum, California Institute of Technology; C. D. Pengelley, Southwest Research Institute.

Comprehensive aeroelastic analyses and wind-tunnel tests have been conducted on a model of a typical high-performance airplane with swept surfaces. The investigation covered the effect of dynamic pressure upon steady-state longitudinal control and stability characteristics as well as aileron effectiveness. The analysis was based upon a superposition method which yields a convergent series which may be applied to any structure on which the load is a function of the deflection. It has been shown that after a few terms this series degenerates to an elementary geometric progression which may be summed to infinity. This conclusion is applicable even to cases where the aeroelastic effects are large and the structure is actually approaching a condition of instability. Wind-tunnel tests were carried out both at the Massachusetts Institute of Technology and the California Institute of Technology. Measured data were compared with the results of the theoretical analysis.

Aeroelastic properties of slender wings. R. L. Halfman, Holt Ashley, Massachusetts Institute of Technology.

A simplified momentum method is used to predict the aerodynamic loads on slender, pointed wings executing arbitrary small motions. This theory is confirmed mathematically for the case of incompressible fluid by systematic reduction of the exact integral equation. Employing rigid and flexible delta models with 26-deg vertex angle, several comparisons are presented between low-speed wind-tunnel measurements and results of the momentum theory. Pitching oscillations of the rigid delta are predicted to be stable for axis positions fixed ahead of the two-thirds chord point; the characteristics of these oscillations are confirmed experimentally. Tests show that a delta flexible only in the chordwise direction is capable of both flutter and chordwise bending divergence. Iteration procedures based

upon the flexural differential equation are employed in an analysis of the critical speeds associated with these phenomena. It is shown how the momentum approach may be applied to more complicated aeroelastic problems.

On the application of station functions to the transient aeroelastic problem. M. D. Schwartz, Massachusetts Institute of Technology.

The solution of the transient aeroelastic problem is of interest for determining the response of an elastic aircraft to excitation arising from gust entry, or from deliberate external excitation such as is used in flight testing for flutter. Rauscher's station-function technique makes it possible to obtain more accurate solutions with less effort than is required in the usual normal-mode approach. The solution is written out using the station-function definition of deflection shapes, Wagner air forces for the unsteady aerodynamic effects, and the Laplace transform technique for handling the transient nature of the problem. For the gust response, Kármán-Sears air forces are employed with specified gust profiles. The inclusion of rigid-body degrees of freedom, and rigidly or elastically mounted nacelles or tip tanks is described. Some results of calculations for the response of a wing to deliberate external excitation are included, where logarithmic dynamic-response templates were employed to simplify the approximate inverse transformation of the response.

Session 16: Buckling of Bars and Plates

Lateral buckling of simply supported beams of rectangular cross section under bending and shear. M. G. Salvadori, Columbia University.

A simply supported beam of rectangular cross section buckles laterally under the action of two bending moments M_2 and $M_1 = rM_2$ applied at its ends. The critical value of M_2 is determined by means of a transcendental equation involving Bessel functions, for values of r varying in steps of 0.1 between -1 and $+1$.

Lateral buckling of eccentrically loaded I and H-section columns. H. N. Hill, J. W. Clark, Aluminum Company of America.

This paper describes an experimental investigation of the behavior of I and H-section aluminum-alloy columns, loaded eccentrically in the plane of the web, and which fail by lateral-torsional buckling. The tests covered a variety of lengths, eccentricities, and cross-section proportions. The proportions were such as to exclude the influence of local buckling. Some failures occurred at stresses within the elastic range of the material, while others involved plastic action. The test results show good agreement with theory, provided that the deflection of the member in the plane of the eccentricity is taken into account in computing the bending moment, and appropriate reduced modulus values are used for buckling in the plastic range. The results indicate that previously proposed design formulas covering this type of failure are unconservative. A new formula is suggested as a basis of design for members of this type.

Torsional instability of a long sandwich cylinder. George Gerard, New York University.

The torsional buckling behavior of a long circular sandwich cylinder was considered. The core material was assumed to be isotropic and the bending rigidity of the faces about their own middle surface was assumed to be negligible, precluding consideration of wrinkling. The results indicate that for a sandwich cylinder with a core very weak in shear, the buckling load depends only upon the shear rigidity of the core. This is the same result obtained for weak core sandwich columns and flat and curved sandwich plates under compressive loads. For strong cores and cores of moderate strength, two-lobe buckling occurs which is the familiar mode for the homogeneous cylinder. In these cases, the equation for the buckling load is essentially of the same form as that obtained for the homogeneous cylinder.

A numerical method for the solution of plate buckling problems. W. J. Austin, N. M. Newmark, University of Illinois.

A numerical method is presented for the solution of problems of buckling of flat, rectangular plates under conditions for which Lévy's solution can be used to reduce the customary partial differential equation of equilibrium to an ordinary differential equation. Fortunately, many practical problems can be solved by this procedure. With some modifications, problems of the buckling of ribbed plates and of plates composed of segments of different thickness are easily solved. The proposed method is a combination of two well-known procedures. A method of successive approximations is used in conjunction with a numerical procedure of integration published by Newmark (Transactions, ASCE, 1943). The numerical work is straightforward, and slide-rule accuracy is sufficient, except for a very few computations. Most of the numerical work consists of simple addition and subtraction. The general procedure is applicable to other problems, since it permits a relatively simple and accurate numerical integration of a class of differential equations.

Bending and buckling of rectangular sandwich plates. A. C. Eringen, Illinois Institute of Technology.

Four partial differential equations are obtained for the bending and buckling of rectangular, flat, sandwich plates having homogeneous cores subjected to various types of loading and boundary conditions, by use of the theorem of minimum total potential. In the present study, the three-dimensional stress distribution in the core is taken into account. Consequently, the bending rigidity and the flattening of the core are not neglected. Also, the face layers, which are customarily assumed to be thin, have bending rigidity. The present theory inherently unifies over-all bending and buckling, and the bending and buckling with flattening of the core. In particular, the differential equations are solved for the bending of a simply supported rectangular sandwich plate subjected to an arbitrary transverse load as well as to a uniformly distributed axial compressive load on two opposite sides. Several special cases are studied. Two formulas for buckling stresses are obtained, one for the instability of the entire sandwich plate, the other for the buckling with flattening of the core. Buckling occurs according to whichever stress has the smaller value. Buckling stresses are plotted against various dimensionless parameters for comparison and for engineering design purposes.

Session 17: Boundary Layer; Laminar Flow

An exact thermal solution in laminar viscous flow. A. N. Tifford, The Ohio State University.

An exact solution of the energy equation in the case of incompressible laminar flow near a forward stagnation point is obtained. This analysis resulted from a desire to gain some insight into the details of the influence upon thermal boundary-layer solutions of extremely large surface-temperature variations. Since under these conditions Prandtl's order-of-magnitude arguments do not simplify significantly the equations, the exact equations are analyzed. It is found that as compared with the usual thermal boundary-layer solution, a new parameter occurs. This dimensionless number may be thought of as the product of the inverse of the local free-stream Reynolds number and an energy ratio, the ratio of the local free-stream kinetic energy to the free-stream thermal energy. Its influence upon the solution may be expressed explicitly. Numerical values of the functions derived are tabulated for several Prandtl numbers. Based upon these values, comparisons are made between approximate and exact solutions.

Self-induced temperature effects on laminar flow of liquids. W. E. Wilson, W. I. Mitchell, South Dakota School of Mines and Technology.

The laminar flow of fluids exhibiting a variation of viscosity with temperature is discussed. Three cases are considered: (1) flow in tubes; (2) flow between stationary, parallel flat plates; (3) flow between parallel flat plates, one of which is in motion parallel to the other. The development of equations describing the flow is based upon several simplifying assumptions, including those common in this type of study, but depends principally upon the assumptions that, (*a*) conditions within an element of differential length in the direction of flow are the same as in flow with constant viscosity, and (*b*) that all the heat generated within the liquid is absorbed internally. The variation of viscosity in the direction of flow and the ratio of the total flow, under the assumptions made, to the flow with constant viscosity are evaluated.

Diffusion from a line source in laminar flow over a wedge and in Blasius flow. Chia-Shun Yih, Colorado Agricultural and Mechanical College.

The velocity distribution in the laminar flow over a semi-infinite plate was calculated by Blasius (1908). The corresponding problem for the laminar symmetric flow over a wedge was solved by Falkner and Skan (1930), in collaboration with Hartree (1937). In the present paper, a line source of mass is considered to be situated at the leading edge of the plate or wedge, which is supposed to be nonconductive of vapor, and the resulting vapor distribution is sought. If free convection is neglected, and the velocity distribution is assumed essentially undisturbed by the variation of vapor concentration, the boundary-layer equation of diffusion for each case can be solved by certain simple substitutions and integrations, the solutions being applicable to similar problems in heat diffusion. Numerical calculations have been carried out for Blasius flow.

Status of the theory of the turbulent boundary layer with pressure rise. N. Tetervin, National Advisory Committee for Aeronautics.

During the past 20 years the problem of calculating the behavior of the turbulent boundary layer in the presence of pressure gradients attracted the attention of a number of investigators without resulting in a satisfactory solution. Critical summaries of the more important papers are given. Each summary gives the major assumptions upon which each method is based and states whether, in the light of present knowledge, the assumptions appear to be valid or not. It seems that the investigations of turbulent boundary layers in the presence of pressure gradients have resulted in only two main findings, namely, that all the velocity profiles form essentially a single parameter family, and that the form of the equation for the rate of change of the profile-shape parameter is obtainable from the Prandtl boundary-layer equation. It is concluded that a sound solution of the problem requires the ability to compute the shearing stresses in turbulent flows of the boundary-layer type.

The laminar-turbulent transition in a boundary layer. Part II. H. W. Emmons, A. E. Bryson, Harvard University.

New experimental observations on the mechanism of transition in a boundary layer and a mathematical formalism to describe it were presented in Part I of this paper. In this second part applications are made to drag and heat-transfer effects in transition on a flat plate, a flat plate with a swept leading edge, a cone, and a blunt-nosed cylinder.

Session 18: Dynamical Problems in Elasticity and Buckling

Effects of an oscillating tangential force on the contact surfaces of elastic spheres. R. D. Mindlin, Columbia University; W. P. Mason, T. F. Osmer, Bell Telephone Laboratory; H. Deresiewicz, The Johns Hopkins University.

When two elastic spheres, held pressed together with a constant normal force, are subjected to a monotonically increasing shearing force tangential to the contact surface, it has been predicted that slip is initiated at the periphery of the contact surface and progresses radially symmetrically inward. Those and other results are extended, in the present paper, to the case of an oscillating tangential force. One of the predictions is that slip on the contact surface progresses back and forth within the confines of an annulus whose dimensions are given by the theory. Experiments were made with sets of three lenses pressed in contact on their spherical surfaces. The outer two were held fixed and the inner lens was vibrated with a barium-titanate cylinder. As anticipated, annular wear patterns were observed on the contact surfaces. The experimental data conform with the theory yielding a coefficient of friction of 0.23, which is in agreement with other measurements.

A one-dimensional theory of compressional waves in an elastic rod. R. D. Mindlin, G. Herrmann, Columbia University.

By means of a method applied previously to plates, the general equations of small motions of an isotropic, elastic medium are reduced to a one-dimensional system applicable to the longitudi-

nal vibrations and the propagation of longitudinal waves in a cylinder of circular cross section. In the process of reduction, both the radial inertia term, due to Rayleigh, and a new radial shear term are retained. Through the latter, the coupling between axial and radial displacements is included and this, in turn, produces dispersion and a singularity with vanishing Poisson's ratio just as in the exact theory. The approximate theory is thus applicable to short bars, high-frequency vibrations, and sharp transients. Since the equations are one-dimensional, solutions are relatively easy to obtain.

The maximum load supported by an elastic column in a rapid compression test. N. J. Hoff, S. V. Nardo, Burton Erickson, Polytechnic Institute of Brooklyn.

Values of the maximum load supported by a perfectly elastic column in a rapid column test are calculated and presented in a diagram for a wide range of values of the dynamic similarity number and of the initial deviation of the column from perfect straightness. The end points of the column are free to rotate, and the loading head of the testing machine descends with a constant velocity. The maximum load exceeds the Euler load considerably when the initial deviation from straightness and the dynamic similarity number are small. In a routine test carried out on a commercial testing machine the maximum load is equal to the Euler load in good approximation.

Numerical analysis of the process of buckling of elastic and inelastic columns. J. P. Chawla, Hughes Aircraft Company.

A numerical method of step-by-step integration of the dynamic equations for the transverse motion of an initially slightly curved column is presented. One of the end points of a pin-ended column is axially displaced at a constant rate in a perfectly rigid testing machine. The results of the calculations are presented in a nondimensional form. The effect of the speed of the loading head of the testing machine and the magnitude of the initial deviations from straightness on the maximum compressive load recorded in a test has been studied and found to be appreciable. When the column buckles at a stress exceeding the elastic limit of the material, the effective bending rigidity is not a constant along the column. For this reason an initially sinusoidal deviation of the axis of a column from a straight line does not increase in proportion to a time-dependent multiplier during the loading process. The curvature increases much more rapidly in the middle than near the ends. The axial compressive load in the column drops suddenly after the maximum value is reached.

The behavior of a simply supported column under constant or varying end load with transverse displacement of one point of support. V. L. Salerno, Polytechnic Institute of Brooklyn; Frances Bauer, Reeves Instrument Corporation; James Sheng, Polytechnic Institute of Brooklyn.

The response of a simply supported column subjected to a constant or linearly varying axial end load is calculated when one end of the column undergoes a prescribed lateral displacement in the form of a pulse. Time-displacement curves of the motion are obtained. These curves show characteristic differences in the motions for the two cases investigated.

Session 19: Turbulence; Motion of Transported Particles; Cavitation

Turbulent diffusion from a nonpunctual source. F. N. Frenkiel, The Johns Hopkins University.

The diffusion of a fluid sphere in a field of homogeneous and isotropic turbulence is investigated. More particularly, the mean concentration distributions within the diffusing sphere are found in function of the time. The character of the turbulence is described by its intensity, the Lagrangian correlation curve, and the corresponding spectrum of turbulence. The time history of the diffusing sphere is then determined as a function of the turbulence characteristics and of the initial diameter of the sphere. Two limiting cases—at the beginning and at the end of the diffusing process—are discussed. Numerical applications are given for various shapes of Lagrangian correlation curves. Referring to some experimental measurements, the case of correlation curves presenting large negative values is also investigated. Finally, the results are compared with those previously obtained by the author for a punctual source.

On the generalized fundamental equations of isotropic turbulence in compressible fluids and in hypersonics. M. Z. E. Krzywoblocki, University of Illinois.

The statistical theory of turbulence is adapted to the case of a compressible, heat-conducting fluid. All the random variables follow the principles of isotropy and homogeneity and are dependent. Four equations are considered: motion, continuity, state, and energy. The results are represented in the forms of three generalized fundamental equations for the propagation of the velocity, temperature, and pressure correlation functions, respectively. For a flow at higher Mach numbers the conventional Navier-Stokes equations are no longer a true description of the physical relations. Following previous authors on the subject of hypersonics, the author assumed as the starting point the equations derived on the basis of the kinetic theory of nonuniform gases. Additional terms are included into the fundamental equations of isotropic turbulence.

The motion of small slender particles in a viscous incompressible fluid. Benjamin Rosenberg, Bureau of Ships.

The motion of slender particles of colloidal size under the action of viscous forces in two-dimensional flow is discussed. An approximate solution is obtained by neglecting inertia forces and Brownian movement and assuming the particle adopts the motion of the surrounding medium without disturbing the flow. It is found that the analysis used to obtain the orientation of these particles in Couette flow is not sufficiently general to be applied to all types of two-dimensional flow. Instead, for any but parallel flow, there are two equilibrium positions. For converging flow, the long axis of the particle lies in the streamline for stable equilibrium. In diverging flow, the stable position is not the streamline but instead, the particle although making the same angle with the plane of maximum shear as does the streamline, lies on the opposite side of the plane of maximum shear.

The collapse or growth of a spherical bubble or cavity in a viscous fluid. H. Poritsky, General Electric Company.

The growth or collapse of cavities in a fluid is of interest in underwater explosions, in cavitation near propellers, and in the

initial stages of foaming in oil. Lord Rayleigh has treated the problem of collapse of a spherical bubble in a perfect (nonviscous) fluid. In this paper the collapse or growth of a spherical bubble in a viscous incompressible fluid is studied; the effect of surface tension is also included. Viscosity shows up in the Navier-Stokes equations in two terms. In the present problem one of these terms vanishes due to incompressibility, the other due to spherical symmetry. However, μ re-enters the problem in the formulation of the boundary condition for the pressure inside the spherical cavity. One is led to a second-order differential equation for a cavity radius R. This equation is put in dimensionless form and integrated numerically for two sets of specific values of the dimensionless constants involved, one for a collapsing bubble, the other for an expanding bubble. The same examples are also treated with surface tension included.

Note on the collapse of a spherical cavity in a viscous incompressible fluid. S. S. Shu, Illinois Institute of Technology.

Lord Rayleigh found that a spherical cavity collapses after a finite time period in an incompressible (nonviscous) fluid. In the presence of viscosity, H. Poritsky found, by numerical integration, that the time of collapsing is infinite for some cases. This result is established rigorously here by means of the Poincaré-Bendixon theory of nonlinear differential equations, with some modifications. A (dimensionless) parameter c of viscosity is found to play an essential role. The time of collapsing is infinite if c is greater than a critical value c_0 ($<\sqrt{6}$) and is finite otherwise. The same method may also be applied to similar problems to find some useful information. One such problem is that in which the surface tension is taken into account; here the time of collapse can always be shown to be finite.

Session 20: Vibrations (miscellaneous)

Electrical analogy for dynamical systems containing broken-linear unsymmetrical elasticity. W. A. Gross, W. W. Soroka, University of California.

A two-degree-of-freedom oscillatory torsional system containing a preset spring is simulated by means of an electrical circuit using the mass-inductance analogy. The preset spring introduces a sharp break, or knee, in the load-deflection curve of the shaft containing this spring. A considerable nonlinearity is present, the ratio of the slopes of the two straight lines meeting at the break being 1:50. An electronic circuit consisting of a cathode follower, Schmitt trigger, and pentode current generator is used to operate a high-speed mechanical relay for introducing the knee characteristic in the analog. Response curves are shown for two representative values of exciting force.

A statical analogue for natural vibrations. P. N. Gustafson, Carnegie Institute of Technology.

This investigation applies to structures which obey a linear force-displacement law, and which carry concentrated weights. In a "natural" mode of vibration of such systems, the dynamic forces exerted on the structure are proportional to the displacement of a point, to the mass at that point, and to the square of the common frequency. It is shown that the displacement at any instant is identical to the displacement produced had these forces been applied gradually, as static loads. Forces which satisfy these conditions may be applied to a model by a cam-and-roller device introduced at points corresponding to concentrated weights. This leads to both the shape and frequency of natural modes of vibration, by means of a purely statical loading. Thus far, only fundamental and second natural modes have been obtained, since higher modes are very unstable. Numerical results have been obtained for a simply supported uniform beam with overhang, but extension to other structures, such as frames, plates, etc., seems practicable.

Statistical mechanics of complex vibrating systems. S. P. Thompson, Naval Research Laboratory.

This paper is a preliminary report on a statistical mechanics of complex vibrating systems. There is practical interest in the vibrations of mechanical systems whose structure is determined, but whose excitations are known only to belong to a class having specified properties. Through statistical mechanics, it is possible in such cases to ascertain typical values of dynamical quantities, and to assess the representativeness of these values. To incorporate into the theory the statistical nature of the excitations, one may introduce a hypothetical ensemble of similar systems, and identify the probability of random selection from the ensemble with the probability to be experienced in observations upon the actual system. Conservative systems are conveniently treated by discussing the distribution of the ensemble in the phase space of the system's normal co-ordinates and their conjugate momenta. For illustration of the kind of information which is derivable from such a theory, conclusions have been drawn from two sets of assumptions regarding the initial distribution-in-phase of linear, conservative systems.

Circular-crested vibrations of an elastic solid bounded by two parallel planes. L. E. Goodman, University of Illinois.

Two fundamental radially symmetric solutions of the linear equations of elasticity are found to describe free vibrations of an elastic plate of finite thickness. It is shown that they correspond to "extensional" and "flexural" motions and are analogous to the straight-crested (plane-strain) waves discovered by Lamb and Rayleigh. At large distances from the origin, the circular-crested and straight-crested motions become indistinguishable. Following the treatment of Lamb, the transcendental equation relating the frequencies of vibration to the wave shape is developed. A numerical tabulation of the solutions of the frequency equation is given and the shapes of the modes are described in detail. For the higher modes there exist surfaces across which no stress is transmitted. These surfaces define shapes for which the motion in question represents a mode of free vibration. In the limit, for very thick plates, the solutions are shown to correspond to Rayleigh surface waves, while, for thin plates, they approach, asymptotically, well-known results in elementary plate theory.

Transverse vibration of one- and of two-span beams under the action of a moving mass load. R. S. Ayre, L. S. Jacobsen, Chieh Su Hsu, Stanford University.

The investigation is one of a series relating to the dynamic effect of traveling loads on continuous beams or bridges. Two earlier studies have dealt with a moving constant force and a moving alternating force. The present study, largely an experimental one, presents the general case of the concentrated mass load moving across a beam having uniformly distributed mass, and compares it with two limiting cases, (1) a mass load traversing

a beam of negligible mass (Stokes, 1849), and (2) a constant force moving on a beam having distributed mass (Kryloff, 1905). The general single-span problem has been included for purposes of comparison of the experimental results with Schallenkamp's analysis (1937), for the single-span beam. The results include the load trajectories as well as diagrams of maximum dimensionless stress in the beam plotted against the dimensionless traversing velocity of the load.

Session 21: Fluid Flow (unsteady, vortex, hypersonic)

On the growth and decay of a vortex filament. Hunter Rouse, Hsieh-ching Hsu, State University of Iowa.

Proceeding from the equations of motion of a viscous fluid, an investigation is made of the temporal variation of a single vortex of arbitrary initial characteristics: (1) The velocity field produced by the action of a vortex filament of infinitesimal diameter is expressed as a function of the strength of the filament, the viscosity of the fluid, and the time of generation. (2) The modification of this field after elimination of the generating filament is described in terms of the three parameters of the generation phase and the time interval thereafter. (3) The resulting equation is rewritten in a form involving three reference parameters which may be related to any three characteristics of an actual vortex at a particular instant; for example, the maximum circulation, the core diameter, and the center-line vorticity. An expression is thus obtained for the prediction of the subsequent change of the vortex characteristics with passage of time in a fluid of any viscosity.

Secondary flows in fluid dynamics. R. E. Kronauer, Harvard University.

Problems of secondary (three-dimensional) flow arise almost universally in experimental investigations of fluid motion. The motions of boundary layers in accelerating force fields may bear little resemblance to the motion of the main bulk of fluid. When the boundary layers become thick, their motions may not be ignored. In many cases the essential character of these motions is relatively independent of local viscous forces. Steady, inviscid, incompressible, three-dimensional, rotational flow solutions are sought to describe the motion of the real fluid in a limited region. An iterative method is proposed for the ideal fluid solutions. The singularities of a three-dimensional rotational flow are examined since certain types are inadmissible if the iterative method is not to degenerate. These inadmissible types are shown to be physically nonrealizable. The flow about a cascade of symmetrical airfoils in a duct with wall boundary layers is analyzed and compared with experimental observation. The agreement is good.

An approximate method for the calculation of nonstationary air forces at subsonic speeds. H. E. Fettis, Office of Air Research.

The computation of the nonstationary air forces and moments, acting on a thin airfoil traveling at subsonic velocity and vibrating with simple harmonic motion, is effected by means of the Possio integral equation which relates the unknown pressure distribution to the known normal velocity (downwash). Instead of attempting to determine an approximate solution to the exact equation, the original integral equation is replaced by one whose nucleus approximates that of the given equation and which possesses a closed solution. The resulting integral equation is solved by means of Kussner's inversion integral for the incompressible case. Computations carried out using only the constant and linear terms of the polynomial show good agreement with previous results, notably those of Dietze obtained by an iteration scheme. In the case of a wing-aileron or wing-flap combination, it is found necessary to introduce a new class of functions which may be considered as a generalization of the Bessel functions of integral order.

Moving sources in Kirchhoff's formula and in nonsteady aerodynamics. I. E. Garrick, National Advisory Committee for Aeronautics.

Kirchhoff's formula, the mathematical formulation of Huygens' principle for sound waves in air, provides a framework for a generic treatment of the role of sources and doublets in linearized nonsteady aerodynamics. It may be extended to apply to a uniformly moving medium with the aid of solutions for moving sources and doublets of arbitrary strength. Formulas for these solutions for subsonic, sonic, and supersonic speeds, for space and for the plane, are discussed, and some geometric properties are shown. Application is made to determine two-dimensional oscillatory air forces at sonic speed, and the results of some calculations for a range of transonic Mach numbers are presented. Other applications to wing flutter and to transient flows are indicated.

Aerodynamic phenomena at Mach numbers in the range from 10 to 20. C. du P. Donaldson, National Advisory Committee for Aeronautics.

A small ballistic range that has been developed to investigate aerodynamics at Mach numbers between 10 and 20 is described. The special problems associated with obtaining smooth and stable projectiles at very high velocities from ordinary rifles are discussed, and the techniques developed to solve these problems are presented. The method of obtaining drag, base pressure, and pressure distribution about bodies of revolution with this apparatus are described. The aerodynamic problems peculiar to very high Mach numbers, such as dissociation and ionization of the gas through which a body is traveling, are discussed. The results of tests of spheres and cones in monatomic gases at Mach numbers between 10 and 20 are presented which indicate ionization of the atoms past which these bodies are traveling. With the aid of the results of these tests, a theoretical discussion of the velocities in any gas required to produce such phase changes, and the aerodynamic effects of such changes, is made.

Session 22: Vibrations (damping)

On the response to external loads of continuous elastic systems with hereditary damping characteristics. Enrico G. Volterra, Illinois Institute of Technology.

In two previous papers the author considered free and forced vibrations of a system of one degree of freedom and free vibrations of continuous elastic systems on the assumption of hereditary damping characteristics. In this paper continuous elastic systems with hereditary damping characteristics are treated in the presence of externally applied loads. In particular, the solution corresponding to the steady-state motion of such systems under the influence of harmonically varying external loads is given explicitly in terms of a definite integral whose value depends upon the specific character of the memory function.

Structural damping in a simple built-up beam. T. H. H. Pian, F. C. Hallowell, Jr., Massachusetts Institute of Technology.

To study the basic mechanism of damping in built-up structures, a theoretical analysis has been formulated for the bending of a simple beam with thin reinforcing spar caps fastened by screws. The analysis assumes that the spar caps and the beam are held together by pressures which depend upon the tightness of the screw joints and that the screws in the holes have sufficient lateral clearance so as not to hinder any sliding motion between the cap and the beam. Following these assumptions, whenever the shear force between the two surfaces has reached the limiting rfiction force, a sliding motion begins and the shear force is redistributed. The load-deflection relation and the energy loss per cycle of static loading are then determined. It has been found that the nonlinear component of the load-deflection curve contains mainly a second-power term and the energy loss per cycle varies approximately as the third power of the amplitude of vibration. The theoretical results have been substantiated by experimental investigations.

Theory of dynamic vibration absorbers for beams. Dana Young, University of Minnesota.

The problem investigated is that of a uniform beam subjected to the action of a harmonic force and carrying a spring-supported mass which is designed to serve as a dynamic-vibration absorber. General equations are developed for the frequency-response characteristics of the system when the absorber is tuned to reduce the amplitudes at any one of the resonant frequencies of the beam. The effect of damping in the absorber system is taken into consideration. An approximate solution is also developed by assuming that the motion of the beam is primarily in one of its normal modes. This approximate solution is correlated both with the exact solution and with the known solution for an ordinary two-degree-of-freedom system. As an example, detailed numerical results are worked out for the case of a cantilever beam with the periodic force applied at the mid-span point and with absorber attached at the free end.

A dynamic method of testing resilient mountings. D. Muster, O. E. Curth, C. A. Arents, Illinois Institute of Technology.

In recent years there has been increased interest in the dynamic characteristics of resilient mountings; particularly in their response to structure-borne vibrations in the audio-frequency range. A method of testing resilient mountings is described which can be adapted to test mountings with load ratings of from 1 to 1000 lb over a frequency range of from 5 to 1500 cycles per second. The practical limits of the method and the possibility of extending the upper limit of the frequency range are discussed. Some data are given which indicate the effect of shape on the decibel drop across the resilient element of a mounting.

Linear noise smoothing and predicting filters. F. W. Bubb, Office of Air Research; R. G. Piety, Phillips Petroleum Company.

A simple method is presented for the design of physical systems such as servomechanisms, communication devices, filters, and the like, which have to operate in the presence of random disturbances (noise). A typical problem in this field is that of synthesizing the smoothing and predicting filter needed in gunfire control, the system being disturbed by radar and other noises. The analysis uses a new operational calculus which remains in the time domain, in sharp contrast to the method of Kolmogoroff and Wiener which employs Fourier analysis on the complex plane. The analysis in this paper culminates in a straightforward arithmetic procedure for solving noise problems, and this is illustrated by a numerical solution of one of Wiener's problems.

Session 23: Fluid Flow (wavefront phenomena)

The velocity and thickness of pressure waves in liquids. R. B. Green, Massachusetts Institute of Technology.

A general solution is obtained for the velocity and thickness of a pressure wave in a Newtonian fluid for which the coefficient of thermal conductivity, viscosity, specific heat at constant pressure, and the partial derivatives of specific volume with pressure and with temperature are constant. The equations of continuity, momentum, and energy are reduced to one third-order, first-degree differential equation in specific volume and distance from the wave center. The velocity of the wave is found from an existence condition, and the maximum slope of specific volume with distance using conditions at the wave center. The thickness of the wave is approximated by dividing the total specific volume change by this maximum slope. The relations between the total changes across the wave of the various properties are found. In a numerical example, a 100-atm pressure wave traveling through water at 20 C and 1 atm is found to have an approach velocity of 1489 m per sec and a thickness of 0.0014 cm.

Transmission of pressure waves in liquid filled tubes. W. T. Thomson, University of Wisconsin.

Propagation of pressure waves in a thin tube filled with liquid is investigated. The effects of inertia, stiffness, Poisson's ratio, and flexural waves in the tube are considered, and the results are reduced to nondimensional form to facilitate the study of variation of any parameter. For any given frequency, the study indicates that a finite number of modes are transmitted. Of these only the lowest mode is transmitted with a velocity less than the characteristic value. The division of energy between the liquid and the tube walls is found to be of importance for the lowest mode. The effect of viscosity on the propagation is investigated by assuming the viscosity to be small and utilizing the velocity distributions of the inviscous cases. Numerical computations are carried out for the first three modes of a particular liquid-pipe system. The paper adds to the work of Lamb, Fay, Jacobi, and others who have treated various phases of the problem.

Generalization and improvement of the hydraulic analogy. V. G. Szebehely, L. F. Whicker, Virginia Polytechnic Institute.

The classical hydraulic analogy between free-surface water flow in a rectangular channel and two-dimensional gas flow is only "qualitative" since the analogy assumes a "hydraulic gas" with an adiabatic constant $\gamma = 2$, instead of the accepted 1.4 for air. In the paper, the analogy is generalized mathematically resulting in a relation between the adiabatic gas constant, the cross section of the hydraulic channel, and the shape of the model. The cross section suggested for $\gamma = 2$ is rectangular, for $\gamma = 1.5$ triangular, and for $\gamma = 1.4$ parabolic. Using the

latter, the analogy becomes exact and "quantitative" measurements are possible. The corresponding temperature, pressure, and density relations for the gas flow are derived for general and special cases. Experimental results using a triangular channel for sub and supersonic flow problems are presented, which show very close agreement with theory and wind-tunnel data. A report on pressure and shock-angle measurements and review of the literature is included.

A simple statistical-mechanical approach to real gas flows with applications to shocks and expansion waves. Paul Lieber, Polytechnic Institute of Brooklyn.

This paper presents a new physical approach to gas-dynamics leading to a simple mathematical formulation for predicting phenomena that depend strongly upon the interaction of viscosity and compressibility effects. The physical concepts used in this development have been to a large extent suggested by the dissipation mechanism previously presented by the author. The principle of contiguous action, which was so effectively used by Maxwell in his formulation of the electromagnetic-field theory, plays a fundamental role in the theory development here. This principle, which asserts that the state of any region in the flow is determined by the states of its immediate neighboring regions, is used to formulate a set of three linear algebraic equations expressing the three conservation laws of mass, energy, and momentum. These equations lead to formulas for calculating the steady state of any region of the flow in accordance with arbitrarily prescribed boundary conditions. A comparison between the numerical results and some available experimental data shows excellent qualitative and some quantitative agreement.

The afterflow theory of the reloading of air-backed plates at underwater explosions. H. M. Schauer, Norfolk Naval Shipyard.

The initial response of an air-backed plate to the shock wave of an underwater explosion is followed by cavitation in the water in front of the plate. In this paper an attempt is made to explain the reloading of the plate which takes place when the cavitation closes. Since calculations based upon shock-wave diffraction fail to yield a satisfactory solution, the influence of the water flow caused by the explosion is investigated. The velocity field in the water caused by the expanding gas globe and modified by the cavitation and the baffle of the plate is calculated, assuming the water to be incompressible. The calculated flow of the water is compared with experimental data; the agreement is satisfactory. An estimation of the final deflection of the plate agrees also well with the measured values. Finally, the difficulties of the theory and the points where further research is necessary are discussed.

Session 24: Nonlinear Vibrations; Path Problems

On the nonlinear vibration of a circular membrane. A. C. Eringen, Illinois Institute of Technology.

Two nonlinear partial differential equations are obtained for the rotationally symmetric vibrations of circular membranes. Radial deformation and transverse deflection are not assumed to be small, contrary to the classical theory. Thus the effect of the additional membrane stresses developed during the vibration are not neglected. The differential equations are solved by use of the perturbation procedure for the case of free vibration. The radial slope and the tangential membrane strain at any point are obtained for a given initial deflection of a Bessel-function type and for an initial stress. The classical theory is found to be a limiting case of the present theory.

Subharmonic resonance of system having nonlinear spring with variable coefficient. M. H. Lee Wu, National Advisory Committee for Aeronautics.

A successive-approximate procedure is presented for solving subharmonic resonances of systems having nonlinear elasticity with variable coefficients and not subjected to a disturbing force. The method also can be applied to solve a subharmonic resonance of other nonlinear systems. In this method, the damping coefficient and frequency are determined for the corresponding values of phase angle and amplitude, although, in an actual physical system, the damping coefficient and the forcing frequency (or the frequency of the variable spring) are known. Detailed discussion and treatment are given for both odd order and even order subharmonic resonance for undamped and damped cases. Numerical calculations are made for third and fourth-order subharmonic resonances. Relations between phase angle and damping coefficient are also obtained for a range of phase angle equal to 2π. The analysis indicates that the results obtained from the calculations can also be applied qualitatively to any odd order and to any even order subharmonic resonance for the system considered.

Nonlinear vibration problems treated by the averaging method of W. Ritz. K. Klotter, Stanford University.

Attention is drawn to the "averaging method" for solving nonlinear differential equations of dynamical problems. The method is readily applicable for calculating steady-state vibrations in both autonomous and nonautonomous systems with whatever restoring forces or damping forces are present. The method allows a treatment in very general terms, thus covering a wide variety of cases. Its chief advantage is that the results are presented in the form of equations and not merely in the form of a prescription, thus allowing general discussions. The equations of the response curves for amplitude and phase angle in a single-degree-of-freedom system with harmonic exciting force and any restoring and any damping force are given explicitly. Some features are discussed. Numerical results for special cases are presented. The method allows a treatment of systems of multiple degrees of freedom also. Furthermore, it is shown that the steady state of a self-excited vibration in an autonomous system is obtained easily by the same method.

Aerodynamic damping of phugoids. Knox Millsaps, Office of Air Research.

The Lindstedt-Glyden perturbation method is applied to determine the effects of a temporal variation in the phugoid constant due to aerodynamic drag on the motion of an aircraft moving in a symmetrical plane. Comparisons between the classical Lanchester undamped phugoids and their electronic analogs and between the aerodynamically damped phugoids and their electronic analogs are made to determine the electronic noise and the validity of the perturbation method, respectively. It is shown that the perturbation method fails to account for the oscillating loss of altitude from an initially level flight due to

aerodynamic drag and that, providing the initial condition is appreciably different from level flight, the method provides a valid determination of the relaxation time of the damped phugoid motion.

Directional stability of ships in a regular seaway. G. P. Weinblum, David Taylor Model Basin.

A highly specialized case has been solved by K. Davidson. In the present paper the general problem of a rectilinear motion for an arbitrary constant speed and heading angle is treated, using approximate expressions for the generalized seaway forces given by the author elsewhere. A differential equation of the Hill type is obtained. In many cases the essential features of the phenomenon can be derived from a Mathieu equation. Here M. F. Strutt's stability chart is applicable. The important influence of the damping which is normally strong can also be estimated. A numerical example is discussed. The quantitative analysis still meets difficulties, since the hydrodynamic magnitudes involved depend upon the effect of the free surface and are known only approximately.

Session 25: Deformation of Bars and Filaments

The applied mechanics of yarn structures as influenced by yarn geometry and inherent fiber properties. W. J. Hamburger, W. G. Klein, M. M. Platt, Fabric Research Laboratories, Inc.

Yarn geometry is idealized by assuming the fiber elements to form a continuum of infinitesimal planetary rings rigid only in the directions of the fiber axes. Such directions are helical, and thus the orientation of the load-resisting elements varies continuously throughout the yarn in accordance with cylindrical helix-curve equations. Thus the yarn is a statically indeterminate structure, and since the fiber stress-strain curve is non-Hookean, yarn properties are dependent upon both inherent elastic characteristics of fiber and yarn geometry. Considering uniform synthetic fibers, theoretical analysis indicates yarn size, yarn twist, and rate of change of fiber stress to strain, important in determining yarn tensile performance. Statistical treatment is applied to natural fibers using the normal-distribution curve of extension to rupture, combined with the afore-mentioned variables found in yarns of synthetic fibers. Theoretical results, presented in the form of graphs covering practical ranges of variables, are compared with experimental data.

Matrix analysis of flexible filaments. J. E. Brock, Washington University.

A slender flexible filament fixed at one end is in the shape of a given space curve C; properties may vary along its length. A force system, consisting of forces in three co-ordinate directions, and couples in three normal planes, is applied at the free end. Displacements of the free end (three displacements and three rotations) are determined. The result is expressed as a 6×6 symmetrical matrix which is obtained by integrating along the curve C a matrix integrand, which, in turn, is obtained by operating on a matrix expressing local elastic properties by transformation matrices depending upon the curve C. As an example, the case of a cylindrical helical spring having constant properties along its length is treated in detail. The derivation of the fundamental matrix equation is given in an appendix using elementary geometry and statics. Validity of results is limited to small deflections.

A theory of twisted Bourdon tubes. Chen Chu, Massachusetts Institute of Technology.

The usual Bourdon tube is thin walled, of nearly rectangular cross-sectional shape, prebent. Consider now, a tube pretwisted instead of prebent. Such a tube will tend to straighten out or untwist by internally applied pressure. A theory for these tubes is worked out in the paper. The most remarkable property of the solution is that the sensitivity (i.e., the untwisting angle per unit pressure) increases with the amount of pretwist only for very small angles of pretwist. Above a certain small pretwist, the sensitivity diminishes rapidly, and a well wound-up tube has practically no sensitivity, and hence is useless as a measuring or control instrument. The theory given in the paper is relatively complicated; the results are shown in diagrams from which the behavior of tubes of most any dimensions can be read. Experimental verification of the theory is quite satisfactory, and the slightly twisted Bourdon tube in many respects is a more sensitive and more practical instrument than the universally used bent type.

The effect of initial twist on the torsional rigidity of thin prismatical bars and tubular members. Chen Chu, Massachusetts Institute of Technology.

Consider a bar of thin cross section, rectangular or otherwise, pretwisted like an aircraft propeller blade or large turbine blade. The pretwist being small (i.e, the helix angle of any horizontal fiber equals the sine of that angle), it has been customary heretofore to neglect the effect of pretwist on the torsional stiffness of the bar. This paper shows that the elastic twist superposed on the pretwist sets up longitudinal tensions of which the small transverse components cause a stiffening torque, making the pretwisted bar stiffer than the straight one. The usual aircraft propeller blade is some 30 per cent stiffer than a nontwisted one, while in an extreme case of a thin rectangular section the actual stiffness can be 5 times greater than that of the straight bar. Experiments verify the theory completely.

On the application of trigonometric series to the twisting of I-type beams. J. E. Goldberg, Purdue University.

In discussing the twisting of I-type beams which are free to warp at the ends and are subjected to one or more torsional loads applied at intermediate locations, the assumption is made that the resistance of the beam to twisting derives primarily from (1) the Saint Venant type of torsional resistance, and (2) the resistance of the flanges to bending in their own planes. Representing the angle of twist as a sine series, the strain energy associated with (1) and (2) and the external work are calculated in terms of the Fourier coefficients. The coefficients are then determined by applying the theorem of virtual work to obtain a general formula for this case. The resulting series converges at a reasonable rate and may be differentiated term by term to evaluate the derivatives which characterize the stress distributions. For other end conditions, a residual solution may be superimposed which liquidates the untenable portions of the warping displacements.

Session 26: Vibrations of Rotors; Transverse Impact of Beams

Critical speeds of uniform shafts under axial torque. Michael Golomb, Purdue University; R. M. Rosenberg, University of Washington.

The effect of axial torques on the critical speeds of uniform shafts with round cross section is investigated. The problem is solved in detail for shafts in self-aligning and in rigid end bearings. It is found that critical speeds always decrease with axial torque. With each critical mode there is associated a critical torque sufficient to cause instability of the nonrotating shaft, i.e., sufficient to reduce the corresponding critical speed to zero. For a given applied torque, the effect of reducing the critical speed is larger for shafts in self-aligning bearings than for those in rigid bearings, and it is larger for lower modes than for higher ones. For the two cases considered in detail, numerical values of the first six critical speeds are given for torques ranging from zero to the lowest critical torque. In addition, formulas are given for determining the critical speeds with good accuracy, provided the modes and torques considered are not too high.

Bending vibrations of a rotating beam. Hsu Lo, J. L. Renbarger, Purdue University.

The bending vibrations of a rotating beam, when vibration takes place in a plane perpendicular to the plane of rotation, have been investigated by many authors. Since in the applications the vibrations may take place in other planes, the present investigation assumes that the beam vibrates in a plane making an arbitrary angle with the plane of rotation. From the equations established, it was proved that the vibration modes are independent of the orientation of the plane of vibration, and the frequencies are related in a very simple manner to the frequencies when vibration is perpendicular to the plane of rotation. This is true for any arbitrary mass and stiffness distribution and hub diameters, as long as the vibration is limited to one plane. In such cases only vibrations perpendicular to the plane of rotation need to be investigated. An extension of the law of similarity by Theodorsen is also given.

Coefficients of irregularity of a rotating system considering torsional elasticities of the shaft. A. P. Boresi, University of Illinois.

The paper presents a method for calculating coefficients of irregularity in a torsional system, which consists of an impeller, generator, and Diesel-engine set. Flexibility, defined as the capability of the system to undergo angular deformations because of the torsional elasticities of the connecting shafts, is accounted for in the calculations. Coefficients of irregularity for specific locations in the system are compared. The maximum coefficient is approximately 4.5 times the minimum. The coefficients are also compared to the coefficient obtained for the system with the usual assumption of rigid shafts. The inclusion of flexibility increases the coefficients from 5 to 22 times. A tabular method, consisting in part of a modified Holzer table, is found to be convenient for the computation. Results are given in tables and curves.

Vibratory response of rigid rotors to dynamic unbalance. R. J. Harker, University of Wisconsin.

In dynamic balancing of rigid rotors it is general practice to allow simultaneous oscillation of the supporting bearings in one plane. Under these conditions the rotor is excited during rotation by two equivalent unbalance forces, one in each correction plane. The practical problem involves the separation of the effects of the two forces on the motion of the two bearings. A method is outlined whereby the speed of rotation may be utilized to effect this separation. General equations of motion are used to develop expressions indicating the response of a rotor at any speed, and also at the balancing condition, which is a particular speed of rotation. Equations are also developed for conventional methods of unbalance separation including the voltage-division and nodal-position methods. A comparison is made of the bearing amplitudes corresponding to a given unbalance condition with different methods of unbalance separation. In all cases the expressions are general, involving only the dimensionless parameters of the system.

Transverse impact of long beams, including rotatory inertia and shear effects. M. A. Dengler, Martin Goland, Midwest Research Institute.

Based upon the Timoshenko differential equation for the transverse bending of elastic beams, closed solutions are deduced for the stresses induced in a long beam of uniform section by the action of an impulsive, concentrated transverse load. For the special case when Young's modulus and the effective transverse shearing modulus of the beam are equal, the results take on a particularly simple form and numerical evaluation of the stresses is readily accomplished. When this equality of properties does not hold, numerical evaluation of the solutions is difficult and methods will have to be developed to permit this. The problem was treated previously in a paper by Uflyand, but his boundary conditions at the load station, and hence his results are shown to be incorrect. This is proved conclusively by treating the beam with equal Young's and effective shear moduli, obtaining the concentrated-load case as the limit of a solution for distributed loading, and noting that the present concentrated-load boundary conditions lead to the correct result. It is hoped that the present solution will help to clarify the stress-propagation phenomena in impacted beams. In a future program, along with numerical evaluation of the analytic results, experimental verification of the solution will be sought.

Session 27: Lubrication; Flow in Engines; Ballistics

Network solutions for lubrication problems. W. W. Soroka, University of California.

The Reynolds equation for fluid-film lubrication has been solved experimentally in the past with the aid of electrolytic tank models. In this paper the general differential equation for a lubricating film is converted to finite-difference form and an electrical resistance network developed to solve the resulting expression. A numerical iteration procedure based upon the Liebmann method is also suggested for solving the finite-difference equation.

The Reynolds lubrication equation with smooth outflow. R. Sedney, A. Charnes, E. Saibel, Carnegie Institute of Technology.

A generalization of the boundary conditions in the Reynolds hydrodynamical theory of lubrication is obtained as natural boundary conditions arising from a variational principle. The name "smooth outflow" suggests itself for this new case. Investigation of the corresponding pressure distributions permits a rigorous treatment and resolution of certain difficulties and questions cited by Gumbel and Vogelpohl.

The effect of leakage on the performance of reciprocating gas-operated mechanisms. E. F. Lype, Armour Research Foundation.

The motion of a free piston in a gas-filled cylinder is investigated for the case that gas leaks out past the piston. Exact solutions are given for the nonlinear differential equations representing the travel-time law and the work of expansion of the moving piston. An example taken from current practice shows that the effect of leakage on the power output can be considerable.

A method of performance analysis for the ducted pulsejet. George Rudinger, Cornell Aeronautical Laboratory, Inc.

Ducting represents a possible approach to the full utilisation of ram precompression in pulsejets. An exact treatment of the periodic flow pulsations of large amplitude that occur in this engine cannot be carried out at present; an approximate method of analysis has been developed which makes allowance for these flow pulsations. It is based upon the concept of a polytropic combustion process, and upon certain assumptions regarding the cyclic variations of the flow. The fuel specific impulse was calculated for various configurations and flight Mach numbers. The results are practically independent of the values of the assumed parameters within the range of their uncertainty. The potential performance of the unducted engine should be superior to that of the ducted engine except for very large duct dimensions, but no way has been found so far to realize this better performance.

Ballistic functions related to the Newtonian law of resistance. Mark Lotkin, Ballistic Research Laboratories.

Ballistic tables that permit the approximate calculation of ballistic elements of trajectories such as range, time of flight, terminal velocity, angle of fall, and the like, fairly easily and relatively quickly, are undoubtedly very useful. This fact was recognized long ago, and there have been many attempts to construct such tables. Thus, in 1842, J. C. F. Otto, following Euler's earlier suggestions based upon the square law of drag, constructed extensive tables of terminal data that are still being used occasionally. The tables of certain ballistic functions, related to the square law of resistance, recently constructed at Aberdeen Proving Ground with the aid of high-speed computing machines, differ in two important aspects from most other tables of a similar nature: (1) They are highly accurate, the tabular entries having an average of seven significant figures. (2) They permit the calculation of complete trajectories for a fairly wide range of the parameters involved. The purpose of this paper is to explain the essential features of the theory employed in the tabulation of the ballistic functions, and to illustrate the use of the tables by means of some pertinent examples. Numerical integrations carried out for a number of cases show the approximate values obtained through the tables to be very satisfactory.

PREPUBLICATION ORDER FORM

For Proceedings of the First U. S. Congress of Applied Mechanics

Amer. Soc. of Mech Engrs.
29 West 39 Street
New York 18, N. Y.

Date_____

Please enter my order for ____ copies of the Proceedings of the First U. S. National Congress of Applied Mechanics, delivery to be made in the spring of 1952. Since this is a prepublication order I understand that copies will be supplied at $10 each. Bill and Proceedings should be sent to me at the following address:

Name _____

Address _____

City _____ Zone _____ State _____

Date _____

For our records please indicate whether you are

☐ an ASME member

☐ nonmember